Polyglycerin-Based Nanogels for Protein Encapsulation

Inaugural-Dissertation

to obtain the academic degree

Doctor rerum naturalium (Dr. rer. nat.)

submitted to the Department of Biology, Chemistry and Pharmacy

of Freie Universität Berlin

by

Alexander Oehrl

2019

Department of Biology, Chemistry and Pharmacy
of Freie Universität Berlin
11.2015 – 11.2019

1. Reviewer:	Prof. Rainer Haag
2. Reviewer:	PD Dr. Kai Licha
Day of Defense:	13.12.2019

The following project was carried out within the research group of Prof. Dr. Rainer Haag from **November, 2015** until **November, 2019** at the Institute of Chemistry and Biochemistry of the Freie Universität Berlin.

Acknowledgements

First, I would like to thank Prof. Dr. Rainer Haag for giving me the opportunity to conduct my doctoral studies in his group, as well as his support during the last years.

I would also like to thank PD Dr. Kai Licha for being the 2nd supervisor of this thesis.

I would like to thank the BCP Core Facility BioSupramol for the numerous measurements.

A big thanks goes to Dr. Wiebke Fischer, for her having an open ear, for the support with every question that I had, and in general for her being the heart of this group. Without you everything would fall to pieces!

Jutta Hass and Eike Ziegler are thanked for handling the financial and organizational issues concerning my scholarship and my “Hausstelle”.

Katharina Tebel is thanked for her fast and friendly help with work trip organization as well as the SFB related part of my position.

A big thanks goes to Sebastian Schötz for his good and efficient labwork.

I would like to thank Dr. Pamela Winchester, Dr. Svenja Ehrmann, Dr. Mathias Dimde and Dr. Magda Ferraro for proofreading my manuscript and parts of this work.

I am thankful for the great time with my lab-mates Dr. Magda Ferraro, Dr. Svenja Ehrmann, Maiko Schulze, Dr. Ehsan Mohammadifar, Dr. Leonhard Urner, and Daniel Braatz. Thank you for the countless days of fun in the lab and the numerous interesting and fruitful discussions. Thank you all for every helping hand and shared moments of achievement.

All members of the lunch group are thanked for the nice breaks from work every day. A sweet thanks goes to the Kuchenkolloquium for the calory rich afternoon breaks with lots of delicious cake.

Era, Magda, Svenja, Wiebke and Yannic! I am grateful to have met you. Thanks for every day and every conversation and every coffee break. Thank you for being friends in good and in bad times. Thank you for all your support and friendship during the years and hopefully the many years to come.

I would like to thank my family for always being part of my life. For your support and your love.

Finally, I would like to thank my boyfriend Frank. Thank you for your love, your understanding, your support, and every day we have together. I love you!

Table of Contents

1. Introduction

1.1 Drugs in Modern Medicine

The treatment of diseases has seen a broad development over the last decades. A variety of different treatment options exist, spanning from small molecule drugs, over liposomal drug formulations[1] and polymer drug conjugates[2] to therapeutic proteins. They all differ regarding their active pharmaceutical ingredient (API) and the formulation of the drug, such as in the form of a tablet, a solution, an aerosol, a cream or an injectable solution. These formulations are considered as a combination of the API and any adjuvant substances, such as tablet filler, solvent, surfactant and preservatives. Depending on the characteristics of the API as well as its formulation, the administration to the body is determined. There are four broad classes of administration routes for drugs, namely oral, local, inhalative, and intravenous administration (**Figure 1A**).[3] The most common route is the oral route via tablets and the most convenient one in terms of patient compliance. However, the type of administration is tied to the specific drug/API and the disease that is treated. Local treatment of diseases is convenient for patients as well, because eye drops, and creams can be easily applied, and most drugs only act in the specific area in which they are applied.[4] This limited drug uptake into systemic circulation is one of the advantages of topical applications. A lot of side effects of a drug come from the systemic distribution of drugs and thus the uptake into tissues that are unrelated to the disease. If, however, a systemic distribution is necessary, oral drug administration is usually the preferred route.

One drawback of orally administered drugs is that they are taken up in the small intestine, which directly supplies the liver with any molecules reaching the blood stream. Liver enzymes, such as the cytochrome P450 system, metabolize many endogenous and foreign substances. This has the aim of detoxification of certain substances or to increase water solubility and thus the excretion rate from the body.[5] This poses a problem for the oral treatment route, as a lot of drugs get metabolized within the first contact with the liver and are most commonly inactivated or modified in a way that leads to a faster excretion. This effect is called the first pass effect and leads to the adjustment of the dose that must be administered to the body. As a large percentage of drug is inactivated, the amount of API must be increased per dose to reach the desired concentration within the blood stream. However, with some drugs the metabolism within the body is used as an advantage, because the compound that is administered to the body is a prodrug, which is converted to the biologically active form.[6]

Another aspect to consider is that some APIs do not have a matching hydrophobicity/hydrophilicity balance. This is corresponding to a too high or too low octanol/water distribution coefficient, also called logP value. It means they are either too hydrophilic to cross the lipid membrane of the small intestines cell lining or so hydrophobic that they are trapped within the membrane and cannot easily pass on into the blood stream.[7] The amount of drug that reaches the blood stream compared to the total amount of drug that was administered is called the bioavailability of the drug.[8] Due to the insolubility and the instability under acidic conditions such as stomach acid of some drugs, as well as slow uptake within the intestine, the bioavailability of a lot of orally administered drugs is quite low.[9] Some drugs are insoluble in water or not taken up at a reasonable rate that the only choice is to administer them intravenously or through inhalation into the lungs. The bioavailability of an intravenously administered drug is therefore 100%, as all the compound reaches the blood stream.

From this point on, the compound is distributed all over the body and depending on the affinity of the API towards certain tissues or cell types, it accumulates there. However, after a certain time every water-soluble compound will also be excreted from the body *via* the kidneys if the molecular mass is below the renal threshold. This threshold lies at a molecular mass around 45 kDa or an aggregate diameter of 5.5 nm. Below this threshold, molecules are easily excreted.[10–12]

The characteristics described above can be combined into the concept of LADMET[13], meaning liberation, administration, distribution, metabolism, excretion, and toxicity of a drug. All these different points must be considered when applying new drugs to the market. Failing to meet the requirements in one of these areas can lead to the end of the development of a certain drug or the discontinuation of a clinical trial. Modern research aims to optimize every aspect of the LADMET concept for the specific disease that must be tackled. The term liberation in this context means the release of the API from tablets, as well as from any drug delivery vehicle that was used. This especially plays a role in the use of nanocarrier systems, which will be discussed in a later paragraph.

Distribution of a drug is mostly dependent on the affinity of the drug molecules to the different tissue types. However, directly after administration the drug is distributed into all kinds of tissues and only after that it accumulates in specific tissues. Usually, small molecular weight drugs do not actively target tissues, but are passively accumulated according to their lipophilicity. The aim of most therapeutic approaches is to make a drug formulation that brings either active targeting into the system by attaching the drug to a ligand for certain cell

receptors, or by taking advantage of the physical properties of some diseased cell types, such as cancers. In these cancerous tissues the blood vessels are malformed and the junctions between epithelial cells are missing, leading to a fenestration of the blood vessel wall. Thus, uptake of larger particles becomes possible, compared to healthy tissues. This opens the opportunity for new therapeutic options, where larger carrier systems transport the drug preferentially into the tumor tissue. Due to an impaired lymphatic system, the carriers are trapped within these tissues and accumulate. Thus, a high local concentration of drug is achieved. This effect is called the enhanced permeation and retention effect (EPR-effect).[1,14,15] An overview on the aspects of LADMET, as well as active and passive targeting, and immune clearance are shown in **Figure 1**.

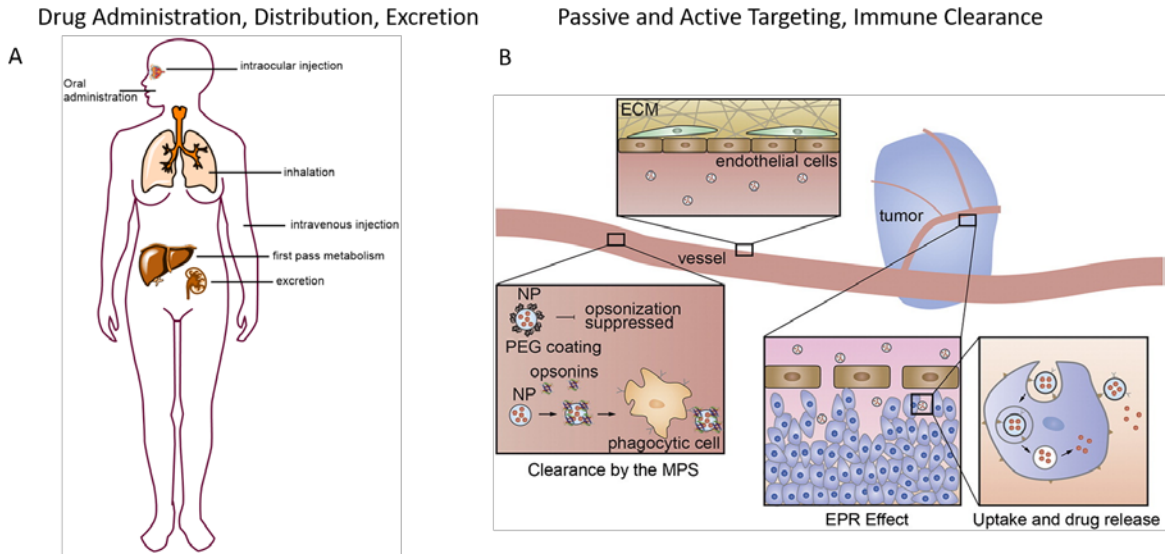

Figure 1. Overview on different aspects of the LADMET concept. A) pathways of drug administration, metabolism and excretion, B) enhanced permeation and retention effect (EPR)-effect in tumorous tissue, immune clearance by the mononuclear phagocyte system (MPS) and cell uptake by active targeting. Reprinted from Journal of Controlled Release **2014**, 187 with permission from Elsevier.[1]

In order to overcome the hurdles that exist in the context of a treatment with small molecules, research has focused on solving the specific issues of non-targeted distribution in the body, increasing the local concentration of drugs, increasing the plasma circulation time by lowering the excretion rate, and reducing side effects and potential toxicity. One promising approach in this regard has been the use of polymers for drug delivery.

1.1.1 Polymer Drug Conjugates

A lot of problems within the LADMET concept can be tackled by using a polymer backbone to which drug molecules are covalently connected to. These polymer-drug conjugates have the advantage of providing a high local drug concentration as a lot of individual drug molecules can be attached to one polymer chain. Furthermore, by addition of cell specific targeting ligands, active targeting to the diseased cells becomes possible.[16–19]

In order to release the drug at the targeted tissue, cleavable linkers between drug and polymer can be introduced. These linkers between the polymer backbone and the drug can be cleaved by or respond to certain specific environmental conditions, including acidic[18,20], reductive[21] or oxidative[22] conditions. This approach leads to enhanced bioavailability and protection of the conjugated drugs during circulation, as well as significantly prolonged excretion times. The design itself corresponds to a prodrug that releases its API upon environmental stimuli.

The polymer backbone can comprise different types of polymers. Polymer drug conjugates have been prepared from e.g. polyethylene glycol (PEG)[23], polyvinyl alcohol (PVA)[24], polylactic acid (PLA)-PEG copolymers[25], alginic acid[26,27], as well as natural polymers such as heparin[28] or even the protein albumin[29] The polymer backbone, however, is also the biggest hurdle to approval, as most polymers cannot be obtained in a monodisperse fashion. Another problem to solve is the accumulation of polymer within the body, as well as potential toxicity of some of the polymer degradation products. Functional groups are mandatory in order to be able to conjugate the desired drug. A variety of different groups can be used as cleavable linkers, such as acetals or hydrazones for acid cleavable systems. In the majority of studied polymer-drug conjugates, drugs such as the anticancer drug doxorubicin, but also a prodrug of the anticancer drug cisplatin were used, among others.[18]

1.1.2 Therapeutic Proteins

Another broad class of therapeutics, apart from small molecules, is the class of therapeutic biomolecules. This includes antibodies[30], hormones, cytokines, regulatory peptides, proteins, and growth factors. Many different types of diseases are treatable with these kinds of therapeutics, however, only quite recently, biotherapeutics emerged on the market.[31] With the advancements in genomics the straightforward preparation of these biomolecules in large quantities and high purities became possible. Prior to this, extraction from human or animal

tissues, which comes with the risk of contamination, was the only option.[32] Additionally, these approaches were time consuming and low yielding.

The great advantage of biotherapeutics is that most members of the class are ligands to one, or only very few receptors within the body. This makes them highly specific with very little side effects from unspecific interactions with other receptors. The specificity is also the reason why, for example, antibodies can be used as the active targeting option in polymer drug conjugates, as they lead to the accumulation within the tissues and cells that present their corresponding antigen on the cell surface.[17,33]

Besides the advantages of antibodies and proteins, they all suffer from a limited amount of administration options. Most proteins do not survive the acidic conditions in the stomach. Furthermore, they are not readily taken up in the small intestine. In most cases, the only option is to administer the protein intravenously, which can only be performed by medical professionals. However, exceptions exist, e.g. in the case of the small peptide insulin, which can be applied by the patient via abdominal injection.[34]

In the circulatory system, additional challenges of biological therapeutics have to be considered. Some compounds are easily recognized by the immune system, which leads to inactivation by the mononuclear phagocyte system (MPS) and thus a loss of function and the requirement for higher doses.[35,36] Furthermore, a lot of therapeutic proteins are small and below the renal threshold of 45 kDa, which leads to fast excretion and low plasma half-lives. As with small molecules, a major strategy to increase plasma half-lives and to reduce immune recognition for proteins is the conjugation of the protein to a polymer backbone. The conjugation leads to an increased overall molecular weight of the modified protein, which is above the renal threshold, thus prolonging plasma circulation. The gold standard, which is today most commonly used for this purpose, is the polymer polyethylene glycol (PEG).[37–41] It is usually covalently bound to the protein at a part of the structure which optimally should not affect the binding affinity between protein and receptor. The conjugation of one PEG chain, as well as multiple PEG chains is possible. The conjugation can be achieved by unspecific modifications of free amine groups of lysine side chains. However, the site-specific modification of certain amino acid residues is preferred, due to the control over protein function. By site specific modification, one can assure that parts of the protein are conjugated that do not have an influence on the active site of the protein. Through genetic modification, an unnatural amino acid can be incorporated at the desired point in the sequence.[40] However, this process is not very efficient and usually leads to lower yields of the modified protein

compared to the natural protein. An example for a PEGylated protein on the market is Oncaspar® which is PEGylated asparaginase.[42]

However, recently it became apparent that PEG can induce an immunogenic response, although it has quite a low overall toxicity. Antibodies against PEG have been found in patients treated with PEGylated proteins, which in some cases lead to a reduced therapeutic response because of fast elimination of the conjugate. In more serious cases, the immune response, can lead to an anaphylactic shock, which actively threatens the life of the patient if not treated immediately. These reasons led research to focus on alternatives for PEGylation of therapeutic proteins. This includes alternative polymers for conjugation, as well as completely different approaches, such as physical encapsulation within polymer networks.[2,43–45]

1.2 Biocompatible Polymers

For any application in the body, polymers must have certain properties. First, they should not show any toxicity towards target tissues, if they are used in implants or prosthetics. Second, if they are directly applied to the blood stream, as in the case of PEGylated proteins, they also should not have any adverse effects. Polymers that are non-toxic in the body are said to be biocompatible, however the definition of biocompatibility is a topic of discussion. One of the most detailed definitions comes from WILLIAMS. He states: “Biocompatibility refers to the ability of a biomaterial to perform its desired function with respect to a medical therapy, without eliciting any undesirable local or systemic effects in the recipient or beneficiary of that therapy, but generating the most appropriate beneficial cellular or tissue response in that specific situation, and optimizing the clinically relevant performance of that therapy.”[46]
The definition he proposes is quite complicated, however, this shows that the concept itself is not clearly defined. In general, one can focus on the absence of toxic effects in the target tissues, as well as on systemic toxicity.

Another big aspect in this context is biodegradability. Biodegradability means that a material can be broken down by processes that happen within living systems. This encompasses metabolic activity, as well as degradation of bulk material by microorganisms. Biodegradability is especially important when it comes to the application of synthetic polymers within the body. Any polymeric material that enters the blood stream must be excretable from the body. However, if the molecular weight of the compound is above the renal threshold, excretion is severely hindered, thus, leading to accumulation in organs, which might be toxic. The goal for a systemic application is to use polymers that can be degraded

under the physiological conditions into non-toxic fragments, which are smaller than the renal threshold and can therefore be easily excreted by the body.[47,48]

This degradability can be achieved by linking polymers with biodegradable linkers or using polymers that have an intrinsically biodegradable backbone. A few examples of biomedically relevant polymers will be discussed in the following section.

1.2.1 Medically Relevant Polymers

Different synthetic and natural polymers have been considered for biomedical applications. Very prominent examples of synthetic polymers include PEG, polylactic acid (PLA), polycaprolactone (PCL), copolymers of lactic and glycolic acid (PLGA). Additionally, natural polymers such as alginate, chitosan, and dextran have been studied (**Figure 2**).

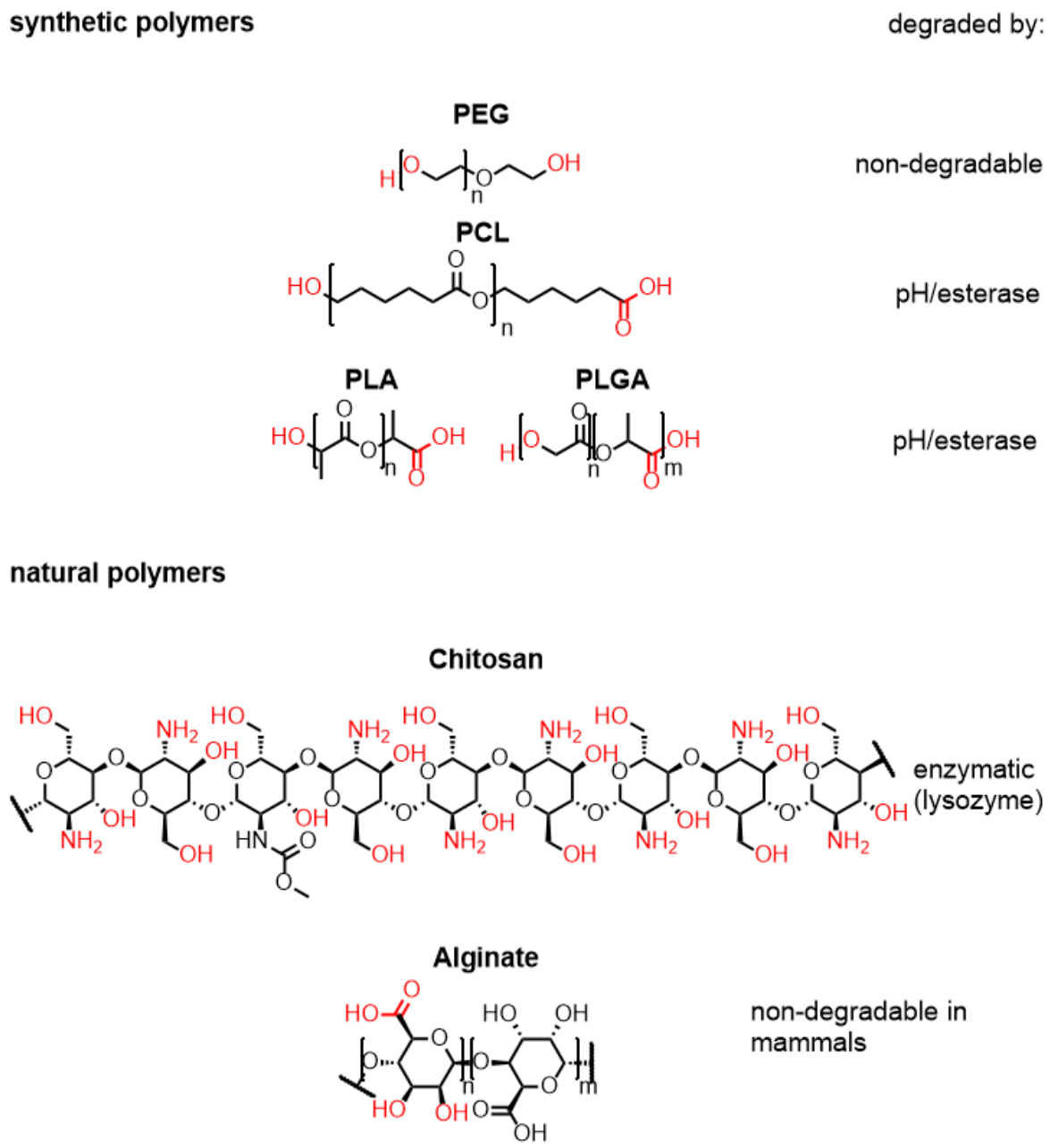

Figure 2. Selection of synthetic and naturally occurring polymers, relevant in biomedical research and application. Functionalizable groups are shown in red. Biodegradation conditions are given for every example.

There have been many studies on the above-mentioned polymers. This can be attributed on one side to the synthetic accessibility, as well as on the other side to the biocompatibility of these polymers. PEG, as mentioned, is the gold standard for the conjugation to proteins, but is also widely used as a linker molecule. It is obtained through either cationic or anionic ring opening polymerization of ethylene oxide. Polymers with narrow polydispersity values can be obtained in this fashion. The polymer itself is hydrophilic and essentially non-toxic, however, PEG-induced allergic reactions have been reported and

discussed. Furthermore, PEG is not biodegradable and only functionalizable at the terminal groups.[39,41,49]

PCL as a polymer is obtained through ring opening polymerization of caprolactone. The polymer itself is quite hydrophobic so it is usually used as a copolymer with more hydrophilic monomers or blocks.[50] This hydrophobicity has the advantage of strong van-der-Waals (vdW) interactions with hydrophobic drugs, which gives it the opportunity to physically bind these drugs in block copolymers, where PCL is the hydrophobic block. It is inherently biodegradable, due to the ester bonds throughout the polymer backbone. Here, the main mode of degradation is the enzymatic cleavage of the ester by esterases. As a result, it does not bioaccumulate and can be excreted from the body after the initial polymer is degraded to fragments below the renal threshold.[51]

PLA and PLGA show excellent biocompatibility and degradability when used as an implantable material.[50,52,53] After some time, natural hydrolysis leads to the polymer breakdown with non-toxic degradation products such as lactic and glycolic acid. However, for use as a conjugatable polymer to proteins, they are too hydrophobic. Furthermore, the functionalization is limited to the terminal groups.

Examples for natural polymers are e.g. chitosan and alginate, both being polysaccharide derivatives. Chitosan is a linear β-(1→4)-linked D-glucosamine which is randomly linked to N-acetyl-D-glucosamine units. It is derived from the shell of shrimp and other crustaceans by treatment of the chitin (fully N-acetylated D-glucosamine) with sodium hydroxide. This gives rise to different polymers with varying degree of acetylation. It is highly hydrophilic and biocompatible and used as a wound dressing polymer and scaffold material for nanoparticles. The material is also inherently biodegradable, as the polysaccharide can be broken down by lysozyme to glucosamine and is thus absorbed and metabolized by the body.[21,54,55]

Alginic acid or the sodium and calcium salt, called alginate is a linear block copolymer of β-(1→4)-linked D-mannuronate and α-(1→4)-linked L-guluronate, and is derived from the cell walls of brown algae and some bacteria. It is also highly hydrophilic and has the property to form polymer networks upon treatment with e.g. calcium-ions. This makes it a good scaffold material for the encapsulation of living cells. The number of functional groups enables further modification, e.g. the addition of growth factors for cells. However, the polymer itself is not degradable by humans as they lack the necessary enzyme.[26,27,55–57]

All these polymers have advantages and disadvantages and there is a variety of other polymers that are currently investigated for use in biomedical applications. Especially for

PEG, as one of the wildly used polymers, new alternatives are needed. One of these alternatives is Polyglycerol, which will be discussed in the next section.

1.2.2 Linear and Dendritic Polyglycerol

Structurally very similar to PEG with its polyether backbone is the linear version of polyglycerol shown in **Scheme 1**.

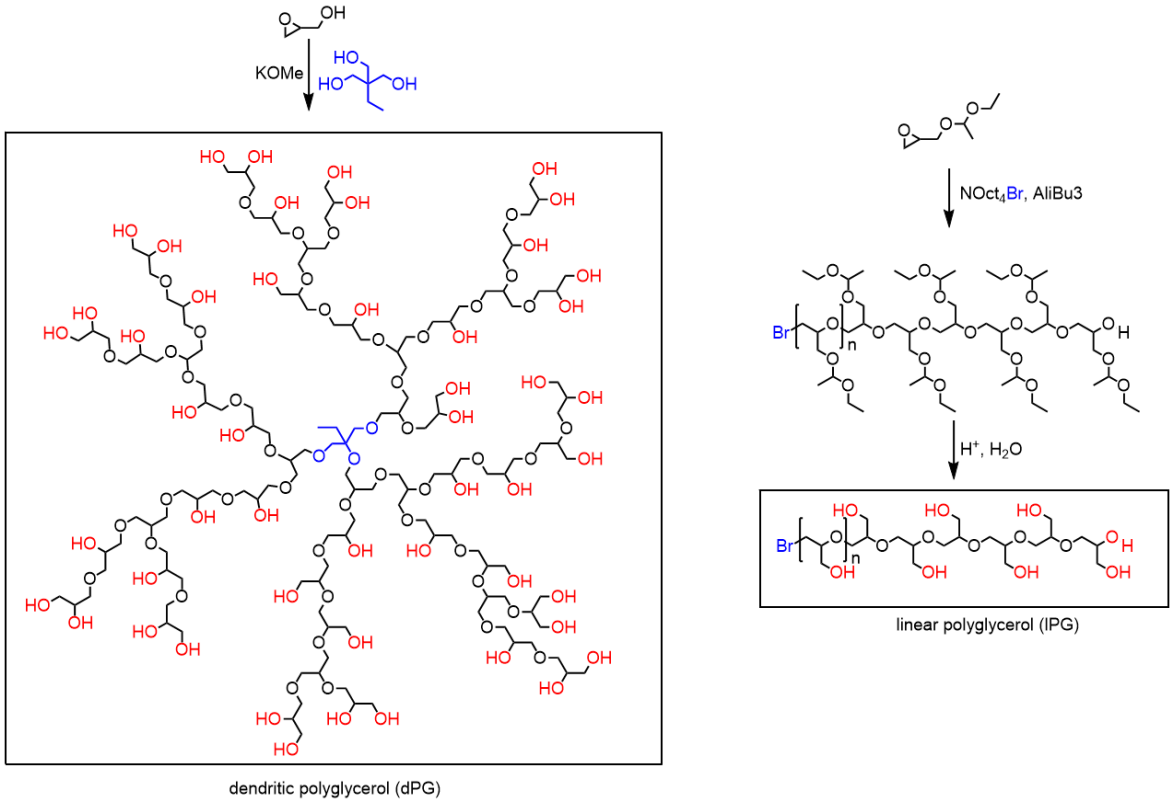

Scheme 1. Simplified reaction scheme for the polymerization of glycidol and acetal protected glycidol to yield dendritic polyglycerol (left) and linear polyglycerol (right), respectively. Initiator molecules are shown in blue, functionalizable groups are shown in red.

Instead of using ethylene oxide to produce PEG, one can use a derivative of ethylene oxide, glycidol, to produce linear or hyperbranched polyglycerol, that are structurally related to PEG.

Monomer activated ring opening polymerization of a protected glycidol derivative yields linear polymers with defined end groups, a polyether backbone and side chains with protected hydroxy groups. In the case of acetal-protected glycidol, the resulting polymer can be deprotected under acidic conditions. The resulting deprotected polymer is a linear

polyglycerol (lPG) and structurally very similar to PEG.[44,58,59] However, it possesses one hydroxy group per monomer at the side chains, which makes it even more hydrophilic than PEG. Side chain functionalization becomes possible, additionally to the terminal functionalization that is available for PEG. These numerous hydroxy groups influence the polymer structure in solution and could have an influence on the evasion from the MPS clearance, offering a stealth effect for a coupled protein. It is anticipated that lPG, due to its higher hydrophilicity, will not induce an immunogenic response and prevent the formation of anti-lPG antibodies.

The anionic ring opening multi-branching polymerization of unprotected glycidol leads to the hyperbranched version of polyglycerol, also called dendritic polyglycerol (dPG) which can be seen in Scheme 2.[60–62] It is a highly hydrophilic polymer and possesses around one hydroxy group per monomer. Thus, dPG has a very biologically inert surface which prevents unspecific protein adsorption and renders it quite biocompatible and non-toxic. The vast number of functional groups can be used for post-functionalization, which makes it an ideal platform for many applications.[63–66] It has been used as a hydrophilic core for core-shell structures[67], as a polymeric support for catalysts[68], as scaffold material for polymeric networks[64,66], and many more. Post-modification of the hydroxy groups to sulfate groups yields potent L-selectin-inhibitors and thus, immune-modulating polymers.[69–72] Due to the mentioned properties it is a highly versatile polymer exhibiting the needed properties for the use in biomedical applications. However, it lacks inherent biodegradability, as the polyether backbone cannot be broken down by the body. Therefore, only polymers with molecular weight below the renal threshold can in general be used for applications, as larger polymers will not be excreted easily by the body and accumulate. Degradable alternatives, including a copolymer of glycerol and caprolactone, have been developed recently and show promising properties as nanocarriers for hydrophobic drugs.[73]

1.3 Nanocarrier Systems

The requirements for a successful nanocarrier are high. Several criteria must be met in order to have the optimal nanocarrier. These criteria include a prolonged blood circulation of the drug, the ability to accumulate via active or passive targeting in the relevant pathological zone, responsiveness to local stimuli, such as pH and/or temperature changes, resulting in accelerated or burst drug release. Furthermore, a nanocarrier has to allow for an effective intracellular drug delivery, bear a contrast/reporter moiety, and is non-toxic or

biodegradable.[74] As mentioned before, a way to overcome low solubility of some drugs or rapid clearance is to covalently attach them to a polymer backbone as seen for polymer-drug conjugates. Analogously, the covalent attachment of PEG, or in general, polymers to therapeutic proteins is also a kind of nanocarrier system, although one can debate, if the polymer in protein-polymer conjugates counts as a carrier. Nevertheless, the polymer increases the blood circulation time and reduces the immune clearance, as well as the renal clearance.

Besides polymer-drug conjugates, there are many more ways to deliver a drug or protein to the side of action and over the last decades a variety of different systems have been developed. These nanocarriers can be divided into different groups, including lipid-based, inorganic, polymeric, and protein based nanocarriers, depending on the material that they are made of. The four main groups can be seen in **Figure 3**.

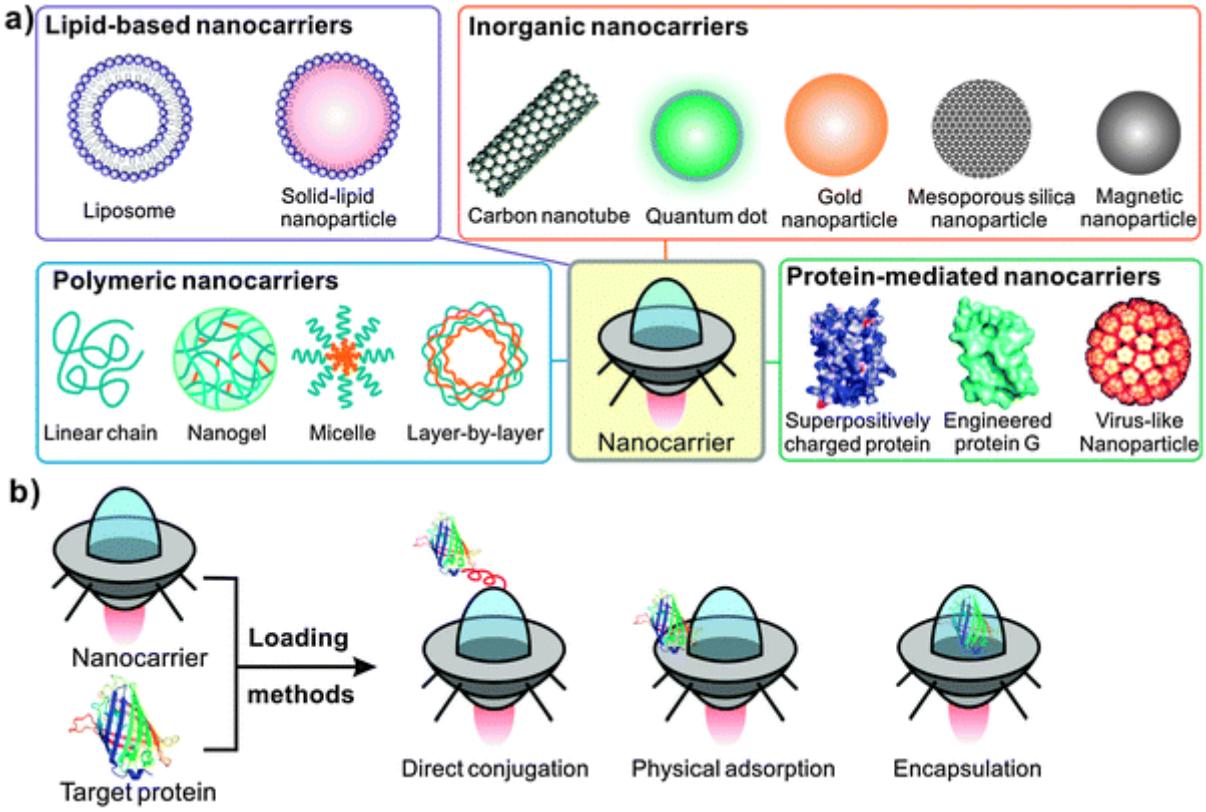

Figure 3. Different groups of nanocarrier systems divided into the class of material that they are made of, a) nanocarrier systems, b) loading methods of drugs/proteins with nanocarriers, reprinted from Chem. Soc. Rev., *2011*, **40**, 3638–3655, with permission from Royal Chemical Society.[75]

There are three methods of loading for nanocarriers. First, the direct conjugation of drug to the carrier. For this method the most prominent example is the polymer-drug conjugate. The second method is to use intermolecular forces to physically adsorb drug

molecules or proteins to the carrier surface. This approach works very well for inorganic carriers, such as carbon nanotubes and graphene, where hydrophobic drugs with aromatic ring system are adsorbed to the aromatic surface via π-π stacking interactions. Another prominent example is protein nanocarriers that can bind drugs to the protein surface. Ionic interactions between a poly-ionic species such as a charged polymer and a charged drug are also possible in this context.[75]

The third loading method involves physical entrapment within the structure of the nanocarrier. The interactions that keep the drug within the carrier are in this case either hydrophobic interactions between parts of the carrier and a drug, or physical entrapment within a network, which strongly hinders diffusion of the encapsulated drug molecule. This method is one of the most commonly used, as the drug is not chemically altered and thus completely keeps its biological effect.

1.3.1 State of the Art

As of 2012, there were around 100 nanomedicines available on the market that were FDA approved.[34,42] The most common nanocarriers in this regard are liposomal formulations of small molecules, such as the anticancer drug doxorubicin. Liposomal formulations work by physical entrapment of a drug within the liposomal aggregates of a lipid. Hydrophilic drugs and hydrophobic drugs alike can be encapsulated at the same time. Hydrophobic drugs are incorporated in the hydrophobic bilayer of the alkyl chain part of the lipids, while hydrophilic drugs are encapsulated within the inner water filled cavity of the liposomes. The size of the liposomes makes it possible to take advantage of the EPR effect, resulting in enhanced uptake into tumors, as compared to normal tissues. The advantage of these formulations is the increased solubility of the drug, a much higher local concentration within the carrier, and decreased side effects due to the smaller amount of free drug. Examples for approved liposomal drug formulations include Doxil®, which is liposomal doxorubicin. It was approved by the FDA in 1995 and is used for the treatment of metastatic ovarian cancer and AIDS-related Kaposi´s Sarcoma.[42,76,77]Other nanocarriers based on protein drug conjugates are available such as Abraxane®, in which the anticancer drug paclitaxel is bound to albumin nanoparticles of around 130 nm. It is used for the treatment of metastatic breast cancer, lung cancer, and metastatic pancreatic adenocarcinoma.[42]

The class of PEGylated proteins includes a lot of different marketed products, one of which is Oncaspar®, a PEGylated version of the protein L-asparaginase. It is used in the treatment of acute lymphoblastic leukemia, and chronic myelogenous leukemia.[78]

However, currently there is no example for polymeric nanocarriers on the market, other than protein-drug conjugates and liposomal formulations.[42] A lot of research effort has been put into the development of polymeric micelles, unimolecular micelles, graphene, carbon nanotubes, and nanogels. The reason for the absence of examples of these nanocarrier types includes either toxicological issues, due to the problem of polydispersity of the polymeric materials used, or an enhanced accumulation of the nanocarriers in organs. Nevertheless, numerous promising examples for nanocarriers that have the potential to reach the market, have been reported in the last years.[34,78] Here one approach is the encapsulation of drugs in unimolecular micelles.

1.3.2 Unimolecular Micelles

The group of nanocarriers that are based on polymers offers a wide variety of different structures which depend on the type of polymer that is used. Block copolymers, consisting of a hydrophobic and a hydrophilic block, for example, can be used for the encapsulation of hydrophobic drugs. This kind of polymers can form polymeric micelles in aqueous solution, with an inner hydrophobic core and an outer hydrophobic shell. Within the hydrophobic core, hydrophobic drugs can be encapsulated by physical interaction of the hydrophobic block with the drug. Upon cell uptake these micelles can release their payload. However, premature disintegration of the micelle limits the applicability of this carrier. Micelles are only stable above a certain critical concentration, also called critical micelle concentration (CMC).[79–81] If this concentration is too high for a certain block copolymer then the micelles fall apart when they encounter the blood stream, as they are quickly diluted below the CMC. This leads to premature disruption of the micelles and thus drug release.[82]

An alternative to the physical stabilization of micelles is the use of core shell structures, especially core multi-shell structures. In these cases, the polymer does not form micelles in solution, but itself has properties of a micelle. Branched polymers or dendritic systems are suitable for these applications. Core-shell structures are constructed by the design of a hydrophobic polymer core which is then modified with a hydrophilic polymer to yield a unimolecular micelle that can encapsulate hydrophobic guests and still is water soluble and protein repellant on the outside. The unimolecular analogue of liposomes can also be formed

in such a fashion. Here, for example, a hydrophilic hyperbranched core such as dPG can be used and covalently modified with a hydrophobic chain, such as a PCL block or a fatty acid, which is then capped with a PEG or lPG chain. Thus, a core multi-shell structure is formed with a hydrophilic dPG-core, a hydrophobic shell and a solubilizing outer shell of PEG. These unimolecular systems can encapsulate hydrophobic drugs within their PCL shell.[83–85]

However, multi-shell systems are generally not very suitable for the encapsulation of therapeutic proteins, as the detergent nature of some of the micelles can denature the protein structure. Many proteins are also large compared to the unimolecular micelles which means that there is no way for the protein to be encapsulated within the shell structure of the carriers. The only way would be that the carriers as a whole surround the protein and form protein-carrier aggregates.

Proteins need a sufficiently large nanocarrier, which does not have detergent-like properties and provides a close to natural environment for the protein. By this, a protein can stay intact and keep its biological function. Very suitable carriers for this purpose are nanogels.

1.4 Nanogels as Drug Delivery Systems

Nanogels are highly water-swollen polymer networks in the size range of 10 to 1000 nm.[56,86] The gels can be formed by physical entanglement of polymer strands, chemical crosslinking, supramolecular interactions, electrostatic interactions, and coordinative bonding.[87,88] This shows the vast variety of possibilities to obtain such polymer networks. As the nanogels are water swollen, the polymers used are usually hydrophilic polymers such as PEG, poly(methacrylate), chitosan, alginate, poly(vinyl alcohol), lPG, and dPG. The porous nanogel network can be tuned regarding polymer density, pore sizes, surface charge and degradability by the use of different scaffold material, as well as crosslinking moieties. The size of the nanogel has a big influence on cell uptake behavior, as cell uptake is usually quite hindered above around 100 nm.[89]

Depending on the polymers and crosslinkers used, the gel network can load a variety of biomedically relevant payloads. If hydrophobic groups are used within the network, hydrophobic drugs can be encapsulated.[90] Positively charged nanogels, based on polypropylene imine (PPI) can load negatively charged ribonucleic acid (RNA) for gene delivery.[91–93] However, one of the most promising encapsulation candidates are therapeutic

proteins. The gel network of hydrophilic and inert polymers provides an optimal environment for protein structure preservation and shielding from immune recognition.

1.4.1 Stimuli Responsive Nanogels

Nanogels that show enhanced or even burst drug release are desired, as they allow for a temporal and spatial control over the release of the payload. Nanogels that are made completely from hydrophilic polymers without any hydrophobic blocks cannot efficiently encapsulate hydrophobic drugs, as there are not strong enough interactions to keep the drug within the network. Even if a hydrophobic block exists and interactions keep the drug, there is a constant loss of drug to the environment due to diffusion. Thus, gels will slowly lose their cargo over time. This slow, constant release can be desirable, however, in most cases a non-leaching carrier is wanted that releases the payload upon certain environmental stimuli. This has the advantage that toxicity in healthy tissues can be reduced if the stimulus exists within the diseased tissue but not in the healthy tissue. Furthermore, if the stimulus is not environmental, but external, the functionality of the carrier increases even more. Environmental stimuli can be for example, changes in pH, ion strength, and redox environment, while external stimuli can be temperature changes, magnetic fields, ultrasound, and light.[94–96] Stimuli-responsiveness must be introduced into the nanogel by using polymers with certain functional groups that react to the change in environmental conditions or the external stimuli. Some examples are shown in **Scheme 2**.

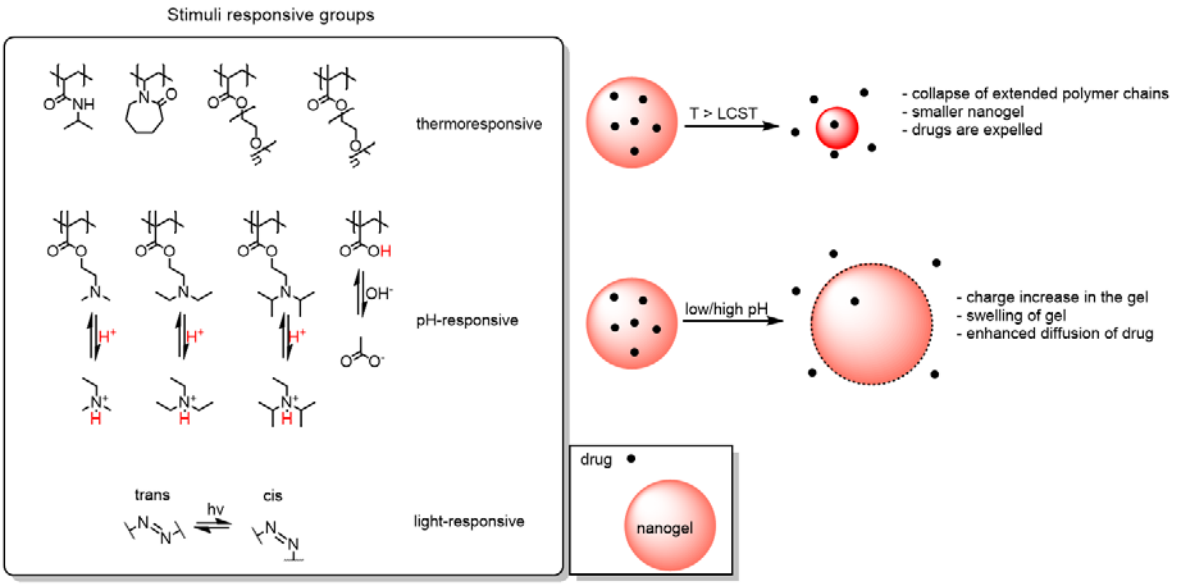

Scheme 2. Examples for functional groups or polymers that exhibit stimuli-responsiveness. Behavior of the corresponding nanogels is shown on the right.

Thermo-responsive systems can be used to target tumors that are near the body surface. When heat is applied from the outside of the skin, the temperature rises above the lower critical solution temperature (LCST) of the thermo-responsive polymers, which triggers the collapse from the extended water-swollen state to the aggregated insoluble state of the polymer. Together with water, the drug is expelled from the carrier.[97–99]

In pH-responsive gels, amine groups or carboxy-groups are usually used. These are protonated or deprotonated at certain pH values. Amines, for example, are protonated at low pH values and gain net electric charge. As more groups within the gel network are protonated, the network draws in more water and expands, thus creating bigger pores and a higher rate of diffusion, which leads to an accelerated drug release.[100] Other stimuli such as magnetic fields can guide nanogels that incorporate magnetic nanoparticles[17,101].

However, all these stimuli and responsive groups usually do not lead to a degradation of the nanogel. Degradation is desired, as nanogels are in a size range where excretion through the kidneys is not possible. This means that after drug release they can accumulate and cause toxicity. Biodegradable nanogels are thus needed for real biomedical applications.

1.4.2 Degradable Nanogels

Degradable nanogels also respond to stimuli, however, the response is the degradation of the polymer network into smaller fragments. The most commonly used environmental stimulus is

a reduced pH-value which is found in tumor tissues (pH 6-7), inflamed tissues (pH 6-6.5), endosomes (pH 5.5), and lysosomes (pH 4.5)[96]. Another commonly exploited stimulus is the reductive environment within cells compared to blood plasma. This reductive environment is due to the presence of free glutathione (GSH) within the cells. Furthermore, the level of GSH in tumor cells is higher compared to normal cells, enabling the specific treatment of tumor cells.[21,102,103] Some examples of cleavable linker groups are shown in **Scheme 3**.

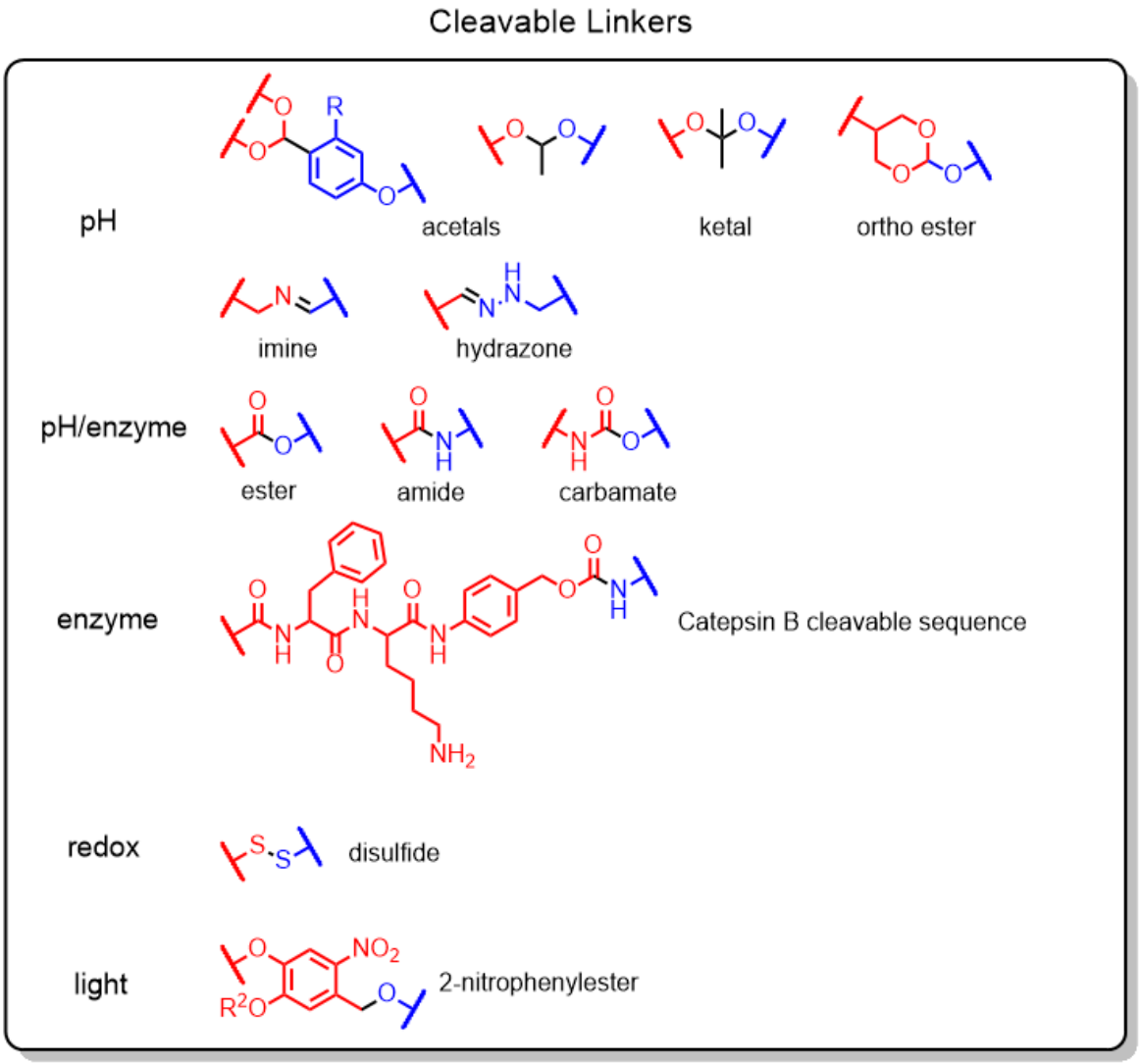

Scheme 3. Selection of linker moieties that are cleaved under certain environmental or external stimuli. Fragments are shown in different colors.

As mentioned, the GSH level in tumor cells is higher than in normal cells, which leads to the reductive cleavage of disulfide bonds. Thus, this is a commonly used motif for redox-sensitive nanocarriers. One example are enzymatically crosslinked nanogels, based on linear polyglycerol with disulfide linking groups developed by SINGH *et al.*[104]

For tumor treatment of the skin, one can use light-sensitive nanogels, were the linking groups degrade upon exposure to certain wavelengths of light, as in the case of 2-nitrophenylesters (UV-light). KLINGER *et al*, for example prepared light and enzymatic sensitive nanogels based on polyacrylamide with acrylate-functionalized dextran that were degraded upon exposure to UV-light of 365 nm.[105]

Especially, a variety of pH-degradable nanogels have been produced in the past. Many different functional groups allow for degradation at endosomal or lysosomal pH values, such as acetals, ketals, orthoesters, imines, and hydrazones. Depending on the application, one can choose a suitable linker for pH-degradation. For example, CHEN *et al* have prepared acetal functionalized polyvinyl alcohol (PVA) based nanogels through UV-crosslinking. Paclitaxel was encapsulated and could be released at a pH of 5.[106] Cell encapsulation and release, based on benzacetal-functionalized microgels was shown by STEINHILBER *et al*.[107]

Slow biodegradation is achieved with esters and amides. They can be hydrolyzed at low pH values but at a much slower rate than acetals or imines. Therefore, long term accumulation is prevented by inclusion of ester or amide bonds into the polymeric network of nanogels. However, for many applications a fast drug release is preferred, so easily cleavable groups are used for a burst drug release.

1.5 Synthetic Methods for Nanogel Preparation

1.5.1 Conventional Methods

Nanogels can be prepared through many different methods. The preparation methods can be divided into polymerization of monomers in a homo- or micro/nanoscale heterogeneous phase, physical self-assembly of polymers, crosslinking of preformed polymers, and template-assisted nanofabrication of nanogel particles using nanolithography.[88]

Self-assembly of polymers leads to nanogels that are either held together by hydrophobic interactions if amphiphilic block-copolymers are used, or that are bound by supramolecular bonds between for example β-cyclodextrin and a guest molecule such as lauryl chains. AKIYOSHI *et al.* entrapped insulin within hydrogels, made by the hydrophobic association of cholesterol-modified pullulan.[108] GREF and co-workers, on the other hand, described the self-assembly of nanogels by supramolecular host-guest interactions of a β-cyclodextrin polymer and lauryl-modified dextran in aqueous solution.[109]

Some of the more common preparation methods are the mini- and microemulsion polymerizations of monomers or macromonomers.[14,60,105,110–115] In these methods, droplets of reactive monomers in the desired size range are obtained by high energy input from ultrasonication in miniemulsion and large amounts of surfactant in microemulsions. Crosslinking of the monomers in the templated droplets leads to polymer beads in the nanometer to micrometer range, which are dispersed in the reaction solvent. However, the use of ultrasonication and surfactants are quite harsh reaction conditions, so the *in situ* encapsulation of proteins is limited or even impossible and problems with surfactant removal can arise.[115–117] An example for the microemulsion process is the work of DESIMONE and co-workers. Cationic PAETMAC nanogels were made by inverse microemulsion polymerization of 2-hydroxyethylacrylate and 2-acryloxyethyltrimethylammonium chloride in heptane, using PEG-bisacrylate as the crosslinker.[114]

Templated synthesis of nanogels using soft lithography is another option to obtain very well-defined and almost monodisperse gels in a variety of shapes from a lot of different organic precursors.[88] DESIMONE and co-workers developed the PRINT method, which stands for particle replication in non-wetting templates. Here, particles in the range of nanometers to several micrometers are obtainable. This technique creates nanogels within non-wetting elastomeric molds, consisting of a perfluoropolyether network. This network is formed on patterned silicon templates by photochemically induced crosslinking of dimethacrylate-functionalized perfluoropolyether oligomers.[118]

Another useful method for the preparation of hydrophobic nanoparticles is the nanoprecipitation method, which is based on the insolubility of some growing polymers in a corresponding non-solvent.[119] For example, polystyrene- (PS),[120] polylactic acid, and copolymers of polylactic and glycolic acid (PLA/PLA-co-PGA)[119,121] nanoparticles have been prepared using a nanoprecipitation protocol. These nanoparticles can be used for the encapsulation of hydrophobic drugs.

1.5.2 Inverse Nanoprecipitation for the Encapsulation of Proteins

Apart from the nanoprecipitation method that produces hydrophobic nanoparticles by precipitation in water, the inverse case has been first described by STEINHILBER *et al.*, where dendritic polyglycerol nanogels were prepared by precipitation in acetone.[122] This method has many advantages compared to the ones described before. No high energy input from

ultrasound or any kind of surfactant is needed, which makes this a very mild method for the preparation of nanogels. Therefore, *in situ* encapsulation of therapeutic proteins is possible, which would be destroyed by alternative nanogel preparation methods. By this method, proteins were encapsulated with high efficiency and retained their functionality upon release.[122]

During inverse nanoprecipitation, the macromonomers form nanoaggregates due to the diffusion of the solvent into the non-solvent. These aggregates are then crosslinked in order to obtain a stable nanogel network that is then subsequently dispersed in water. In a last step, the final gels are obtained by removal of acetone.

A further improvement to the batch-wise inverse nanoprecipitation method is the continuous method of using a microfluidic system for the controlled synthesis of polymer nanoparticles. The hydrodynamic flow ensures a rapid and controllable mixing of solvent and non-solvent within the microfluidic channels.[119] VALENCIA *et al*. showed the feasibility for a PLGA-b-PEG copolymer in acetonitrile/water.[123] Furthermore, a flow-based approach enables the production of large amounts of nanogels and might be suitable for upscaling for biomedical applications.

However, fast screening of conditions is done in a much easier way in the batch-wise inverse nanoprecipitation method, which is the reason that it was chosen for this work.

1.6 Click-Type Reactions for Crosslinking

The crosslinking chemistry is an important aspect when it comes to nanogel formation from polymeric precursors. If sensitive cargos, such as proteins has to be encapsulated, the cross-linkable reactive groups should not react with the protein in any way. This refers to the term biorthogonality which was introduced as a concept by BERTOZZI in 2003. Bioorthogonal reactions are defined by her as reactions that are inert to functional groups within biological systems. The functional groups must, however, exhibit a specific reactivity with each other under cell- and organism friendly conditions. The size of the reactive groups has to be relatively small to prevent undesired interactions with biological systems. A reaction that already occurs in living organisms cannot be, by definition, a bioorthogonal reaction. Finally, reaction kinetics have to be reasonably high, reactants and products have to be stable in water, and functional groups have to be installable in a straightforward manner.[124]

Click reactions are especially suitable as linking chemistries. SHARPLESS *et al.* defined click chemistry as reactions that must be high yielding, have easily accessible starting materials, generate no- or non-toxic side-products, have a high thermodynamic driving force, and must be performable in a benevolent solvent such as water.[125] **Figure 4** shows an overview on the most prominent examples of click chemistry.

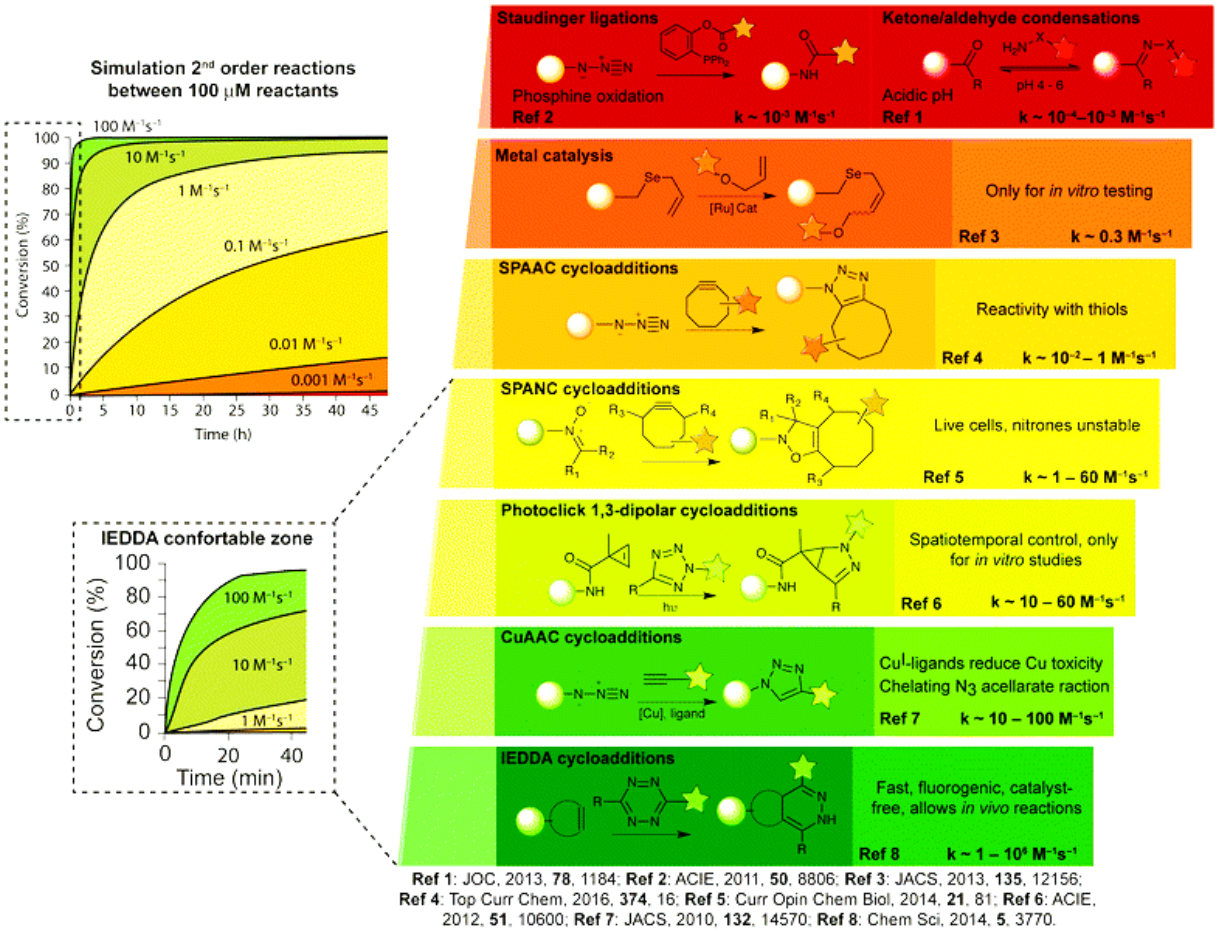

Figure 4. Overview on the different click chemistries, their properties, functional groups, and reaction kinetics. Reprinted from [126], copyright from The Royal Society of Chemistry.[126]

From the available click type chemistries only a few are considered completely bioorthogonal, however, for some applications the biorthogonality does not play the most important role as in the case of production of nanoparticles and nanogels for the encapsulation of hydrophobic drugs. For the encapsulation of proteins or even living cells it is far more important to have completely bioorthogonal nanogel formation reactions. As in this work the inverse nanoprecipitation of pre-functionalized polymers is used for the formation of nanogels, the crosslinking chemistry is very important. The crosslinking chemistry has to be fast and with

high conversion, without producing toxic side products and be bioorthogonal. Therefore, different chemistries have been explored for the purpose of the gelation of polymers.

The Huisgen 1,3-dipolar cycloaddition between azides and alkynes that forms a triazole ring is one very prominent example for a predecessor of click reactions.[127] Slow reaction kinetics, however, limited the biomedical applicability of this reaction until the copper-catalyzed azide-alkyne cycloaddition (CuAAC) was discovered by SHARPLESS and MELDAL, independently. The catalyzed version proceeds even at room temperature.[128,129] Although azides and alkynes are functional groups that are non-existent and inert in living organisms, CuAAC only partially meets the requirements for bioorthogonality.[125,130] This is due to the harming effects of copper ions that can bind or damage sensitive biomolecules, such as proteins.[131] Furthermore, copper contaminations may induce oligonucleotide[132] and polysaccharide degradation[133], which is the main reason for cytotoxicity coming from DNA damage. Still, CuAAC has been used for bioconjugation, polymer and dendrimer synthesis[134] as well as for the encapsulation of cells[135] into hydrogels. CuAAC is a useful tool for many applications that do not require full biocompatibility and allow for the removal of trace amounts of copper ions. However, for applications in which copper cannot be fully eliminated from the product, it is not a suitable crosslinking chemistry. This has led to the development of copper free alternatives, such as the strain promoted azide-alkyne cycloaddition (SPAAC).

KREBS and co-workers discovered in 1961 that the cycloaddition between phenylazide and cyclooctyne proceeds with a very high reaction rate even at room temperature.[136] The enhanced reaction rates are due to ring-strain relief upon reaction of alkynes that are part of an eight-membered ring system with organic azides. The activation barrier for the reaction is significantly reduced, therefore the reaction proceeds very fast even without the addition of a catalyst. BERTOZZI and co-worker screened different cyclooctyne derivatives, used in SPAAC chemistry, regarding their reactivity.[137] The fast reaction rates even allowed for fluorescent labeling of cell membranes in vitro and in vivo.[138,139]

The broad application of SPAAC in biomedical applications, however, is limited by long and low yielding routes for the preparation of the cyclooctyne derivatives. The synthesis of DIFO, a fluorinated cyclooctyne derivative, for example, requires eight consecutive steps.[133] Other more elaborate derivatives, such as bicyclo[6.1.0]non-4-yne (BCN) still require at least four steps to obtain a precursor for polymer conjugation.[140] Cross-reactivity of these strained cyclooctynes with free thiols has been observed,[141] thus limiting bioorthogonality of this reaction due to the presence of free thiols in many proteins and on cellular surfaces.[142] However, the reaction between organic azides and strained cyclooctynes

is considerably faster than the side reaction of free thiols with cyclooctynes, thus allowing the encapsulation of cells without many problems.[143,144] As of today, upscaling is still very limited and thus hinders the application of SPAAC for problems where a large amount of material is needed.

In terms of scalability Thio-Michael addition reactions outperform SPAAC. The synthetic precursors are readily accessible or inexpensive. Hereby, a nucleophilic free thiol is connected to a Michael-acceptor, e.g. acrylates, vinylsulfone, and maleimide. All of these groups can be introduced to a polymer backbone in a straightforward fashion. The reaction can be conducted in water, under mild conditions, such as room temperature and under physiological pH values, which makes it well optimal for gelation reactions for protein and cell encapsulation. However, the main drawback is the cross-reactivity of free thiols with maleimides and acrylates that are present in some proteins and on cell surfaces.[142,145] Therefore, the reaction is not considered as bioorthogonal. However, for applications, where cross-reactivity can be prevented or is negligible, this crosslinking chemistry is very useful and easily scalable.

1.6.1 Inverse Electron Demand Diels-Alder

The fastest- and in terms of biorthogonality, most promising click-reaction to this day, is the inverse electron demand Diels-Alder (iEDDA). This reaction is based on the combination of tetrazines and electron rich or strained dienophiles. It was first reported by CARBONI and LINDSEY who observed a very fast reaction between tetrazines and unsaturated compounds under mild conditions.[146] A general proposed mechanism is described in **Scheme 4**.

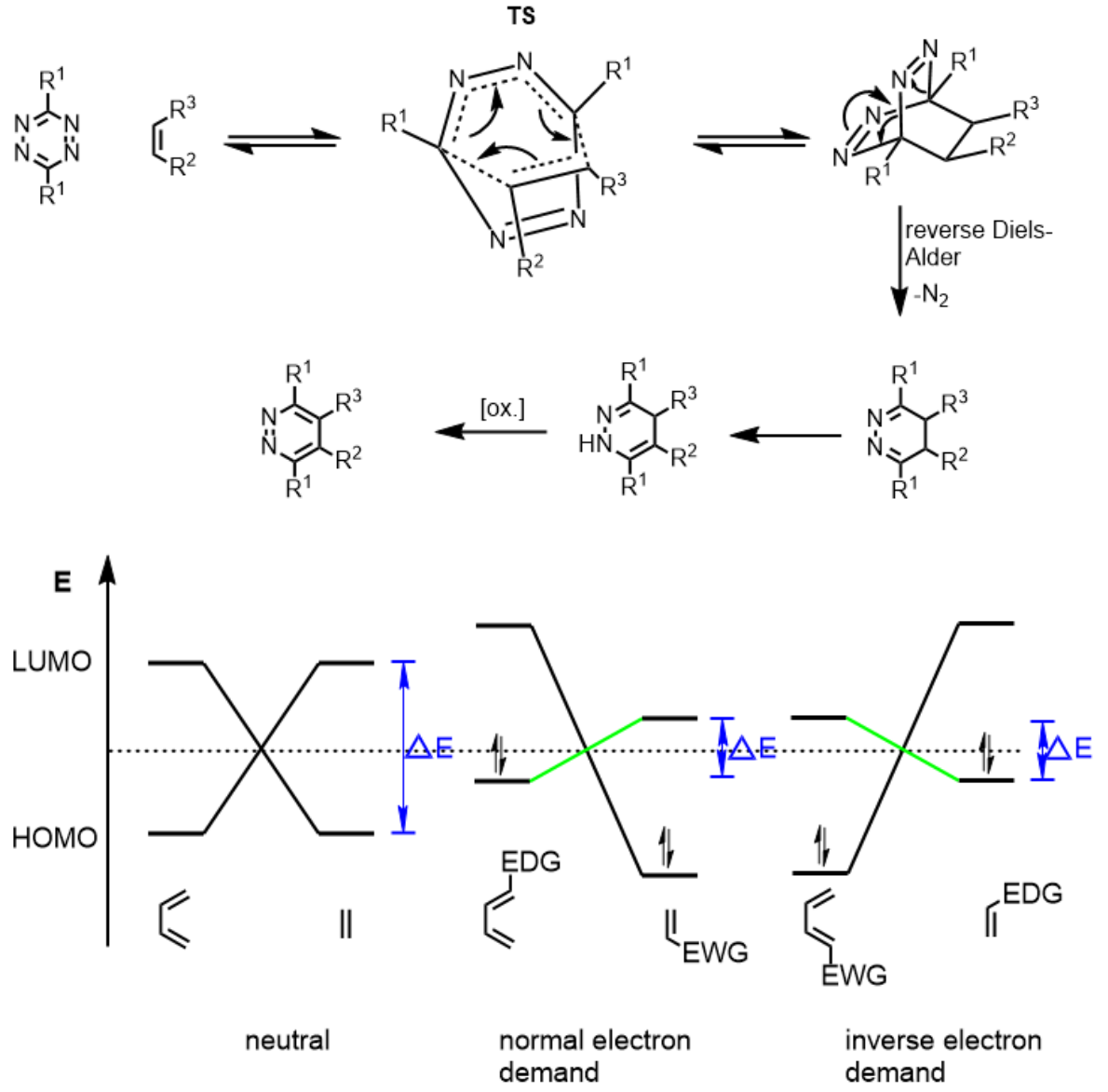

Scheme 4. Proposed mechanism of the reaction between a tetrazine and a dienophile. Energy diagram for the LUMO and HOMO of a neutral, normal electron demand, and inverse electron demand Diels-Alder reaction is shown, EDG = electron donating group, EWG = electron withdrawing group.

The reaction starts with the [4+2] Diels-Alder cycloaddition between tetrazine and a corresponding dienophile to form the bicyclic adduct with two nitrogen bridges. This expels nitrogen in an immediately occurring reverse Diels-Alder reaction.[126,147–149] The removal of nitrogen in this case is irreversible. SAUER and co-workers studied the reactivity of a large variety of different tetrazines and electron rich and poor dienophiles.[150] Reaction rates span about nine orders of magnitude, which mostly depends on the dienophile that is used. Internal olefins react only slowly with tetrazines, which is an advantage, preventing the side reaction with cis-alkenes of the lipid components of cell membranes.[150] DARKO et al. reported on the

fastest rate constant so far of about 3300000 $M^{-1}s^{-1}$ for a conformationally strained trans-cyclooctene.[151]Cis-cyclooctene, however, was reported to react much slower in a comparable setting, with a rate constant of 0.03 $M^{-1}s^{-1}$. Due to fact, that the alkenes of the cell membranes are not presented on the outside of the cells, side reactions are further suppressed. IEDDA has been used as a bioorthogonal linking strategy for fluorescent labeling of antibodies,[152] DNA-tagging,[153] and cell labeling.[154] Due to the fast reaction rates iEDDA is considered more bioorthogonal than SPAAC, as possible side reactions with biological systems are slower.[99] There is a big variety of synthetically accessible tetrazine[155] derivatives and dienophiles. They offer different reactivities and synthetic accessibility, as well as stability in water.[155] Depending on the application, and the reaction rates needed, suitable combinations of tetrazine and dienophile can be chosen. Due to the easy accessibility of the precursors, this method can be used for the upscaling of applications such as the formation of nanogels for the encapsulation of therapeutic proteins.

As argued in the sections of this introduction, the design of nanocarriers and their properties remains challenging. The choice and combination of scaffold materials, as well as production method and linking chemistry plays a critical role for the viability and applicability of nanocarriers. For the encapsulation of therapeutic proteins, the use of the mild and surfactant-free inverse nanoprecipitation, together with the fast, scalable, and bioorthogonal iEDDA crosslinking chemistry would provide optimal conditions and properties. Therefore, in this thesis, the design, synthesis, and properties of a hydrophilic, pH-degradable nanogel, based on the biocompatible and functionalizable dPG, that fulfils most of the desired criteria described by the LADMET concept, was studied.

2. Scientific Goals

Biotherapeutics, such as antibodies and therapeutic proteins gain ever more importance in modern medicine. The specificity of these protein drugs is superior to small molecules, which means less side effects and an improved treatment effect. However, most proteins cannot be orally administered, as the very low pH-value in the stomach denatures their structure. Furthermore, uptake in the small intestine is also not efficient for most of the biotherapeutics. If systemic treatment is needed, in most cases, the intravenous administration route is the only option to deliver protein drugs to the body. Yet, within the blood stream, proteins are especially sensitive to the body´s detoxification mechanisms. Small proteins with molecular weights below the renal excretion limit of around 45 kDa are easily eliminated from the body in a short period of time. Furthermore, blood proteins can bind to administered biotherapeutics and thus mark them for elimination by mononuclear phagocyte system (MPS), which is a part of the innate immune system.

The gold standard to counteract the aforementioned problems is the covalent modification of the proteins with biocompatible polyethylene glycol (PEG). This PEGylation leads to increased molecular weights and thus, longer circulation times, as well as somewhat reduced blood protein binding and reduced MPS clearance. However, PEG modification can lead to a reduced activity of the proteins and has recently been found to induce an immune response in some patients.

Alternative approaches are thus needed which also improve blood circulation times, and immune evasion, while not reducing the activity of the protein or provoke an immune response. A promising alternative for the covalent modification with PEG is the physical encapsulation within hydrophilic nanogels. These water-swollen polymer networks (10 -1000 nm) provide room for proteins and keep them physically intact and shielded from blood proteins or antibodies. The total loaded nanogel is well above the renal excretion limit and thus provide prolonged circulation times. Nanogels can be produced in a size range that provide enhanced uptake into tumorous tissue through the enhanced permeation and retention (EPR) effect. Through the incorporation of environmentally responsive groups, the gels can be designed as smart carriers that degrade upon stimuli such as acidic- or reductive environments. This can be used as a way of triggered protein release at the site of action.

As a preparation method that provides mild and surfactant free conditions, the inverse nanoprecipitation in acetone has shown promising features. These mild conditions help to

prevent loss of protein function and assure high encapsulation efficiencies due to the in-situ encapsulation during gel formation.

As a crosslinking chemistry, inverse-electron demand Diels-Alder (iEDDA) based on tetrazines and dienophiles, shows the most promising kinetics, biocompatibility, accessibility of the precursors, as well as biorthogonality compared to other click type reactions such as strain promoted azide alkyne cycloaddition reactions (SPAAC).

Thus, the aim of this work is to design a macromonomer platform based on the polymer dendritic polyglycerol (dPG) which is easily functionalizable, biocompatible, and highly hydrophilic. This polymer shall be functionalized with a selection of different dienophiles and tetrazine, in order to obtain for the first time a library of substances, which is easily accessible and/or reactive during an inverse nanoprecipitation to form nanogels. The macromonomers will be studied regarding their properties in context of nano gelation, including gelation times, aggregation, and stability in aqueous solution. Influencing parameters, such as solvent to non-solvent ratio, quenching times, and macromonomer concentration will be screened to find optimal conditions for nanogel formation in the desired size range of 20 to 200 nm. The most promising candidates in terms of reactivity, stability in aqueous solution, and accessibility will then be used for the co-precipitation of a model protein, such as myoglobin.

Based on the screening results, environmentally degradable dPG-macromonomers will be designed. pH-degradability of the nanogels should be achieved by the incorporation of acetal linking groups in-between the polymer and the reactive dienophile functional groups. Different acetal linkers will be used to obtain nanogels that can be cleaved at different pH-values. The most promising dienophile from the screening will be used as the dienophile and compared to the commercially available bicyclo[6.1.0]non-4-yne (BCN). The obtained macromonomers will be tested regarding their cytocompatibility and then used in the preparation of pH-degradable nanogels using inverse nanoprecipitation. Degradability of the gels will be tested by subjection to different pH values. The therapeutic protein Asparaginase will be co-precipitated to observe the ability of the gels to encapsulate other functional proteins.

3. Publications

3.1 Systematic Screening of Different Polyglycerin-Based Dienophile Macromonomers for Efficient Nanogel Formation through IEDDA Inverse Nanoprecipitation

Alexander Oehrl, Sebastian Schötz, Rainer Haag, *Macromol Rapid Commun*, accepted. DOI: 10.1002/marc.201900510

Abstract

Alternatives for strain-promoted azide–alkyne cycloaddition (SPAAC) chemistries are needed because of the employment of expensive and not easily scalable precursors such as bicyclo[6.1.0]non-4-yne (BCN). Inverse electron demand Diels Alder (iEDDA)-based click chemistries, using dienophiles and tetrazines, offer a more bioorthogonal and faster toolbox especially in the biomedical field. Here, the straightforward synthesis of dPG-dienophiles and dPG-methyl tetrazine (dPG-metTet) as macromonomers for a fast, stable, and scalable nanogel formation by inverse nanoprecipitation is reported. Nanogel size influencing parameters are screened such as macromonomer concentration and water to acetone ratio are screened. dPG-norbonene and dPG-cyclopropene show fast and stable nanogel formation in the size range of 40–200 nm and are thus used for the coprecipitation of the model protein myoglobin. High encapsulation efficiencies of more than 70% at a 5 wt% feed ratio are obtained in both cases, showing the suitability of the mild gelation chemistry for the encapsulation of small proteins.

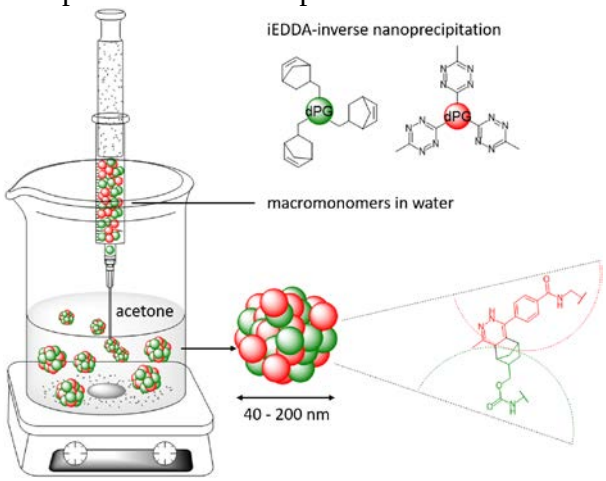

Contributions: Study design, synthesis of precursors and parts of macromonomers, synthesis and characterization of nanogels, protein determination assay, manuscript preparation, manuscript revision.

Macromolecular Rapid Communications
www.mrc-journal.de

Systematic Screening of Different Polyglycerin-Based Dienophile Macromonomers for Efficient Nanogel Formation through IEDDA Inverse Nanoprecipitation

Alexander Oehrl, Sebastian Schötz, and Rainer Haag*

Alternatives for strain-promoted azide–alkyne cycloaddition (SPAAC) chemistries are needed because of the employment of expensive and not easily scalable precursors such as bicyclo[6.1.0]non-4-yne (BCN). Inverse electron demand Diels Alder (iEDDA)-based click chemistries, using dienophiles and tetrazines, offer a more bioorthogonal and faster toolbox especially in the biomedical field. Here, the straightforward synthesis of dPG-dienophiles and dPG-methyl tetrazine (dPG-metTet) as macromonomers for a fast, stable, and scalable nanogel formation by inverse nanoprecipitation is reported. Nanogel size influencing parameters are screened such as macromonomer concentration and water to acetone ratio are screened. dPG-norbonene and dPG-cyclopropene show fast and stable nanogel formation in the size range of 40–200 nm and are thus used for the coprecipitation of the model protein myoglobin. High encapsulation efficiencies of more than 70% at a 5 wt% feed ratio are obtained in both cases, showing the suitability of the mild gelation chemistry for the encapsulation of small proteins.

Therapeutic protein drugs are on the rise in the treatment of various diseases, due to their increased specificity compared to small molecules. However, they suffer the drawback of increased immune recognition and undergo renal clearance if their size is below the renal threshold of 45 kDa or a hydrodynamic diameter of about 5.5 nm.[1,2] In order to prevent the rapid clearance, the proteins are usually PEGylated to increase their total molecular weight and reduce immune recognition.[3–6] However, PEG seems to be able to induce an immune response, as well as hypersensitivity reactions in some patients.[6]

Moreover, to prevent the immune recognition, therapeutic proteins can be masked by non-covalent encapsulation in nanocarriers such as nanogels.[7–10]

These nanogels are commonly highly water-swollen polymer networks in the size range of 10–1000 nm that offer a stealth effect to any protein cargo inside, due to their hydrophilic nature and small and unspecific interactions with blood proteins.[10–14] The size of a nanogel is typically above the renal threshold, yielding increased circulation times for the encapsulated proteins. Furthermore, nanogels only physically entrap the protein instead of forming covalent bonds such as in the case of PEGylation, preventing any detrimental influence of covalent modifications.[3,6]

A variety of different methods are available for the preparation of nanogels. The most common preparation methods are the mini- and microemulsion polymerizations of monomers or macromonomers.[15–23] These methods utilize droplets of reactive monomers in the desired size range which are obtained by high energy input from ultrasonication in miniemulsion and large surfactant amounts in microemulsions. Subsequent crosslinking of the monomers in those templated droplets led to a dispersion of polymer beads in the nanometer to micrometer range. However, the use of ultrasonication and surfactants has the downside of not providing mild conditions for the in situ encapsulation of proteins and poses problems with purification.[23–25]

A very useful method for the preparation of hydrophobic nanoparticles is the nanoprecipitation method, which is based on the insolubility of certain growing polymers in a corresponding non-solvent.[26] For example, polystyrene (PS),[27] polylactic acid, and copolymers of polylactic and glycolic acid (PLA/PLA-co-PGA)[26,28] nanoparticles have been prepared in such a fashion. These polymers can be used for the encapsulation of hydrophobic drugs. Our group reported the use of an inverse nanoprecipitation method with hydrophilic macromonomers based on dendritic polyglycerol (dPG).[7] Due to the reversal of polarity in this method, a surfactant-free, mild, and easy to purify way of producing nanogels is offered. Proteins were encapsulated with high efficiency and retained their functionality upon release.

During inverse nanoprecipitation, the macromonomers form nanoaggregates due to the diffusion of the solvent into the non-solvent. These aggregates then must be crosslinked in order to obtain a stable polymer network that does not break up upon dilution with water. The type of crosslinking chemistry has thus a very big impact on the gel formation process. Click-type reactions are especially suitable for this application. They are fast and usually proceed in a quantitative fashion.[29]

A. Oehrl, S. Schötz, Prof. R. Haag
Institute for Chemistry and Biochemistry
Department of Biology, Chemistry, and Pharmacy
Freie Universität Berlin
Takustr 3 D-14195, Berlin, Germany
E-mail: haag@chemie.fu-berlin.de

The ORCID identification number(s) for the author(s) of this article can be found under https://doi.org/10.1002/marc.201900510.

DOI: 10.1002/marc.201900510

Copper-catalyzed Huisgen 2 + 3 cycloaddition, for example, is based on the reaction of organic azides with terminal organic alkynes and has been used for the preparation of nanoparticles and nanogels.[29] The reactive groups are easily obtained, although the need of copper as a catalyst is a major drawback. Copper ions are usually hard to remove and can bind to some proteins and therefore subject cells to oxidative stress due to the production of reactive oxygen species, diminishing the biocompatibility of nanogels produced in such a manner.[30] Copper-free alternatives exist, where the terminal alkyne is replaced by a strained version, usually embedded in an eight-membered ring system.[31] These highly strained systems allow for the complete elimination of copper, because the ring-strain release upon reaction with the azide provides the driving force for the coupling reaction. Yet, some major drawbacks of these strain-promoted azide–alkyne cycloaddition (SPAAC) reactions are the high price for the precursor molecules, as well as the tedious and low-yielding synthetic protocols, especially for BCN.

Another common crosslinking method, the thiol-ene reaction, is based on free thiols reacting with olefin derivatives. This method has the advantage of easily accessible macromonomers, which makes the process scalable and comparatively inexpensive. However, it is incompatible with proteins that contain free thiols.[32]

We have previously reported on nanogels, which are based on a hydrophilic, biocompatible, and easy to functionalize dPG-backbone.[33,34] A lot of the aforementioned different linking strategies have been used, such as CuAAC,[7] thiol-ene,[35,36] and the SPAAC reaction.[37]

Due to the drawbacks of some of these methods, the need for newer generations of click reactions arose. One of the most recent advances in "click chemistry" was the development of inverse electron demand Diels-Alder (iEDDA) reactions based on tetrazine derivatives and different dienophiles.[38–41] Depending on the dienophiles and tetrazines used, the reaction kinetics can be orders of magnitude faster than the corresponding SPAAC alternatives.[41]

IEDDA has been used as a bioorthogonal linking strategy for fluorescent labeling of antibodies,[42] DNA-tagging,[43] and even cell labeling.[44] Due to the fast reaction rates, iEDDA is considered more bioorthogonal than SPAAC, as any possible side reactions with biological systems are much slower.[45] There is a big variety of synthetically accessible tetrazine[46] derivatives and dienophiles. They all offer different reactivities and synthetic accessibility as well as stability in aqueous solutions.[46] Depending on the application, one can choose the most suitable combination of tetrazine and dienophile.

We hypothesize that these characteristics of iEDDA reactions are thus optimal for the substitution of SPAAC in the formation of nanogels by inverse nanoprecipitation.

We present the synthesis of new dPG-based macromonomers functionalized with methyl-tetrazine and different dienophiles such as the well-known norbonene, methyl-cyclopropene, and dihydropyran (DHP). The macromonomers are characterized by NMR and DLS and tested regarding their ability to form macrogels, as well as stable nanogels during inverse nanoprecipitation in acetone. The most promising macromonomers dPG-norbonene and dPG-cyclopropene are used for the in situ coprecipitation of the small protein myoglobin (17 kDa) and show very good encapsulation efficiencies up to 93%. The fast and efficient synthetic route to dPG-norbonene and dPG-metTet, as well as the stable and scalable nanogels that are obtained from them, while avoiding the drawbacks of other crosslinking strategies makes this a possible new platform for the bioorthogonal encapsulation of therapeutic proteins.

The success of a nanocarrier depends on its key physical properties, such as the nature of the material that it is made of (e.g., functional groups), hydrophilicity/hydrophobicity balance, and the size, as well as the synthetic accessibility of the respective crosslinkers. We chose, for the purpose of a high biocompatibility and ease of functionalization, the already well known dPG.[33,34,47,48] Due to its large amount of terminal hydroxyl groups, it is highly hydrophilic and easy to functionalize without losing its hydrophilicity upon a low degree of functionalization. The polymer itself can be synthesized in kilogram scale which makes it a very suitable candidate as a macromonomer for nanogel synthesis.

We chose the inverse nanoprecipitation method for the formation of the nanogel network as no surfactant is needed and thus a mild encapsulation of proteins becomes possible. In order to achieve a stable gel in a fast way, the iEDDA chemistry was chosen as a gel crosslinking strategy due to its biorthogonality and high reaction rates. However, the stability of the reactive groups to reaction conditions, as well as storage conditions is also very important for potential applications.

For our work, we therefore selected a water stable tetrazine derivative, which still has a moderate reactivity toward dienophiles and can be easily attached to the dPG-core. 4-(6-Methyl-1,2,4,5-tetrazin-3-yl)benzoic acid was thus chosen, which can be attached via simple amide bond formation to a dPG-amine core. As the counterpart, four different dienophiles were chosen, in order to compare their reactivity during gel formation and the stability of the final nanogels in terms of aggregation. As can be seen in **Scheme 1**, we obtained four different dPG-dienophiles with approximately the same degree of functionalization starting from a 6 kDa dPG core. The different dPG-macromonomers are depicted as the corresponding colored spheres.

The synthetic overview for the precursor molecules **(1–5)** can be found in Scheme S1, Supporting Information.

One great advantage of using iEDDA chemistry compared to strained alkyne–azide cycloaddition is the accessibility of the reactive tetrazines and dienophiles. The tetrazine precursor 4-(6-methyl-1,2,4,5-tetrazin-3-yl)benzoic acid was obtained according to a one-pot reaction reported in literature in a moderate yield of 40% but can be used for functionalization with any kind of amine and has a good stability in water and buffer.[46] The different dienophiles were synthesized as the reactive carbonate derivatives. In this form, they can be reacted with any kind of amine, yielding the corresponding carbamate-linked dienophiles. In contrast, the synthesis of BCN is quite lengthy, with five steps and an overall yield of only 27%. In the series of dienophiles reported here, BCN is known to be one of the most reactive dienophiles in tetrazine click-reactions.[49] The next one in line in terms of reactivity is the cyclopropene derivative, which we obtained in four steps with a low overall yield of 19%. We chose the structural motive of bicyclo[2.2.1]hept-5-ene-2-carbaldehyde as a precursor as it is commercially

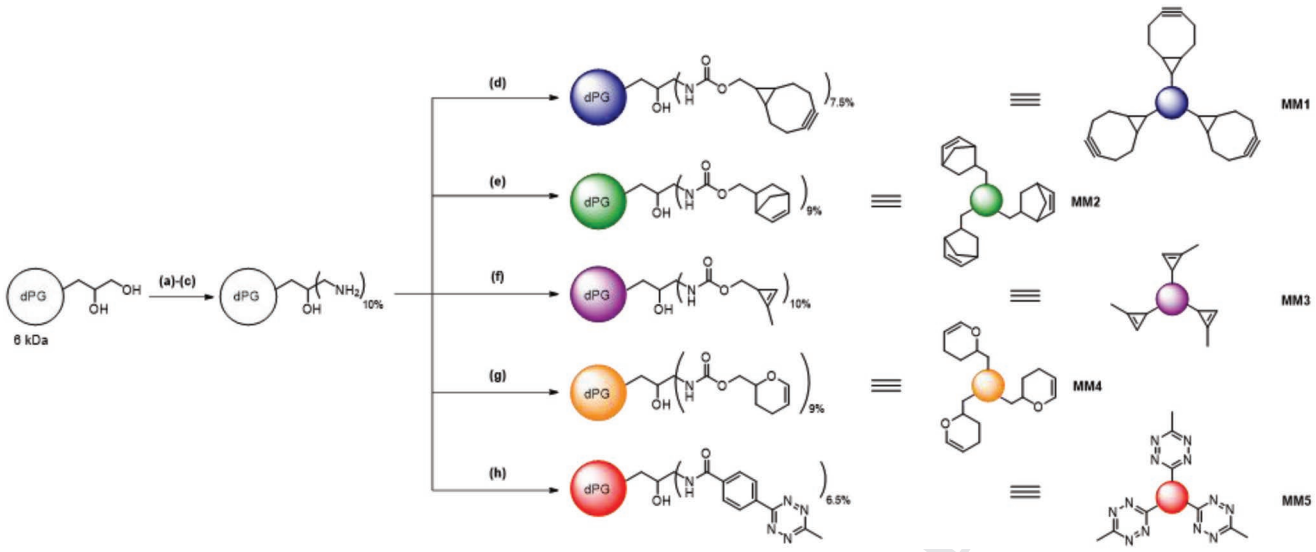

Scheme 1. Synthetic overview for the different macromonomers dPG-BCN, dPG-norbonene, dPG-cyclopropene, dPG-DHP, and dPG-metTet. The following conditions were used: a) MsCl, NEt_3, DMF, rt, overnight; b) NaN_3, 60 °C, 3 d; c) PPh_3, water/THF, rt, 3 d; d) 1, NEt_3, DMF, rt, overnight; e) 2, NEt_3, DMF, rt, overnight; f) 3, NEt_3, DMF, rt, overnight; g) 4, NEt_3, DMF, rt, overnight; and h) 5, HATU, DIPEA, DMF, rt, overnight. Number of reactive groups not representative; just for clearness.

available at a low price and was easily transformed in two steps with a good overall yield of 84% to the reactive carbonate form bicyclo[2.2.1]hept-5-en-2-ylmethyl (4-nitrophenyl) carbonate. Thus, norbonene was the most promising and well-known dienophile candidate in terms of potential upscaling and commercial use, even though it presents a relatively moderate reactivity.[50] The last dienophile we tested, was based on a common protecting group for alcohols. The (3,4-dihydro-2H-pyran-2-yl) methanol is commercially available for a relatively low price and is structurally related to 3,4-dihydropyrane (DHP). The commercial precursor was transformed to the activated DHP carbonate (3,4-dihydro-2H-pyran-2-yl)methyl (4-nitrophenyl) carbonate in one step, with a yield of 79%. This structural motif is known as a dienophile in literature; although, the reaction rates are considerably lower compared to the other structural motives used in this work.[51]

With the reactive dienophiles and tetrazine in hand, the functionalization of the polymer core, dPG-amine, was performed in a straightforward fashion using the same procedure for every dienophile (Scheme 1). This provided us with a toolbox of macromonomers for the formation of nanogels. The macromonomers were characterized by NMR, IR, and DLS, as can be seen in the Supporting Information.

In a first screening, we used the macromonomers in the formation of macroscopic hydrogels to determine the reactivity of each type of dienophile. This was investigated by measuring the time required for the gelation of a mixture of dPG-metTet with the respective dPG-dienophile. As can be seen in **Figure 1**, the dPG-cyclopropene was the macromonomer with the fastest gelation time. It was followed in reactivity by dPG-norbonene. dPG-BCN and dPG-DHP did not show any macrogel formation even after 30 min.

Only an increased viscosity was observed for dPG-BCN. As BCN was supposed to have the highest reaction rates, we expected it to have the fastest macrogel formation. We hypothesized that, due to the fast reaction, the dPG-BCN was quenched almost instantaneously before a network formation could happen. The lower reactivity of cyclopropene and norbonene led to diffusion of macromonomers within the network and thus to a stable gel formation. As expected, the cyclopropene derivative reacted faster than the norbonene derivative. However, both showed macrogel formation in a reliable manner. Only dPG-DHP was too unreactive and did not yield even an increased viscosity of the macromonomer mix.

Subsequently, we performed the synthesis of nanogels via inverse nanoprecipitation. The process works by fast injection of a dilute macromonomer solution into the corresponding non-solvent. In our case, the non-solvent for dPG-based

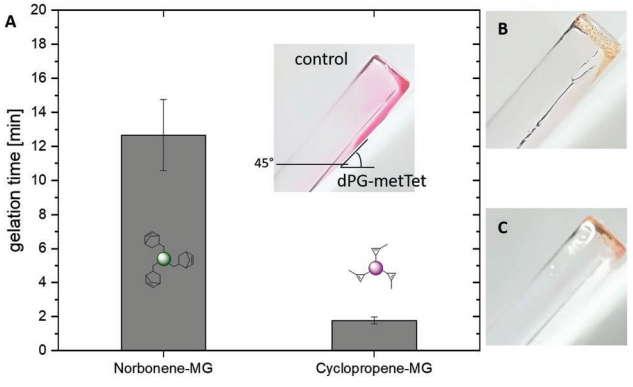

Figure 1. Macrogelation for the dPG-dienophiles MM2 and MM3, n = 3. A) Gelation times of MM2 and MM3 measured in triplicate. Control depicts the measurement setup with a small glass vial at an angle of 45° and MM5 without crosslinker. B) Macrogel of MM2 after 30 min. C) Macrogel of MM3 after 30 min.

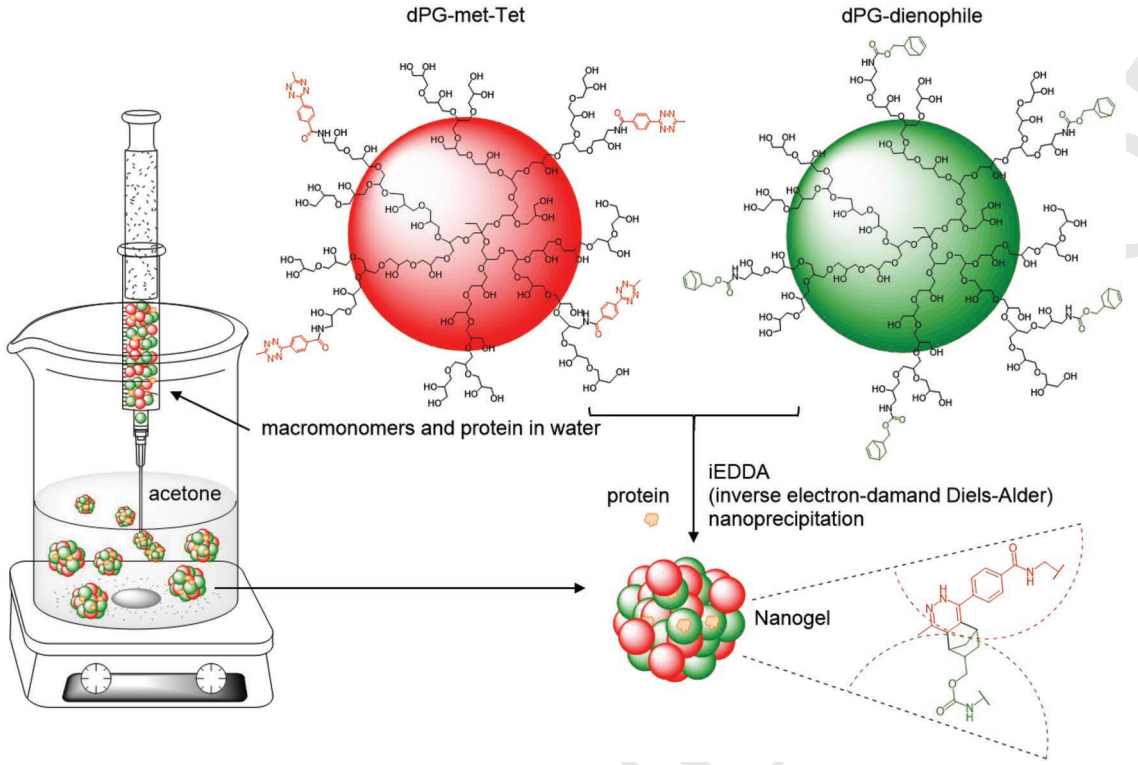

Scheme 2. Overview on nanogel formation by inverse nanoprecipitation in acetone with dPG-norbonene as an example. Linking points and structure of dPG-polymer core are shown. Possible encapsulation of myoglobin is shown.

polymers was acetone. The schematic overview on the inverse nanoprecipitation process can be seen in **Scheme 2**.

A lot of parameters can influence the outcome of the nanoprecipitation method such as macromonomer concentration, solvent/non-solvent ratio, stirring speed, temperature, macromonomer ratio, and reaction time. Usually, the size distribution and polydispersity are influenced by the parameters described above. For biomedical applications, nanogel sizes in the range of 20–200 nm are desirable.[52,53] We investigated most of these parameters for the most promising dienophile dPG-norbonene. The gels were produced by separately dissolving the respective macromonomers in water and then mixing dPG-dienophile with dPG-metTet, just prior to injection into acetone. Depending on the experiment, different amounts of the stock solutions were employed. The macromonomer solutions were cooled to 4 °C in order to prevent premature crosslinking.

First, the influence of the macromonomer concentration in water on the nanogel formation was studied. As can be seen in **Table 1**, the concentration was changed between 0.5 and 5 mg mL^{-1}.

The macromonomer concentration apparently did not have a relevant influence on the size or the polydispersity of the nanogels. However, for a concentration of 1 mg mL^{-1}, we observed a disturbed gel formation, that led to very large gels with a high polydispersity. As the macromonomer concentration in water directly correlates with the scalability of the process, we chose the highest concentration of 5 mg mL^{-1} for further studies.

In order to prevent subsequent crosslinking of already formed nanogels, an excess of one of the macromonomers was used. The ratio of reactive groups was set to 1:1.5. dPG-metTet exhibits a pink color, which can be used as an indicator of the status of the reaction. For this reason, dPG-metTet was used in shortfall to the other macromonomer to observe completion

Table 1. Concentration dependence of dPG-norbonene/dPG-metTet-NGs.

Entry	Macromonomer		V(H_2O): V(acetone)	$T_{q,\,chem}$ [min]	$T_{q,\,water}$ [min]	Z-average [nm]	PDI
	Ratio (A:B)	C [mg mL^{-1}]					
1	1:1.5	5	1:40	5	30	163 ± 13	0.02 ± 0.01
2	1:1.5	2.5	1:40	5	30	209 ± 21	0.03 ± 0.02
3	1:1.5	1	1:40	5	30	1528 ± 801	0.6 ± 0.1
4	1:1.5	0.5	1:40	5	30	190 ± 20	0.03 ± 0.02

A, dPG-metTet; B, dPG-norbonene; size values correspond to the mean of three individual gels.

Table 2. Dependance of water quenching time on dPG-norbonene/dPG-metTet-NGs.

Entry	Macromonomer		$T_{q,\ water}$ [min]	Z-average [nm]	PDI
	Ratio (A:B)	C [mg mL^{-1}]			
1	1:1.5	5	On	nd	nd
2	1:1.5	5	60	194 ± 6	0.07 ± 0.02
3	1:1.5	5	30	188 ± 9	0.07 ± 0.02
4	1:1.5	5	10	136 ± 5	0.07 ± 0.01
5	1:1.5	5	5	121 ± 4	0.06 ± 0.02
6	1:1.5	5	2.5	41 ± 4	0.40 ± 0.03
7	1:1.5	5	1	nd	nd

A, dPG-metTet; B, dPG-norbonene; nd, measurement quality criteria not achieved due to very high polydispersity; V(H_2O):V(acetone) = 1:40; $T_{q,\ chem}$ = 10 min; on = overnight.

of the reaction. Additionally, a chemical quencher (2-(vinyloxy)ethan-1-ol) was used in order to deactivate the remaining methyl-tetrazine groups. The influence of the time, after which the chemical quencher was added, on the nanogel formation is reported in Table S2 and Figure S2, Supporting Information.

No clear trend could be seen, as the size was in the same range for all different time points and the PDI stayed below 0.1. Apparently, the reaction rates were so fast for the crosslinking reaction that the chemical quencher did not have an influence on the nanogel formation, whatsoever. Aggregation of already formed nanogels was also not an issue, as even without the addition of a chemical quencher, the gels stayed stable and maintained their size (Table S2, Supporting Information, entry 1). In order to assure that no crosslinking would happen, we chose to add the chemical quencher anyway and used 10 min as the delay time for its addition.

Due to the stability of the system, which gave in most of the cases, reproducibly nanogels in the size range of 180–200 nm, we wanted to see if it is possible to influence the particle size while still maintaining a good PDI. As the crosslinking seemed to be almost complete after 10 min, we tried to physically quench the nanogel formation after defined time spans. Water was added to decrease the local macromonomer concentration and to break up any preformed aggregates that did not crosslink yet. As can be seen in **Table 2** and **Figure 2**, the nanogel size was not really affected after roughly 30 min. If the gels were not quenched at all, then complete precipitation occurred overnight (Table 2, entry 1). For quenching times of 60 and 30 min, there was no difference in nanogel size. However, quenching after 10 and 5 min showed a significant reduction in nanogel size while still maintaining a low PDI value of less than 0.1. Quenching at 1 and 2.5 min nanogel formation was severely hampered. Only small aggregates of around 40 nm were observed in DLS (vol%) for a reaction time of 2.5 min, whereas no reliable measurement could be obtained for a reaction time of 1 min. This trend of smaller particles after short reaction times can be explained with the dissolution of non-crosslinked aggregates. **Figure 3** shows the overall trend between water quenching time and nanogel size.

Due to the fast reaction rates the size distribution quickly reached saturation. Therefore, there is only a small time window to influence the size of the nanogels towards smaller values.

Another way to control the size of nanogels is to change the ratio of solvent to non-solvent. The right ratio depends on the actual solubility of the macromonomers in each solvent. For extremely high ratios of solvent to non-solvent, there will not be nanogel formation anymore as the macromonomers do not aggregate in very low amounts of the non-solvent. As the ratio decreases, the macromonomers can aggregate due to their decreasing solubility in the mixture of solvent and non-solvent.

The effect of several ratios of solvent and non-solvent, ranging from 1:20 to 1:200, are reported in **Table 3**.

For low ratios such as 1:200 to 1:80, the nanogel formation was strongly disturbed, leading to precipitation. Meaningful size values could not be determined, because the measurement quality was not achieved in DLS. Ratios of 1:60 to 1:20, however, were suitable for nanogel formation, with higher ratios leading to smaller nanogels. The polydispersity of the gels was in all cases below 0.1, which suggested a stable gel formation for such high ratios of solvent to non-solvent. This was a very promising result, as the main drawback of the inverse nanoprecipitation method is that very high amounts of non-solvent are needed for the preparation of relatively small amounts of

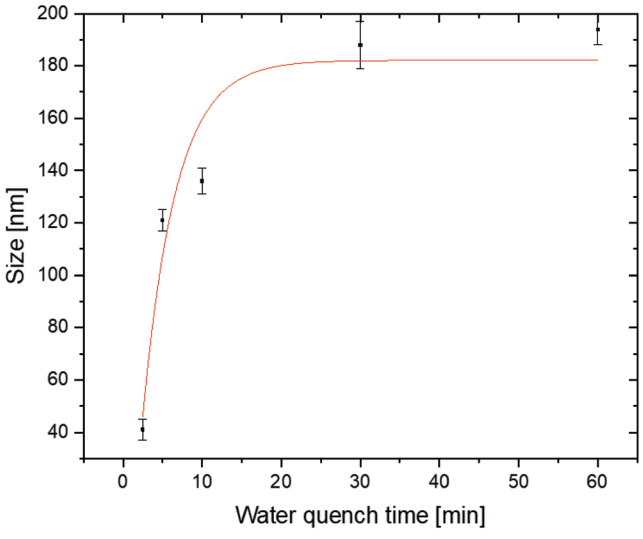

Figure 2. Dependency of nanogel size on water quenching time.

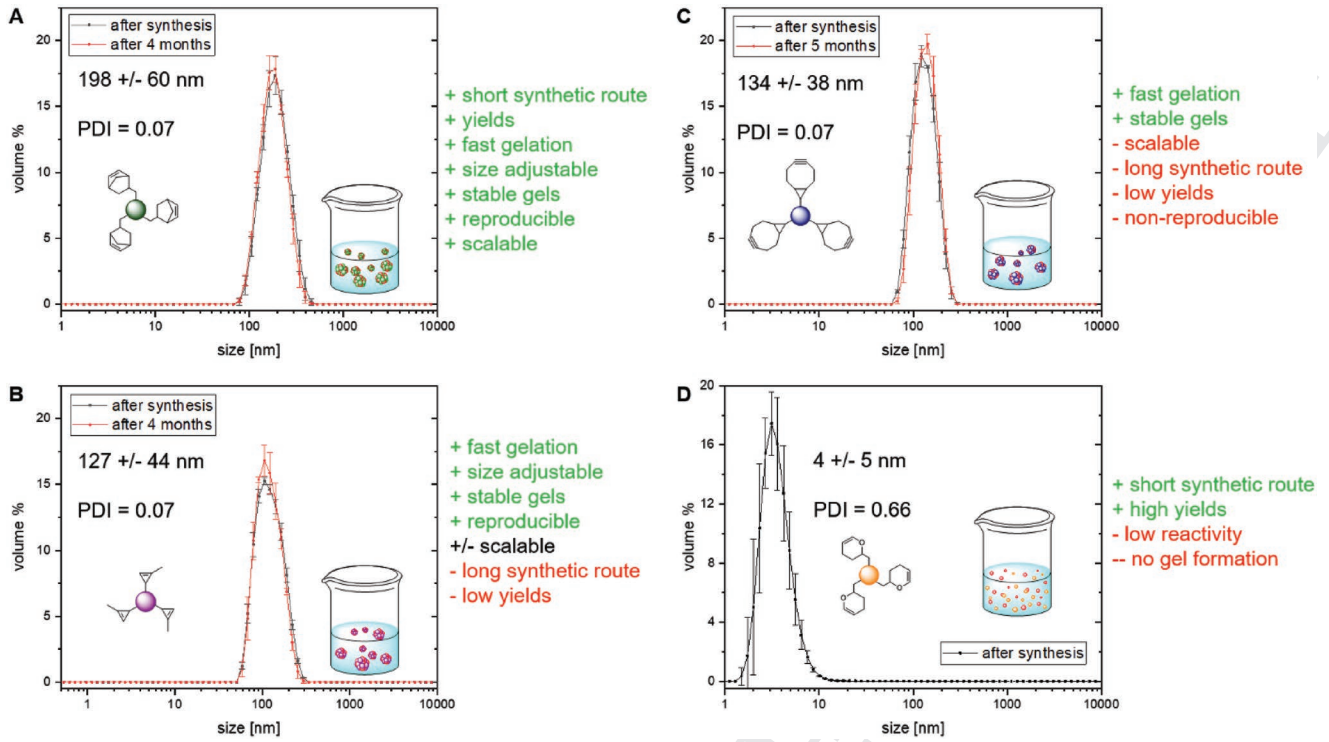

Figure 3. Overview on nanogel formation behavior, synthetic accessibility, and reactivity of the different macromonomers. DLS measurement of an exemplary gel is shown for each macromonomer, directly after synthesis and purification (black line) and after 4 to 5 months (red line). A) dPG-norbonene NG, B) dPG-cyclopropene NG, C) dPG-BCN NG, and D) dPG-DHP + dPG-metTet.

nanogels, usually a ratio of 1:200. Obtaining stable and almost monodisperse nanogels with a relatively high ratio of 1:20 means that the nanogel formation is scalable. For all batches, we used 5 mg of macromonomers, as higher amounts make it usually time consuming to remove acetone. To obtain relevant amounts of nanogels, we wanted to confirm if the production process is scalable to ten times the amount that is usually taken for a gel batch. **Table 4** shows the obtained nanogels for 50 mg batches.

Gels in the size range of 100–120 nm were obtained with PDI values below 0.1. The three gels were combined to yield a single dispersion of nanogel in water, with an average size distribution between the three gels and a PDI value of 0.1. This showed that several batches could be combined without a big increase in polydispersity. The scalability of a single batch and the possible combination of several batches into one batch thus holds the possibility to produce these nanogels in gram scale.

The stirring speed can also influence the nanogel formation. Table S3 and Figure S3, Supporting Information show the effect of different stirring speeds on the size and polydispersity of the nanogels. The stirring speed had no relevant influence on the size and PDI of the nanogels, although the same volume of non-solvent was used for each stirring speed. Thus, the highest stirring speeds were used for all the experiments.

The other combinations of macromonomers were then studied. Starting with the lowest reactivity, dPG-DHP was

Table 3. dPG-norbonene/dPG-metTet-NGs; water:acetone ratios.

Entry	Macromonomer		V(H_2O): V(acetone)	Z-average [nm]	PDI
	Ratio (A:B)	C [mg mL^{-1}]			
1	1:1.5	5	1:200	nd	nd
2	1:1.5	5	1:150	nd	nd
3	1:1.5	5	1:100	nd	nd
4	1:1.5	5	1:80	nd	nd
5	1:1.5	5	1:60	233 ± 10	0.06 ± 0.01
6	1:1.5	5	1:40	165 ± 7	0.06 ± 0.01
7	1:1.5	5	1:20	110 ± 4	0.09 ± 0.01

A, dPG-metTet; B, dPG-norbonene; nd, measurement quality criteria not achieved due to very high polydispersity; $T_{q,\,chem}$ = 10 min and $T_{q,\,water}$ = 30 min.

Table 4. Nanogel formation of dPG-norbonene/dPG-metTet (50 mg batch size).

Entry	Macromonomer		Z-average [nm]	PDI
	Ratio (A:B)	C [mg mL^{-1}]		
1	1:1.5	5	122 ± 1	0.07 ± 0.01
2	1:1.5	5	129 ± 2	0.07 ± 0.01
3	1:1.5	5	104 ± 2	0.07 ± 0.01
Avg.	1:1.5	5	118 ± 11	0.07 ± 0.01

A, dPG-metTet; B, dPG-norbonene; V(H_2O):V(acetone) = 1:40; $T_{q,\,chem}$ = 5 min; and $T_{q,\,water}$ = 30 min.

tested regarding its ability to form nanogels. As already shown, the macrogel experiments did not yield any gel after extended periods of time for dPG-DHP. Even after a reaction time of 18 h, only the non-crosslinked macromonomers could be seen by DLS (Figure 3). This showed that the reactivity of the DHP moiety was far too low for a nanogel formation. Thus, we decided to not investigate the dPG-DHP macromonomer further as useful time spans for gel formation could not be achieved.

dPG-BCN showed a delayed and incomplete gelation during macrogel formation. As can be seen in Tables S4 and S5, Supporting Information, the optimal conditions for nanogel formation, which were observed for dPG-norbonene, were also tested for dPG-BCN. The nanogel formation leads almost in all cases to big aggregates with high polydispersities, which are also not dependent on the preparation conditions. No reproducibility could be observed under the tested conditions, as size values scattered from 100 to 2000 nm, with PDI values between 0.2 and 0.8. We assumed that the high reactivity of BCN led to premature crosslinking and further crosslinking of the nanoaggregates that formed during the inverse nanoprecipitation. This resulted in a very fast growth of bigger and bigger aggregates. This might explain the big and polydisperse gels we observed with this macromonomer.

The last macromonomer that was tested was dPG-cyclopropene. The cyclopropene moiety is rather small compared to the alternatives presented in this work and in literature. In general, it does not have as big of an influence on hydrophilicity as dienophiles, such as BCN. Moreover, the reactivity toward tetrazine derivatives is also reported to be moderately high.[54] However, the synthesis reported in literature is quite lengthy. Hence, it could be an alternative to norbonene, in cases where very small and less hydrophobic crosslinkers are needed, despite the drawback of low scalability. As for the other macromonomers, different conditions were tested, which are summarized in Table S6, Supporting Information. dPG-cyclopropene, as well as dPG-norbonene, showed stable nanogel formation in the size range of 70–120 nm. This macromonomer also yielded nanogels with very low polydispersity indices of below 0.1.

Zeta potential measurements (Figure S4, Supporting Information) showed that all gels had a close to neutral surface charge. dPG-norbonene and dPG-cyclopropene nanogels were slightly positively charged and dPG-BCN nanogels slightly negatively charged.

A summary of the nanogel formation process for the different macromonomers is described in Figure 3 and the corresponding NTA measurements can be found in Figure S5, Supporting Information.

Of all the dienophiles, dPG-norbonene and dPG-cyclopropene showed reliably nanogel formation in the biologically relevant size range of below 100–200 nm. The most influencing parameters on nanogel size and polydispersity were water to acetone ratio and the water quenching time $T_{q,water}$. dPG-norbonene, however, is by far the most promising candidate for the easy upscaling and robust application, due to the straightforward synthesis of the precursors and the stable and monodisperse nanogels which can be obtained.

Due to their stable and reproducible nanogel formation, dPG-norbonene and dPG-cyclopropene were used in coprecipitation experiments with the protein myoglobin. During the mild coprecipitation, the protein was first physically encapsulated by the formation of nanoaggregates in the acetone phase. This polyglycerol shell around the protein protects it from the organic solvent and provides, due to the many hydroxyl groups, an almost natural environment to it. As the aggregates of polyglycerol macromonomers start to crosslink, the protein stays physically entrapped in the growing polymer network and diffusion gets ever more hindered. Due to the very mild reaction conditions of iEDDA and the absence of surfactants, high temperature and radicals, the sensitive protein cargo is very likely to be intact after nanogel formation.

Myoglobin, a small 17 kDa protein which is mostly responsible for oxygen transport within muscle tissue, was used as an inexpensive and abundant model protein for coprecipitation. We tested two different myoglobin feed ratios, a higher 5 wt% and lower 2.5 wt% of myoglobin compared to macromonomer. Tables S7 and S8, Supporting Information summarize the conditions we used and the nanogel sizes and polydispersity values that were obtained for dPG-norbonene and dPG-cyclopropene macromonomers, respectively.

The addition of a protein to the system changes the aggregation behavior during inverse nanoprecipitation significantly. The sizes of the nanogels at least doubled compared to the same conditions without protein (**Figure 4**A). However, the polydispersity indices of the formed nanogels, stayed low (below 0.1).

The determination of protein concentration within the gels was performed by a bicinchoninic acid (BCA) assay using bovine serum albumin (BSA) and myoglobin standard curves (Figures S6 and S7, Supporting Information). The total amount of protein was determined by multiplying the concentration of protein, determined in the BCA assay, by the total volume

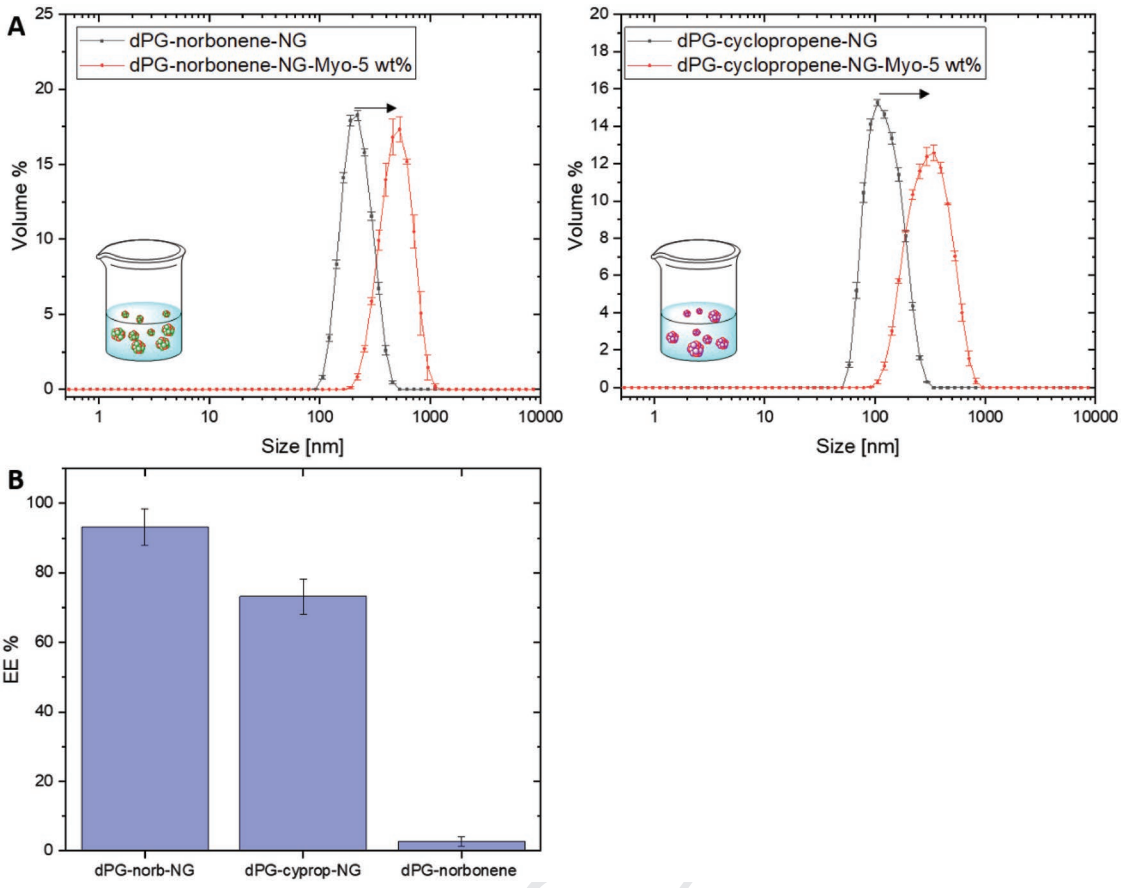

Figure 4. Influence of coprecipitation of myoglobin on nanogel size for dPG-norbonene and dPG-cyclopropene nanogels at 5 wt% myoglobin feed. A) left: DLS data for a dPG-norbonene-NG without (black line) and with (red line) encapsulated myoglobin; right: DLS data for dPG-cyclopropene-NG without (black line) and with (red line) encapsulated myoglobin. B) Encapsulation efficiency at 5 wt% feed of myoglobin in dPG-norbonene and dPG-cyclopropene nanogels. dPG-norbonene without dPG-tetrazine was used as a control, $n = 3$.

of the individual gel dispersions and then divided by the feed amount of protein. The results can be seen in Figure 4.

Both dPG-norbonene as well as dPG-cyclopropene nanogels could encapsulate myoglobin with a very high encapsulation efficiency of 75–93% at 5 wt% feed. The control shows only dPG-norbonene without dPG-metTet as crosslinker. The control sample was treated in the same way as the other samples, however, as no crosslinker was present, no gel formation was expected. Thus, no protein should have been present after centrifugal filtration. As confirmation, almost no protein was observed in the control experiments.

The results clearly showed, that the nanogels, which were formed through iEDDA click chemistry, especially the dPG-norbonene-based NGs, could efficiently encapsulate myoglobin.

We have shown the synthesis of different amine-reactive dienophiles as a toolbox for the functionalization of dPG-amine. The activated carbonates of norbonene, BCN, cyclopropene, and DHP were synthesized. The corresponding carbamate-linked dPG-dienophiles were obtained by a standardized procedure. The macromonomers dPG-norbonene and dPG-cyclopropene showed a fast macrogel formation within 12 min and nanogels in the size range of 40–200 nm were obtained with excellent polydispersity indices of 0.1 and below. dPG-norbonene-based nanogels were reproducibly synthesized under a wide range of conditions and showed batch scalability to at least 50 mg per batch. Combination of different batches yielded gels that retained the low polydispersity of the individual batches. dPG-BCN and dPG-DHP showed non-reproducible or no gel formation at all, respectively. In case of dPG-BCN, the reason was probably due to very high reaction rates and thus premature cross-linking and, in the case of dPG-DHP, a very low reactivity and hence, no crosslinking at all.

Coprecipitation of myoglobin (17 kDa) showed excellent encapsulation efficiencies of up to 93% for nanogels made from dPG-norbonene and dPG-cyclopropene, respectively.

All in all, dPG-norbonene is the most promising candidate for nanogel formation with dPG-metTet, within the series of dienophile macromonomers presented in this work, in terms of synthetic access to the precursors, scalability, and reproducibility of the system. Thus, the goal for future studies will be the preparation of responsive nanogels based on dPG-norbonene/dPG-metTet for the triggered degradation and release of therapeutic proteins.

Experimental Section

Materials: The solvents *n*-pentane, ethyl acetate, and diethyl ether were obtained from the technically pure solvents by distillation before use. DCM and acetone (HPLC grade) were used without further purification. Dry DCM and THF were taken from a SPS-800 type MBRAUN solvent drying system. Dry methanol and DMF were acquired from Acros and Fischer Chemical. All other chemicals and deuterated solvents were purchased from Sigma Aldrich, Merck, Acros, and Fisher Chemicals and were used as reagent grade without further purification. Qualitative thin layer chromatography (TLC) was performed on silica gel-coated aluminum plates serving as stationary phase (silica gel 60 F254 from Macherey-Nagel). The analytes were identified by irradiation of the TLC plates with UV light ($\lambda = 254$ nm) or by treatment with a potassium-permanganate-based staining reagent (100 mL deionized water, 200 mg potassium permanganate) or anis aldehyde-based (450 mL EtOH, 25.0 mL anis aldehyde, 25.0 mL conc. sulfuric acid, 8.0 mL acetic acid). Column chromatography was performed with silica gel of the company Macherey-Nagel (grain size 40–63 µm, 230–400 mesh) as stationary phase and the indicated eluent mixtures as mobile phase.

Analytical Methods: IR spectra were recorded on a JASCO FT/IR-4100 spectrometer. The characteristic absorption bands were given in wave numbers. ^{1}H NMR spectra were recorded at 300 K on Joel ECX 400 (400 MHz) and AVANCE III (700 MHz) instruments. Chemical shifts δ were indicated in parts per million (ppm) relative to tetramethyl silane (0 ppm) and calibrated as an internal standard to the signal of the incompletely deuterated solvent ($CDCl_3$: $\delta = 7.26$ ppm, MeOD: $\delta = 3.31$ ppm). Coupling constants J were given in Hertz. ^{13}C NMR spectra were recorded at 300 K on AVANCE III instruments (176 MHz). Chemical shifts δ were given in ppm relative to tetramethyl silane (0 ppm) and calibrated as an internal standard to the signal of the incompletely deuterated solvent ($CDCl_3$: $\delta = 77.16$ ppm, MeOD: $\delta = 49$ ppm). Coupling constants J were given in Hertz. The spectra were decoupled from proton broadband. DLS and Zeta potential were measured on a Malvern zeta-sizer nano ZS 90 with He–Ne laser ($\lambda = 532$ nm) at 173° backscatter and automated attenuation at 25 °C. Three measurements were performed per sample with between 10 and 16 individual measurements, yielding a mean size value plus standard deviation. Sample concentration was kept at 1 mg mL^{-1}. GPC was performed on an Agilent 1100 at 5 mg mL^{-1} using a pullulan standard, 0.1 M NaNO3 solution as eluent, and a PSS Suprema column 10 µm with a flow rate of 1 mL min^{-1}. Signals were detected with an RI detector.

Precursors and Macromonomers: All air- and moisture-sensitive reactions were carried out in flasks in an inert atmosphere (argon) using conventional Schlenk techniques. Reagents and solvents were added via argon rinsed disposable syringes. Solids were added in argon counterflow or in solution.

The synthesis of the literature known precursors is described in the Supporting Information, showing the modified procedures.

Bicyclo[2.2.1]hept-5-en-2-ylmethyl (4-nitrophenyl) Carbonate (1): In a dried 500 mL Schlenk flask, bicyclo[2.2.1]hept-5-en-2-ylmethanol (2.5 g, 20 mmol) and pyridine (4 mL, 50 mmol) were dissolved in dry DCM (235 mL) under an argon atmosphere and stirred for 5 min. Then, 4-nitrophenyl chloroformate (6 g, 30 mmol) was added and the reaction was stirred at room temperature for 90 min. After quenching with 200 mL of saturated ammonium chloride solution, the water phase was extracted three times with 100 mL DCM each. The organic phases were united and dried over sodium sulfate and the solvent was removed under reduced pressure. The raw product was purified with column chromatography using silica and pentane:EtOAc as solvent system (10:1; $R_f = 0.6$ in pentane:EtOAc 10:1). The product was obtained as a colorless solid and stored in the freezer (5.5 g, 87%). ^{1}H NMR (700 MHz, CD_3OD): δ 8.27 (m, 2 H, aryl), 7.43–7.34 (m, 2 H), 6.22–5.98 (m, 2 H, $R^1HC = CHR^2$), 4.36–3.86 (m, 2 H, RCH_2OCO_2R), 2.96–2.80 (m, 2 H, bridgehead-H), 2.57–2.46 (m, 1 H, $R^3R^4CHCH_2OR^5$), 1.94–0.58 (m, 4 H, bridge-H atoms + $R^6CH_2CR^7CH_2OR^5$). ^{13}C NMR (176 MHz, CD_3OD): δ 157.3, 154.1, 146.9, 139.0, 138.2, 137.3, 133.1, 126.3, 123.4, 74.4, 73.8, 50.5, 45.9, 45.2, 44.9, 43.6, 42.9, 39.4, 39.1, 30.4, 29.8.

General Procedure for dPG-Dienophiles: All dPG-dienophiles were synthesized according to the same general procedure. As an example, dPG–norbonene is described in detail.

dPG-Norbonene$_{9\%}$ (MM2): In a 50 mL Schlenk flask, dry DMF (15 mL) was added to a methanolic solution of dPG-amine (22.22 mL, 0.09 g mL^{-1}). Methanol was removed under reduced pressure, fresh dry DMF (15 mL) was added, the solution was constricted under reduced pressure to 25 mL and Et_3N (0.82 g, 8.11 mmol, 1.12 mL) was added. Bicyclo[2.2.1]hept-5-en-2-ylmethyl (4-nitrophenyl) carbonate (0.94 g, 2.97 mmol) (or other activated carbonate of dienophile) was dissolved in DMF (10 mL) and the solution was added dropwise via syringe to the dPG-amine solution. The resulting reaction mixture was stirred at room temperature overnight. The crude product was dialyzed against a mixture of water and acetone (1:1) for 3 days and methanol for 2 days (MWCO = 1 kDa). The product was obtained as a slightly yellow methanolic solution (9% functionalization, 83%). ^{1}H NMR (700 MHz, CD_3OD, δ): 6.25–6.21 (m, 1 H, H-olefin), 6.05–6.00 (m, 1 H, H-olefin), 3.98–3.48 (dPG-backbone), 2.98–2.92 (m, 1 H, H-bridgehead), 2.89–2.84 (m, 1 H, H-bridgehead), 2.49–2.42 (m, 1 H, H-bridgehead), 1.94–1.88 (m, 1 H, H-bridge), 1.51–1.47 (m, 1 H, H-bridge), 1.37–1.32 (m, 1 H, H-bridge), 0.64–0.59 (m, 1 H, H-ring). ^{13}C NMR (176 MHz, CD_3OD, δ): 159.3, 138.6, 138.0, 137.4, 133.3, 81.4, 79.9, 74.0, 72.6, 72.4, 72.24, 70.7, 69.4, 64.4, 62.8, 50.4, 49.9, 45.1, 44.9, 43.5, 42.8, 39.8, 39.5, 30.5, 29.9. IR (ATR): $\tilde{\nu}$ = 3364, 2910, 2871, 1697, 1540, 1418, 1457, 1418, 1327, 1254, 1107, 1076 cm^{-1}.

dPG-BCN$_{7.5\%}$ (MM1): dPG-BCN was synthesized according to a literature protocol. dPG-amine (22.22 mL, 0.09 g mL^{-1}); Et_3N (0.82 g, 8.11 mmol, 1.12 mL); BCN (0.94 g, 2.97 mmol). The product was obtained as a yellow methanolic solution (7.5% functionalization, 85%). ^{1}H NMR (700 MHz, CD_3OD, δ): 4.22–3.35 (dPG-backbone), 2.47–2.12 (m, 4 H, H-vinyl), 1.72–1.32 (m, 4 H, H-ring), 1.04–0.93 (m, 1 H, H-cyclopropane), 0.85–0.71 (m, 2 H, H-cyclopropane). ^{13}C NMR (176 MHz, CD_3OD, δ): 99.7, 81.5, 80.0, 74.0, 73.1, 72.6, 72.3, 72.3, 71.0, 70.7, 64.5, 64.4, 63.0, 34.5, 30.3, 25.1, 24.2, 22.1, 21.4. IR (ATR): $\tilde{\nu}$ = 3379, 2915, 2873, 1696, 1614 1517, 1457, 1394, 1304, 1244, 1078, 934 cm^{-1}.

dPG-Cyclopropene$_{8\%}$ (MM3): dPG-amine (5.55 mL, 0.09 g mL^{-1}); Et_3N (0.21 g, 2.03 mmol, 0.28 mL); (2-methylcycloprop-2-en-1-yl)methyl 2-(4-nitrophenyl)acetate (0.22 g, 0.88 mmol). The product was obtained as a colorless methanolic solution (8% functionalization, 85%). ^{1}H NMR (700 MHz, CD_3OD, δ): 6.76–6.69 (m, 1 H, H-olefin), 3.97–3.46 (m, dPG-backbone), 2.25–2.15 (m, 3 H, methyl), 1.73–1.63 (m, 1 H, H-ring). ^{13}C NMR (176 MHz, CD_3OD, δ): 122.2, 103.1, 81.5, 79.9, 74.0, 73.4, 72.5, 72.2, 70.9, 70.7, 64.5, 64.4, 62.8, 18.4, 11.8. IR (ATR): $\tilde{\nu}$ = 3374, 2912, 2876, 1697, 1541, 1457, 1325, 1259, 1110, 1080, 874, 848 cm^{-1}. EA ($C_{72}H_{136}N_2O_{43}$): calc. C (50.34%), found C (50.36%); calc. N (1.63%), found N (2.45%); calc. H (7.98%), found (7.96%).

dPG-DHP$_{9\%}$ (MM4): dPG-amine (5.55 mL, 0.09 g mL^{-1}); Et_3N (0.15 g, 1.52 mmol, 0.21 mL); (3,4-dihydro-2H-pyran-2-yl)methyl (4-nitrophenyl) carbonate (0.16 g, 0.56 mmol). The product was obtained as a colorless methanolic solution (9% functionalization, 82%). ^{1}H NMR (700 MHz, CD_3OD, δ): 6.41–6.34 (m, 1 H, $R^1HC = CHOR^2$), 4.78–4.72 (m, 1 H, $R^3OHC = CHR^1$), 4.22–4.13 (m, 2 H, $R^4OCHR^5R^6$), 4.07–3.44 (dPG-backbone), 2.19–1.96 (m, 2 H, H-ring), 1.96–1.67 (m, 2 H, H-ring). ^{13}C NMR (176 MHz, CD_3OD, δ): 101.8, 101.7, 81.7, 81.5, 79.9, 74.5, 74.0, 73.0, 72.5, 72.3, 71.0, 71.0, 70.7, 67.8, 64.5, 64.4, 62.7, 49.9, 25.3, 20.2. IR (ATR): $\tilde{\nu}$ = 3384, 2913, 2874, 1701, 1650, 1541, 1457, 1418, 1329, 1240, 1111, 1070 cm^{-1}. EA ($C_{726}H_{1366}N_{20}O_{435}$): calc. C (50.30%), found C (48.86%); calc. N (1.62%), found (2.18%); calc. H (7.94%), found H (8.47%).

dPG-metTet$_{6.5\%}$ (MM5): In a 250 mL Schlenk flask, dry DMF (50 mL) was added to a methanolic solution of dPG-amine (44.44 mL, 0.09 g mL^{-1}). Methanol was removed under reduced pressure, fresh dry DMF (50 mL) was added, and the solution was constricted under reduced pressure to 75 mL. The 4-(6-methyl-1,2,4,5-tetrazin-3-yl)benzoic acid (0.89 g, 4.05 mmol), EDC·HCl (1.04 g, 5.41 mmol), HOBT (0.73 g, 5.41 mmol), and DIPEA (1.05 g, 5.41 mmol, 1.38 mL) were dissolved in dry DMF (50 mL) and the solution was added dropwise via syringe to the

dPG-amine solution. The resulting reaction mixture was stirred at room temperature overnight. The crude product was dialyzed against DMF for 4 days and methanol for 4 days (MWCO = 1 kDa). The product was obtained as a red methanolic solution (6.5% functionalization, 85%). ^{1}H NMR (700 MHz, CD_3OD, δ): 8.69–8.53 (m, 2 H, H-aryl), 8.12–7.98 (m, 2 H, H-aryl), 4.05–3.48 (m, dPG-backbone), 3.10 (s, 3 H, methyl-H).^{13}C NMR (CD_3OD, 176 MHz, δ): 169.4, 169.2, 164.8, 139.1, 136.3, 129.4, 128.9, 81.7, 81.4, 80.2, 79.8, 74.0, 73.0, 72.5, 72.2, 71.0, 70.7, 70.3, 64.5, 64.4, 62.8. IR (ATR): $\tilde{\nu}$ = 3348, 2871, 1644, 1548, 1456, 1404, 1364, 1327, 1305, 1258, 1070, 931 cm^{-1}.

Macrogel Formation: The time required for the gelation of a mixture of dPG-metTet with the respective dPG-dienophile was measured. For each experiment, 50 µL of macromonomer solution was used (20 µL of dPG-metTet + 30 µL of dPG-dienophile) at a concentration of 200 mg mL^{-1}. The mixture was added to a small glass vial and after defined time spans, the vial was tilted at an angle of 45° to see if the mixture started to gelate. This was confirmed by the inability of the gels to flow down the glass vial. For samples that did not gelate even after 30 min, the time it took for the macromonomer mixture to flow from the top of the vial to the bottom of the vial was measured and compared to just dPG-metTet solution.

Nanogel Formation: General Procedure—The ratios of macromonomer A (dPG-metTet) to macromonomer B (dPG-dienophile) were set to 1:1.5. Acetone was utilized as the non-solvent. Parameters, such as solvent to non-solvent ratio (1:10–1:200), macromonomer concentration in water (0.5–7.5 mg mL^{-1}), stirring speed (300–1200 rpm), chemical quenching time $T_{q,chem}$ (0–∞ min), and water quenching time $T_{q,water}$ (0–120 min) were varied according to the tables described in the results and discussion section, as well as the Supporting Information. As an example, a general procedure for one set of parameters is described below.

Macromonomers A and B were stored as stock-solutions in water. An aliquot was taken and separately diluted with water to a final volume of 1 mL. For this, 15 µL of macromonomer A were diluted with 485 µL water and 22.5 µL of macromonomer B with 477.5 µL water. Both solutions were cooled in an ice bath to 4 °C. Macromonomer A solution was added fast to solution B and shortly vortexed for 5 s. Then, the mixed solution was added very fast via syringe to a glass vial containing magnetically stirred acetone (40 mL) at 1200 rpm. The turbid dispersion was stirred for another 2 s and then kept still for 10 min. The reaction was then quenched by the addition of 20 µL of 2-(vinyloxy)ethan-1-ol. Water (1/3 of acetone) was added after 30 min and the acetone was removed under reduced pressure. Purification was performed by centrifugal filtration, using a membrane with a cutoff of 300 kDa and three consecutive washing steps with 10 mL each. Nanogels were obtained as stable dispersions in water and characterized using DLS, NTA, and Zeta-potential measurements.

Coprecipitation of Myoglobin: The inverse nanoprecipitation was performed as described in Section 2.5. Varying amounts of a stock solution of myoglobin were added to the dPG-metTet macromonomer solution and thoroughly mixed. The total volume of water was kept at 1 mL. 2.5 and 5 wt% of myoglobin were encapsulated each for dPG-norbonene- and dPG-cyclopropene-NGs (n = 3). The gels were purified by centrifugation filtration, using filters with a molecular weight cutoff of 1 MDa at 234 rcf. The gel volume was reduced to 1 mL and fresh PBS buffer solution was added (10 mL). Then, the volume was reduced to 1 mL again and the whole process was repeated three times to ensure the complete removal of the nonencapsulated protein.

Protein Content Determination Assay: A standard Pierce BCA assay kit was used for the determination of protein content within the nanogels. 25 µL of the purified nanogels were added to a 96-well plate. Then, 200 µL of working reagent was added to each well and the plate was shaken for 30 s on a plate shaker. The plate was then incubated at 37 °C for 1 h. After cooling to room temperature, the absorbance was measured at 562 nm on a plate reader. Samples were recorded in triplicates and for three independent gels of the same type. Calibration curves were prepared for a dilution series of albumin and myoglobin in the range of 0–750 µg mL^{-1}. Concentrations of myoglobin in the samples were determined via the fitted standard curves of myoglobin (Figure S6, Supporting Information).

Supporting Information

Supporting Information is available from the Wiley Online Library or from the author.

Acknowledgements

The authors like to acknowledge Cathleen Schlesener for providing dPG and dPG-NH_2 and the BioSupraMol core facility for NMR and ESI measurements. Dr. Pamela Winchester is thanked for careful proofreading this manuscript. SFB 765 is thanked for funding.

Conflict of Interest

The authors declare no conflict of interest.

Keywords

inverse electron demand Diels Alder, nanogels, nanoprecipitation, protein encapsulation

Received: September 24, 2019
Revised: October 25, 2019
Published online:

[1] H. S. Choi, W. Liu, P. Misra, E. Tanaka, J. P. Zimmer, B. Itty Ipe, M. G. Bawendi, J. V Frangioni, *Nat. Biotechnol.* **2007**, *25*, 1165.
[2] L. W. Seymour, R. Duncan, J. Strohalm, J. Kopeček, *J. Biomed. Mater. Res.* **1987**, *21*, 1341.
[3] P. Zhang, F. Sun, S. Liu, S. Jiang, *J. Controlled Release* **2016**, *244*, 184.
[4] P. L. Turecek, M. J. Bossard, F. Schoetens, I. A. Ivens, *J. Pharm. Sci.* **2016**, *105*, 460.
[5] R. Haag, F. Kratz, *Angew. Chem., Int. Ed.* **2006**, *45*, 1198.
[6] K. Knop, R. Hoogenboom, D. Fischer, U. S. Schubert, *Angew. Chem., Int. Ed.* **2010**, *49*, 6288.
[7] D. Steinhilber, M. Witting, X. Zhang, M. Staegemann, F. Paulus, W. Friess, S. Küchler, R. Haag, *J. Controlled Release* **2013**, *169*, 289.
[8] S. Singh, F. Topuz, K. Hahn, K. Albrecht, J. Groll, *Angew. Chem., Int. Ed.* **2013**, *52*, 3000.
[9] C. Wu, C. Böttcher, R. Haag, *Soft Matter* **2015**, *11*, 972.
[10] T. Nochi, Y. Yuki, H. Takahashi, S. Sawada, M. Mejima, T. Kohda, N. Harada, I. G. Kong, A. Sato, N. Kataoka, D. Tokuhara, S. Kurokawa, Y. Takahashi, H. Tsukada, S. Kozaki, K. Akiyoshi, H. Kiyono, *Nat. Mater.* **2010**, *9*, 572.
[11] D. Steinhilber, S. Seiffert, J. A. Heyman, F. Paulus, D. A. Weitz, R. Haag, *Biomaterials* **2011**, *32*, 1311.
[12] E. Mauri, G. Perale, F. Rossi, *ACS Appl. Nano Mater.* **2018**, *1*, 6525.
[13] D. Steinhilber, A. L. Sisson, D. Mangoldt, P. Welker, K. Licha, R. Haag, *Adv. Funct. Mater.* **2010**, *20*, 4133.
[14] A. V. Kabanov, S. V. Vinogradov, *Angew. Chem., Int. Ed.* **2009**, *48*, 5418.
[15] H. Zhou, D. Steinhilber, H. Schlaad, A. L. Sisson, R. Haag, *React. Funct. Polym.* **2011**, *71*, 356.
[16] D. Klinger, K. Landfester, *J. Polym. Sci., Part A: Polym. Chem.* **2012**, *50*, 1062.

[17] A. L. Sisson, D. Steinhilber, T. Rossow, P. Welker, K. Licha, R. Haag, *Angew. Chem., Int. Ed.* **2009**, *48*, 7540.
[18] A. L. Sisson, I. Papp, K. Landfester, R. Haag, *Macromolecules* **2009**, *42*, 556.
[19] D. Steinhilber, S. Seiffert, J. A. Heyman, F. Paulus, D. A. Weitz, R. Haag, *Biomaterials* **2011**, *32*, 1311.
[20] M. Antonietti, *Angew. Chem. Int. Ed.* **1988**, *27*, 1743.
[21] J. Z. Du, T. M. Sun, W. J. Song, J. Wu, J. Wang, *Angew. Chem., Int. Ed.* **2010**, *49*, 3621.
[22] K. McAllister, P. Sazani, M. Adam, M. J. Cho, M. Rubinstein, R. J. Samulski, J. M. DeSimone, *J. Am. Chem. Soc.* **2002**, *124*, 15198.
[23] R. Jenjob, T. Phakkeeree, F. Seidi, M. Theerasilp, D. Crespy, *Macromol. Biosci.* **2019**, *19*, e1900063.
[24] R. L. Grant, C. Yao, D. Gabaldon, D. Acosta, *Toxicology* **1992**, *76*, 153.
[25] Â. S. Inácio, K. A. Mesquita, M. Baptista, J. Ramalho-Santos, W. L. C. Vaz, O. V. Vieira, *PLoS One* **2011**, *6*, e19850.
[26] S. Schubert, J. T. Delaney, U. S. Schubert, *Soft Matter* **2011**, *7*, 1581.
[27] C. Zhang, V. J. Pansare, R. K. Prud'homme, R. D. Priestley, *Soft Matter* **2012**, *8*, 86.
[28] R. Tong, L. Yala, T. M. Fan, J. Cheng, *Biomaterials* **2010**, *31*, 3043.
[29] Y. Dai, X. Chen, X. Zhang, *Macromol. Rapid Commun.* **2019**, *40*, 1.
[30] D. C. Kennedy, C. S. McKay, M. C. B. Legault, D. C. Danielson, J. A. Blake, A. F. Pegoraro, A. Stolow, Z. Mester, J. P. Pezacki, *J. Am. Chem. Soc.* **2011**, *133*, 17993.
[31] N. J. Agard, J. a. Prescher, C. R. Bertozzi, *J. Am. Chem. Soc.* **2004**, *126*, 15046.
[32] D. P. Nair, M. Podgórski, S. Chatani, T. Gong, W. Xi, C. R. Fenoli, C. N. Bowman, *Chem. Mater.* **2014**, *26*, 724.
[33] A. L. Sisson, R. Haag, *Soft Matter* **2010**, *6*, 4968.
[34] J. Khandare, M. Calderón, N. M. Dagia, R. Haag, *Chem. Soc. Rev.* **2012**, *41*, 2824.
[35] M. Dimde, D. Steinhilber, F. Neumann, Y. Li, F. Paulus, N. Ma, R. Haag, *Macromol. Biosci.* **2016**, *17*, 1600190.
[36] M. Dimde, F. Neumann, F. Reisbeck, S. Ehrmann, J. L. Cuellar-Camacho, D. Steinhilber, N. Ma, R. Haag, *Biomater. Sci.* **2017**, *5*, 2328.
[37] P. Dey, T. Bergmann, J. L. Cuellar-Camacho, S. Ehrmann, M. S. Chowdhury, M. Zhang, I. Dahmani, R. Haag, W. Azab, *ACS Nano* **2018**, *12*, 6429.
[38] R. A. Carboni, R. V. Lindsey, *J. Am. Chem. Soc.* **1959**, *81*, 4342.
[39] J. Sauer, D. K. Heldmann, J. Hetzenegger, J. Krauthan, H. Sichert, J. Schuster, *Eur. J. Org. Chem.* **1998**, *1998*, 2885.
[40] G. Clavier, P. Audebert, *Chem. Rev.* **2010**, *110*, 3299.
[41] B. L. Oliveira, Z. Guo, G. J. L. Bernardes, *Chem. Soc. Rev.* **2017**, *46*, 4895.
[42] D. S. Liu, A. Tangpeerachaikul, R. Selvaraj, M. T. Taylor, J. M. Fox, A. Y. Ting, *J. Am. Chem. Soc.* **2012**, *134*, 792.
[43] J. Schoch, M. Staudt, A. Samanta, M. Wiessler, A. Jäschke, *Bioconjugate Chem.* **2012**, *23*, 1382.
[44] J. Yang, J. Šečkute, C. M. Cole, N. K. Devaraj, *Angew. Chem., Int. Ed.* **2012**, *51*, 7476.
[45] M. Witting, M. Molina, K. Obst, R. Plank, K. M. Eckl, H. C. Hennies, M. Calderón, W. Frieß, S. Hedtrich, *Nanomed.: Nanotechnol., Biol. Med.* **2015**, *11*, 1179.
[46] M. R. Karver, R. Weissleder, S. A. Hilderbrand, *Bioconjugate Chem.* **2011**, *22*, 2263.
[47] D. Ekinci, A. L. Sisson, A. Lendlein, *J. Mater. Chem.* **2012**, *22*, 21100.
[48] C. Siegers, M. Biesalski, R. Haag, *Chem. - Eur. J.* **2004**, *10*, 2831.
[49] K. Lang, L. Davis, S. Wallace, M. Mahesh, D. J. Cox, M. L. Blackman, J. M. Fox, J. W. Chin, *J. Am. Chem. Soc.* **2012**, *134*, 10317.
[50] N. K. Devaraj, R. Weissleder, S. A Hilderbrand, *Communications* **2008**, *19*, 2297.
[51] F. Thalhammer, U. Wallfahrer, J. Sauer, *Tetrahedron Lett.* **1990**, *31*, 6851.
[52] B. D. Chithrani, A. A. Ghazani, W. C. W. Chan, *Nano Lett.* **2006**, *6*, 662.
[53] S. Mitragotri, J. Lahann, *Nat. Mater.* **2009**, *8*, 15.
[54] D. M. Patterson, L. A. Nazarova, B. Xie, D. N. Kamber, J. A. Prescher, *J. Am. Chem. Soc.* **2012**, *134*, 18638.

Supporting Information

Systematic Screening of Different Polyglycerin-based Dienophile Macromonomers for Efficient Nanogel Formation through IEDDA Inverse Nanoprecipitation

*Alexander Oehrl, Sebastian Schötz, Rainer Haag**

Materials and Analytical Methods

The solvents *n*-pentane, ethyl acetate, and diethyl ether were obtained from the technically pure solvents by distillation before use. DCM and acetone (HPLC grade) were used without further purification. Dry DCM and THF were taken from a SPS-800 type MBRAUN solvent drying system. Dry methanol and DMF were acquired from Acros and Fischer Chemical. All other chemicals and deuterated solvents were purchased and used without further purification. Qualitative thin layer chromatography (TLC) was performed on silica gel-coated aluminum plates serving as stationary phase (silica gel 60 F254 from Macherey-Nagel). The analytes were identified by irradiation of the TLC plates with UV light (λ = 254 nm) or by treatment with a potassium permanganate-based staining reagent (100 mL deionized water, 200 mg potassium permanganate) or anis aldehyde-based (450 mL EtOH, 25.0 mL anis aldehyde, 25.0 mL conc. sulfuric acid, 8.0 mL acetic acid). Column chromatography was performed with silica gel of Macherey-Nagel, grain size 40 – 63 µm, 230 - 400 mesh as the stationary phase, and the indicated eluent mixtures as mobile phase. IR spectra were recorded on a JASCO FT/IR-4100 spectrometer. The characteristic absorption bands are given in wave numbers. ^{1}H–NMR spectra were recorded at 300 K on Joel ECX 400 400 MHz and AVANCE III (700 MHz) instruments. Chemical shifts δ are indicated in parts per million (ppm) relative to tetramethyl silane (0 ppm) and calibrated as an internal standard to the signal of the incompletely deuterated solvent ($CDCl_3$: δ = 7.26 ppm, MeOD: δ = 3.31 ppm). Coupling constants J are given in Hertz (Hz).

^{13}C–NMR spectra were recorded at 300 K on AVANCE III instruments (176 MHz). Chemical shifts δ are given in parts per million (ppm) relative to tetramethyl silane (0 ppm) and calibrated as an internal standard to the signal of the incompletely deuterated solvent ($CDCl_3$: δ = 77.16 ppm, MeOD: δ = 49 ppm). Coupling constants J are given in Hertz (Hz). The spectra are decoupled from proton broadband. GPC was performed on an Agilent 1100 at 5 mg mL^{-1} using a pullulan standard,0.1 M $NaNO_3$ solution as eluent, and a PSS Suprema column 10 μm with a flow rate of 1 mL/min. Signal was detected with an RI detector. DLS and Zeta potential were measured on a Malvern zeta- sizer nano ZS 90 with He–Ne laser (λ = 532 nm) at 173° backscatter and automated attenuation at 25 °C. Three measurements were performed per sample with between 10 and 16 individual measurements, yielding a mean size value plus standard deviation. Sample concentration was kept at 1 mg mL^{-1}. The readout for the protein assay was performed with an infinite M200 Pro from TECAN.

Precursor Synthesis

Activated carbonate precursors of the different dienophiles were partially synthesized according to literature-known procedures. Some procedures were modified as indicated. Norbonene- and DHP activated carbonates are here described for the first time.

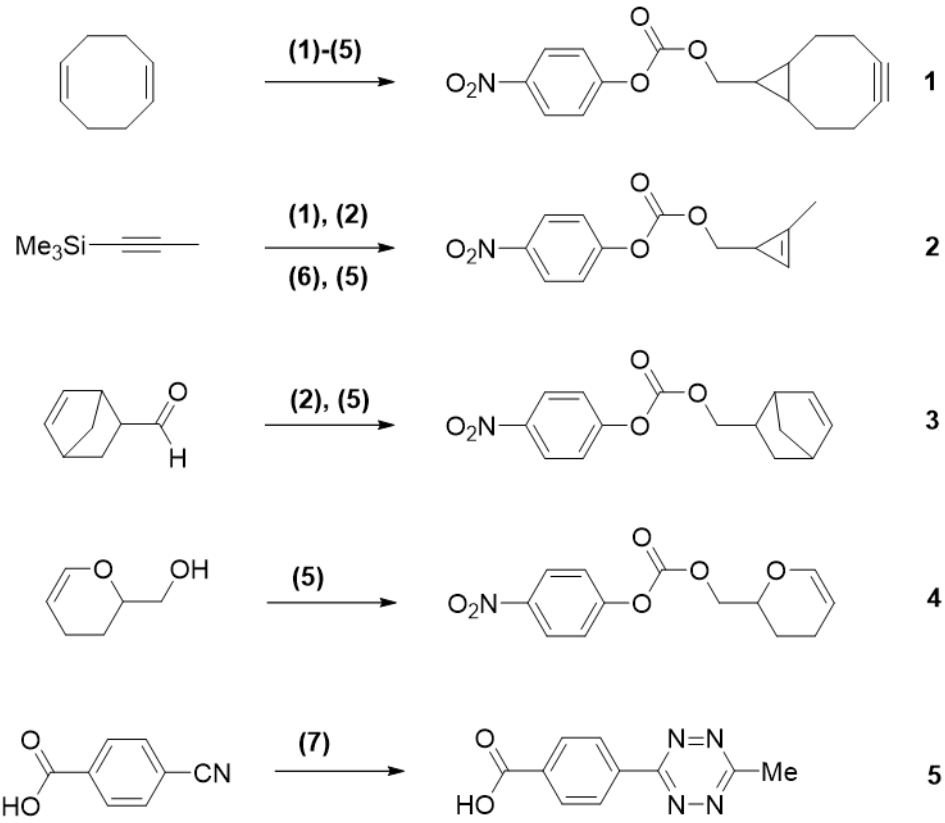

Scheme S1. Synthetic overview of the precursor molecules: (1) Rh-acetate dimer, ethyl diazoacetate, DCM, (2) $LiAlH_4$, THF, (3) Br_2, DCM, (4) KO^tBu, THF, (5) 4-nitrophenyl chloroformate, py, DCM, (6) TBAF, THF and (7) acetamidine hydrochloride, hydrazine, $Zn(OTf)_2$, then $NaNO_2$, HCl.

BCN was synthesized according to a modified literature procedure.[1]

ethyl (Z)-bicyclo[6.1.0]non-4-ene-9-carboxylate

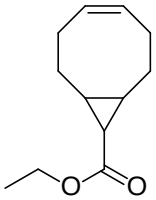

In a 2 L three-neck round bottom flask, cycloocatadiene (310 mL, 2.87 mol) and rhodium acetate dimer (750 mg, 1.72 mmol) were dissolved in 300 mL of dry DCM under an argon atmosphere. Ethyl diazoacetate (52.8 g, 458 mmol) dissolved in 150 mL dry DCM was then added dropwise to the magnetically stirred solution over the course of 8 h and the reaction

mixture was stirred at room temperature for 3 d. The solvent was removed under reduced pressure and the crude product was purified by column chromatography using hexane:EtOAc (100:1 → 50:1 → 20:1 → 5:1 → 0:1) as a solvent system (R_f (endo+exo) = 0.2/0.25 in Hex:EtOAc 5:1). The product (endo/exo-mixture) was obtained as a colorless liquid (85 g, 95%).[1]H NMR (400 MHz, $CDCl_3$, δ): 5.77 – 5.45 (m, 2 H), 4.20 – 3.94 (m, 2 H), 2.53 – 1.99 (m, 6 H), 1.86 – 1.35 (m, 5 H), 1.23 (m, 3 H).

(Z)-bicyclo[6.1.0]non-4-en-9-ylmethanol

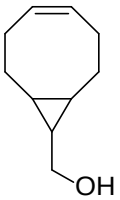

In a dried 2 L three-neck round bottom flask, $LiAlH_4$ (7.3 g, 193 mmol) was suspended in 250 mL of dry diethylether under an argon atmosphere. The suspension was cooled to 0 °C using an ice bath. Ethyl (Z)-bicyclo[6.1.0]non-4-ene-9-carboxylate (25 g, 129 mmol) was dissolved in 250 mL of dry diethylether and added dropwise to the magnetically stirred solution over the course of 1 h using a dropping funnel. After complete addition, the reaction was warmed to room temperature and stirred for another hour. The reaction was then cooled to 0 °C again and carefully quenched with water until the precipitate turned white. After extraction with 3 x 300 mL of diethylether, the organic phase was dried over sodium sulfate and the solvent was removed under reduced pressure. The product was obtained without further purification as a colorless liquid (20 g, quant.). [1]H NMR (400 MHz, $CDCl_3$, δ): 5.62 (td, J = 4.1, 1.9 Hz, 2H), 3.58 (dd, J = 94.5, 7.3 Hz, 2H), 2.42 – 1.90 (m, 4H), 1.64 – 0.90 (m, 3H), 0.80 – 0.56 (m, 2H).

(4,5-dibromobicyclo[6.1.0]nonan-9-yl)methanol

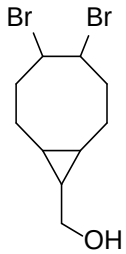

In a dried 1 L Schlenk flask, (Z)-bicyclo[6.1.0]non-4-en-9-ylmethanol (20 g, 129 mmol) was dissolved in 450 mL of dry DCM under an argon atmosphere. The suspension was cooled to 0 °C using an ice bath. Bromine (8 mL, 154 mmol) was dissolved in 50 mL of dry DCM and added dropwise to the magnetically stirred solution until the yellow color persisted. The reaction was quenched with 150 mL saturated sodium sulfite solution, turning the reaction mixture milky white. After extraction with 3 x 200 mL of DCM, the organic phase was dried over sodium sulfate and the solvent was removed under reduced pressure. The product was obtained without further purification as honey-like substance and used without further purification (42 g, quant.). ^{1}H NMR (500 MHz, $CDCl_3$, δ): 4.93 – 4.58 (m, 2 H), 3.87 – 3.34 (m, 1 H), 2.77 – 2.50 (m, 2 H), 2.33 – 1.81 (m, 4 H), 1.70 – 1.02 (m, 3 H), 0.97 – 0.76 (m, 1 H), 0.74 – 0.57 (m, 1 H).

bicyclo[6.1.0]non-4-yn-9-ylmethanol

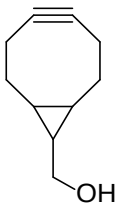

In a dried 2 L Schlenk flask, (4,5-dibromobicyclo[6.1.0]nonan-9-yl)methanol (42 g, 129 mmol) was dissolved in 250 mL of dry THF under an argon atmosphere. The suspension was cooled to 0 °C using an ice bath. KO^{t}Bu (48 g, 425 mmol) was suspended in 250 mL of dry THF and the supernatant was added dropwise to the magnetically stirred solution over the course of 8 h. The reaction was stirred at room temperature for 2 d and another 20 g of KO^{t}Bu was added

directly to the suspension. The reaction mixture was then stirred for another 2 d. After quenching with 200 mL of saturated ammonium chloride solution, the THF was removed under reduced pressure and the water phase was extracted 3 times with 300 mL DCM each. The organic phases were united and dried over sodium sulfate and the solvent was removed under reduced pressure. The raw product was purified with column chromatography using silica and hexane:EtOAc as solvent system (100:1 → 50:1 → 20:1 → 5:1 → 2:1). The product was obtained as a slightly yellow liquid (7 g, 37%). ^{1}H NMR (500 MHz, $CDCl_3$, δ): 4.93 – 4.58 (m, 2 H), 3.87 – 3.34 (m, 1 H), 2.77 – 2.50 (m, 2 H), 2.33 – 1.81 (m, 4 H), 1.70 – 1.02 (m, 3 H), 0.97 – 0.76 (m, 1 H), 0.74 – 0.57 (m, 1 H).

bicyclo[6.1.0]non-4-yn-9-ylmethyl (4-nitrophenyl) carbonate (1)

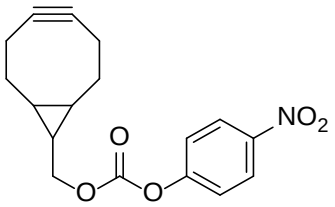

In a dried 2 L Schlenk flask, bicyclo[6.1.0]non-4-yn-9-ylmethanol (7 g, 47 mmol) and pyridine (9,5 mL, 117 mmol) were dissolved in 750 mL of dry DCM under an argon atmosphere and stirred for 5 min. Then 4-nitrophenyl chloroformate (14.1 g, 70 mmol) was added and the reaction was stirred at room temperature for 90 min. After quenching with 200 mL of saturated ammonium chloride solution, the water phase was extracted 3 times with 300 mL DCM each. The organic phases were united and dried over sodium sulfate and the solvent was removed under reduced pressure. The raw product was purified with column chromatography using silica and pentane:EtOAc as solvent system (20:1 → 10:1; R_f = 0.7 in pentane:EtOAc 3:1). The product was obtained as a colorless solid and stored in the freezer (11.4 g, 78 %).^{1}H NMR (400 MHz, $CDCl_3$, δ): 8.32 – 8.23 (m, 2 H), 7.43 – 7.33 (m, 2 H), 5.30 (d, J = 0.7 Hz, 1 H), 4.40 (dd, J = 8.2, 0.7 Hz, 1 H), 4.21 (dd, J = 6.8, 0.7 Hz, 1 H), 2.45 (dd, J = 13.3, 2.9 Hz, 1 H), 2.39 –

2.24 (m, 3 H), 2.29 – 2.12 (m, 2 H), 1.60 (d, *J* = 10.9 Hz, 1 H), 1.50 (td, *J* = 9.0, 8.3 Hz, 1 H), 1.13 – 0.99 (m, 1 H), 0.92 – 0.76 (m, 2 H).

bicyclo[2.2.1]hept-5-en-2-ylmethanol

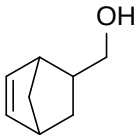

In a dry 1 L three-neck round bottom flask, $LiAlH_4$ (7.3 g, 193 mmol) was suspended in 300 mL of dry diethylether under an argon atmosphere. The suspension was cooled to 0 °C using an ice bath. Bicyclo[2.2.1]hept-5-ene-2-carbaldehyde (5 g, 129 mmol) was dissolved in 30 mL of dry diethylether and added dropwise to the magnetically stirred solution over the course of 1 h using a dropping funnel. After complete addition, the reaction was warmed to room temperature and stirred for another hour. The reaction was then cooled to 0 °C again and carefully quenched with water until the precipitate turned white. After extraction with 3 x 250 mL of diethylether, the organic phase was dried over sodium sulfate and the solvent was removed under reduced pressure. The product was obtained without further purification as a colorless liquid (5.5 g, 93%). ^{1}H NMR (400 MHz, $CDCl_3$, δ): 6.06 (dd, *J* = 5.8, 3.0 Hz, 1H, RC*H*=CHR), 5.89 (dd, *J* = 5.8, 2.9 Hz, 1H, RCH=C*H*R), 3.60 (m, 1H, CH_2OH), 3.28 (m, 1H, CH_2OH), 2.86 (s, 1H, bridgehead), 2.72 (s, 1H, bridgehead), 2.31 – 2.11 (m, 1H, R_2C*H*CH_2OH), 1.74 (ddd, *J* = 11.6, 9.2, 3.8 Hz, 1H,), 1.44 – 1.33 (m, 1H), 1.32 – 1.17 (m, 1H), 0.43 (ddd, *J* = 11.6, 4.5, 2.6 Hz, 1H).

The cyclopropene derivatives were synthesized according to modified literature procedures.[2,3]

ethyl 2-methyl-3-(trimethylsilyl)cycloprop-2-ene-1-carboxylate

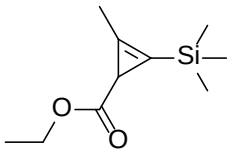

In a 100 mL three-neck round bottom flask, trimethylsilylpropyne (6.5 g, 58 mmol) and rhodium acetate dimer (25 mg, 0.06 mmol) were dissolved in dry DCM (30 mL) under an argon atmosphere. Ethyl diazoacetate (4 g, 35 mmol), dissolved in 20 mL dry DCM was then added dropwise to the magnetically stirred solution over the course of 8 h and the reaction mixture was stirred at room temperature for 1 d. The solvent was removed under reduced pressure and the crude product was purified by column chromatography using pentane:EtOAc (100:1) as a solvent system. Further purification was performed using HPLC. The product was obtained as a colorless liquid (2.37 g, 34%). ^{1}H NMR (400 MHz, $CDCl_3$, δ): 5.77 – 5.45 (m, 2 H), 4.20 – 3.94 (m, 2 H), 2.53 – 1.99 (m, 6 H), 1.86 – 1.35 (m, 5 H), 1.23 (m, 3 H)

(2-methyl-3-(trimethylsilyl)cycloprop-2-en-1-yl)methanol

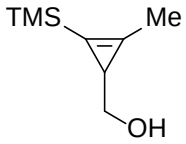

In a 50 mL Schlenk flask, DIBAL–H (10.08 mmol, 10.08 mL, 1.0 M in THF) was dissolved in dry Et_2O (25 mL). The ethyl 2-methyl-3-(trimethylsilyl)cycloprop-2-ene-1-carboxylate (1.00 g, 5.05 mmol) was added dropwise with a syringe. The solution was stirred at room temperature for 30 minutes. Saturated aqueous solution of Rochelle's salt (10 mL) was added. The phases were separated and the aqueous phase was extracted with Et_2O (3x10 mL). The combined organic phases were dried with sodium sulfate. The solvent was removed under reduced pressure. The crude product was purified by column chromatography (DCM/EtOAc, 10:1) to give the product as a colorless oil (0.59 g, 3.80 mmol, 75%). ^{1}H NMR (400 MHz,

$CDCl_3$, δ): 3.48 (d, J = 4.6 Hz, 2H, HOCH_2R^1), 2.21 (s, 3H, methyl-H), 1.56 (t, J = 4.6 Hz, 1H; $HOCH_2CHR^2R^3$), 0.17 (s, 9H, TMS-H).

(2-methylcycloprop-2-en-1-yl)methyl 2-(4-nitrophenyl)acetate (3)

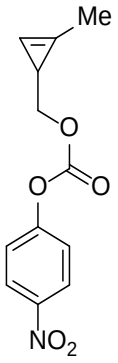

In a 100 mL Schlenk flask, (2-methyl-3-(trimethylsilyl)cycloprop-2-en-1-yl)methanol (0.67 g, 4.28 mmol) was dissolved in THF (45 mL). TBAF (5.00 mL, 1.4 M in THF) was added and the solution was stirred for 30 min at room temperature. Water and DCM were added, the phases separated, and the aqueous phase was extracted with DCM (3x40 mL). The combined organic phases were dried with sodium sulfate. The solvent was removed under reduced pressure. The crude product was purified by a short silica pad. Without any further purification, the desilylated cyclopropene was dissolved in dry DCM (40 mL) and pyridine (0.21 g, 2.63 mmol, 0.21 mL) was added. The solution was stirred for 5 min at room temperature. *p*-nitrophenylchloroformate (0.32 g, 1.58 mmol) was added and the resulting solution was stirred for 45 min at room temperature. Saturated aqueous NH_4Cl-solution was added, and the phases were separated. The aqueous phase was extracted with DCM (3x40 mL). The combined organic phases were washed with saturated aqueous NH_4Cl-solution and dried with sodium sulfate. The solvent was removed under reduced pressure. The crude product was purified by column chromatography (pentane/EtOAc, 10:1). The product (0.19 g, 0.77 mmol, 73% over 2 steps) was obtained as a yellow oil. ^{1}H NMR (400 MHz, $CDCl_3$, δ): 8.30–8.26 (m, 2 H H–aromatic), 7.41–7.37 (m, 2 H, aromatic), 6.61 (s, 1 H, H–olefin), 4.32–4.12 (m, 2 H, aliphatic), 2.17 (s, 3 H, Me), 1.79–1.76

(m, 1 H, H–ring). EA ($C_{12}H_{11}NO_5$): calc. C (57.83%), found C (58.45%); calc. N (5.62%), found N (5.75%); calc. H (4.45%), found H (4.55%).

(3,4-dihydro-*2H*-pyran-2-yl)methyl (4-nitrophenyl) carbonate (4)

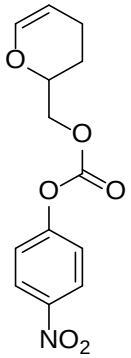

In a 250 mL Schlenk flask, (3,4-dihydro-2H-pyran-2-yl)methanol (2.00 g, 17.52 mmol) was dissolved in dry DCM (80 mL) and pyridine (3.46 g, 43.81 mmol, 3.53 mL) was added. The solution was stirred for 5 min at room temperature. *p*-nitrophenylchloroformate (5.30 g, 26.28 mmol) was added and the resulting solution was stirred for 45 min at room temperature. Saturated aqueous NH_4Cl-solution was added and the phases were separated. The aqueous phase was extracted with DCM (3x40 mL). The combined organic phases were washed with saturated aqueous NH_4Cl solution and dried with sodium sulfate. The solvent was removed under reduced pressure. The crude product was purified by column chromatography (pentan/EtOAc, 10:1). The product (3.44 g, 13.78 mmol, 79%) was obtained as a yellow solid. ^{1}H NMR (400 MHz, $CDCl_3$, δ): 8.30–8.26 (m, 2 H, H–aromatic), 7.42–7.38 (m, 2 H, H–aromatic), 6.42–6.39 (m, 1 H H–olefin-O), 4.78–4.73 (m, 1 H, H–olefin), 4.38 (d, J = 5.2 Hz, 2 H, H–C–carbonate), 4.19–4.13 (m, 1 H, H–C(tertiary)), 2.20–1.71 (m, 4 H, H–ring). ^{13}C NMR (176 MHz, CD_3OD, δ): 157.1, 154.0, 146.9, 144.2, 126.3, 123.2, 101.7, 73.7, 71.70, 24.9, 20.1. EA ($C_{13}H_{13}NO_6$): calc. C (55.92 %), found C (55.96 %); calc. N (4.69 %), found N (5.25 %); calc. H (4.77 %), found H (4.77 %).

4-(6-methyl-1,2,4,5-tetrazin-3-yl)benzoic acid was synthesized according to a modified literature protocol.[4]

4-(6-methyl-1,2,4,5-tetrazin-3-yl)benzoic acid (5)

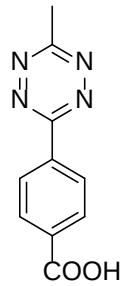

4-cyanobenzoic acid (1.5 g, 10 mmol), acetamidine hydrochloride (4.82 g, 41 mmol) and $Zn(OTf)_2$ (1 g, 3 mmol) were ground in a mortar, added to a 100 mL Schlenk flask under argon atmosphere, and cooled to 0 °C. Anhydrous hydrazine (12 mL, 377 mmol) was then slowly added under constant stirring; the reaction mixture was allowed to warm to room temperature and stirred for 72 h. $NaNO_2$ (10 g) dissolved in 30 mL of water was then added to the reaction mixture. After cooling to 0 °C, the pH was adjusted to 2-3 by the slow addition of conc. HCl_{aq}. The color of the solution turned bright pink and a pink solid precipitated. After stirring at 0 °C for another 1 h, the precipitate was filtered and washed with deionized water and MeOH. The product was obtained as a pink solid without further purification (1.1 g, 50 %). ^{1}H NMR (400 MHz, C_3D_7NO, δ): 13.80 (s, 1 H, COO*H*), 8.67 – 8.65 (m, 2 H, ArH), 8.32 – 8.29 (m, 2 H, ArH), 3.09 (s, 3 H, -CH_3).^{13}C NMR (101 MHz, C_3D_7NO, δ): 168.9, 167.9, 137.2, 135.5, 131.4, 128.7, 21.6.

Polymer Core

dPG and dPG-amine were synthesized according to literature protocols.[5,6]

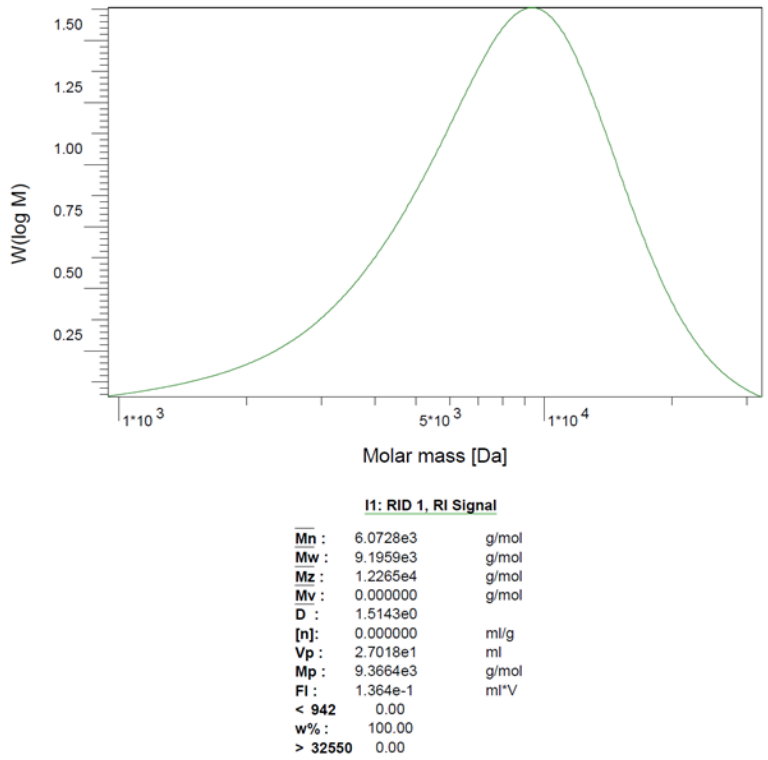

Figure S1. GPC-analysis of the dPG core.

Table S1: DLS data of the different macromonomers.

Entry	dF by NMR %	Size by Volume [nm]	PDI
dPG-BCN	7.5	12 ± 2	0.30 ± 0.01
dPG-norbonene	9	4 ± 1	0.80 ± 0.02
dPG-DHP	9	3 ± 1	0.60 ± 0.05
dPG-metTet	6.5	160 ± 140	0.50 ± 0.01
dPG-cyclopropene	8	3 ± 1	0.70 ± 0.05

Nanogels

Table S2. dPG-norbonene/dPG-metTet-NGs. Chemical quenching time.

Entry	Macromonomer		V(H_2O): V(acetone)	$T_{q, chem}$ [min]	$T_{q, water}$ [min]	Z-Average [nm]	PDI
	Ratio (A:B)	c [mg mL^{-1}]					
1	1:1.5	5	1:40	none	120	192 ± 5	0.07 ± 0.04
2	1:1.5	5	1:40	30	120	191 ± 3	0.07 ± 0.01
3	1:1.5	5	1:40	10	120	211 ± 2	0.11 ± 0.01
4	1:1.5	5	1:40	5	120	180 ± 1	0.07 ± 0.02
5	1:1.5	5	1:40	2.5	120	185 ± 3	0.08 ± 0.02
6	1:1.5	5	1:40	1	120	203 ± 1	0.10 ± 0.01
7	1:1.5	5	1:40	0	120	175 ± 1	0.08 ± 0.02

A = dPG-metTet, B = dPG-norbonene

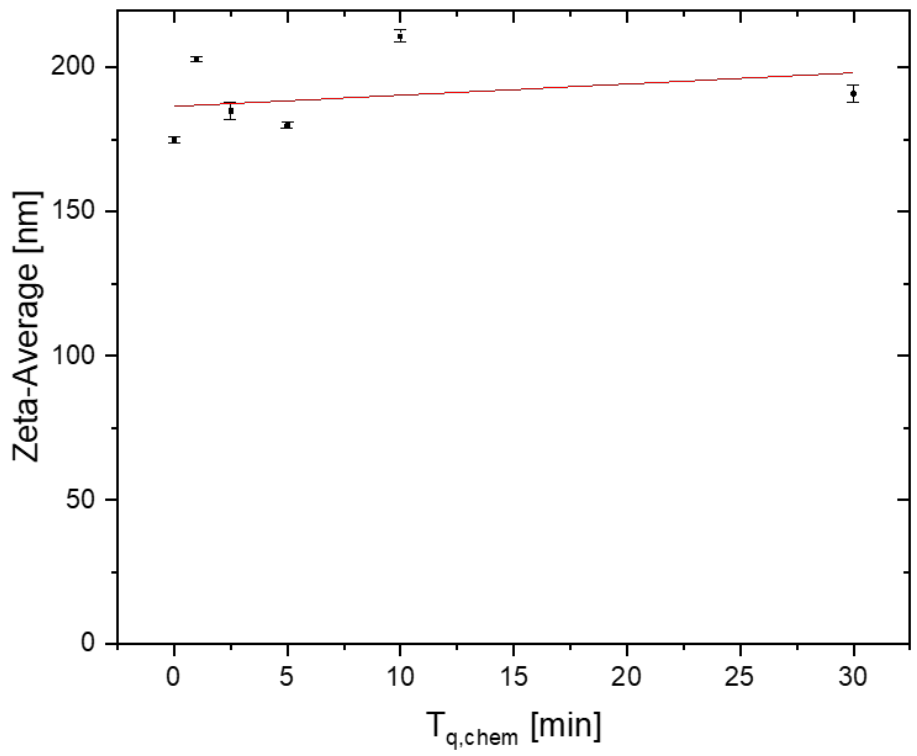

Figure S2. Relationship between chemical quenching time and size of nanogels.

Table S3. dPG-norbonene/dPG-metTet-NGs. Stirring speed

Entry	Macromonomer		V(H_2O): V(acetone)	$T_{q,\ chem}$ [min]	$T_{q,\ water}$ [min]	Stirring speed [rpm]	Z-Average [nm]	PDI
	Ratio (A:B)	c [mgmL^{-1}]						
1	1:1.5	5	1:40	10	60	300	150 ± 30	0.07 ± 0.03
2	1:1.5	5	1:40	10	60	600	119 ± 7	0.04 ± 0.01
3	1:1.5	5	1:40	10	60	900	140 ± 30	0.07 ± 0.03
4	1:1.5	5	1:40	10	60	1200	130 ± 40	0.07 ± 0.04

A = dPG-metTet; B = dPG-norbonene.

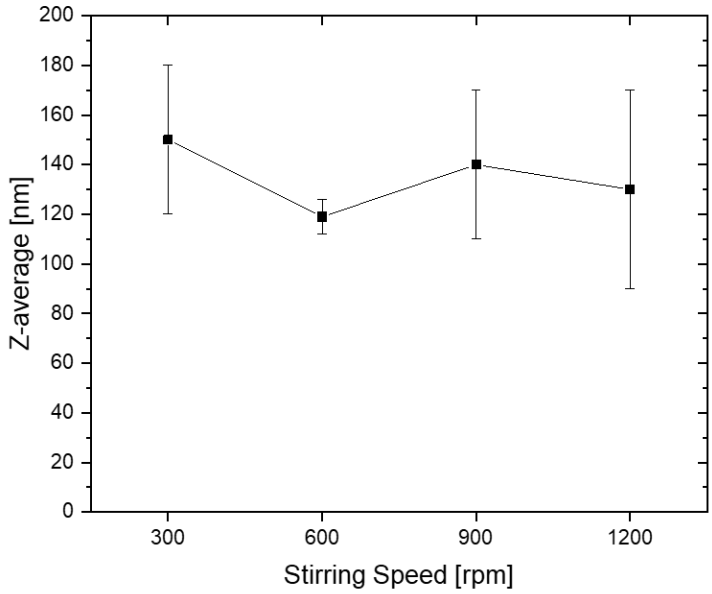

Figure S3. Dependency of nanogel size on stirring speed during nanoprecipitation.

Table S4. dPG-BCN/dPG-metTet-NGs. Water/acetone ratio.

Entry	Macromonomer		$V(H_2O)$: V(acetone)	$T_{q,\ chem}$ [min]	$T_{q,\ water}$ [min]	Z-Average [nm]	PDI
	Ratio (A:B)	c [mg mL^{-1}]					
1	1:1.5	5	1:80	5	30	[a]	1
2	1:1.5	5	1:60	5	30	[a]	1
3	1:1.5	5	1:40	5	30	800 ± 23	0.20 ± 0.03
4	1:1.5	5	1:20	5	30	132 ± 2	0.07 ± 0.04

A = dPG-metTet, B = dPG-BCN, [a] = measurement quality criteria not achieved due to very high polydispersity.

Table S5. dPG-BCN/dPG-metTet-NGs. Water quench time.

Entry	Macromonomer		$V(H_2O)$: V(acetone)	$T_{q,\ chem}$ [min]	$T_{q,\ water}$ [min]	Z-Average [nm]	PDI
	Ratio (A:B)	c [mg mL^{-1}]					
1[a]	1:1.5	5	1:40	5	2	950 ± 150	0.34 ± 0.02
2[a]	1:1.5	5	1:40	5	5	1800 ± 300	0.50 ± 0.02
3[a]	1:1.5	5	1:40	5	10	2300 ± 500	0.80 ± 0.30
4	1:1.5	5	1:40	5	30	359 ± 7	0.20 ± 0.05

[a] = Quality criteria for DLS measurements not fulfilled.

Table S6. dPG-cyclopropene/dPG-metTet nanogels. Water quenching time and water/acetone ratio.

Entry	Macromonomer		$V(H_2O)$: V(acetone)	$T_{q,chem}$ [min]	$T_{q,water}$ [min]	Z-Average [nm]	PDI
	Ratio (A:B)	c [mg mL^{-1}]					
1	1:1.5	5	1:40	5	5	78 ± 1	0.10 ± 0.01
2	1:1.5	5	1:40	5	30	81 ± 1	0.06 ± 0.01
3	1:1.5	5	1:40	5	60	101 ± 2	0.10 ± 0.01
4	1:1.5	5	1:20	5	30	76 ± 1	0.15 ± 0.01
5	1:1.5	5	1:40	5	30	93 ± 2	0.10 ± 0.01
6	1:1.5	5	1:60	5	30	124 ± 2	0.07 ± 0.01

A = dPG-metTet, B = dPG-cyclopropene.

Zeta-Potential

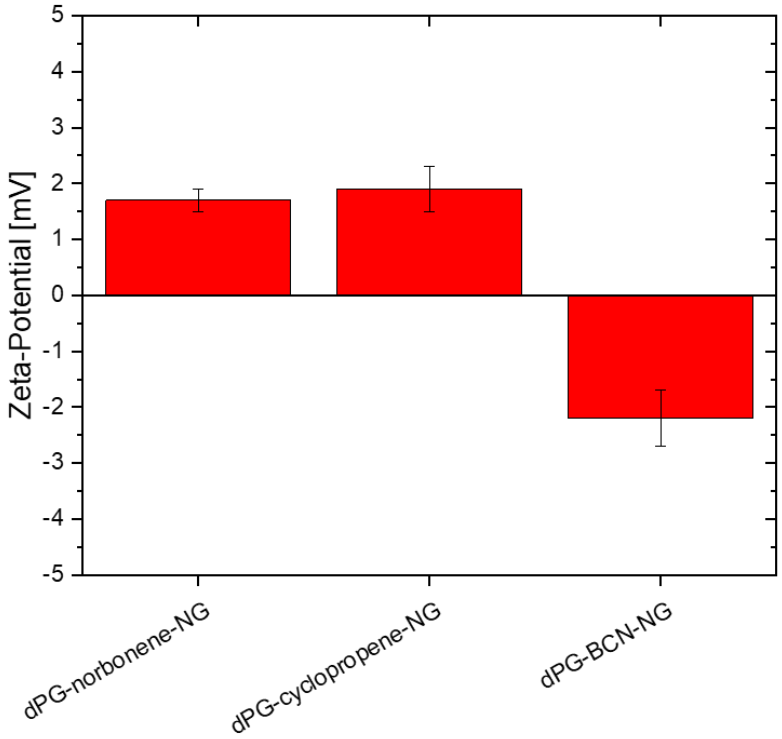

Figure S4. Zeta potential measurements of dPG-norbonene-, dPG-cyclopropene-, and dPG-BCN-NGs. Average of 3 measurements +SD.

Table S7. dPG-norbonene/dPG-metTet-NGs. Myoglobin.

Entry	Macromonomer		Myoglobin Feed [wt.%]	Z-Average [nm]	PDI
	Ratio (A:B)	c [mg mL^{-1}]			
1	1:1.5	5	5	265 ± 5	0.07 ± 0.02
2	1:1.5	5	5	435 ± 5	0.10 ± 0.02
3	1:1.5	5	2.5	191 ± 1	0.04 ± 0.02
4	1:1.5	5	2.5	241 ± 2	0.04 ± 0.03

A = dPG-metTet, B = dPG-norbonene, V(H_2O):V(acetone) = 1:40, $T_{q,\ chem}$ = 10 min and $T_{q,\ water}$ = 30 min.

Table S8. dPG-cyclopropene/dPG-metTet-NGs. Myoglobin

Entry	Macromonomer		Myoglobin Feed [wt.%]	Z-Average [nm]	PDI
	Ratio (A:B)	c [mg mL^{-1}]			
1	1:1.5	5	5	185 ± 2	0.04 ± 0.02
2	1:1.5	5	5	185 ± 2	0.08 ± 0.02
3	1:1.5	5	2.5	154 ± 1	0.07 ± 0.01
4	1:1.5	5	2.5	182 ± 3	0.07 ± 0.01

A = dPG-metTet, B = dPG-cyclopropene, V(H_2O):V(acetone) = 1:40; $T_{q,\ chem}$ = 10 min and $T_{q,\ water}$ = 30 min.

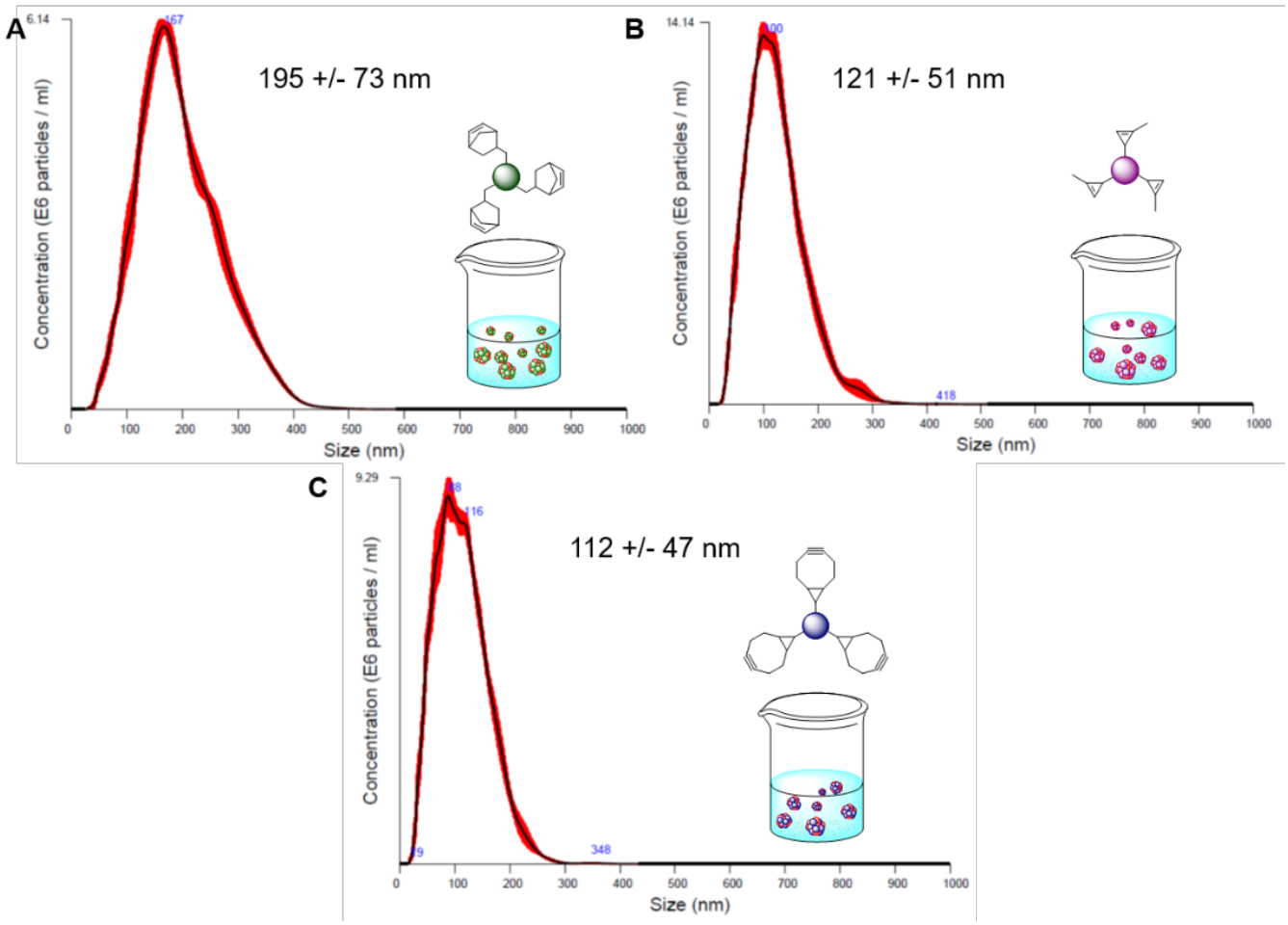

Figure S5. NTA measurements for the nanogels shown in *Figure 4.* (A) dPG-norbonene NG, (B) dPG-cyclopropene NG and (C) dPG-BCN NG. Measurements performed in triplicate at 10 µg mL^{-1}.

BCA Protein Assay

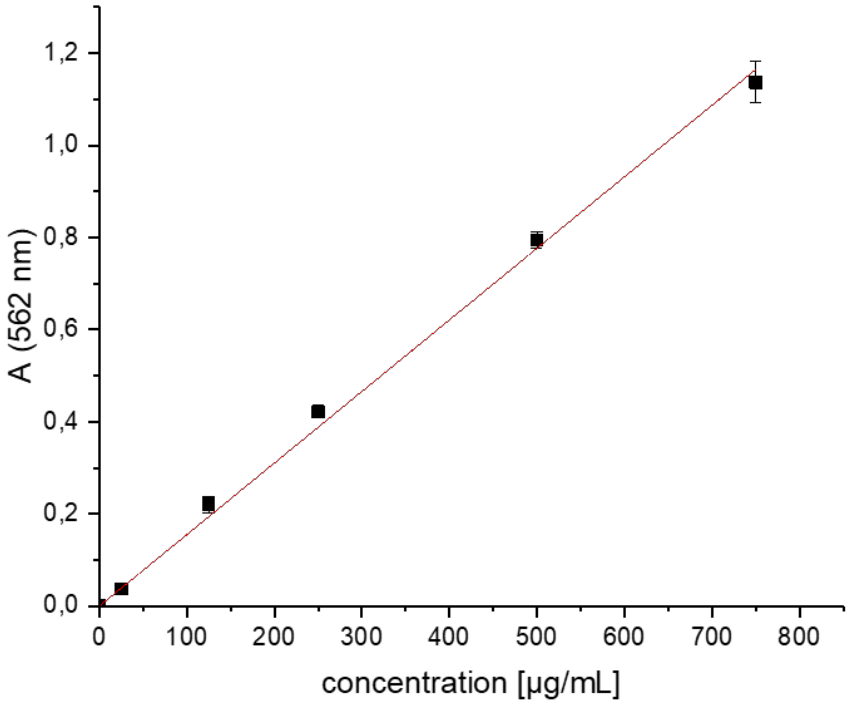

Figure S6. Albumin calibration curve.

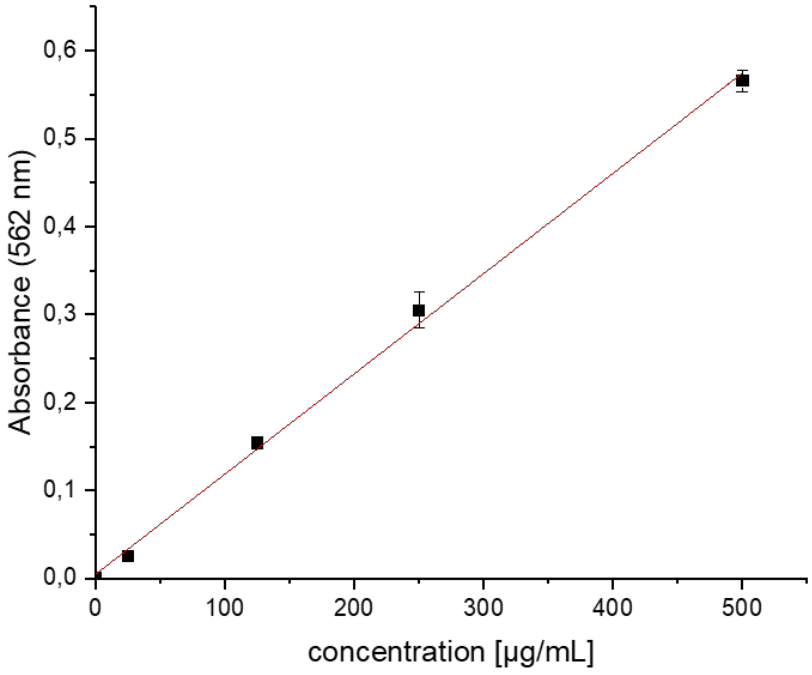

Figure S7. Calibration curve of myoglobin.

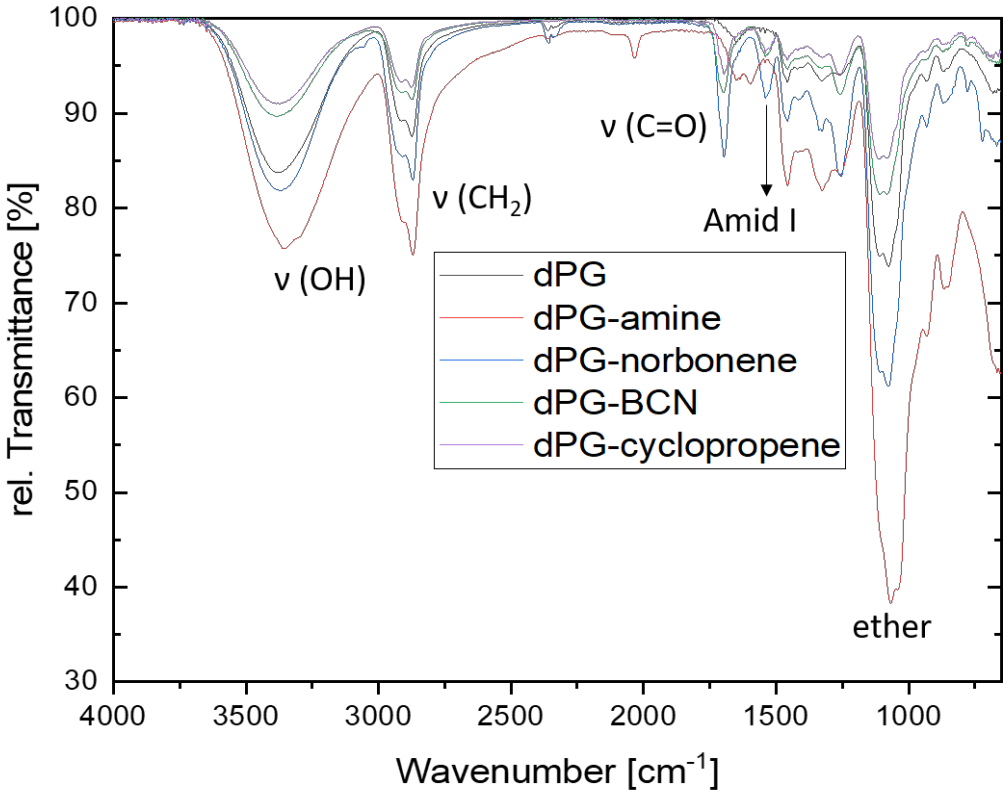

Figure S8. IR-spectra of dPG-macromonomers.

NMR Spectra

BCN (**1**)

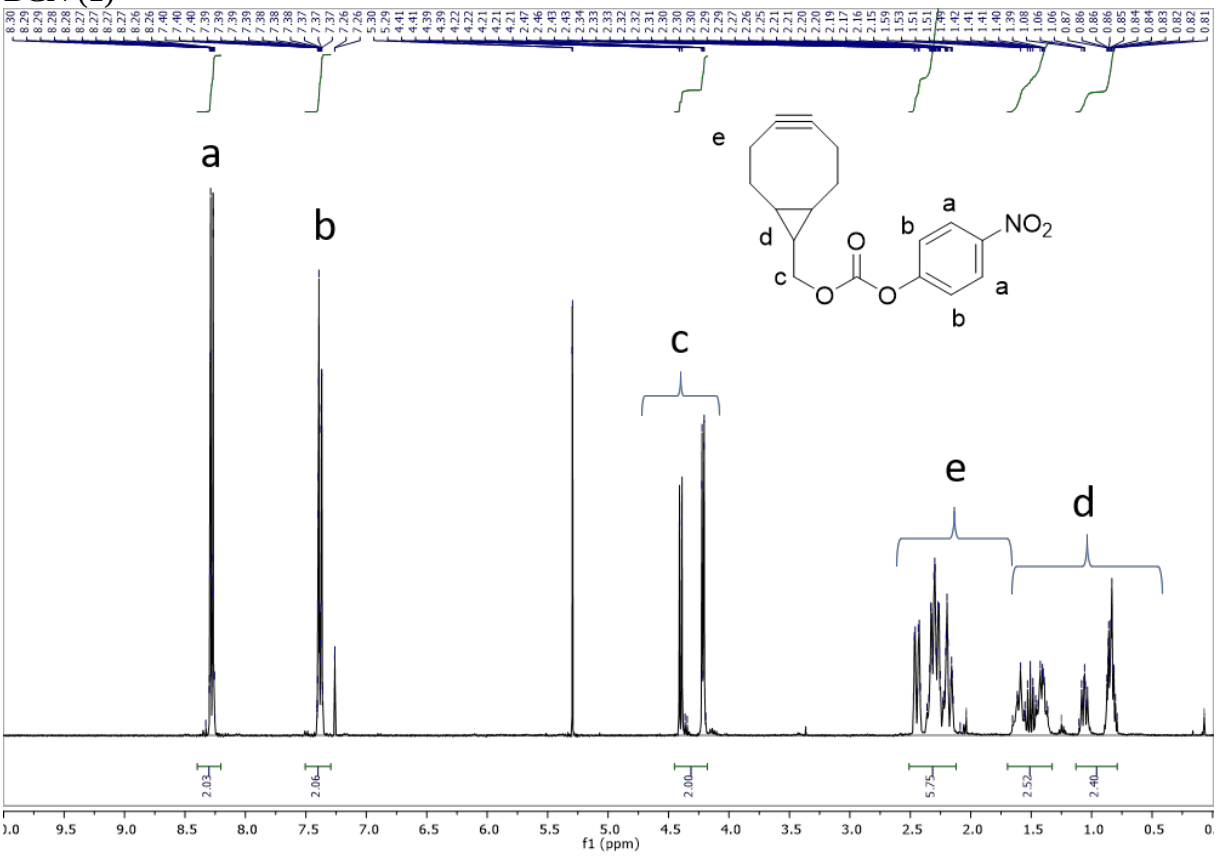

Norbonene-alcohol (^{1}H)

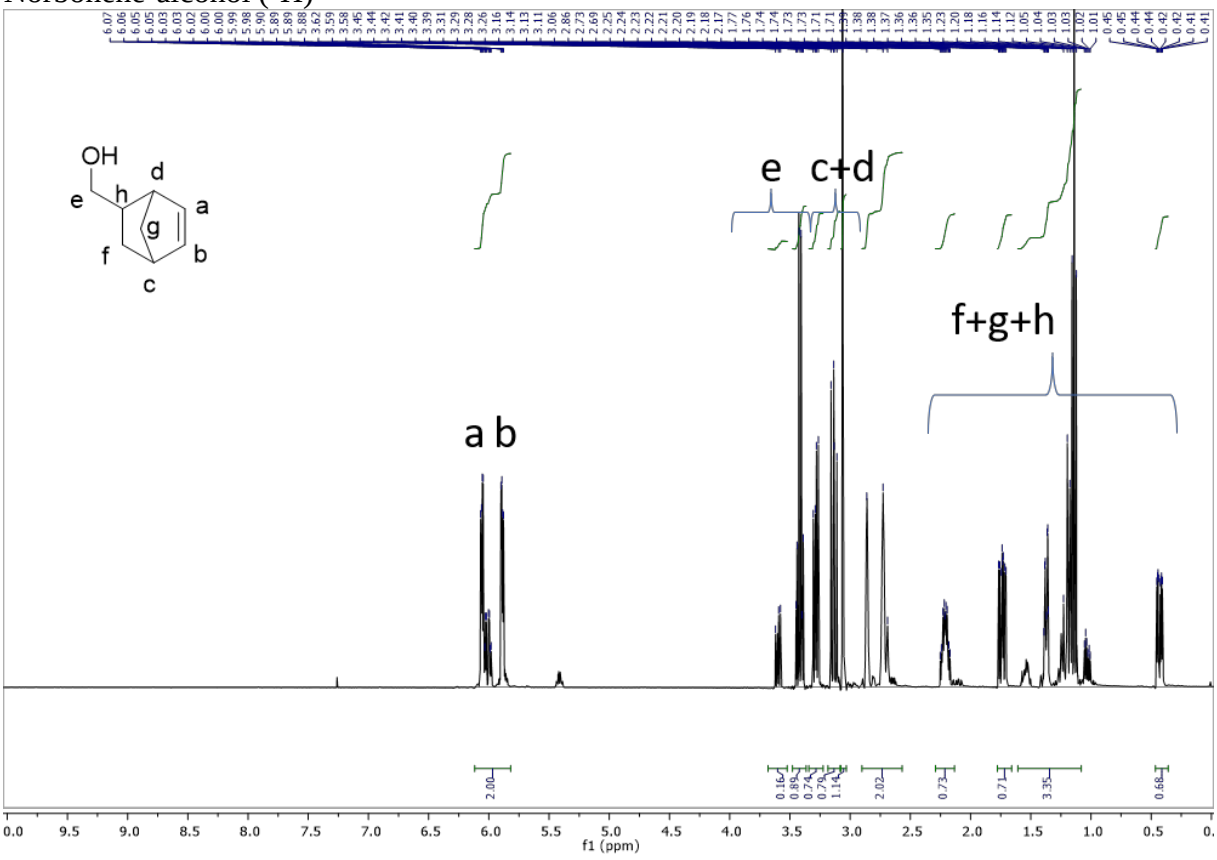

Norbonene-active ester (^{1}H)

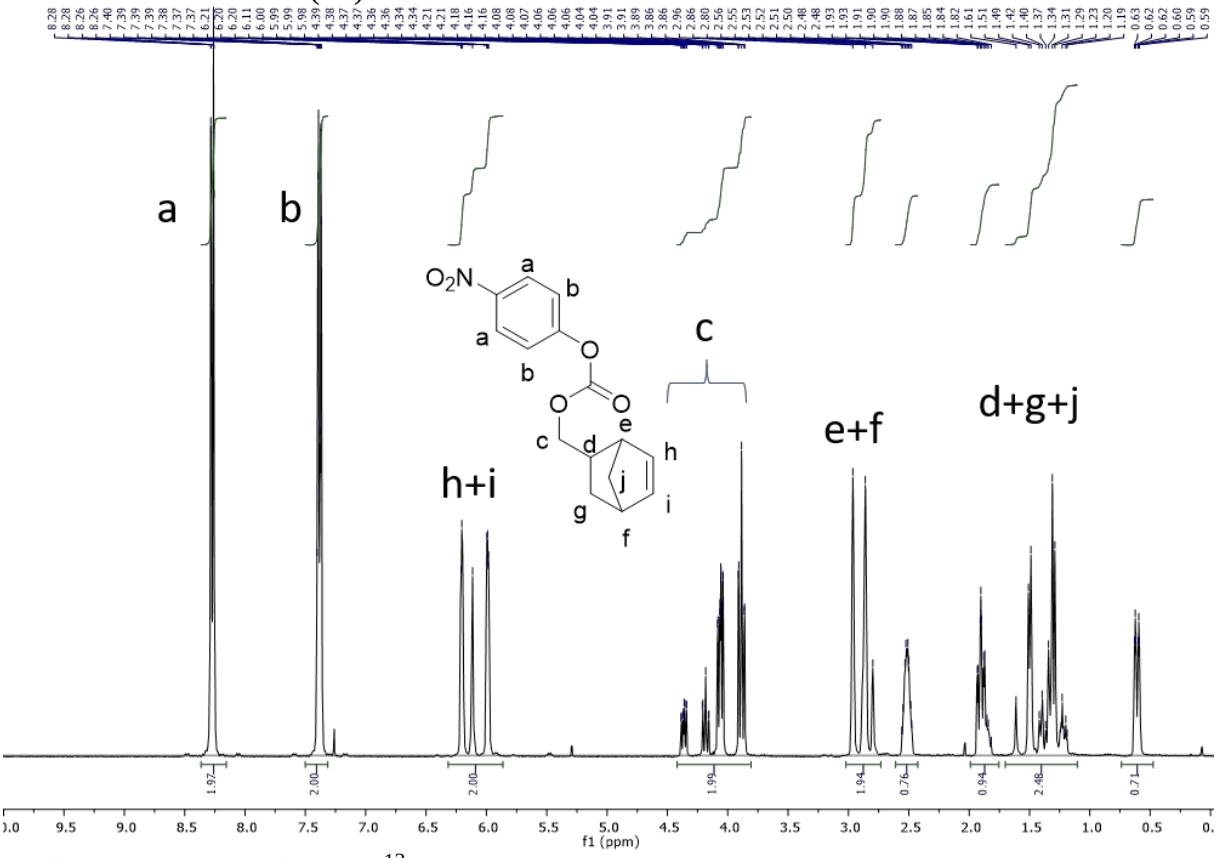

Norbonene-active carbonate (^{13}C)

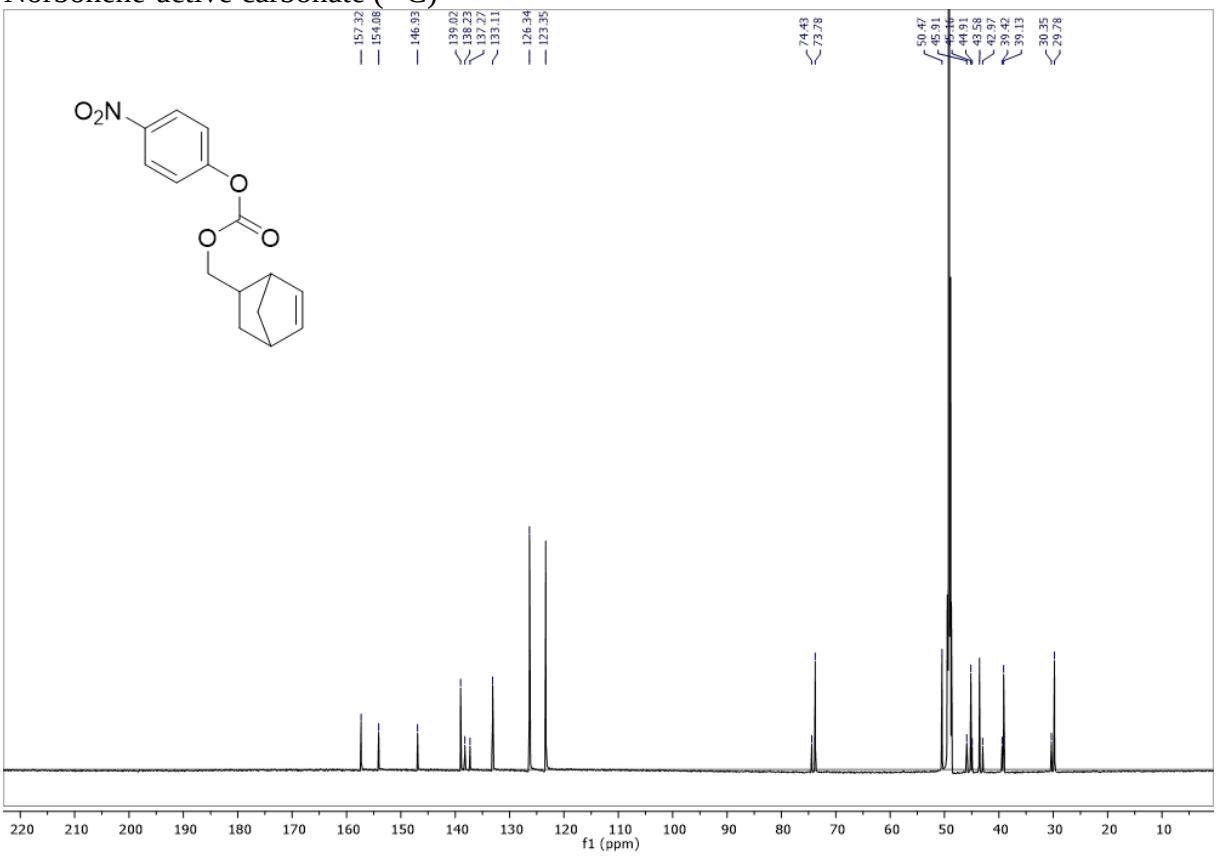

Cyclopropene-active carbonate (^{1}H)

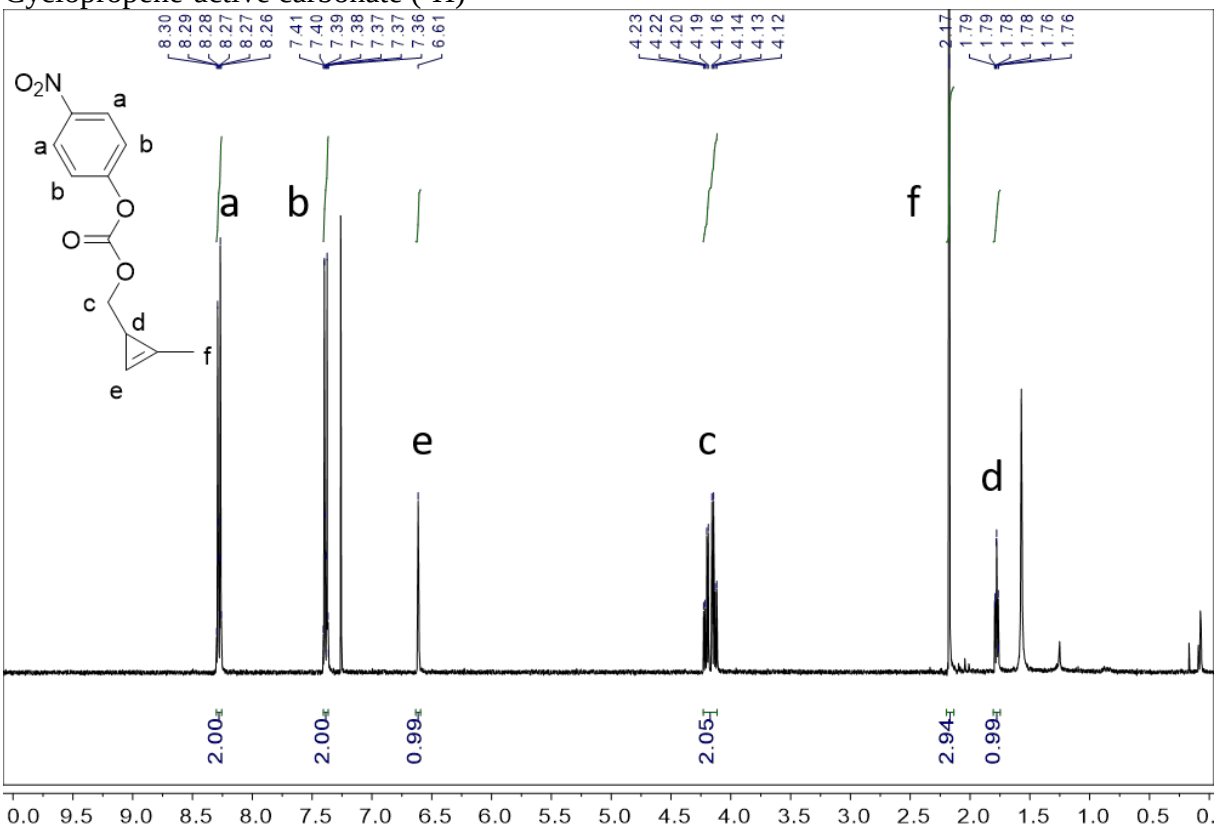

DHP-active carbonate (^{1}H)

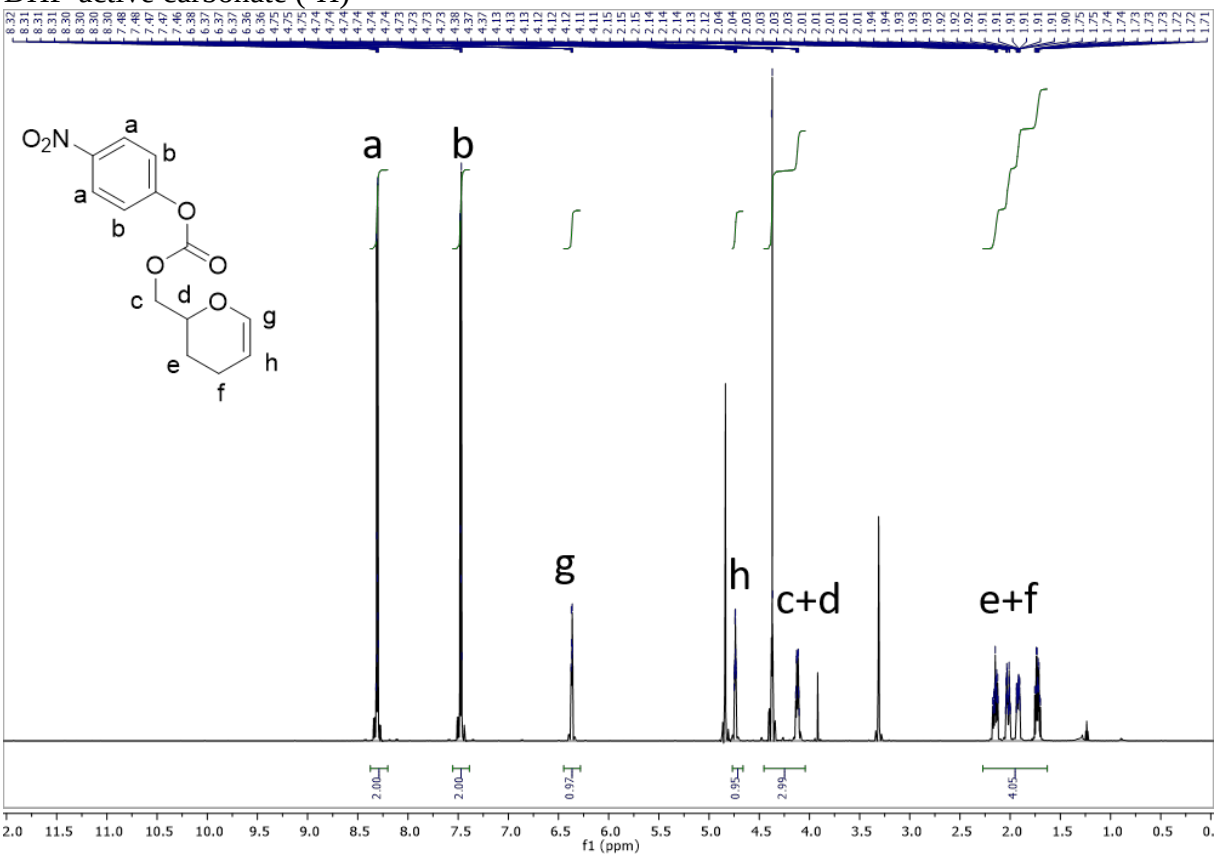

DHP-active carbonate (^{13}C)

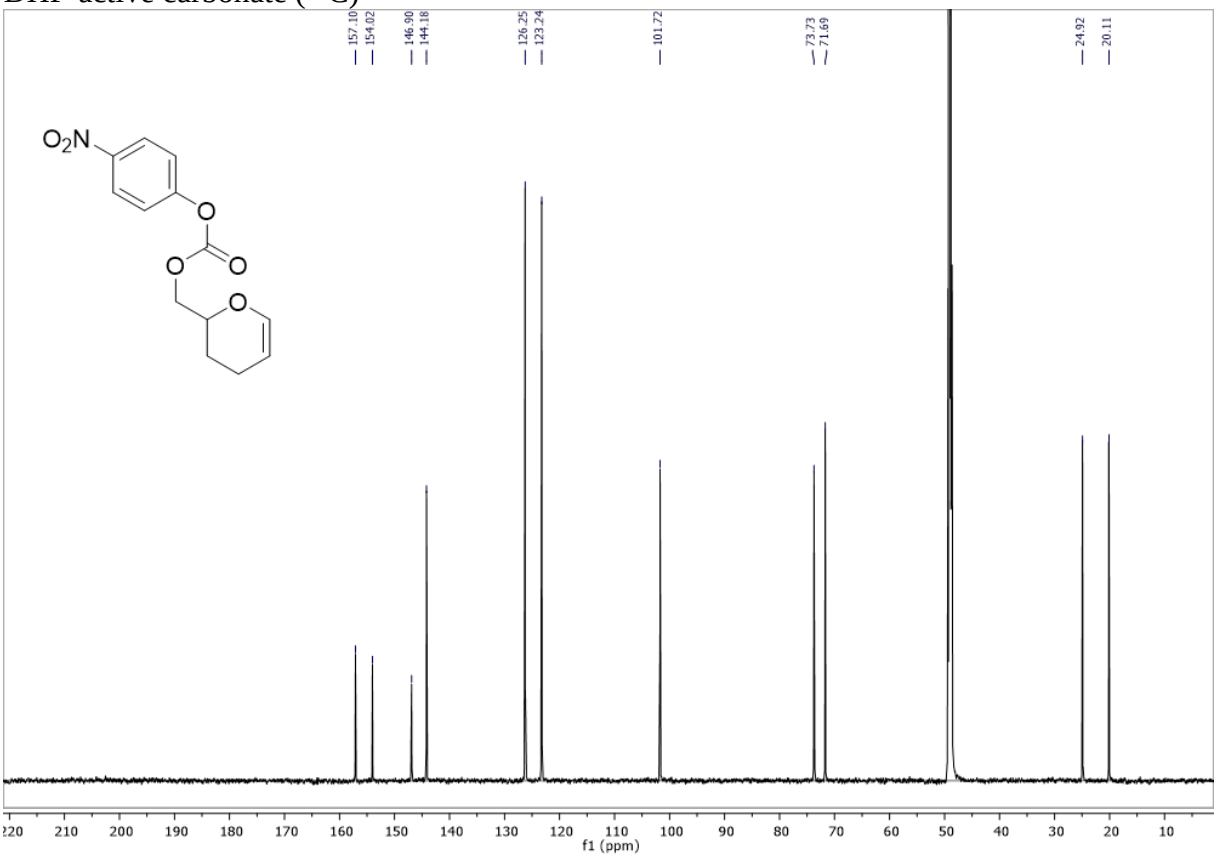

4-(6-methyl-1,2,4,5-tetrazin-3-yl)benzoic acid (^{1}H)

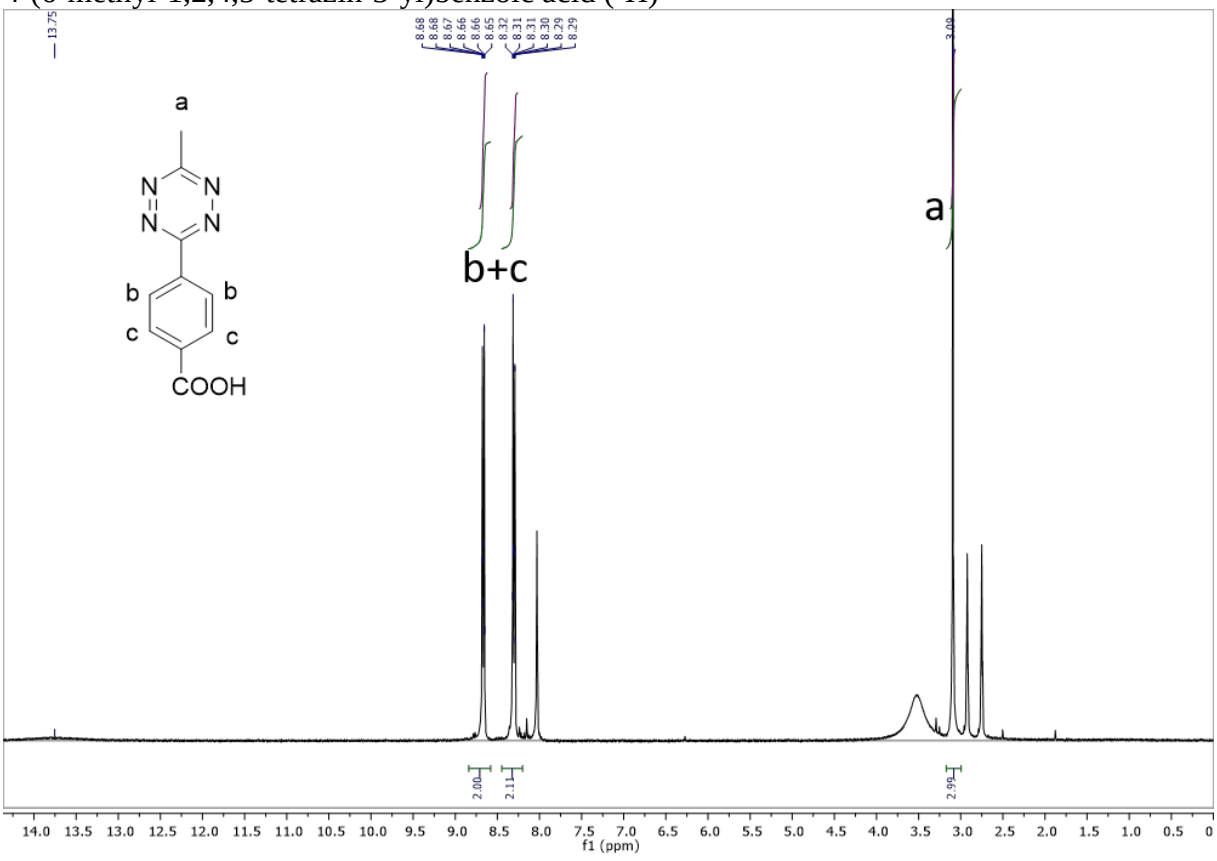

4-(6-methyl-1,2,4,5-tetrazin-3-yl)benzoic acid (^{13}C)

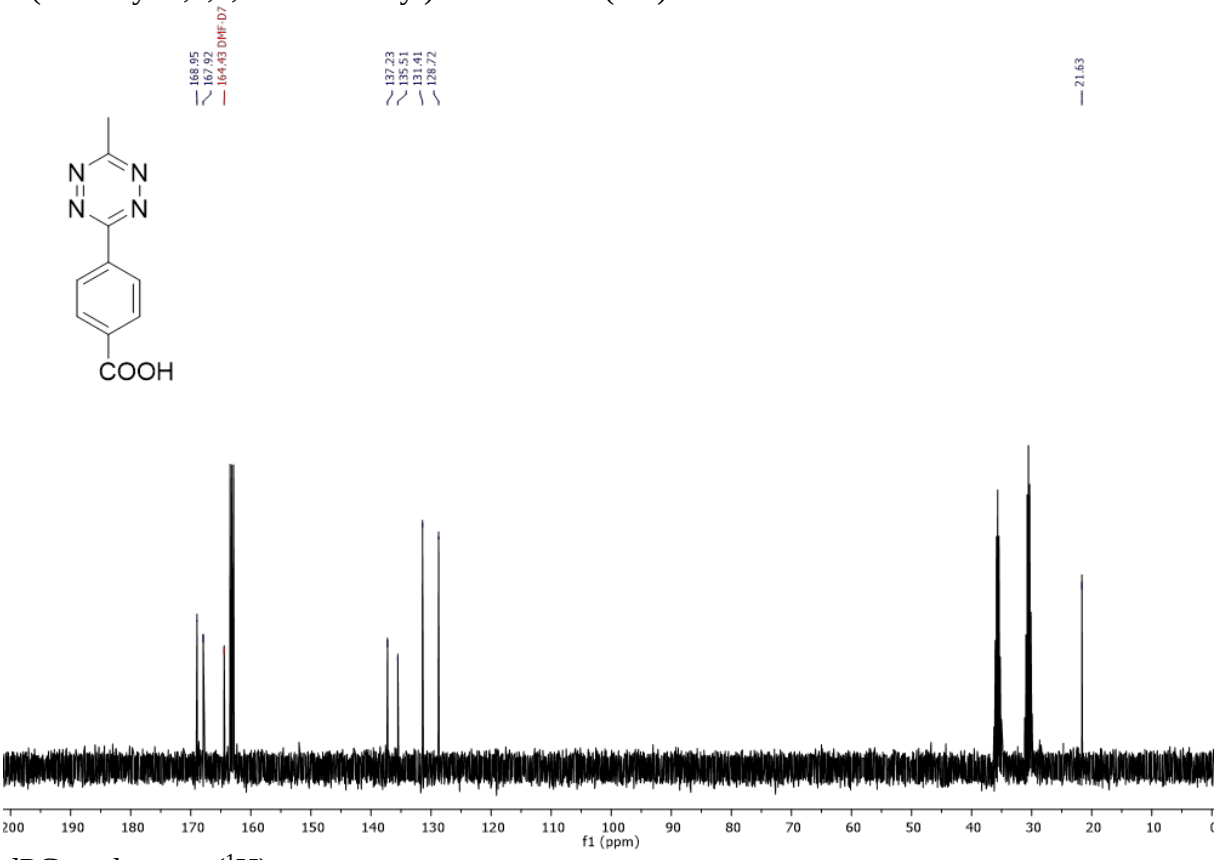

dPG-norbonene (^{1}H)

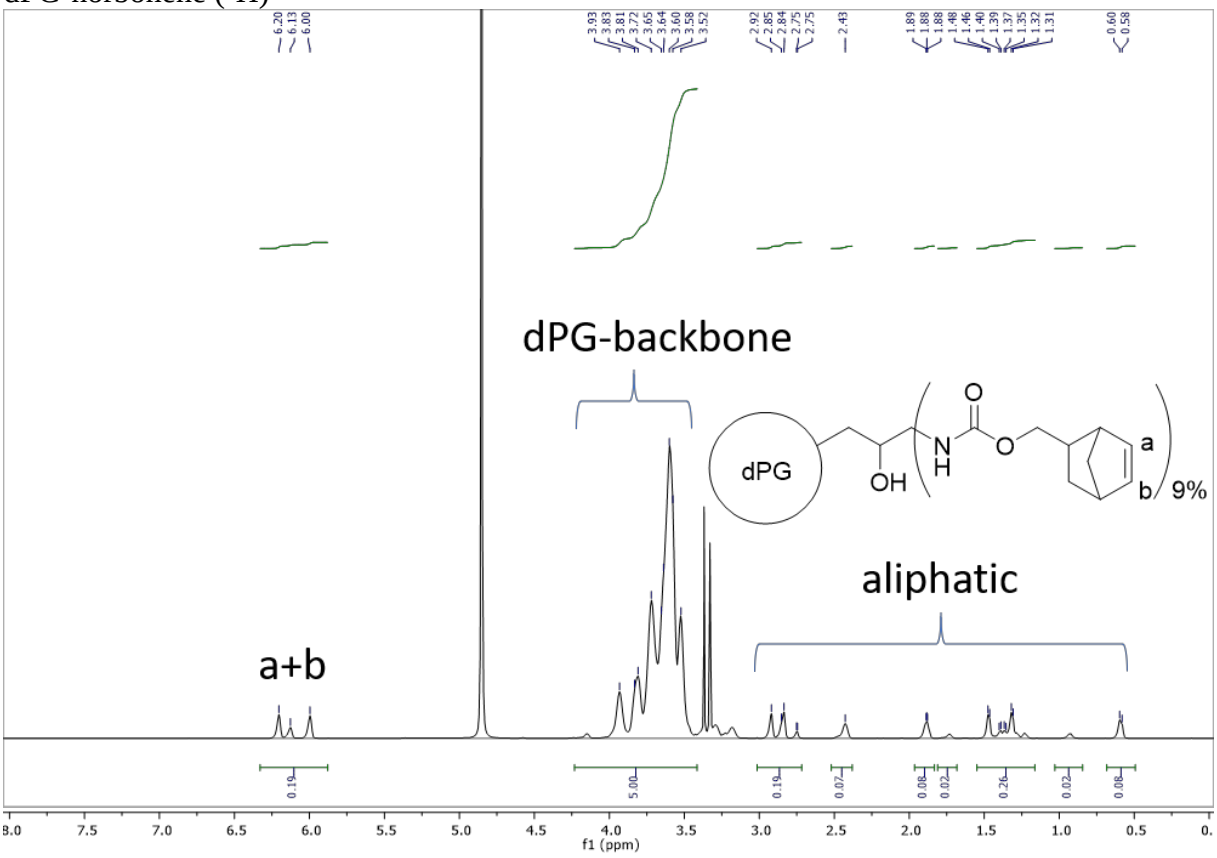

dPG-norbonene (^{13}C)

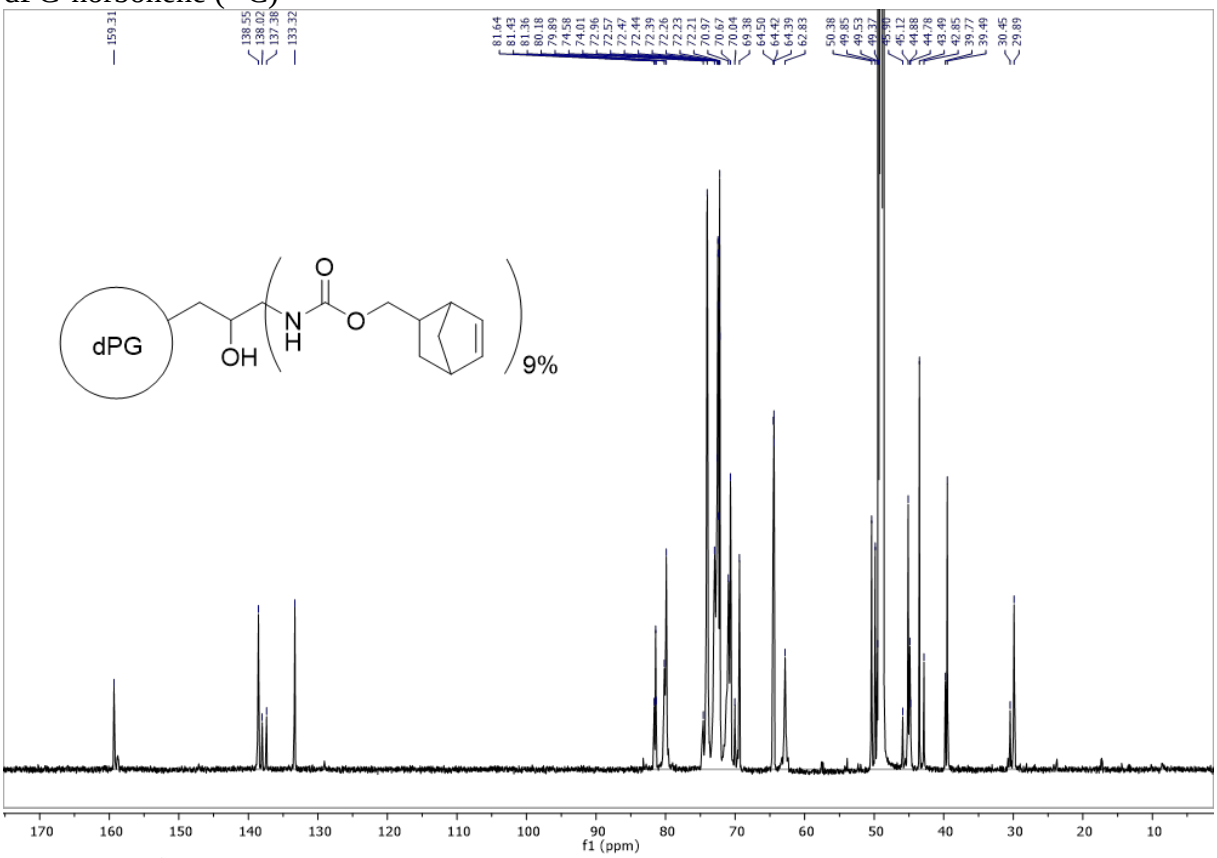

dPG-BCN (^{1}H)

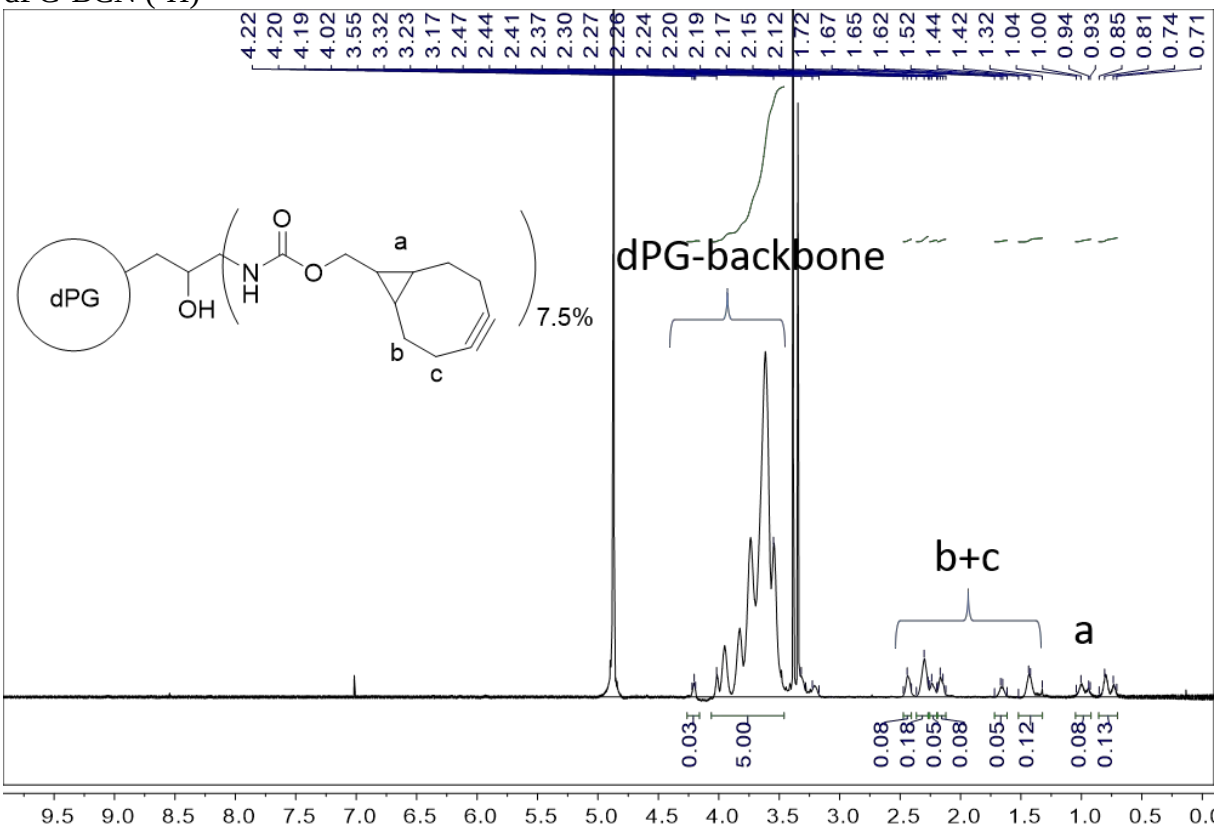

dPG-BCN (^{13}C)

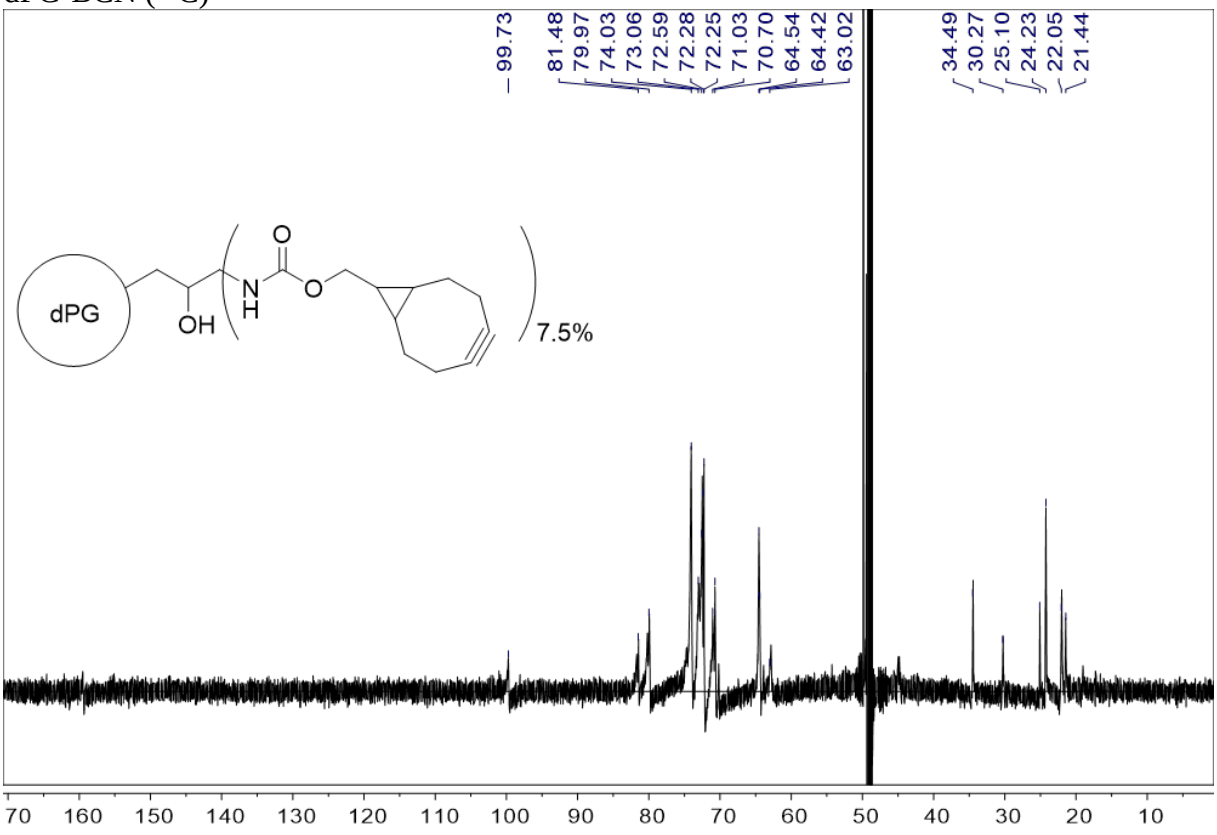

dPG-metTet (^{1}H)

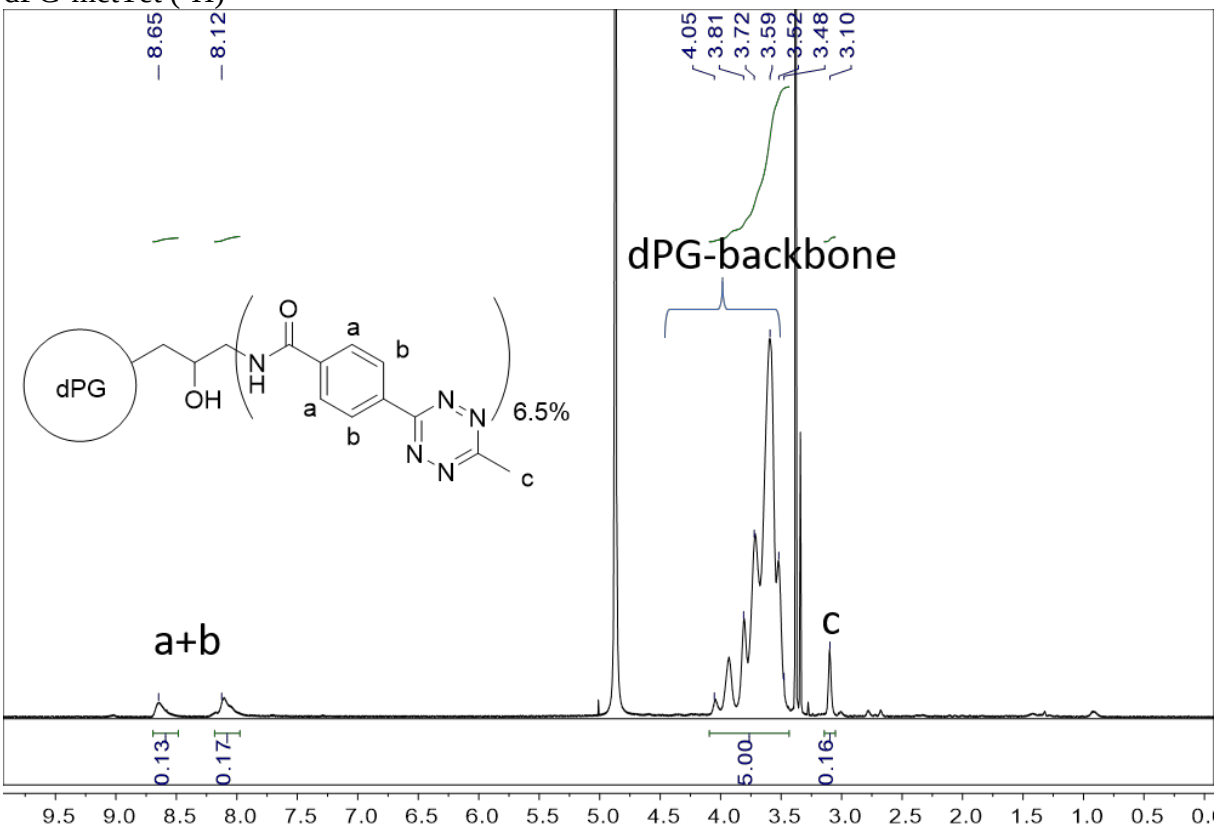

dPG-metTet (^{13}C)

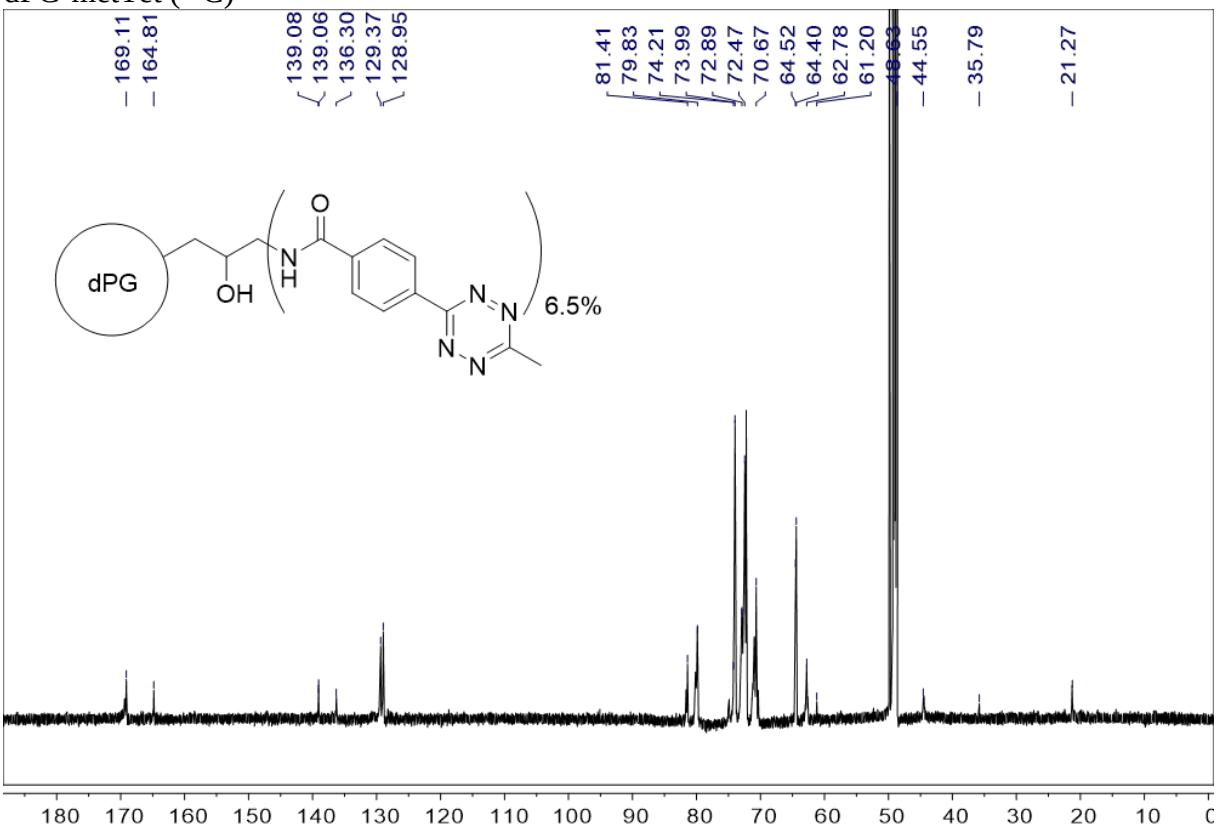

dPG-cyclopropene (^{1}H)

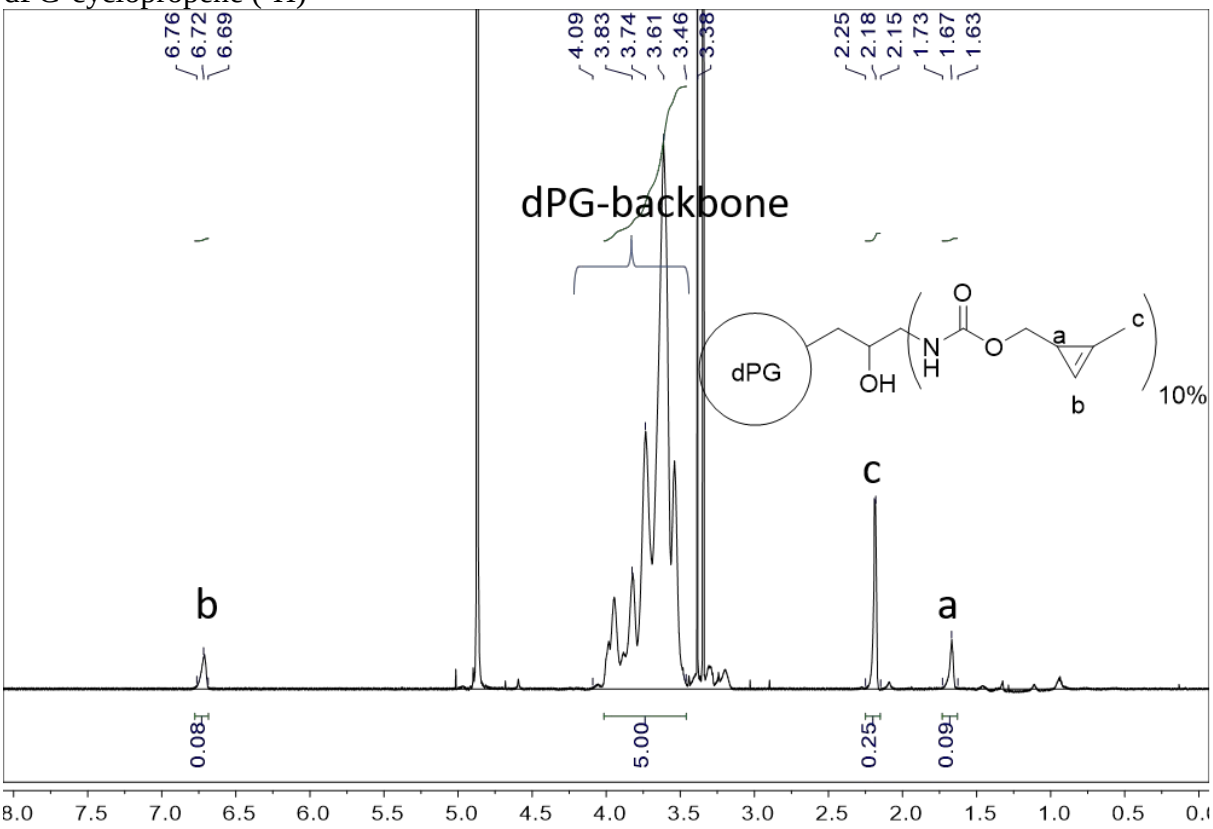

dPG-cyclopropene (^{13}C)

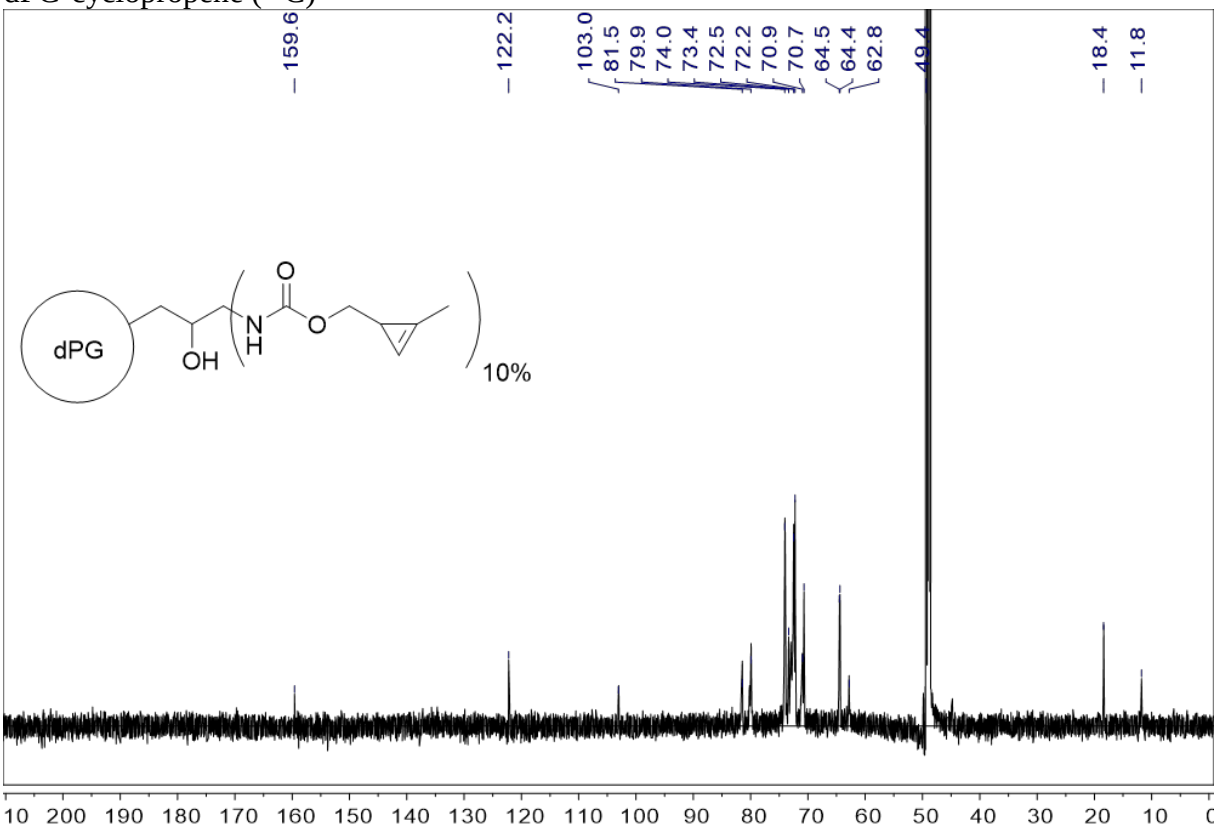

References

[1] J. Dommerholt, S. Schmidt, R. Temming, L. J. a Hendriks, F. P. J. T. Rutjes, J. C. M. Van Hest, D. J. Lefeber, P. Friedl, F. L. Van Delft, *Angew. Chemie - Int. Ed.* **2010**, *49*, 9422–9425.

[2] J. Yang, J. Šečkute, C. M. Cole, N. K. Devaraj, *Angew. Chemie - Int. Ed.* **2012**, *51*, 7476–7479.

[3] D. M. Patterson, L. A. Nazarova, B. Xie, D. N. Kamber, J. A. Prescher, *J. Am. Chem. Soc.* **2012**, *134*, 18638–18643.

[4] M. R. Karver, R. Weissleder, S. A. Hilderbrand, *Bioconjug. Chem.* **2011**, *22*, 2263–2270.

[5] A. Sunder, R. Hanselmann, H. Frey, R. Mülhaupt, *Macromolecules* **1999**, *32*, 4240–4246.

[6] S. Roller, H. Zhou, R. Haag, *Mol. Divers.* **2005**, *9*, 305–316.

3.2 Synthesis of pH-Degradable Polyglycerin-Based Nanogels by iEDDA-Mediated Crosslinking for Encapsulation of Asparaginase Using Inverse Nanoprecipitation

Alexander Oehrl, Sebastian Schötz, Rainer Haag, *Colloid Polym. Sci*, submitted

Abstract

Biocompatible, environmentally responsive, and scalable nanocarriers are needed for targeted and triggered delivery of therapeutic proteins, such as the anticancer protein asparaginase are needed. For this purpose, suitable polymer scaffolds, preparation methods and crosslinking chemistries have to be considered. Good options include, biocompatible dendritic polyglycerol (dPG) as the polymer, the mild surfactant-free inverse nanoprecipitation method for nanogel preparation, and the fast, bioorthogonal, and scalable inverse electron demand Diels-Alder (iEDDA) as a crosslinking chemistry. In this work, the synthesis of pH-degradable nanogels, based on tetrazine, norbonene and bicyclo[6.1.0]nonyne (BCN) functionalized macromonomers is reported. Cell viability assays show the cell-compatibility of the macromonomers at concentrations of up to 2.5 mg mL^{-1} for three different cell lines. Nanogels are obtained in the size range of 47 to 200 nm and can be degraded within 48 h at pH 4.5 for the benzacetal (BA) nanogels, and at pH 3 for the tetrahydropyran (THP) based nanogels. Encapsulation of the therapeutic protein asparaginase (32 kDa) yield encapsulation efficiencies of up to 93% at 5 wt.% feed. Overall, iEDDA crosslinked pH-degradable dPG-nanogels from inverse nanoprecipitation are promising candidates for biomedical applications.

Contributions: Study design, synthesis of precursors and parts of macromonomers, synthesis and characterization of nanogels, protein encapsulation and protein determination assay, degradation studies with loaded nanogels, manuscript preparation, manuscript revision.

Synthesis of pH-Degradable Polyglycerin-Based Nanogels by iEDDA-Mediated Crosslinking for Encapsulation of Asparaginase Using Inverse Nanoprecipitation

Journal:	*Colloid and Polymer Science*
Manuscript ID	Draft
Manuscript Type:	Special issue dedicated to Prof. Ballauff
Date Submitted by the Author:	n/a
Complete List of Authors:	Oehrl, Alexander; Freie Universitat Berlin Schötz, Sebastian; Freie Universitat Berlin Haag, Rainer; Freie Universitat Berlin
Keywords:	iEDDA, nanogels, inverse nanoprecipitation, pH degradability, protein encapsulation

Synthesis of pH-Degradable Polyglycerin-Based Nanogels by iEDDA-Mediated Crosslinking for Encapsulation of Asparaginase Using Inverse Nanoprecipitation

Alexander Oehrl, Sebastian Schötz, Rainer Haag

Alexander Oehrl, Sebastian Schötz, Prof. Rainer Haag
Freie Universität Berlin, Institute for Chemistry and Biochemistry, Takustr. 3, D-14195 Berlin, Germany
E-mail: haag@chemie.fu-berlin.de
ORCID: 0000-0003-3840-162X

Keywords: iEDDA, nanogels, inverse nanoprecipitation, pH degradability, protein encapsulation

Abstract

Biocompatible, environmentally responsive, and scalable nanocarriers are needed for targeted and triggered delivery of therapeutic proteins. Suitable polymers, preparation methods and crosslinking chemistries must be considered for nanogel formation. Biocompatible dendritic polyglycerol (dPG) is used in the mild, surfactant-free inverse nanoprecipitation method for nanogel preparation. The biocompatible, fast, and bioorthogonal inverse electron demand Diels-Alder (iEDDA) crosslinking chemistry is used. In this work, the synthesis of pH-degradable nanogels, based on tetrazine, norbonene and bicyclo[6.1.0]nonyne (BCN) functionalized macromonomers is reported. The macromonomers are non-toxic up to 2.5 mg mL^{-1} in three different cell lines. Nanogels are obtained in the size range of 47 to 200 nm and can be degraded within 48 h at pH 4.5 (BA-gels), and pH 3 (THP-gels), respectively. Encapsulation of asparaginase (32 kDa) yield encapsulation efficiencies of up to 93% at 5 wt.% feed. Overall, iEDDA crosslinked pH-degradable dPG-nanogels from inverse nanoprecipitation are promising candidates for biomedical applications.

Funding: SFB 765; Deutsche Forschungsgemeinschaft (DFG)

1. Introduction

Modern medicine has a high demand for new and smart nanocarrier systems for drug delivery, that improve pharmacokinetics, permit the use of less overall drug, thus reduce side effects, lead to prolonged drug circulation time, and can deliver their cargo specifically to diseased tissue and not to healthy tissue.[1] Additionally, these carrier systems must be biocompatible and either biodegradable or be easily excreted by the body after delivering their cargo.[2, 3] Any degradation products and metabolites must be non-toxic. Attempts have been made to design such nanocarriers for a variety of drugs. In the class of hydrophobic drugs there are already some examples on the market, such as liposomal formulations of the anticancer drugs doxorubicin (Doxil®) and daunorubicin (DaunoXome®), and micellar estradiol (Estrasorb™)[4]. However, liposomal formulations cannot be considered smart or responsive carriers, as they lack the structural properties to respond to external stimuli. For the more sensitive drugs, such as therapeutic proteins, liposomal formulations are not very suitable. The detergent nature of the liposomes can disrupt the natural folding of the proteins and thus lead to a loss of function. However, especially this type of drug needs improved delivery systems. Proteins are usually injected intravenously to the body, due to low stability in the strongly acidic environment of the stomach or due to very low absorption within the small intestine.[5] In the blood stream, the mononuclear phage system (MPS), a part of the immune system, effectively removes foreign substances from the body. Proteins are easily recognized by the MPS and are thus eliminated quite fast.[4, 6, 7] Apart from the MPS, small proteins are also excreted via the kidney if their molecular weight is below the renal threshold of 45 kDa or hydrodynamic diameter of 5.5 nm.[8–10] This shows, that nanocarriers are needed for protein delivery, which are able to increase the total molecular weight of the therapeutics to prolong circulation times

and offer evasion from the MPS clearance. Currently, the only type of carriers that fulfill these criteria and are on the market, are polyethylene glycol (PEG) protein conjugates. PEG is a hydrophilic and size-tunable, biocompatible polymer that is attached randomly, or site specific to the protein. This increases the total molecular weight above the renal threshold and leads to increased circulation times and reduced clearance through the MPS.[11–13] However, recently PEG has shown to be able to induce immune responses in some patients, leading to reduced effectivity of the treatment.[14, 15] Furthermore, targeted delivery is not possible with PEG conjugation and can also reduce the activity of the protein that it is conjugated to. Thus, alternatives that provide the same advantages as PEG, but additionally also allow for a targeted delivery and release of the protein are needed.

Alternatively nanogels consist of hydrophilic polymer networks in the size range of 10 to 1000 nm and offer a hydrophilic environment that shields any cargo encapsulated inside.[16–21] The properties of these gels can be tuned, based on the polymers that are used for the network formation. A variety of options exist and have been intensively studied. Natural polymers such as e.g. alginate[22], dextran[23] and chitosan[24] have been used for nanogel preparation. However, synthetically easily accessible polymers such as PEG[25], copolymers of polylactic and glycolic acid (PLA/PLA-co-PGA)[26], linear polyglycerol (lPG)[27] and dendritic polyglycerol (dPG)[27–30] have also been successfully used for nanogel formation. The introduction of environmentally responsive groups, such as pH-sensitive acetals[31–33], or redox-sensitive disulfides[16, 34] can then be used for the preparation of degradable nanogels. For example, within endosomes and lysosomes, the pH value drops to values between 4 and 6.[35]

Beside network material, the preparation method also has ab big influence on the suitability of the carrier for biomedical applications. Nanogels have been prepared by methods such as micro- and miniemulsion polymerization.[23, 36–38] However, the use of surfactants,

heat, and ultrasound can be detrimental for the encapsulation of sensitive biotherapeutics. Furthermore, surfactants are sometimes hard to remove and can have a negative impact on cell viability and applicability in vitro and in vivo.

Technologies such as the nanoprecipitation method, where nanoparticles are formed by precipitation in their corresponding non-solvent water have been adjusted to hydrophilic macromonomers.[39–42] This inverse nanoprecipitation leads to hydrophilic nanogels by precipitation of the macromonomers in solvents like acetone. Thus, very mild conditions for the encapsulation of proteins are present, as no surfactants or ultrasound are used.[28, 30]

For the inverse nanoprecipitation method, usually macromonomers are used, that crosslink in situ during the precipitation process. In order to have a reasonably fast gelation, the type of crosslinking chemistry plays a major role for successful preparation of nanogels. Suitable chemistries include the click-type copper catalyzed azide alkyne cycloaddition (CuAAC)[30], the strain promoted version of CuAAC (SPAAC)[27], Thio-Michael addition[43], and inverse electron demand Diels-Alder (iEDDA). CuAAC is suitable for gel formation, however, the toxic copper ions are hard to remove and can have toxicity in vivo. Thio-Michael addition is fast and scalable, however, not suitable for proteins containing thiols, as a cross-reactivity exists. SPAAC offers a fast gelation, as well as very low cross-reactivity with free thiols. However, the synthetic precursors are expensive and exhibit low yielding, long synthetic procedures. In contrast, iEDDA reactions between tetrazine derivatives and dienophiles are so fast and bioorthogonal[44–47], that they have been used for fluorescent labeling of antibodies,[48] DNA-tagging,[49] and even cell labeling.[50] The synthetic precursors are inexpensive and prepared in a straightforward manner. Depending on the application, one can choose between different reactivities and thus gelation times. As there are no side reactions with biological systems, this method is one of the most bioorthogonal reactions available so far. Furthermore, no toxic catalysts, such as copper ions are needed,

which makes iEDDA a very promising coupling strategy for the preparation of biocompatible nanogels.

We present the synthesis of new pH-cleavable macromonomers based on the biocompatible and easy to functionalize dPG[12, 51–53] with methyl-tetrazine and the dienophiles norbonene and bicyclo[6.1.0]non-4-yne (BCN) as iEDDA reactive functional groups. pH-degradability is introduced by incorporation of benzacetal (BA) and tetrahydropyran-based (THP) acetals into the macromonomers which cleave at pH values of 5 and 3, respectively. The macromonomers are characterized by NMR, IR and DLS and tested regarding their ability to form stable nanogels during inverse nanoprecipitation in acetone under various reaction conditions. dPG-BA-norbonene and dPG-THP-norbonene are used for encapsulation of the therapeutic protein asparaginase with excellent encapsulation efficiencies of up to 93%. The BA-based gels are cleaved completely within 48 h at pH 4.5, while the THP-based gels were degraded at pH 3 within 48 h. The macromonomers were tested in a cell viability assay with three different cell lines and did not show toxicity up to about 2.5 mg mL^{-1}.

The fast and efficient synthetic route to pH-cleavable macromonomers with iEDDA reactive groups, as well as the stable and scalable nanogels that are obtained from them, while avoiding the drawbacks of toxic catalysts or side reactivity in other crosslinking strategies, makes this a nanocarrier system with potential biomedical application.

2. Materials and Methods

2.1 Materials

Ethyl acetate, *n*-pentane and diethyl ether were obtained from the technically pure solvents by distillation before use. Dry DCM and THF were used from a SPS-800 type MBRAUN solvent drying system. Acetone and DCM (HPLC grade) were used without further purification. Dry methanol and DMF were purchased from Acros and Fischer Chemical. All other chemicals and deuterated solvents were obtained from Sigma Aldrich, Acros, Merck, and Fisher Chemicals and were used as without further purification. Thin layer chromatography (TLC) was performed on silica gel-coated aluminum plates, serving as stationary phase (silica gel 60 F254 from Macherey-Nagel). Identification of analytes was done by UV-irradiation (λ = 254 nm) of the TLC plates or by treatment with a potassium permanganate-based (100 mL deionized water, 200 mg potassium permanganate) or anis aldehyde-based staining solution (450 mL EtOH, 25 mL anis aldehyde, 25 mL conc. sulfuric acid, 8.0 mL acetic acid). Column chromatography was performed with silica gel (Macherey-Nagel, grain size 40 - 63 µm, 230 - 400 mesh) as stationary phase and the indicated eluent mixtures as the mobile phase.

2.2 Analytical Methods

IR spectra were recorded on a JASCO FT/IR-4100 spectrometer. The characteristic absorption bands are given in wave numbers. ^{1}H NMR spectra were recorded at 300 K on Joel ECX 400 400 MHz and AVANCE III (700 MHz) instruments. Chemical shifts δ are indicated in parts per million (ppm) relative to tetramethyl silane (0 ppm) and calibrated as an internal standard to the signal of the incompletely deuterated solvent ($CDCl_3$: δ = 7.26 ppm, MeOD: δ = 3.31 ppm). Coupling constants J are given in Hertz (Hz). ^{13}C NMR spectra were recorded at 300 K on AVANCE III instruments (176 MHz). Chemical shifts δ are given in ppm relative to tetramethyl silane (0 ppm) and calibrated as an internal standard to the signal of the

incompletely deuterated solvent ($CDCl_3$: δ = 77.16 ppm, MeOD: δ = 49 ppm). Coupling constants J are given in Hertz (Hz). The spectra are decoupled from proton broadband. DLS and Zeta potential were measured on a Malvern zeta- sizer nano ZS 90 with He–Ne laser (λ = 532 nm) at 173° backscatter and automated attenuation at 25 °C. Three measurements were performed per sample, yielding a mean size value plus standard deviation. Sample concentration was kept at 1 mg mL^{-1}. GPC was performed on an Agilent 1100 at 5 mg mL^{-1} using a pullulan standard, 0.1 M NaNO3 solution as eluent and a PSS Suprema column 10 µm with a flow rate of 1 mL min^{-1}. Signals were detected with an RI detector.

2.3 Precursors and Macromonomers

All air- and moisture-sensitive reactions were carried out in flasks in an inert atmosphere (argon) using conventional Schlenk techniques. Reagents and solvents were added *via* argon rinsed syringes. Solids were added in argon counterflow as solutions in the corresponding solvent.

The synthesis of the literature known precursors is described in the Supporting Information, showing the modified procedures.

2-(azidomethyl)-3,4-dihydro-2H-pyran (5)

(3,4-dihydro-2H-pyran-2-yl)methanol (1.58 g, 13.84 mmol) and Et_3N (2.10 g, 20,76 mmol, 2.88 mL) were dissolved in DCM (25 mL). Methane sulfonyl chloride (1.74 g, 15.23 mmol, 1.18 mL) was added dropwise *via* syringe. The solution was stirred for 45 minutes at 0 °C. Saturated aqueous $NaHCO_3$-solution was added, phases were separated, and the aqueous phase was extracted with DCM (3x25 mL). The combined organic layers were dried with Na_2SO_4. The solvent was removed under reduced pressure.

The crude product (2.84 g, 14.77 mmol) was dissolved in DMF (20 mL) and NaN_3 (9.60 g, 147.67 mmol) was added. The solution was stirred at 55 °C for three days. Water (20 mL) was added, the phases were separated, and the aqueous phase was extracted with DCM (3x25 mL). The combined organic layers were dried with Na_2SO_4. The solvent was removed under reduced pressure. The crude product was purified by column chromatography (pentan/EtOAc, 10:1) to give the product (**30**) (1.91 g, 13.76 mmol, 93 % over 2 steps) as a colorless oil.

^{1}H–NMR (400 MHz, CD_3OD): δ = 6.38 (d, *J* = 6.2 Hz, 1 H, H–olefin–O), 4.74–4.72 (m, 1 H, H–olefin), 4.01–3.96 (m, 1 H, H–tertiary), 3.48–3.32 (m, 2 H, H–CN3), 2.16– 1.58 (m, 4 H, H–ring) ppm.

dPG-THP-azide$_{5\%}$

dPG (0.12 g, 1.44 mmol) was dried under HV at 70 °C overnight and dissolved in dry DMF (10 mL). The DHP-azide (**5**) (0.02 g, 0.15 mmol) was dissolved in dry DMF (5 mL) and added to the dPG–solution *via* syringe and *p*-TSA (1.90 µg, 0.01 mmol) was added. The resulting solution was stirred at room temperature overnight. After quenching with a small excess of NEt_3 the crude product was constricted under reduced pressure and dialyzed against H_2O and methanol 1:1 for 4 days and methanol for 3 days (MWCO = 1 kDa). The product was obtained as methanolic solution (5.0% functionalization, 85%).

^{1}H–NMR (700 MHz, CD_3OD): δ = 4.59–4.53 (m, 1 H, H–$C_2H_2N_3$), 4.21–14 (m, 1 H, H–C_2H_2–carbamate), 4.04 (dPG – backbone), 3.33–3.20 (m, 2 H, H–C–carbamate), 1.99–1.39 (m, 6 H, H–ring) ppm.

^{13}C–NMR (176 MHz, CD_3OD): δ = 101.4, 80.0, 79.9, 79.5, 79.3, 79.1, 74.1, 74.0, 72.6, 72.5, 72.2, 70.7, 70.67, 64.5, 64.4, 33.1, 29.1 ppm.

IR (ATR): $\tilde{\nu}$ = 3375, 2919, 2871, 2357, 2332, 2099, 1649, 1450, 1324, 1300, 1261, 1067 cm^{-1}.

EA ($C_{66}H_{31}N_3O_{42}$): calc. C (48.37%), found C (49.46%); calc. N (2.56%), found N (2.62%), calc. H (8.06%), found H (8.47%).

dPG-THP-amine$_{5\%}$

The dPG-THP-azide (1.67 g, 22.21 mmol, 1.13 mmol azide) was dissolved in THF (70 mL). Distilled water (80 mL) and PPh_3 (3.50 g, 13.33 mmol) were added and the solution was stirred for seven days at room temperature. THF was removed under reduced pressure and the crude product was filtered. The filtrate was constricted under reduced pressure. The crude product was dialyzed against methanol for 5 days (MWCO = 1 kDa). The product was obtained as a methanolic solution (5.0% functionalization, 95%).

^{1}H–NMR (700 MHz, CD_3OD): δ = 4.76–4.65 (m, 2 H, H–acetal), 4.24–4.03 (m, 2 H, H–C2H6N), 4.00–3.43 (dPG – backbone), 2.96–2.68 (m, 2 H, H–tertiary), 2.02–1.17 (m, 6 H, H–ring) ppm.

^{13}C–NMR (176 MHz, CD_3OD): δ = 170.3, 142.7, 103.3, 81.7, 81.4, 80.2, 79.9, 73.98, 74.0, 73.0, 72.4, 72.2, 71.0, 70.7, 70.7, 64.5, 64.4, 62.8, 49.4 ppm.

IR (ATR): $\tilde{\nu}$ = 3359, 2913, 1871, 2380, 1650, 1456, 1327, 1067, 1030, 931, 866. 748 cm $^{-1}$.

General Procedure for dPG-dienophiles

All dPG-dienophiles were synthesized according to the same general procedure. As an example, dPG-BA-norbonene is described in detail.

dPG-BA-norbonene$_{8\%}$ (MM4)

Dry DMF (7.50 mL) was added to a methanolic solution of dPG–benzacetal-amine (10.00 mL, 0.062 g/mL). Methanol was removed under reduced pressure. Fresh dry DMF (7.50 mL) was added, the solution was constricted under reduced pressure to 15 mL and Et3N (0.18 g, 1,83

mmol, 0.25 mL) was added. Norbonene active carbonate (**2**) (0.19 g, 0.67 mmol) was dissolved in DMF (10 mL) and the solution was added dropwise *via* syringe to the dPG – amine solution. The resulting reaction mixture was stirred at room temperature overnight. The crude product was dialyzed against a mixture of water and acetone (1:1) and methanol for 4 days (MWCO = 1 kDa). The product was obtained as a yellow methanolic solution (88%, 7.5 % functionalization).

^{1}H–NMR (700 MHz, CD_3OD): δ = 7.49–7.35 (m, 2 H, H–aromatic), 7.02–6.88 (m, 2 H, H–aromatic), 6.20–6.06 (m, 1 H, H–olefin), 5.99–5.84 (m, 1 H, H–olefin), 5.78–5.68 (m, 1 H, H–acetal), 4.63–4.54 (m, 2 H, H–C–carbamate), 4.47–4.22 (m, 2 H, H–C–OPh), 4.11–3.44 (dPG – backbone), 3.32–3.28 (m, 2 H, H–C–NH), 2.91–2.85 (m, 1 H, H– ring), 2.85–2.80 (m, 1 H, H–ring), 2.03–1.94 (m, 2 H, H–ring), 1.90–1.82 (m, 1 H, H– ring), 1.42–1.14 (m, 2 H, H–aliphatic) ppm.

^{13}C–NMR (176 MHz, CD_3OD): δ = 161.4, 161.2, 159.2, 138.6, 138.0, 137.4, 133.3, 129.6, 129.3, 115.4, 105.6, 104.9, 81.4, 80.2, 79.9, 76.6, 74.1, 74.0, 73.0, 73.0, 72.6, 72.5, 72.4, 72.2, 71.0, 70.8, 69.2, 68.6, 66.7, 64.5, 64.4, 62.8, 50.4, 45.9, 45.1, 43.5, 42.8, 39.5, 38.9, 30.8, 30.4, 29.9 ppm. 48

IR (ATR): $\tilde{\nu}$ = 3374, 2871, 1696, 1614, 1517, 1458, 1394, 1327, 1304, 1244, 1075, 977 cm-1.

EA ($C_{847}H_{1475}N_{13}O_{440}$): calc. C (53.88%), found C (53.29%); calc. N (0.96%), found N (1.94%); calc. H (7.87%), found (8.21%).

dPG-THP-norbonene$_{5\%}$ (MM6)

DMF (10 mL), dPG-THP-NH_2 (440 mg, 0.3 mmol NH_2), NEt_3 (170 µL, 3 eq), BCN (132 mg, 0.42 mmol) in DMF (3 mL). The product was stored as the methanolic solution in the freezer (5%, 91%).

^{1}H–NMR (700 MHz, CD_3OD): δ = 6.23–6.02 (m, 2 H, H-olefin), 3.95–3.54 (m, dPG–backbone, 2.94–0.61 (m, 6 H, aliphatic-H).

^{13}C–NMR (176 MHz, CD_3OD): δ = 159.23, 138.54, 133.31, 98.72, 81.64, 81.43, 80.16, 79.89, 73.99, 72.96, 72.46, 72.23, 70.98, 70.68, 69.33, 64.42, 62.83, 50.37, 49.85, 45.12, 43.49, 42.86, 39.79, 39.50, 30.62, 29.88, 29.06, 24.55, 18.79.

dPG-THP-BCN$_{5\%}$ (MM7)

DMF (10 mL), dPG-THP-NH_2 (440 mg, 0.3 mmol NH_2), NEt_3 (170 µL, 3 eq), BCN (144 mg, 0.45 mmol) in DMF (3 mL). The product was stored as the methanolic solution in the freezer (5%, quantitative).

^{1}H–NMR (700 MHz, CD_3OD): δ = 3.96–3.55 (m, dPG–backbone), 2.44–0.73 (m, 11 H, aliphatic-H-BCN).

^{13}C–NMR (176 MHz, CD_3OD): δ = 157.96, 98.28, 80.25, 80.04, 78.82, 78.51, 72.62, 71.58, 71.07, 70.84, 69.61, 69.30, 67.87, 63.11, 63.03, 61.43, 48.46, 33.07, 28.85, 28.04, 23.72, 22.84, 20.63, 20.05, 17.62, 17.40.

2.4 Inverse Nanoprecipitation of Macromonomers

General Procedure: The ratio of macromonomer A (dPG-metTet) to macromonomer B (dPG-dienophile) was set to 1:1.5. Acetone was used as the non-solvent. Parameters, such as solvent to non-solvent ratio (1:20 – 1:80) and water quenching time $T_{q,\,water}$ (0 – 120 min) were varied according to the tables described in the results and discussion section. As an example, a general procedure for one set of parameters is described in detail below.

Macromonomers A and B were stored as stock-solutions of 100 to 150 mg mL^{-1} in water. Aliquots were taken and separately diluted with water to a final volume of 1 mL. For this, 15 µL of macromonomer A were diluted with 485 µL water and 22.5 µL of macromonomer B with 477.5 µL water. Both solutions were cooled in an ice bath to 4 °C. Macromonomer A solution was added fast to solution B and vortexed for 5 seconds. Then, the solution was added fast *via*

syringe to a 60 mL glass vial containing magnetically stirred acetone (40 mL) at 1200 rpm. The turbid dispersion was stirred for another 2 seconds and then kept still for 10 min. The reaction was then quenched by the addition of 20 µL of 2-(vinyloxy)ethan-1-ol. Water (1/3 of acetone) was added after 30 min and the acetone was removed under reduced pressure. Purification was performed by centrifugal filtration, using a membrane with a cutoff of 1 MDa and 3 consecutive washing steps with 10 mL distilled water/PBS buffer each. Nanogels were obtained as stable dispersions in water and characterized using DLS, NTA, and Zeta-potential measurements.

2.5 Coprecipitation of Asparaginase

The inverse nanoprecipitation was performed as described in Section 2.4. 225 µL of a 1.11 mg/mL stock solution of asparaginase were added to the dPG-metTet macromonomer solution and thoroughly mixed. The total volume of water was kept at 1 mL. 5 wt.% of asparaginase were encapsulated each for dPG-norbonene-, dPG-BA-norbonene and dPG-THP-norbonene-NGs (n = 3). The gels were purified by centrifugation filtration, using filters with a molecular weight cut-off of 1 MDa at 234 rcf. The gel volume was reduced to 1 mL and fresh PBS buffer was added (10 mL). Then the volume was reduced to 1 mL again and the whole process was repeated three times to ensure the complete removal of the non-encapsulated protein.

2.6 Protein Content Determination Assay

A standard Pierce BCA assay kit was used for the determination of asparaginase content within the nanogels. 25 µL of the purified nanogels were added to a 96-well plate. Then 200 µL of working reagent was added to each well and the plate was shaken for 30 seconds on a plate

shaker. The plate was then incubated at 37 °C for 1 h. After cooling to room temperature, the absorbance was measured at 562 nm on a plate reader. Samples were recorded in triplicates and for three independent gels of the same type. Calibration curves were prepared for a dilution series of albumin and asparaginase in the range of 0 to 1000 µg mL^{-1}. Concentrations of asparaginase in the samples were determined *via* the fitted standard curves of asparaginase (**Figure S4**).

2.7 Degradation of Nanogels

For the continuous degradation experiments, 100 µL of 2 mg/mL were diluted with buffer to 200 µL total volume. For each pH value a different buffer was used. In case of pH 7.4, a 10 mM PBS buffer, in case of pH 4.5 10 mM acetate buffer and in case of pH 3 the same acetate buffer with addition of 1M HCl were used.

The solutions were placed in a disposable UV-cuvette and measured continuously with a Malvern zeta- sizer nano ZS 90 with He–Ne laser (λ = 532 nm) at 173° backscatter and automated attenuation at 25 °C for 16 h.

For nanogels with protein content 333 µL of 1.1 mg/mL nanogel dispersion were diluted with 500 µL of the buffer solutions and agitated continuously with a vortex at lowest agitation speed for 48 h. At 30 min, 1 h, 3 h, 5 h, 8 h, 24 h, and 48 h a sample of 70 µL was taken for each pH value, snap frozen in liquid nitrogen and stored at -20 °C in the freezer. Particle size distributions were measured for each time point and pH value using a Malvern zeta- sizer nano ZS 90 with He–Ne laser (λ = 532 nm) at 173° backscatter and automated attenuation at 25 °C. A mean of three measurements is reported.

2.8 Cell Viability Assay

Cell viability was determined using a CCK-8 Kit (Sigma-Aldrich) according to the manufacturer's instructions. A549, HeLa and MCF-7 cells were obtained from Leibniz-Institut DSMZ - Deutsche Sammlung von Mikroorganismen und Zellkulturen GmbH and cultured in DMEM (A549 cells) or RPMI 1640 (HeLa and MCF-7 cells) supplemented with 10% (v/v) FBS, 100 U/mL penicillin and 100 µg mL^{-1} streptomycin.

A549, HeLa and MCF-7 cells were seeded in a 96-well plate at a density of 5 x 10^4 cells/mL in 90µl DMEM/RPMI Medium per well over night at 37°C and 5% CO_2. 10 µL of dPG-metTet or dPG-dienophile (solved in deionized water) were added in serial dilutions including positive (1% and 0,1% SDS) and negative controls (cell culture medium and 10% H_2O in cell culture medium) and incubated for another 24 h at 37°C and 5% CO_2.

For background subtraction, also wells containing no cells but only sample were used. After 24h incubation the CCK8 solution was added (10 µL/well) and absorbance (450nm/650nm) was measured after approximately 3 h incubation of the dye using a Tecan plate reader (Infinite pro200, TECAN-reader Tecan Group Ltd.).

Measurements were performed in triplicates and repeated three times. The cell viability was calculated by setting the non-treated control to 100% and the non-cell control to 0% after subtracting the background signal using the Excel software.

3. Results and Discussion

3.1 Synthesis of Precursors and Macromonomers

The synthetic accessibility of macromonomers and precursors for nanogel formation is quite important, as any useful application needs scalable and high yielding reactions. For the inverse nanoprecipitation itself a highly efficient and bioorthogonal crosslinking chemistry is needed. The iEDDA crosslinking chemistry we used, provides the efficient and fast reaction to produce nanogels in a reliable fashion. The synthetic focus of this work thus lies on the synthetic description of the pH-cleavable THP linker that was used, to our knowledge, for the first time and the different macromonomers that were obtained from the dPG-benzacetal- and dPG-THP-amine cores.

The second most important property for a biological application is the biocompatibility of the synthetic polymers that are used. Dendritic polyglycerol is a platform for straightforward post-modification and has already been shown to be biocompatible.[54] The polymer itself can be obtained on a multigram to kilogram scale and is easy to functionalize either directly *via* the hydroxyl groups or by a short reaction sequence that leads to the dPG-amine derivative. This dPG-amine can then be reacted with a large variety of molecules to further introduce functionality to the polymer. In this way many different non-degradable macromonomers for iEDDA can be generated in a straightforward and scalable fashion.

The synthetic routes for the activated carbonates of the dienophiles (**1** + **2**), the methyl tetrazine carboxylic acid (**3**), the benzacetal-azide precursor (**4**) and the DHP-azide (**5**) can be found in **Scheme S1** in the Supporting information. These precursors were then used to functionalize dPG, as well as dPG-amine to the corresponding macromonomers that were used in this work. The synthetic routes are described in **Scheme 1**.

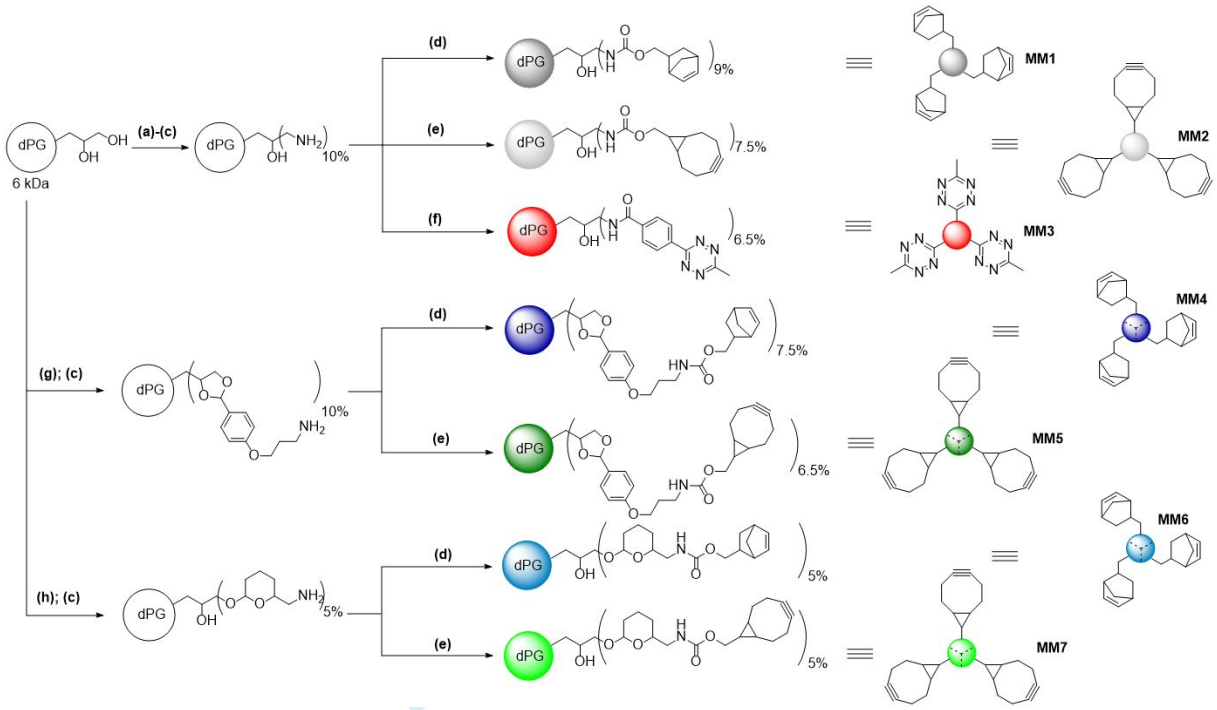

Scheme 1 Synthetic overview for the different macromonomers. The following conditions were used: (a) MsCl, NEt_3, DMF, rt, overnight, (b) NaN_3, 60 °C, 3 d, (c) PPh_3, water/THF, rt, 3 d, (d) **1**, NEt_3, DMF, rt, overnight, (e) **2**, NEt_3, DMF, rt, overnight, (f) **5**, HATU, DIPEA, DMF, rt, overnight, (g) 1-(3-azidopropoxy)-4-(dimethoxymethyl)benzene, pTSA, DMF, 40°C, overnight and (h) **3**, pTSA, DMF, rt, overnight. Number of reactive groups not representative; just for clearness

Norbonene was chosen as the reactive dienophile because its activated carbonate form can be obtained in a high yielding two step reaction from the commercially available and quite inexpensive precursor bicyclo[2.2.1]hept-5-ene-2-carbaldehyde. The methyl tetrazine carboxylic acid (**3**) has also been shown to be easily attached to the dPG-amine core *via* simple amide bond formation and the corresponding macromonomer is stable for extended periods of time in MeOH and water.

BCN was used as a comparison to norbonene, as it can be obtained from commercial sources, although the price is quite high, and the synthetic route is low yielding and lengthy.[55] It is most commonly used in SPAAC click reactions in combination with organic azides, however it has some cross-reactivity with thiols, limiting its biorthogonality.

In order to introduce pH-degradability to the system, we chose two different types of acetal linkers between the dPG core and the dienophiles. The benzacetal (BA) linker (**4**) is known to degrade at pH values below 5 and the cyclic aliphatic acetal that is generated in macromonomers **6** and **7** can degrade at pH values below 3. Synthetically, the BA precursor was obtained in 4 steps and was directly attached to the dPG core by trans-acetalization of the terminal 1,3 diols of the polymer to form the cyclic aromatic acetal motif that can be seen in Scheme 1. The precursor for the aliphatic acetal linking groups can be obtained by modification of a common protecting group for alcohols in organic synthesis, the DHP protecting group. A slightly modified precursor is commercially available ((3,4-dihydro-2H-pyran-2-yl)methanol). This was transformed in two steps to the corresponding DHP-azide (**5**) which was then attached to the dPG-core by an acid catalyzed addition reaction.

The polymer azides that were obtained in this fashion were then reduced to the corresponding amines, using a Staudinger reduction. The dPG-acetal amines are the platform for the attachment of the activated carbonate forms of the dienophiles. These dPG-acetal-dienophiles (**MM 4 - MM7**) were obtained in high yields of 85 to >99% applying the same synthetic method for each macromonomer. This toolbox of monomers was then characterized using NMR, IR, and DLS. The degradable macromonomers were then employed to produce nanogels via inverse nanoprecipitation in acetone.

3.1 Nanogel Preparation by Inverse Nanoprecipitation

In general, the inverse nanoprecipitation method works by injection of a solution of macromonomers in a suitable solvent, such as water, into the corresponding non-solvent of said macromonomers, in this case acetone. While the water is dispersed within the acetone, the

insoluble macromonomers precipitate out of solution. First small aggregates are formed which, with time, form larger and larger conglomerates. Due to the local concentration of these macromonomers within the aggregates being high, the reaction of the dienophiles with methyl tetrazin proceeds very fast and thus leads to the crosslinking of the aggregates to form a hydrohilic nanogel network. As time proceeds, the small gel networks come into contact and crosslink further until almost all macromonomers are consumed, yielding the stable dispersions of nanogels acetone. By the addition of water, the gel formation is quenched and upon removal of acetone the nanogels are obtained as stable dispersions in water. The simplified process can be seen in **Scheme 2** with dPG-BA-norbonene and dPG-metTet as an example.

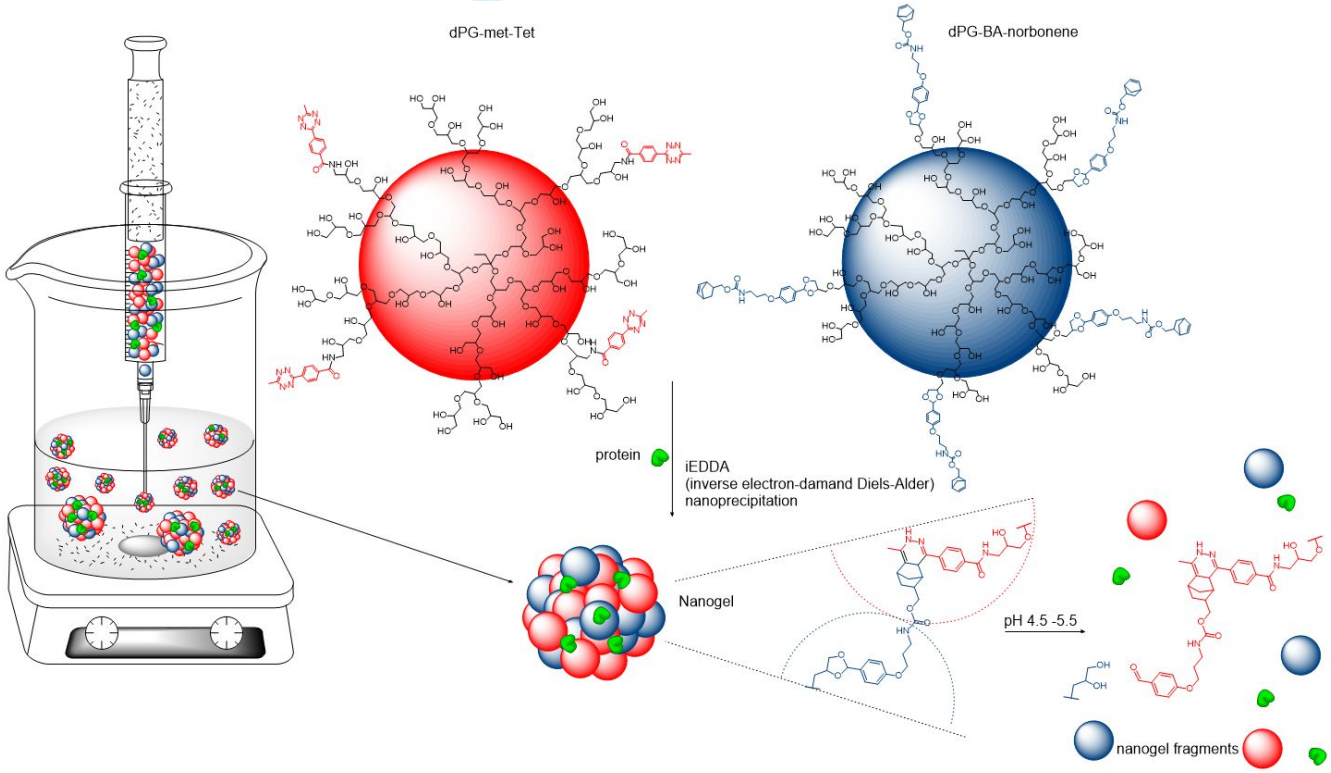

Scheme 2 Simplified overview on the inverse nanoprecipitation process, pH decrease leads to disintegration of the network and the release of the protein cargo

We studied the parameters that have the most influence on nanogel formation with this type of macromonomers. It was observed that the time when water is added to the reaction mixture and the water/acetone ratio are the most influential parameters on nanogel size.

As can be seen in **Table 1** and **Table 2** we investigated the influence of water to acetone ratios on nanogel size and polydispersity for dPG-BA-norbonene and dPG-BA-BCN nanogels, respectively.

Table 1 Influence of water to acetone ratio on the size of dPG-BA-norbonene/dPG-metTet-NGs

Entry	Macromonomer		V(H_2O): V(acetone)	Z-Average [nm]	PDI
	Ratio (A:B)	c [mg/mL]			
1	1:1.5	5	1:80[a]	102 ± 2	0.03 ± 0.01
2	1:1.5	5	1:60	120 ± 2	0.02 ± 0.01
3	1:1.5	5	1:40	91 ± 1	0.04 ± 0.02
4	1:1.5	5	1:20	62 ± 1	0.08 ± 0.01

A = dPG-metTet; B = dPG-BA-norbonene, [a] = different container used for gelation compared to other water/acetone ratios, $T_{q,\ chem}$ = 10 min, $T_{q,\ water}$ = 30 min

Table 2 Influence of water to acetone ratio on the size of dPG-BA-BCN/dPG-metTet-NGs

Entry	Macromonomer		V(H_2O): V(acetone)	Z-Average [nm]	PDI
	Ratio (A:B)	c [mg/mL]			
1	1:1.5	5	1:80[a]	94 ± 1	0.06 ± 0.01
2	1:1.5	5	1:60	147 ± 2	0.10 ± 0.01
3	1:1.5	5	1:40	88 ± 1	0.07 ± 0.01
4	1:1.5	5	1:20	47 ± 1	0.10 ± 0.01

A = dPG-metTet; B = dPG-BA-BCN, [a] = different container used for gelation compared to other water/acetone ratios, $T_{q,\ chem}$ = 10 min, $T_{q,\ water}$ = 30 min

The overall trend is summarized in **Figure 1**.

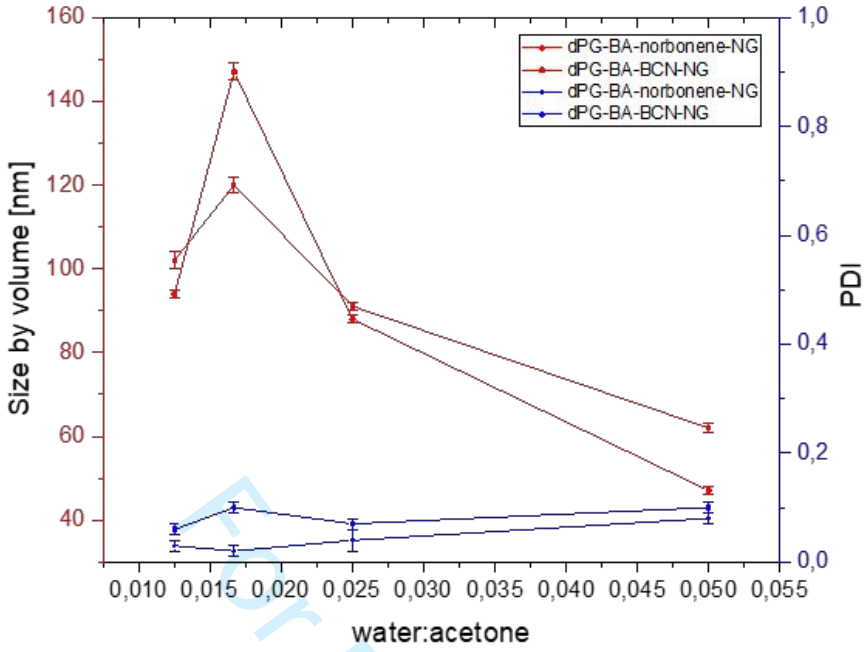

Figure 1 Size trend and polydispersity of nanogels formed from MM 4 and MM5 with varying water to acetone ratio during inverse nanoprecipitation

It is evident that there is a trend towards smaller nanogels when the ratio of water to acetone becomes bigger. This is expected, as a higher water content increases the solubility of the macromonomers in the mixture of water and acetone, thus leading to smaller aggregates in the non-solvent. The ratio of 1:80, however, is an outlier since the glass vial that was used for the experiments had a maximum volume of 60 mL. Therefore, this ratio was performed in a different glass container which influenced the nanogel formation. This trend is observed for both macromonomers indicating that the geometry of the container has an impact on gel size.

Moreover, the polydispersity of the final nanogels in water is not significantly influenced by the high ratios of water:acetone which offers the opportunity to produce small nanogels without a negative impact on the polydispersity of the gels and using relatively low amounts of organic solvent, which simplifies the overall process of nanogel production.

The second most influencing parameter we tested was the time when water was added to the mixture in order to stop any further crosslinking between already formed nanoaggregates. The results for a variety of quenching times between 4 and 60 min is shown for dPG-BA-norbonene/dPG-metTet in **Table 3.**

Table 3 Influence of water quenching time on the size of dPG-BA-norbonene/dPG-metTet-NGs

Entry	Macromonomer		$T_{q,\ water}$ [min]	Z-Average [nm]	PDI
	Ratio (A:B)	c [mg/mL]			
1	1:1.5	5	60	88 ± 1	0.04 ± 0.01
2	1:1.5	5	30	92 ± 1	0.04 ± 0.01
3	1:1.5	5	10	75 ± 1	0.20 ± 0.01
4	1:1.5	5	5	nd	nd
5	1:1.5	5	4	nd	nd

A = dPG-metTet; B = dPG-BA-norbonene, nd = measurement quality criteria not achieved due to very high polydispersity, V(H_2O):V(acetone) = 1:40, $T_{q,\ chem}$ = 10 min

One can see that immediate quenching after four- or five-minutes leads to a complete disruption of nanogel formation as the resulting gel/macromonomer mixtures were so polydisperse that they did not reach the measurement quality to report a reliable value. After ten minutes the gel seemed to have formed, however, the polydispersity was quite high compared to other batches, which indicates that at this timepoint there is still unreacted small aggregates present. After around 30 min the gel is fully formed and no significant change in nanogel size can be observed. The polydispersity, however, reaches very good values of below 0.05.

We decided to test only larger quenching times for **MM5** as it was evident that a real control over nanogel size using small quenching times was not possible. The results for quenching times between 30 and 60 min are summarized in **Table 4**.

Table 4 Influence of water quenching time on the size of dPG-BA-BCN/dPG-metTet-NGs

Entry	Macromonomer		$T_{q, water}$ [min]	Z-Average [nm]	PDI
	Ratio (A:B)	c [mg/mL]			
1	1:1.5	5	30	73 ± 1	0.08 ± 0.01
2	1:1.5	5	40	65 ± 1	0.07 ± 0.01
3	1:1.5	5	50	62 ± 1	0.10 ± 0.01
4	1:1.5	5	60	72 ± 1	0.07 ± 0.01

A = dPG-metTet; B = dPG-BA-BCN, V(H_2O):V(acetone) = 1:40, $T_{q, chem}$ = 10 min

As expected, the longer quenching times did not have an influence on nanogel size as most of the crosslinking happened in the first few minutes. However, it also showed that most of the reactive surface groups were consumed within the first hour, which prevented bigger aggregates and possibly complete precipitation of the nanogels. PDI values were also not significantly affected using these quenching times and stayed between 0.07 and 0.1.

The nanogels were obtained in a reproducible manner. We thus chose the norbonene derivative to perform co-precipitation of the therapeutic protein asparaginase.

3.2 Asparaginase Encapsulation by Coprecipitation

The protein asparaginase is used as a drug to treat acute lymphoblastic leukaemia (ALL). A PEGylated version is available on the market (Oncaspar®)[3].

5 wt.% of protein compared to the total amount of macromonomers were chosen for encapsulation, without severely impacting the polydispersity of the gels. However, the size of the nanogels almost always increased to higher values when compared to gels that were produced without the addition of a protein.

The norbonene derivatives of the macromonomers (**MM1**, **MM4**, **MM6**) were used to perform the coprecipitation of asparaginase, as the precursors are synthetically more accessible compared to the BCN derivatives and should have negligible reactivity towards biological systems. As a control we used nanogels that were prepared without the addition of asparaginase during nanoprecipitation. The results are summarized in **Figure 2**.

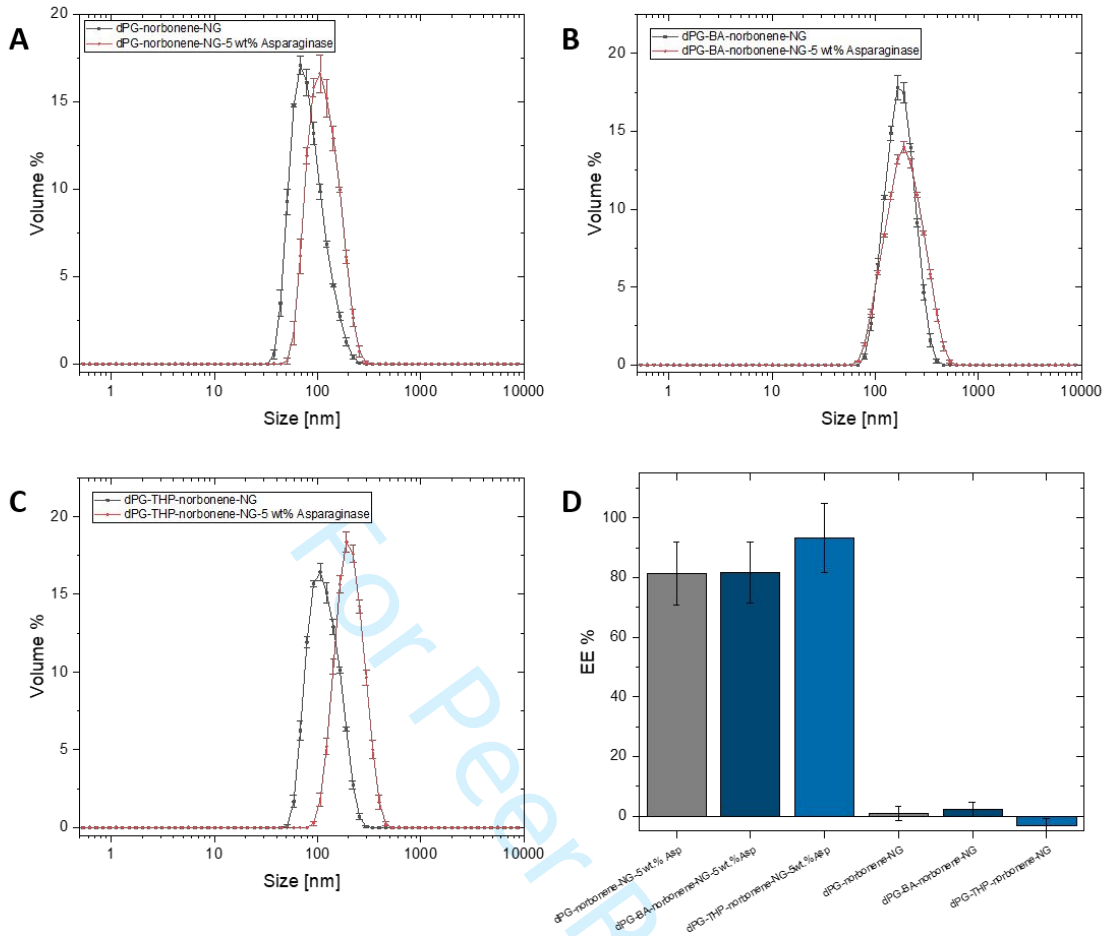

Figure 2 Co-precipitation of asparaginase at 5 wt.% feed with **MM1/MM3**, **MM4/MM3**, and **MM6/MM3**. (A) DLS data for a gel without (black) and with asparaginase (red) present during gel formation (dPG-norbonene-NG), (B) DLS data for a gel without (black) and with asparaginase (red) present during gel formation (dPG-BA-norbonene-NG), (C) DLS data for a gel without (black) and with asparaginase (red) present during gel formation (dPG-THP-norbonene-NG), (D) encapsulation efficiency determined by a BCA assay for gels with asparaginase and control gels without; the readout of the control gels was subtracted from the values that were determined for the gels containing asparaginase

It is evident, that the coprecipitation of a protein influenced the size of the resulting nanogels to higher values. We hypothesize that this was due to interactions of the protein with the macromonomers during the inverse nanoprecipitation process which lead to the formation of bigger initial aggregates which grew faster during the gel formation process, thus resulting in bigger nanogels.

After a purification process, where the gels were washed in a centrifugal filter with PBS, most of any free protein should be removed from the gel dispersions. The gels were then tested regarding their protein content, using a standard BCA assay with a dilution series of free asparaginase as the standard curve (**Figure S4**). Gels that were formed without the addition of asparaginase were used as a control and the OD values for these gels were subtracted from the gels that contained asparaginase. The results of the encapsulation efficiency can be seen in **Figure 2 D**. All three types of gels, namely dPG-norbonene, dPG-BA-norbonene-, and dPG-THP-norbonene nanogels reached very good encapsulation efficiencies of between 81 and 93%, showing the suitability of these macromonomers to form gels that efficiently entrap asparaginase within their gel network.

The pH-degradability of the different types of acetal functionalized nanogels was then tested at different pH-values.

3.3 pH-Triggered Degradation of Nanogels

In order to study the degradation behavior of the gels we added the different types of gels which contained asparaginase to buffer at different pH values. Every group of gel was exposed to pH 7.4, pH 4.5, and pH 3 at moderate agitation and room temperature. The degradation was then followed over the course of 48 h. At each time point a sample was taken and snap frozen in liquid nitrogen to be later measured by DLS. The results are shown in **Figure 3** and **Figure S8**.

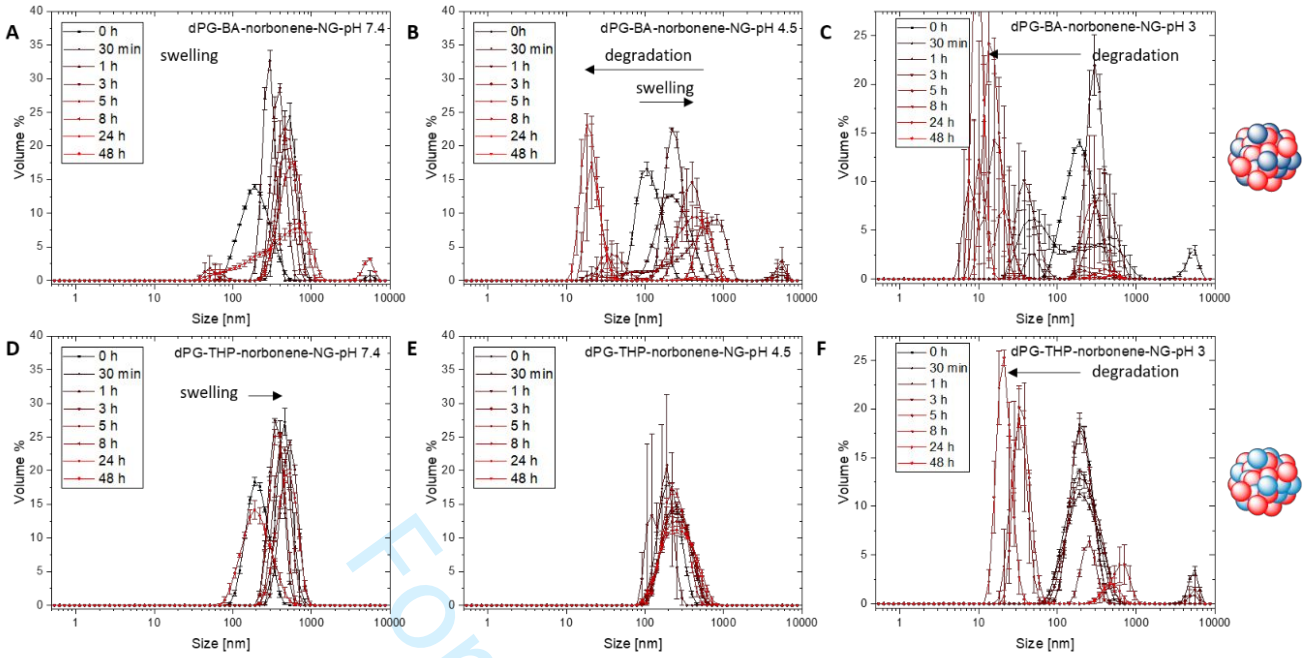

Figure 3 Degradation profiles of dPG-BA-norbonene- and dPG-THP-norbonene at pH 7.4, pH 4.5 and pH 3. (A)-(C) dPG-BA-norbonene-NG at pH 7.4, 4.5, and 3. (D)- (F) dPG-THP-NG at pH 7.4, 4.5, and 3

At pH 7.4 (**A** + **D**) both gels do not show degradation at all. Through the strong agitation, however, the particles tend to aggregate and show a strong increase in polydispersity. In terms of degradation, there was no significant amount of small particles observable. However, at pH 4.5 nanogel degradation was observed for the gel with BA linking groups (**B**). At first, swelling of the nanogels was observed, which shifted the distribution towards bigger size values, while only after 24 h small particles appeared at around 20 nm in a mix with still intact nanogels. After 48 h, however, most particles were in the size range of around 20 nm. In contrast, even after 48 h no degradation was observed for the aliphatic THP-acetal linker containing gel (**E**). This was expected, as these kinds of acetals degrade usually only at pH values of below 3.

At pH 3, the dPG-BA-norbonene NG (**C**)degraded much faster than at pH 4.5. After already 3 h particles of around 50 nm were observed and after 8 h mostly particles of around 20 nm remained. At 48 h nearly all particles were degraded to around 10 nm, which signaled the complete breakdown of the gels into mostly macromonomers.

The dPG-THP-norbonene-NG at pH 3 in contrast to pH 4.5, started to degrade and showed smaller particles of around 50 nm after 8 h. After 48 h almost complete degradation to particles of around 20 nm was observed.

In order to see a more detailed degradation profile of the dPG-BA-norbonene-NGs a continuous monitoring over the course of 18 h was performed. For this, a nanogel without protein was degraded in acetate buffer at pH 4.5 within a DLS cuvette and measured continuously while every measurement corresponds to roughly 2 min. The results are shown in **Figure 4**.

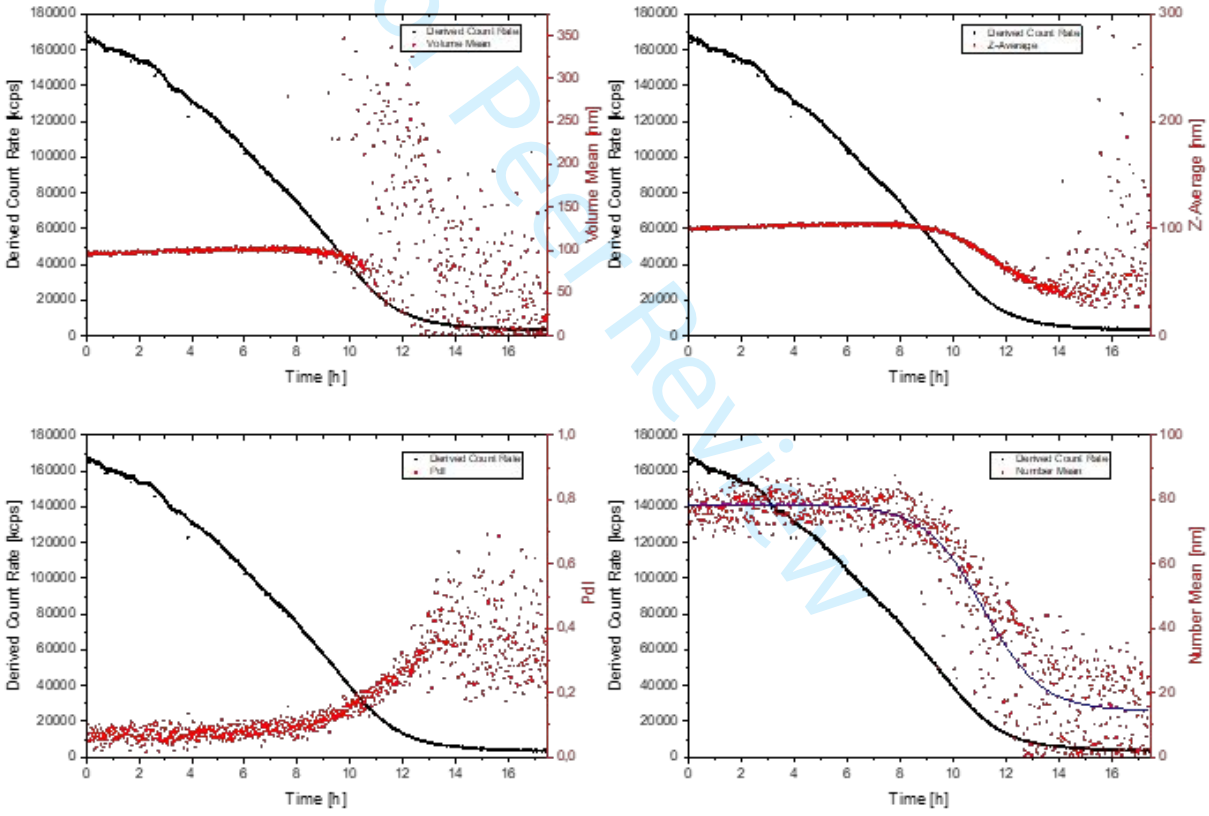

Figure 4 Continuous degradation profile of dPG-BA-norbonene-NG at pH 4.5 in acetate buffer. Size by volume, Z-Average, size by number and PDI are shown. The derived count rate is shown for comparison

The black curve in every diagram corresponds to the derived count rate. This was constantly decreasing over time, which indicated less, and less particle counts over time. However, over a long period of time of around 8 to 9 h not much change could be observed in the volume and number distributions. If at all, there is a slight increase in size, probably due to swelling of the

gels. After around 9 h, the PDI value slowly started to rise, which showed that a mixture of particles must be present with a wider distribution of sizes. This could also be observed in the size by volume and number distributions. From this point on, the size values continued to decrease until at around 13 h the count rate became too low for the measurement quality to obtain reliable results. This was indicated by the fluctuation of measurement values and the strong spreading of the distribution of values. However, at least a trend could be observed, which showed that the gels disintegrated between 9 h and 14 h to values below 20 nm.

All in all, this shows that the gels based on the BA linkers that were used can be degraded at pH values that can be found in endosomes and lysosomes. At pH 7.4 all gels were stable for extended periods of time, as can be seen in **Figure S6**. NTA measurements of the same gels also confirmed, that the particle sizes obtained from DLS are comparable (**Figure S7**).

3.4 CCK8 Cell Viability Test

For any application handling living cells or *in vivo* experiments, it is necessary to know if the macromonomers that are used are non-toxic to the cells at reasonable concentrations. In the case of the nanogels we presented here, no free macromonomers remain, however for applications such as microgelation and co-encapsulation of living cells it is absolutely mandatory to see if the macromonomers are toxic, because they come into direct contact with the cells they encapsulate. After gel formation the gels are mostly appearing as hydrophilic networks, presenting a lot of hydroxyl groups and it has been demonstrated before that nanogels, based on dPG do not impact the cell viability negatively within a certain concentration range.[56]

The results for three different cell lines are summarized in **Figure 5**.

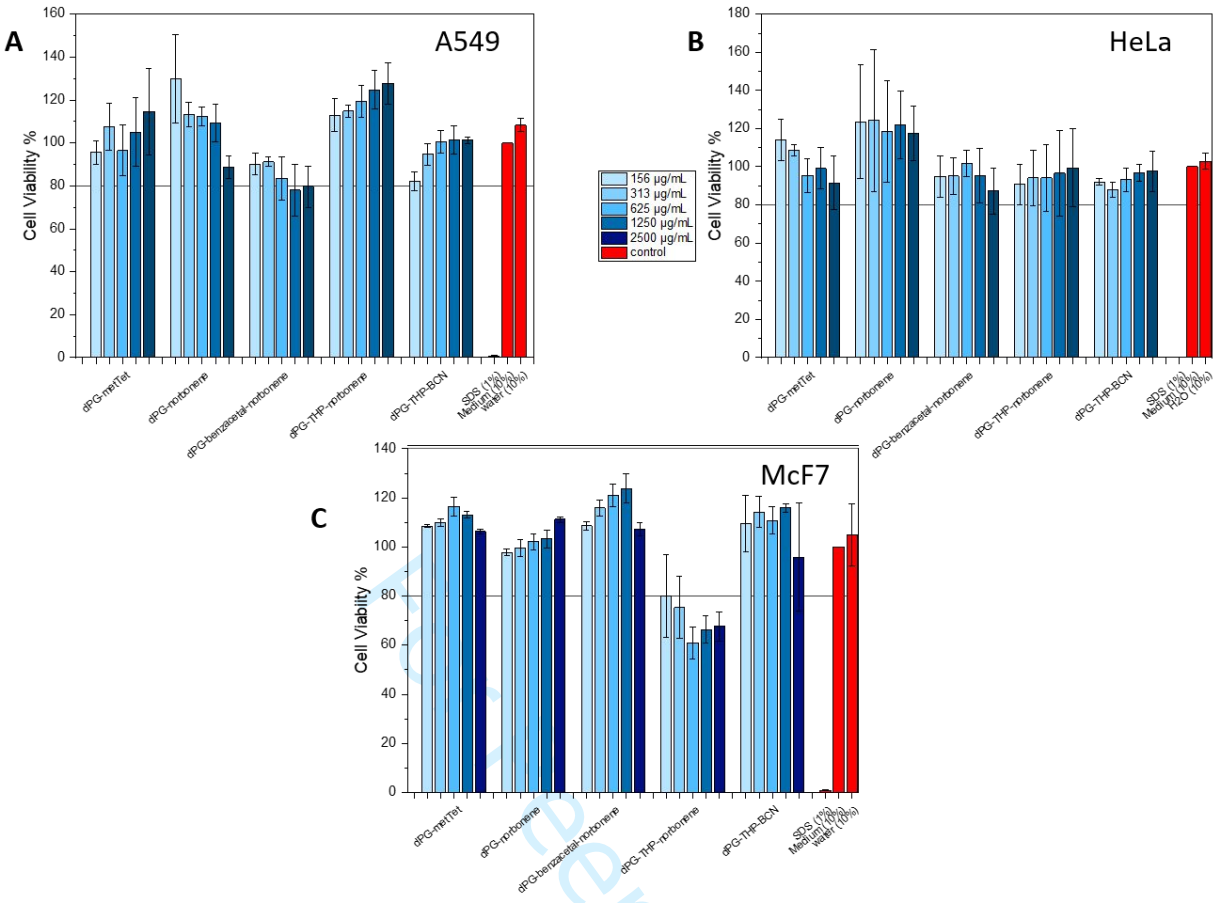

Figure 5 Cell viability assay of all different macromonomers using three different cell lines, A) A549 cell line, B) HeLa cell line, C) McF7 cell line.

All macromonomers did not have a big impact on cell viability up to approximately a concentration of 156 µg mL^{-1}, however, dPG-THP-norbonene exhibited slight cytotoxicity at concentrations higher than this. The rest of the macromonomers were non-toxic even up to concentrations of 2.5 mg mL^{-1}. This indicated that the macromonomers are suitable even for applications with living cells.

Conclusion

We have shown the synthesis of different reactive macromonomers for iEDDA click chemistry mediated production of pH-degradable nanogels that are degraded at their acetal linking points. Three different groups of nanogels were produced. Non-degradable gels, degradable gels, based

on an aromatic BA linker, and degradable gels based on an aliphatic THP acetal were obtained. The NGs were synthesized in the size range of 47 -200 nm with excellent polydispersity indices of 0.1 and below.

Co-precipitation of the therapeutic protein asparaginase showed excellent encapsulation efficiencies of between 81 and 93% for nanogels made from dPG-norbonene and dPG-BA-norbonene, respectively.

Gels based on the aromatic BA linker, were degraded at pH values of 4.5, within 24 h, while THP-linked gels were not degraded at all at this pH. dPG-BA-norbonene gels were degraded fast within 9 h at pH 3 and dPG-THP gels showed complete degradation within 24 h at this pH showing the applicability of the dPG-BA-dienophile gels for degradation within endosomal to lysosomal pH windows. All gels were stable in PBS at pH 7.4 for extended periods of time. The macromonomers used, did not show cell toxic effects up to about 2.5 mg mL^{-1}, except for dPG-THP-norbonene.

The low toxicity of the macromonomers, as well as the reproducible gel formation within a reasonable size range and low polydispersity, together with the excellent encapsulation efficiency, make the nanogels ideal for the delivery of therapeutic proteins. As a future perspective, functionalization of the dPG-core with targeting ligands could be performed, in order to obtain nanocarriers that have active-, as well as passive targeting properties.

Acknowledgements

We like to acknowledge Cathleen Schlesener for providing dPG and dPG-NH_2 and the BioSupraMol core facility for NMR measurements. Elisa Quaas is thanked for performing the CCK8 assay and Dr. Pamela Winchester is thanked for careful proofreading this manuscript. The SFB 765 of the German Science Foundation (DFG) is thanked for funding.

Conflict of Interest

The authors declare no conflict of interest.

References

1. Ruiz-Garcia A, Bermejo M, Moss A, Casabo VG (2008) Pharmacokinetics in Drug Discovery. J Pharm Sci 97:654–690. https://doi.org/10.1002/jps.21009

2. Raemdonck K, Demeester J, De Smedt S (2009) Advanced nanogel engineering for drug delivery. Soft Matter 5:707. https://doi.org/10.1039/b811923f

3. Farjadian F, Ghasemi A, Gohari O, et al (2019) Nanopharmaceuticals and nanomedicines currently on the market: challenges and opportunities. Nanomedicine 14:93–126. https://doi.org/10.2217/nnm-2018-0120

4. Choi YH, Han HK (2018) Nanomedicines: current status and future perspectives in aspect of drug delivery and pharmacokinetics. J Pharm Investig 48:43–60. https://doi.org/10.1007/s40005-017-0370-4

5. Jiskoot W, Randolph TW, Volkin DB, et al (2012) Protein Instability and Immunogenicity: Roadblocks to Clinical Application of Injectable Protein Delivery Systems for Sustained Release. J Pharm Sci 101:946–954. https://doi.org/10.1002/jps.23018

6. Alexis F, Pridgen E, Molnar LK, Farokhzad OC (2008) Factors affecting the clearance and biodistribution of polymeric nanoparticles. Mol Pharm 5:505–515. https://doi.org/10.1021/mp800051m

7. Dobrovolskaia MA, Neun BW, Man S, et al (2014) Protein corona composition does not accurately predict hematocompatibility of colloidal gold nanoparticles.

Nanomedicine Nanotechnology, Biol Med 10:1453–1463. https://doi.org/10.1016/j.nano.2014.01.009

8. Gröger D, Kerschnitzki M, Weinhart M, et al (2014) Selectivity in Bone Targeting with Multivalent Dendritic Polyanion Dye Conjugates. Adv Healthc Mater 3:375–385. https://doi.org/10.1002/adhm.201300205

9. Seymour LW, Duncan R, Strohalm J, Kopeček J (1987) Effect of molecular weight (Mw) ofN-(2-hydroxypropyl)methacrylamide copolymers on body distribution and rate of excretion after subcutaneous, intraperitoneal, and intravenous administration to rats. J Biomed Mater Res 21:1341–1358. https://doi.org/10.1002/jbm.820211106

10. Haag R, Kratz F (2006) Polymer therapeutics: Concepts and applications. Angew Chem Int Ed 45:1198–1215. https://doi.org/10.1002/anie.200502113

11. Greenwald RB, Choe YH, McGuire J, Conover CD (2003) Effective drug delivery by PEGylated drug conjugates. Adv Drug Deliv Rev 55:217–250. https://doi.org/10.1016/S0169-409X(02)00180-1

12. Thomas A, Müller SS, Frey H (2014) Beyond Poly(ethylene glycol): Linear Polyglycerol as a Multifunctional Polyether for Biomedical and Pharmaceutical Applications. Biomacromolecules 15:1935–1954. https://doi.org/10.1021/bm5002608

13. Baca QJ, Leader B, Golan DE (2017) Protein Therapeutics. Springer International Publishing, Cham

14. Turecek PL, Bossard MJ, Schoetens F, Ivens IA (2016) PEGylation of Biopharmaceuticals: A Review of Chemistry and Nonclinical Safety Information of Approved Drugs. J Pharm Sci 105:460–475. https://doi.org/10.1016/j.xphs.2015.11.015

15. Zhang P, Sun F, Liu S, Jiang S (2016) Anti-PEG antibodies in the clinic: Current issues and beyond PEGylation. J Control Release 244:184–193.

https://doi.org/10.1016/j.jconrel.2016.06.040

16. Singh S, Topuz F, Hahn K, et al (2013) Embedding of Active Proteins and Living Cells in Redox-Sensitive Hydrogels and Nanogels through Enzymatic Cross-Linking. Angew Chem Int Ed 52:3000–3003. https://doi.org/10.1002/anie.201206266

17. Chacko RT, Ventura J, Zhuang J, Thayumanavan S (2012) Polymer nanogels: A versatile nanoscopic drug delivery platform. Adv Drug Deliv Rev 64:836–851. https://doi.org/10.1016/j.addr.2012.02.002

18. Karg M, Pich A, Hellweg T, et al (2019) Nanogels and Microgels: From Model Colloids to Applications, Recent Developments, and Future Trends. Langmuir 35:6231–6255. https://doi.org/10.1021/acs.langmuir.8b04304

19. Sivaram AJ, Rajitha P, Maya S, et al (2015) Nanogels for delivery, imaging and therapy. Wiley Interdiscip Rev Nanomedicine Nanobiotechnology 7:509–533. https://doi.org/10.1002/wnan.1328

20. Ekkelenkamp AE, Elzes MR, Engbersen JFJ, Paulusse JMJ (2018) Responsive crosslinked polymer nanogels for imaging and therapeutics delivery. J Mater Chem B 6:210–235. https://doi.org/10.1039/C7TB02239E

21. Kabanov A V., Vinogradov S V. (2009) Nanogels as Pharmaceutical Carriers: Finite Networks of Infinite Capabilities. Angew Chem Int Ed 48:5418–5429. https://doi.org/10.1002/anie.200900441

22. Bazban-Shotorbani S, Dashtimoghadam E, Karkhaneh A, et al (2016) Microfluidic Directed Synthesis of Alginate Nanogels with Tunable Pore Size for Efficient Protein Delivery. Langmuir 32:4996–5003. https://doi.org/10.1021/acs.langmuir.5b04645

23. Klinger D, Landfester K (2012) Enzymatic- and light-degradable hybrid nanogels: Crosslinking of polyacrylamide with acrylate-functionalized Dextrans containing

photocleavable linkers. J Polym Sci Part A Polym Chem 50:1062–1075. https://doi.org/10.1002/pola.25845

24. Thomann-Harwood LJ, Kaeuper P, Rossi N, et al (2013) Nanogel vaccines targeting dendritic cells: Contributions of the surface decoration and vaccine cargo on cell targeting and activation. J Control Release 166:95–105. https://doi.org/10.1016/j.jconrel.2012.11.015

25. Gratton SEA, Pohlhaus PD, Lee J, et al (2007) Nanofabricated particles for engineered drug therapies: A preliminary biodistribution study of PRINT™ nanoparticles. J Control Release 121:10–18. https://doi.org/10.1016/j.jconrel.2007.05.027

26. Modi S, Anderson BD (2013) Determination of drug release kinetics from nanoparticles: overcoming pitfalls of the dynamic dialysis method. Mol Pharm 10:3076–89. https://doi.org/10.1021/mp400154a

27. Dey P, Bergmann T, Cuellar-Camacho JL, et al (2018) Multivalent Flexible Nanogels Exhibit Broad-Spectrum Antiviral Activity by Blocking Virus Entry. ACS Nano 12:6429–6442. https://doi.org/10.1021/acsnano.8b01616

28. Witting M, Molina M, Obst K, et al (2015) Thermosensitive dendritic polyglycerol-based nanogels for cutaneous delivery of biomacromolecules. Nanomedicine 11:1179–87. https://doi.org/10.1016/j.nano.2015.02.017

29. Wu C, Böttcher C, Haag R (2015) Enzymatically crosslinked dendritic polyglycerol nanogels for encapsulation of catalytically active proteins. Soft Matter 11:972–980. https://doi.org/10.1039/C4SM01746C

30. Steinhilber D, Witting M, Zhang X, et al (2013) Surfactant free preparation of biodegradable dendritic polyglycerol nanogels by inverse nanoprecipitation for encapsulation and release of pharmaceutical biomacromolecules. J Control Release

169:289–295. https://doi.org/10.1016/j.jconrel.2012.12.008

31. Seidi F, Jenjob R, Crespy D (2018) Designing Smart Polymer Conjugates for Controlled Release of Payloads. Chem Rev 118:3965–4036. https://doi.org/10.1021/acs.chemrev.8b00006

32. Zhang J, Jia Y, Li X, et al (2011) Facile Engineering of Biocompatible Materials with pH-Modulated Degradability. Adv Mater 23:3035–3040. https://doi.org/10.1002/adma.201100679

33. Chen W, Hou Y, Tu Z, et al (2017) pH-degradable PVA-based nanogels via photo-crosslinking of thermo-preinduced nanoaggregates for controlled drug delivery. J Control Release 259:160–167. https://doi.org/10.1016/j.jconrel.2016.10.032

34. Yang H, Wang Q, Chen W, et al (2015) Hydrophilicity/Hydrophobicity Reversable and Redox-Sensitive Nanogels for Anticancer Drug Delivery. Mol Pharm 150409150353009. https://doi.org/10.1021/acs.molpharmaceut.5b00068

35. Pang X, Jiang Y, Xiao Q, et al (2016) pH-responsive polymer–drug conjugates: Design and progress. J Control Release 222:116–129. https://doi.org/10.1016/j.jconrel.2015.12.024

36. Mauri E, Perale G, Rossi F (2018) Nanogel Functionalization: A Versatile Approach To Meet the Challenges of Drug and Gene Delivery. ACS Appl Nano Mater 1:6525–6541. https://doi.org/10.1021/acsanm.8b01686

37. O'Donnell JM (2012) Reversible addition-fragmentation chain transfer polymerization in microemulsion. Chem Soc Rev 41:3061–3076. https://doi.org/10.1039/c2cs15275d

38. Antonietti M, Landfester K, Willert M, et al (2001) Polyreactions in non-aqueous miniemulsions. Prog Polym Sci 27:689–757

39. Hamidi M, Azadi A, Rafiei P (2008) Hydrogel nanoparticles in drug delivery. Adv Drug Deliv Rev 60:1638–1649. https://doi.org/10.1016/j.addr.2008.08.002

40. Schubert S, Delaney, Jr JT, Schubert US (2011) Nanoprecipitation and nanoformulation of polymers: from history to powerful possibilities beyond poly(lactic acid). Soft Matter 7:1581. https://doi.org/10.1039/c0sm00862a

41. Perevyazko IY, Delaney JT, Vollrath A, et al (2011) Examination and optimization of the self-assembly of biocompatible, polymeric nanoparticles by high-throughput nanoprecipitation. Soft Matter 7:5030–5035. https://doi.org/10.1039/c1sm05079f

42. Schubert S, Delaney JT, Schubert US (2011) Nanoprecipitation and nanoformulation of polymers: From history to powerful possibilities beyond poly(lactic acid). Soft Matter 7:1581–1588. https://doi.org/10.1039/c0sm00862a

43. Nair DP, Podgórski M, Chatani S, et al (2014) The Thiol-Michael Addition Click Reaction: A Powerful and Widely Used Tool in Materials Chemistry. Chem Mater 26:724–744. https://doi.org/10.1021/cm402180t

44. Späte A-K, Bußkamp H, Niederwieser A, et al (2014) Rapid Labeling of Metabolically Engineered Cell-Surface Glycoconjugates with a Carbamate-Linked Cyclopropene Reporter. Bioconjug Chem 25:147–154. https://doi.org/10.1021/bc4004487

45. Oliveira BL, Guo Z, Bernardes GJL (2017) Inverse electron demand Diels-Alder reactions in chemical biology. Chem Soc Rev 46:4895–4950. https://doi.org/10.1039/c7cs00184c

46. Wu H, Devaraj NK (2016) Inverse Electron-Demand Diels–Alder Bioorthogonal Reactions. Top Curr Chem 374:3. https://doi.org/10.1007/s41061-015-0005-z

47. Knall A-C, Slugovc C (2013) Inverse electron demand Diels-Alder (iEDDA)-initiated conjugation: a (high) potential click chemistry scheme. Chem Soc Rev 42:5131–5142.

https://doi.org/10.1039/c3cs60049a

48. Liu DS, Tangpeerachaikul A, Selvaraj R, et al (2012) Diels-alder cycloaddition for fluorophore targeting to specific proteins inside living cells. J Am Chem Soc 134:792–795. https://doi.org/10.1021/ja209325n

49. Schoch J, Staudt M, Samanta A, et al (2012) Site-specific one-pot dual labeling of DNA by orthogonal cycloaddition chemistry. Bioconjug Chem 23:1382–1386. https://doi.org/10.1021/bc300181n

50. Yang J, Šečkute J, Cole CM, Devaraj NK (2012) Live-cell imaging of cyclopropene tags with fluorogenic tetrazine cycloadditions. Angew Chem Int Ed 51:7476–7479. https://doi.org/10.1002/anie.201202122

51. Frey H, Haag R (2002) Dendritic polyglycerol: A new versatile biocompatible material. Rev Mol Biotechnol 90:257–267. https://doi.org/10.1016/S1389-0352(01)00063-0

52. Kurniasih IN, Keilitz J, Haag R (2015) Dendritic nanocarriers based on hyperbranched polymers. Chem Soc Rev 44:4145–4164. https://doi.org/10.1039/C4CS00333K

53. Steinhilber D, Seiffert S, Heyman JA, et al (2011) Hyperbranched polyglycerols on the nanometer and micrometer scale. Biomaterials 32:1311–1316. https://doi.org/10.1016/j.biomaterials.2010.10.010

54. Khandare J, Mohr A, Calderón M, et al (2010) Structure-biocompatibility relationship of dendritic polyglycerol derivatives. Biomaterials 31:4268–4277. https://doi.org/10.1016/j.biomaterials.2010.02.001

55. Dommerholt J, Schmidt S, Temming R, et al (2010) Readily Accessible Bicyclononynes for Bioorthogonal Labeling and Three-Dimensional Imaging of Living Cells. Angew Chem Int Ed 49:9422–9425. https://doi.org/10.1002/anie.201003761

56. Sisson AL, Haag R (2010) Polyglycerol nanogels: Highly functional scaffolds for biomedical applications. Soft Matter 6:4968–4975. https://doi.org/10.1039/c0sm00149j

Synthesis of pH-Degradable Polyglycerin-Based Nanogels by iEDDA-Mediated Crosslinking for Encapsulation of Asparaginase Using Inverse Nanoprecipitation

Alexander Oehrl, Sebastian Schötz, Rainer Haag

Alexander Oehrl, Sebastian Schötz, Prof. Rainer Haag

Freie Universität Berlin, Institute for Chemistry and Biochemistry, Takustr. 3, D-14195 Berlin, Germany

E-mail: haag@chemie.fu-berlin.de

Supplementary Information

Materials and Analytical Methods

Ethyl acetate, *n*-pentane and diethyl ether were obtained from the technically pure solvents by distillation before use. Dry DCM and THF were used from a SPS-800 type MBRAUN solvent drying system. Acetone and DCM (HPLC grade) were used without further purification. Dry methanol and DMF were purchased from Acros and Fischer Chemical. All other chemicals and deuterated solvents were obtained from Sigma Aldrich, Acros, Merck, and Fisher Chemicals and were used as without further purification. Thin layer chromatography (TLC) was performed on silica gel-coated aluminum plates, serving as stationary phase (silica gel 60 F254 from Macherey-Nagel). Identification of analytes was done by UV-irradiation (λ = 254 nm) of the TLC plates or by treatment with a potassium permanganate-based (100 mL deionized water, 200 mg potassium permanganate) or anis aldehyde-based staining solution (450 mL EtOH, 25 mL anis aldehyde, 25 mL conc. sulfuric acid, 8.0 mL acetic acid). Column chromatography was performed with silica gel (Macherey-Nagel, grain size 40 - 63 µm, 230 - 400 mesh) as stationary phase and the indicated eluent mixtures as the mobile phase.

IR spectra were recorded on a JASCO FT/IR-4100 spectrometer. The characteristic absorption bands are given in wave numbers. ^{1}H NMR spectra were recorded at 300 K on Joel ECX 400 400 MHz and AVANCE III (700 MHz) instruments. Chemical shifts δ are indicated in parts per million (ppm) relative to tetramethyl silane (0 ppm) and calibrated as an internal standard to the signal of the incompletely deuterated solvent ($CDCl_3$: δ = 7.26 ppm, MeOD: δ = 3.31 ppm). Coupling constants J are given in Hertz (Hz). ^{13}C NMR spectra were recorded at 300 K on AVANCE III instruments (176 MHz). Chemical shifts δ are given in ppm relative to tetramethyl silane (0 ppm) and calibrated as an internal standard to the signal of the incompletely deuterated solvent ($CDCl_3$: δ = 77.16 ppm, MeOD: δ = 49 ppm). Coupling constants J are given in Hertz (Hz). The spectra are decoupled from proton broadband. DLS and Zeta potential were measured on a Malvern zeta- sizer nano ZS 90 with He–Ne laser (λ = 532 nm) at 173° backscatter and automated attenuation at 25 °C. Three measurements were performed per sample, yielding a mean size value plus standard deviation. Sample concentration was kept at 1 mg mL^{-1}. GPC was performed on an Agilent 1100 at 5 mg mL^{-1} using a pullulan standard, 0.1 M NaNO3 solution as eluent and a PSS Suprema column 10 µm with a flow rate of 1 mL min^{-1}. Signals were detected with an RI detector.

Precursor Synthesis

Activated carbonate precursors of the different dienophiles were partially synthesized according to literature-known procedures. Some procedures were modified as indicated.

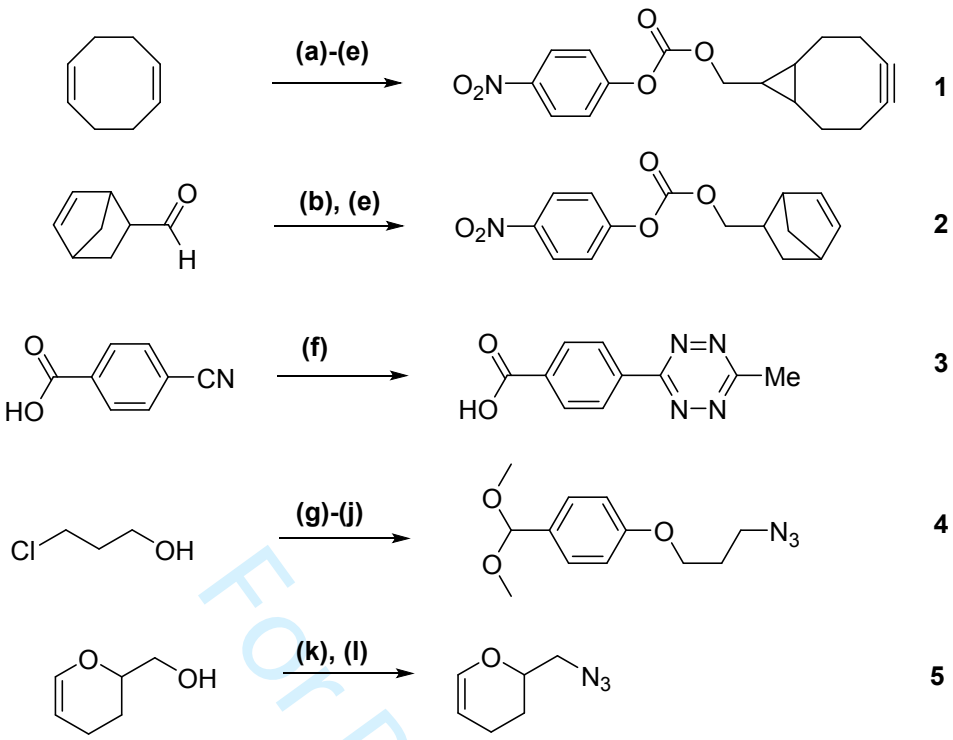

Scheme S1 Synthetic overview of the precursor molecules. (a) Rh-acetate dimer, ethyl diazoacetate, DCM; (b) $LiAlH_4$, THF; (c) Br_2, DCM; (d) KO^tBu, THF; (e) 4-nitrophenyl chloroformate, py, DCM; (f) acetamidine hydrochloride, hydrazine, $Zn(OTf)_2$, then $NaNO_2$, HCl; (g) NaN_3, $NBut_4$ HSO_4, H_2O, 80 °C, overnight; (h) 3-azidopropanol, TsCl, NEt_3, DCM, 0 °C to rt, overnight; (i) 4-hydroxybenzaldehyde, 3-azidopropyl 4-toluenesulfonate, K_2CO_3, acetone, reflux, overnight, (j) 4-(3-azidopropoxy) benzaldehyde, trimethyl orthoformate, pTSA, MeOH, reflux, 24 h, (k) MsCl, NEt_3, DMF, 0 °C to rt, overnight and (l) NaN_3, DMF, 80 °C, 2 days

BCN (**1**) was synthesized according to literature procedure.[1]

dPG-BCN (**MM2**) was synthesized according to literature protocol.[2]

dPG-norbonene was synthesized according to literature protocol.

4-(6-methyl-1,2,4,5-tetrazin-3-yl)benzoic acid (**3**) was synthesized according to a modified literature protocol:[3]

4-(6-methyl-1,2,4,5-tetrazin-3-yl)benzoic acid

4-cyanobenzoic acid (1.5 g, 10 mmol), acetamidine hydrochloride (4.82 g, 41 mmol) and $Zn(OTf)_2$ (1 g, 3 mmol) were ground in a mortar, added to a 100 mL Schlenk flask under argon atmosphere and cooled to 0 °C. Anhydrous hydrazine (12 mL, 377 mmol) was then slowly added under constant stirring, the reaction mixture was allowed to warm to room temperature

and stirred for 72 h. $NaNO_2$ (10 g) dissolved in 30 mL of water was then added to the reaction mixture. After cooling to 0 °C, the pH was adjusted to 2-3 by the slow addition of conc. HCl_{aq}. The color of the solution turned bright pink and a pink solid precipitated. After stirring at 0°C for another 1 h, the precipitate was filtered and washed with deionized water and MeOH. The product was obtained as a pink solid without further purification (1.1 g, 50 %).

^{1}H-NMR (400 MHz, DMF-d_7): δ = 13.80 (s, 1 H, COO*H*), 8.67 – 8.65 (m, 2 H, ArH), 8.32 – 8.29 (m, 2 H, ArH), 3.09 (s, 3 H, -CH_3) ppm.

^{13}C-NMR (101 MHz, DMF-d_7): δ = 168.95, 167.92, 137.23, 135.51, 131.41, 128.72, 21.63 ppm.

Polymer Core

dPG and dPG-amine were synthesized according to literature protocols.[4, 5]

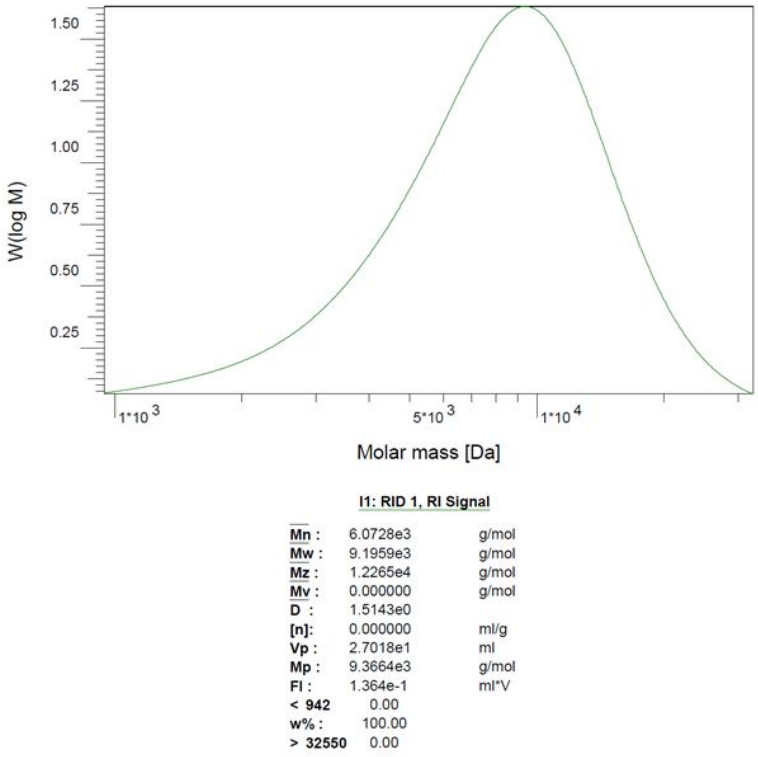

Figure S1: GPC-analysis of the dPG-core.

Macromonomers

dPG-BA-azide$_{8\%}$ was synthesized according to a modified literature protocol[6]:

dPG-BA-azide$_{8\%}$

dPG (4.16 g, 55.39 mmol) was dried at the HV at 70 °C overnight and dissolved in dry DMF (50 mL). The benzacetal (**4**) (1.48 g, 5.76 mmol) was dissolved in dry DMF (50 mL) and added to the dPG – solution *via* syringe and *p*-TSA (0.04 g, 0.22 mmol) was added. The resulting solution was stirred at 40 °C and MeOH was continuously removed through distillation. The crude product was constricted under reduced pressure and dialyzed against water and methanol 1:1 for four days and methanol for nine days (MWCO = 1 kDa). The product was obtained as methanolic solution (8 % functionalization, 85 %).

^{1}H–NMR (700 MHz, CD_3OD): δ = 7.48–7.40 (m, 2 H, H–aromatic), 7.00–6.93 (m, 2 H, H–aromatic), 5.90–5.87 (m, 1 H, H–acetal), 4.49–4.34 (m, 2 H, H–C–N3), 4.10–3.46 (m, dPG – backbone), 2.09–2.01 (m, 2 H, H–aliphatic) ppm.

^{13}C–NMR (176 MHz, CD_3OD): δ = 129.6, 115.4, 105.6, 104.9, 79.9, 74.0, 73.0, 72.3, 66.0, 64.4, 29.9 ppm.

IR (ATR): *v* = 3350, 2913, 2876, 2361, 2342, 2098, 1653, 1245, 1070, 1024 cm-1.

EA ($C_{80}H_{140}N_6O_{43}$): calc. C (51.27%), found C (49.46%); calc. N (4.48%), found N (5.78%), calc. H (7.53%), found H (8.47%).

dPG-BA-amine$_{10\%}$ was synthesized according to a modified literature protocol[6]:

dPG-BA-amine$_{10\%}$

The solvent of the dPG–benzacetal-azide (2.00 g, 26.62 mmol, 14.40 mL) solution was removed under reduced pressure. THF (70 mL), water (80 mL) and PPh_3 (3.50 g, 13.33 mmol) was added and the solution was stirred for seven days at room temperature. THF was removed under reduced pressure and the crude product was filtered. The filtrate was constricted under reduced pressure. The crude product was dialyzed against methanol for (MWCO = 1 kDa) for 3 days. The product was obtained as a methanolic solution (8.5% functionalization, 93%).

^{1}H–NMR (700 MHz, CD_3OD): δ = 7.47–7.39 (m, 2 H, H–aromatic), 7.01–6.92 (m, 2 H, H–aromatic), 5.89–5.71 (m, 1 H, H–acetal), 4.46–4.35 (m, 1 H, H–C–O), 4.13–3.46 (dPG – backbone), 2.97–2.88 (m, 1 H, H–C–NH2), 2.06–1.95 (m, 1 H, H–aliphatic) ppm.

^{13}C–NMR (176 MHz, CD_3OD): δ = 129.6, 129.3, 115.3, 105.6, 104.9, 81.5, 81.4, 80.2, 79.8, 76.6, 74.1, 74.0, 73.0, 72.5, 72.2, 71.1, 70.7, 68.5, 67.0, 67.0, 64.4, 62.9, 39.5, 32.2 ppm.

IR (ATR): $\tilde{\nu}$ = 3360, 2827, 2360, 2341, 1613, 1589, 1516, 1457, 1438, 1392, 1116, 1069 cm-1.

dPG-BA-BCN$_{6.5\%}$ was synthesized according to a modified literature protocol[6]:

dPG-BA-BCN$_{6.5\%}$

DMF (14 mL), dPG–BA-amine (10.00 mL, 0.062 g/mL), Et_3N (0.16 g, 1,62 mmol, 0.22 mL), BCN (0.19 g, 0.59 mmol) in DMF (10 mL). The product was obtained as a yellow methanolic solution (6.5% functionalization, 94%).

^{1}H–NMR (700 MHz, CD_3OD): δ = 7.47–7.38 (m, 2 H, H–aromatic), 6.99–6.92 (m, 2 H, H–aromatic), 5.89–5.72 (m, 1 H, H–acetal), 4.46–4.33 (m, 1 H, H–C–O), 4.30–4.13 (m, 2 H, H–C–carbamate), 4.13–3.44 (dPG – backbone), 2.40–2.08 (m, 4 H, H–2, H– 2'), 2.02–1.93 (m,

ring), 1.66–1.33 (m, 4 H, H–ring), 0.98–0.71 (m, 2 H, H–ring), 0.71– 0.65 (m, 1 H, H–ring) ppm.

^{13}C–NMR (176 MHz, CD_3OD): δ = 129.6, 129.3, 115.4, 111.4, 81.6, 79.9, 74.0, 72.2, 70.7, 64.5, 63.7, 62.8, 34.4, 30.8, 30.2, 25.1, 24.2, 22.0, 21.4 ppm.

IR (ATR): *v* = 3379, 2915, 2873, 1696, 1614, 1517, 1457, 1394, 1304, 1244, 1078, 934 cm-1.

EA ($C_{873}H_{1501}N_{13}O_{440}$): calc. C (54.55%), found C (53.11%); calc. N (0.95%), found N (1.63%); calc. H (7.87%), found H (7.90%).

Table S1 DLS data of the different macromonomers

Entry	dF by NMR %	Size by Volume [nm]	PDI
dPG-BCN	7.5	12 ± 2	0.30 ± 0.01
dPG-norbonene	9	4 ± 1	0.80 ± 0.02
dPG-metTet	6.5	160 ± 140	0.50 ± 0.01
dPG-BA-BCN	8	3 ± 1	0.75 ± 0.01
dPG-BA-norbonene	8	3 ± 1	0.75 ± 0.04
dPG-THP-BCN	5	9 ± 4	0.30 ± 0.04
dPG-THP-norbonene	5	5 ± 1	0.40 ± 0.04

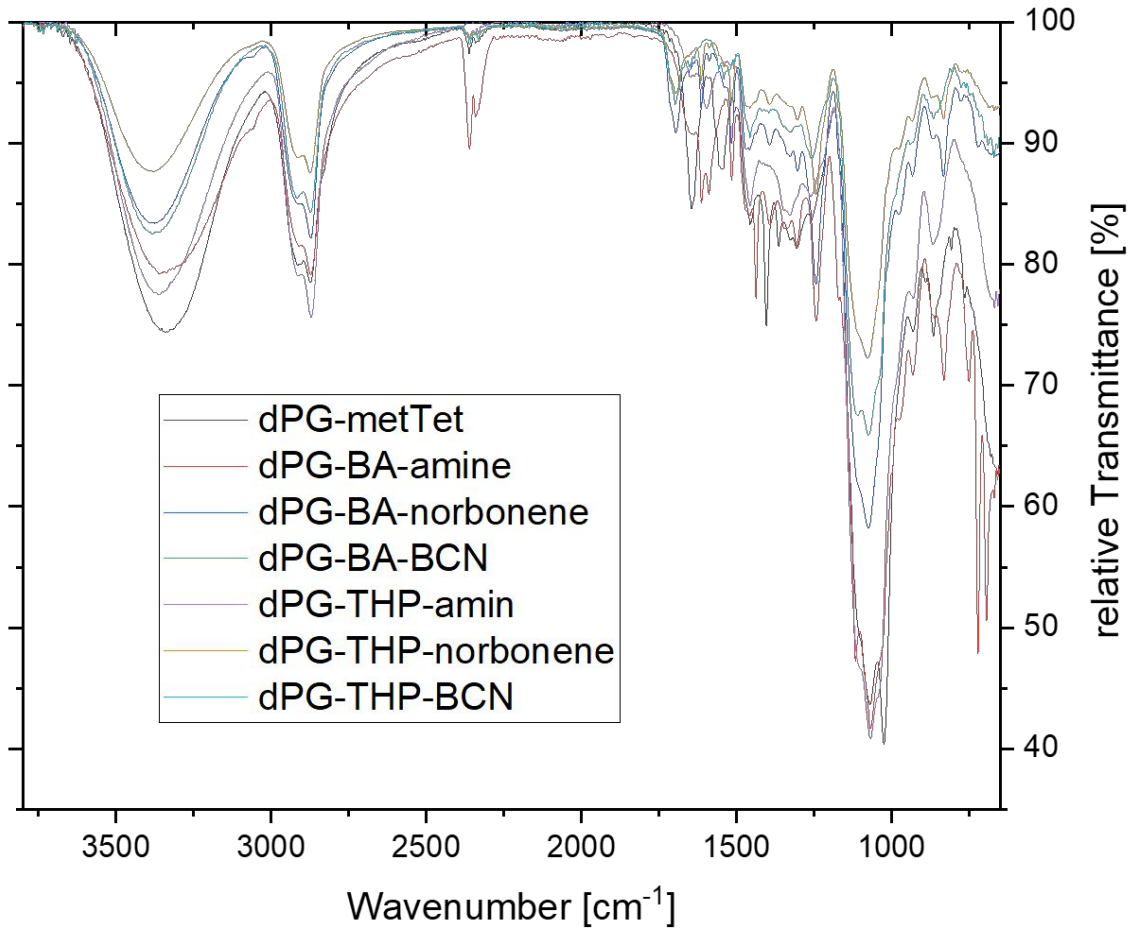

Figure S2 IR-spectra of the different macromonomers

Nanogels:

Table S2 Influence of concentration on nanogel size and polydispersity of dPG-BA-norbonene/dPG-metTet-NGs.

Entry	Macromonomer		$V(H_2O)$: V(acetone)	T_c [min]	T_{water} [min]	Z-Average [nm]	PDI
	Ratio (A:B)	c [mg/mL]					
1	1:1.5	5	1:40	10	60	105 ± 2	0.09 ± 0.01
2	1:1.5	5	1:40	10	60	115 ± 1	0.07 ± 0.01
3	1:1.5	7.5	1:40	10	60	112 ± 1	0.07 ± 0.01
4	1:1.5	7.5	1:40	10	60	120 ± 1	0.09 ± 0.01

Asparaginase Encapsulation

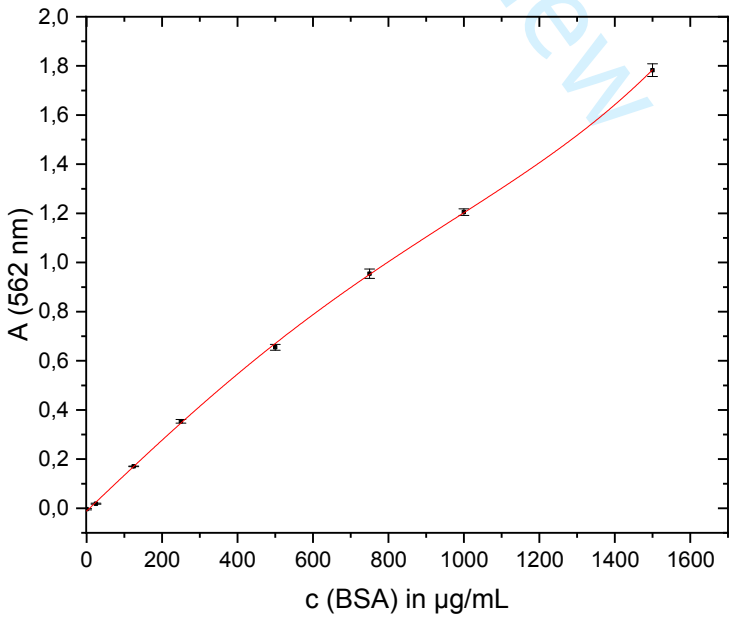

Figure S3 Standard curve of BSA in BCA assay

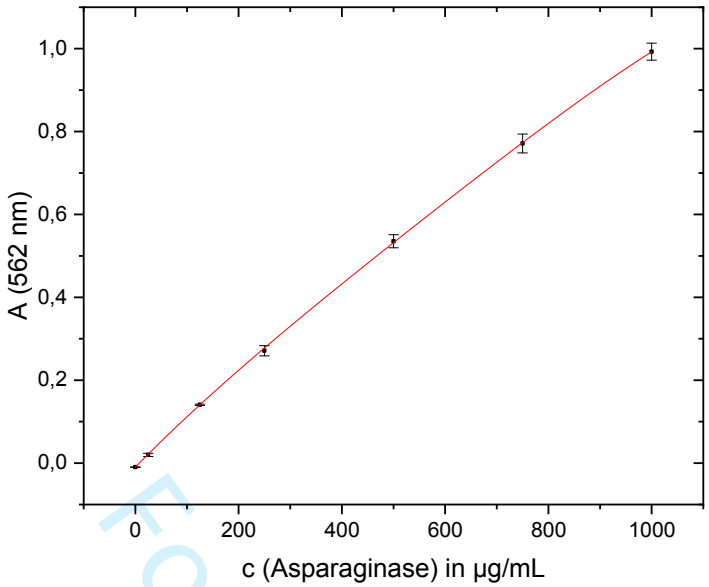

Figure S4 Standard curve of asparaginase in BCA assay

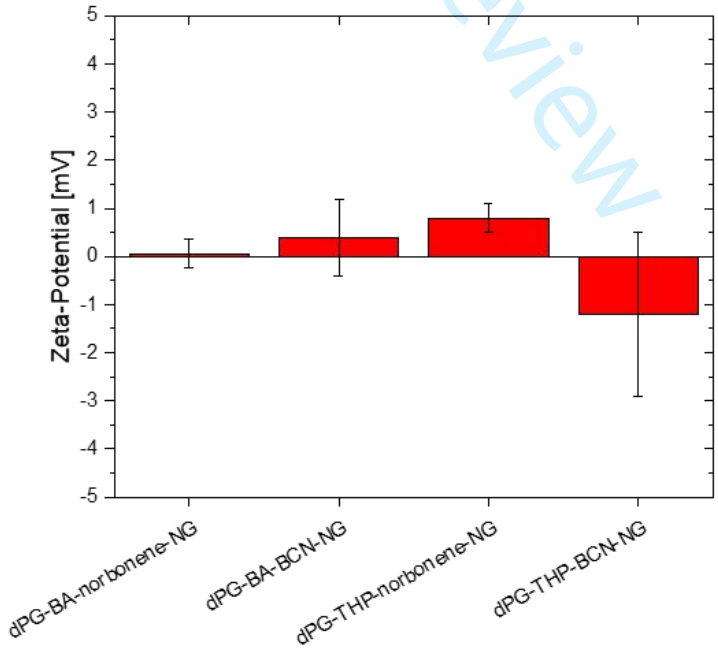

Figure S5 Zeta-Potential of Nanogels, derived from the different macromonomers

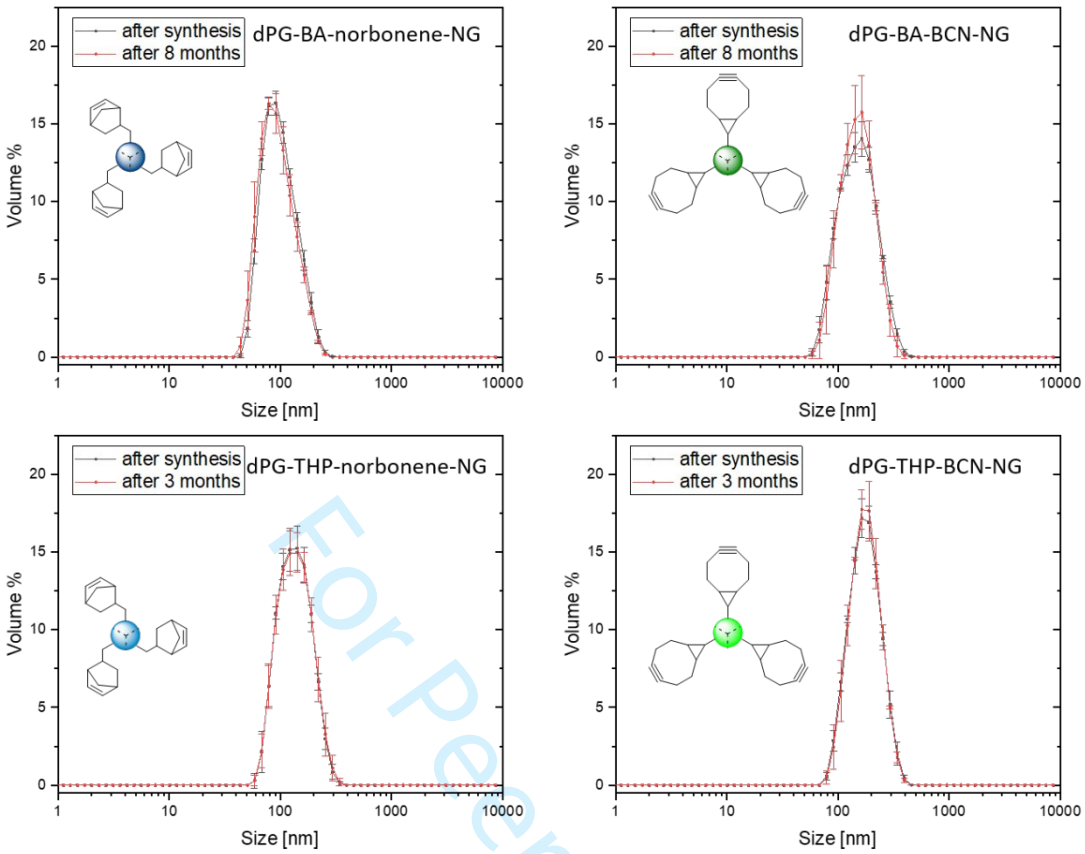

Figure S6 DLS distribution of nanogels after synthesis and after 3 to 8 months of storage in 10 mM PBS at pH 7.4 and 4 °C

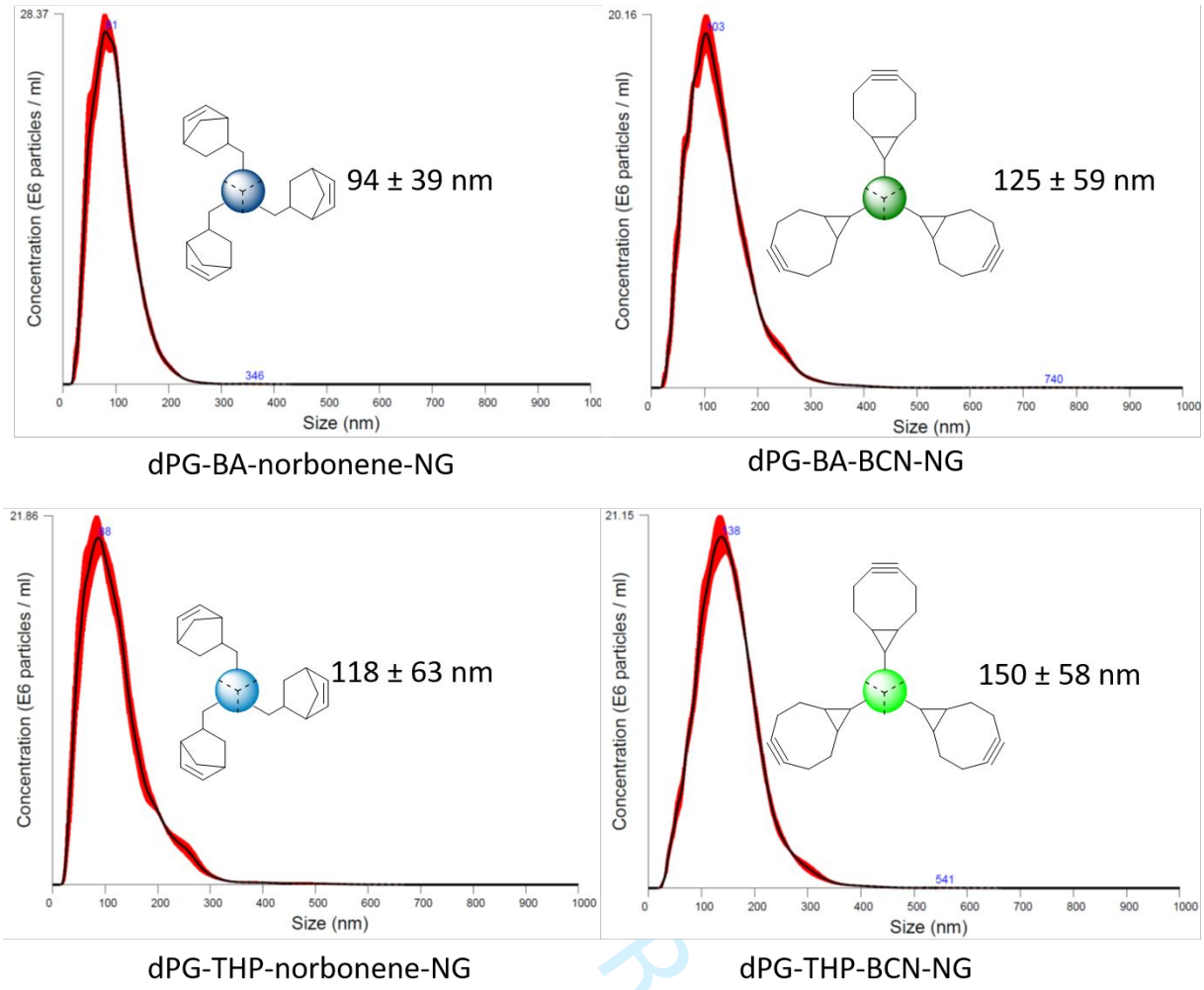

Figure S7 NTA measurements of Gels depicted in **Figure S5**, size values plus SD

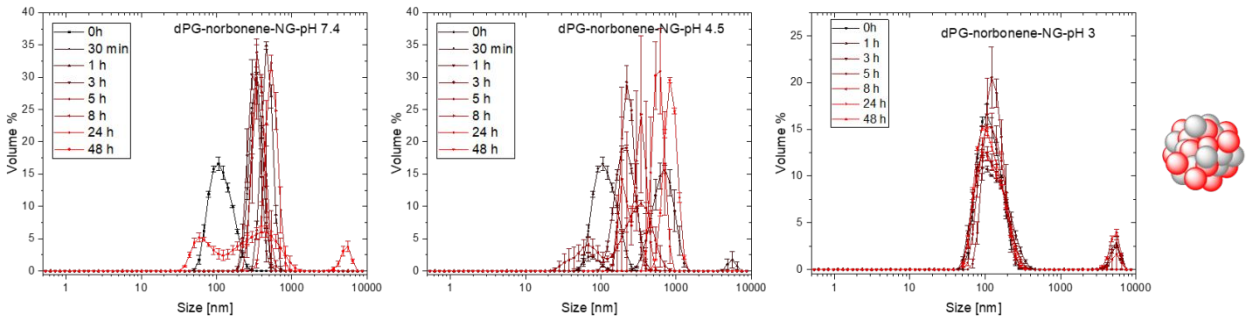

Figure S8 Degradation profile for dPG-norbonene-NG at 3 different pH values, size by volume is shown

NMR-Spectra:

BCN (**1**) (^{1}H)

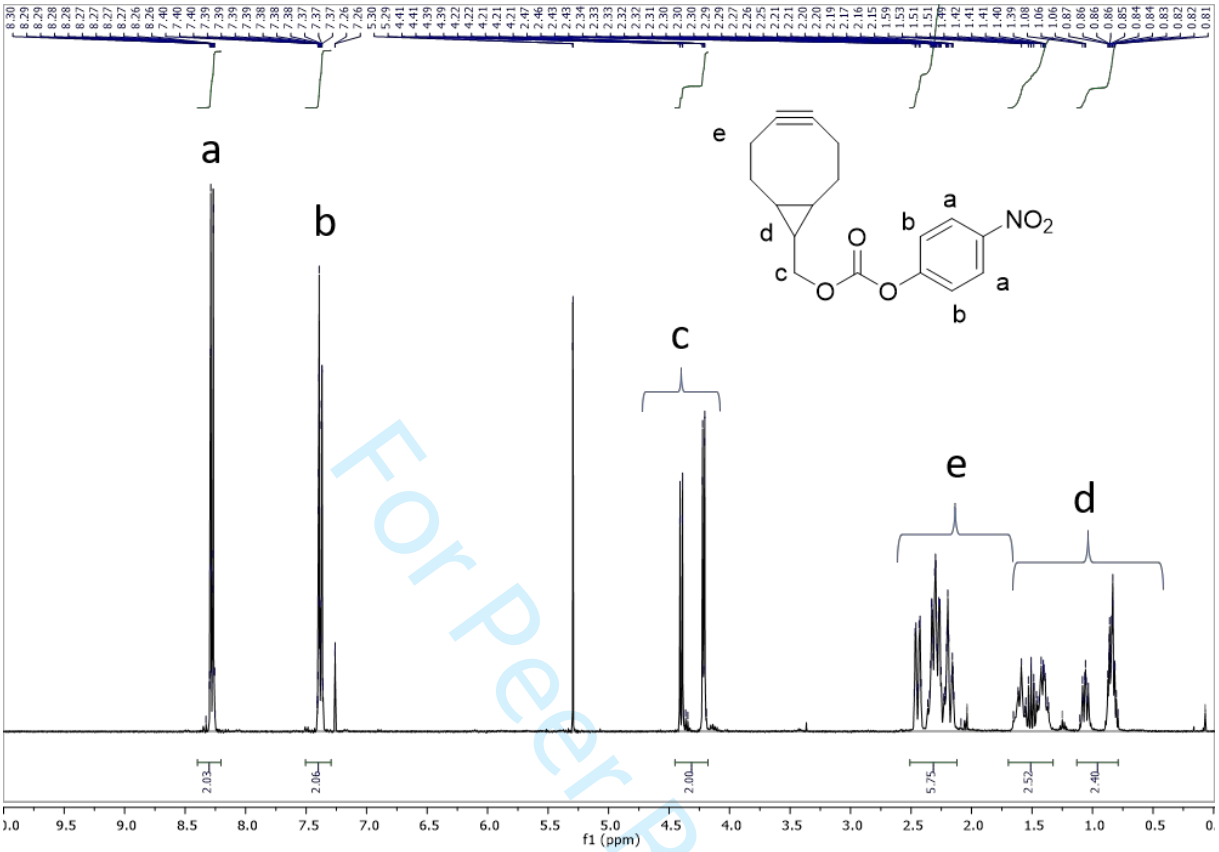

Norbonene-active ester (**2**) (^{1}H)

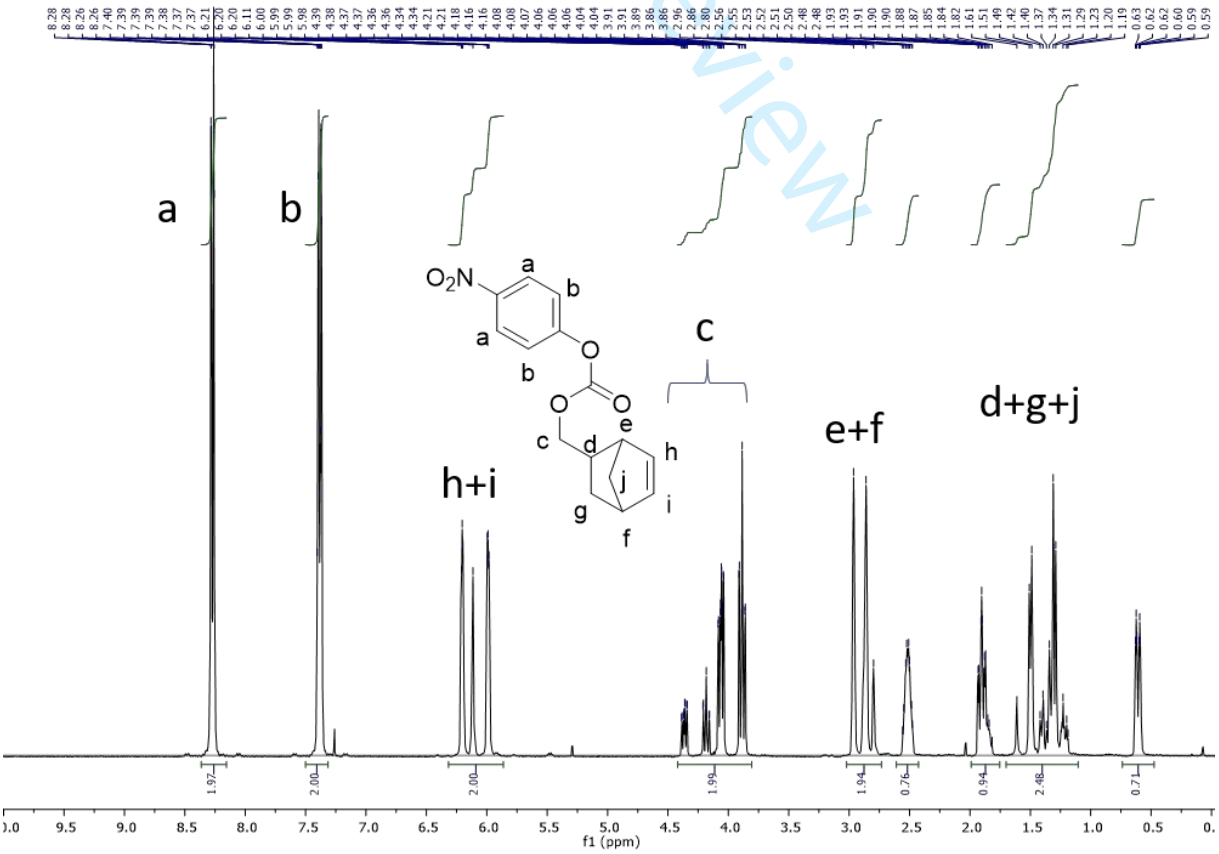

1-(3-azidopropoxy)-4-(dimethoxymethyl)benzene (**3**) (^{1}H)

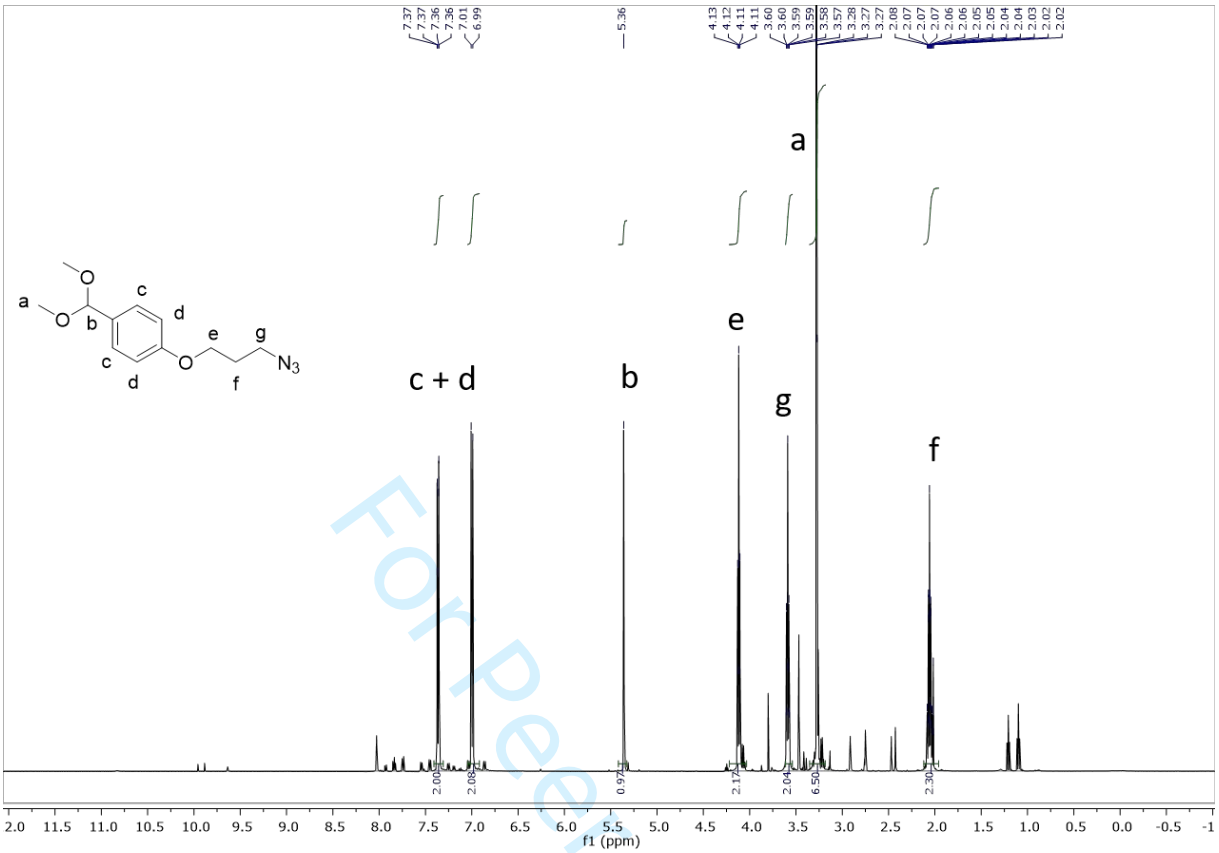

2-(azidomethyl)-3,4-dihydro-2H-pyran (**4**) (^{1}H)

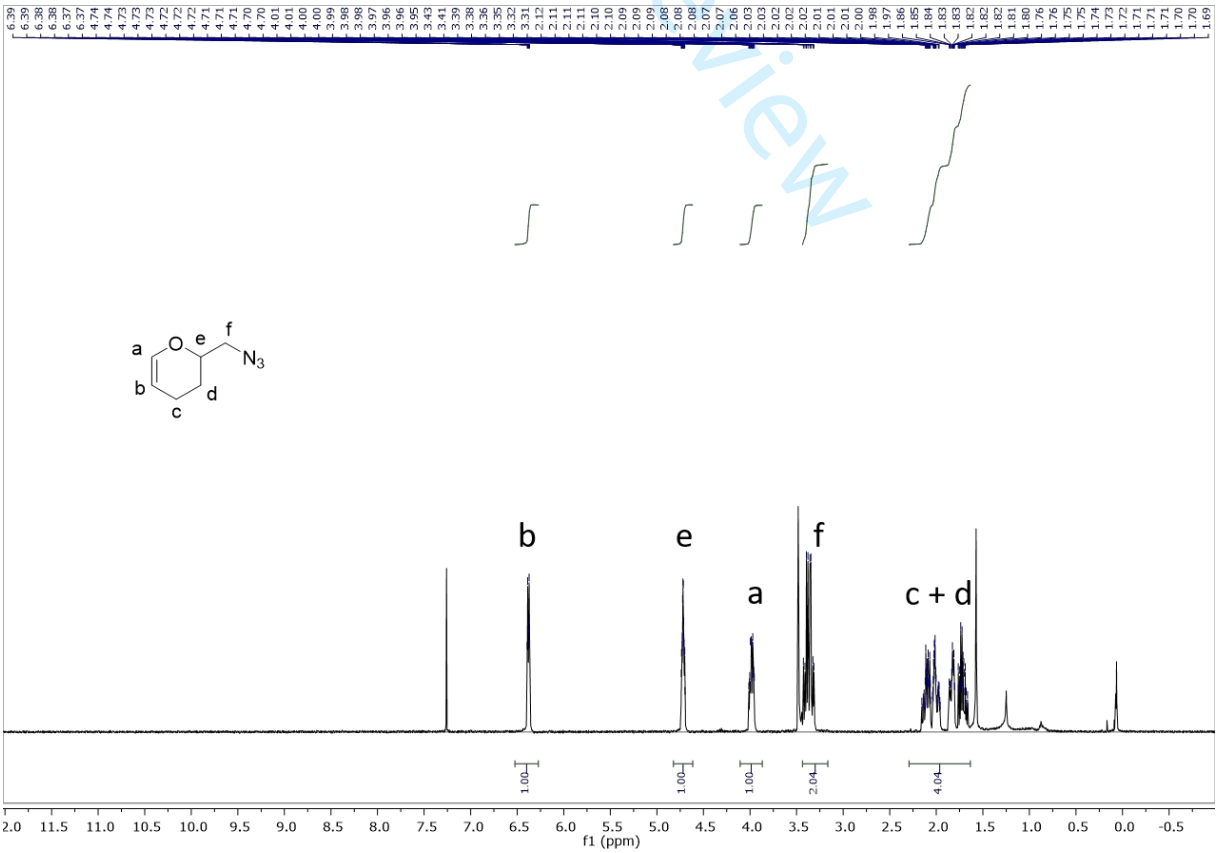

4-(6-methyl-1,2,4,5-tetrazin-3-yl)benzoic acid (**5**) (^{1}H)

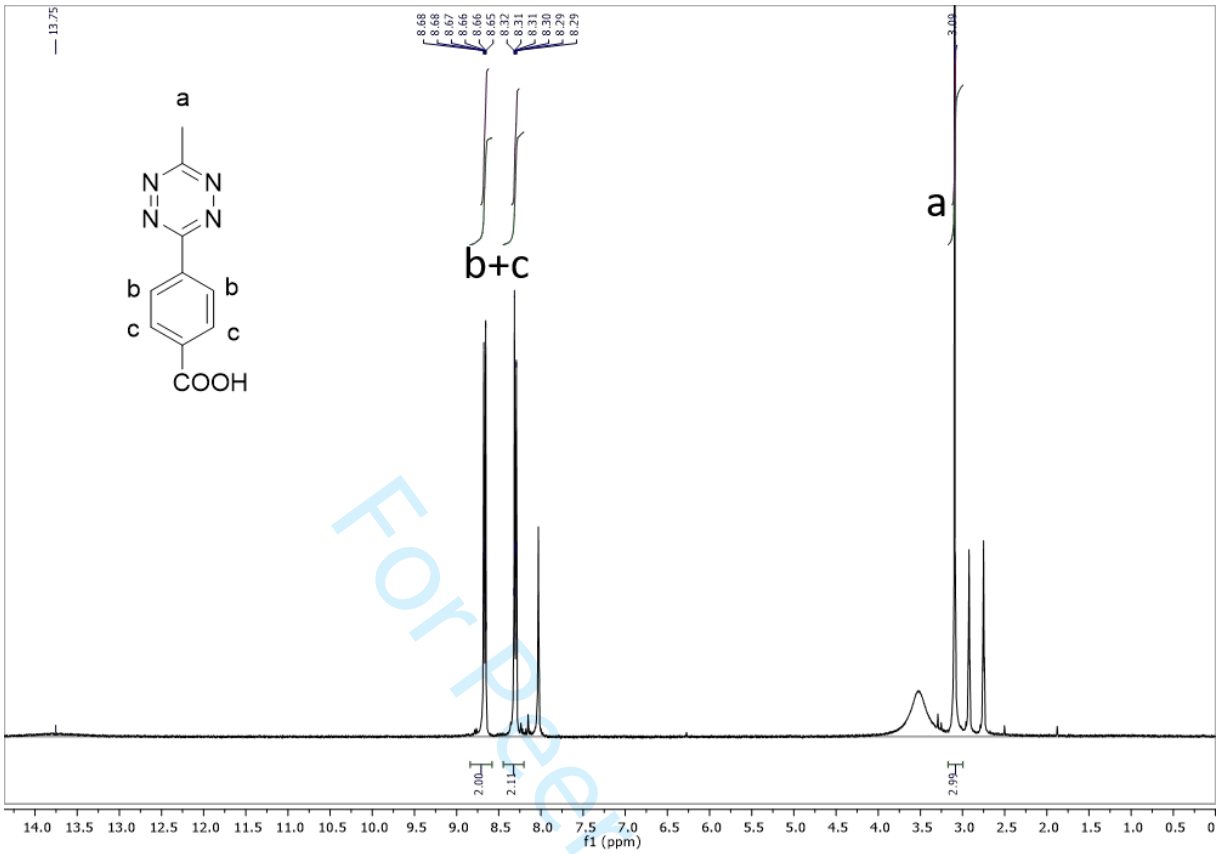

dPG-norbonene (**MM1**) (^{1}H)

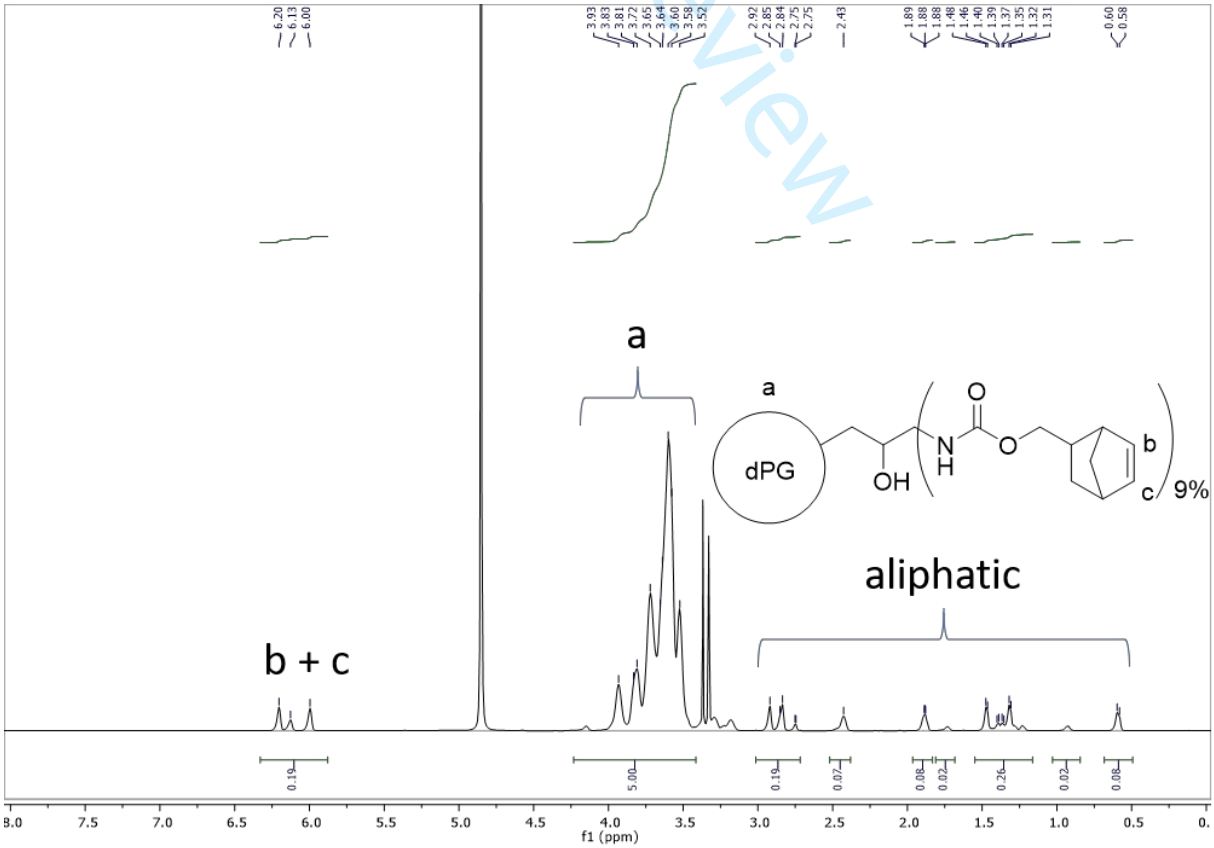

dPG-BCN (**MM2**) (^{1}H)

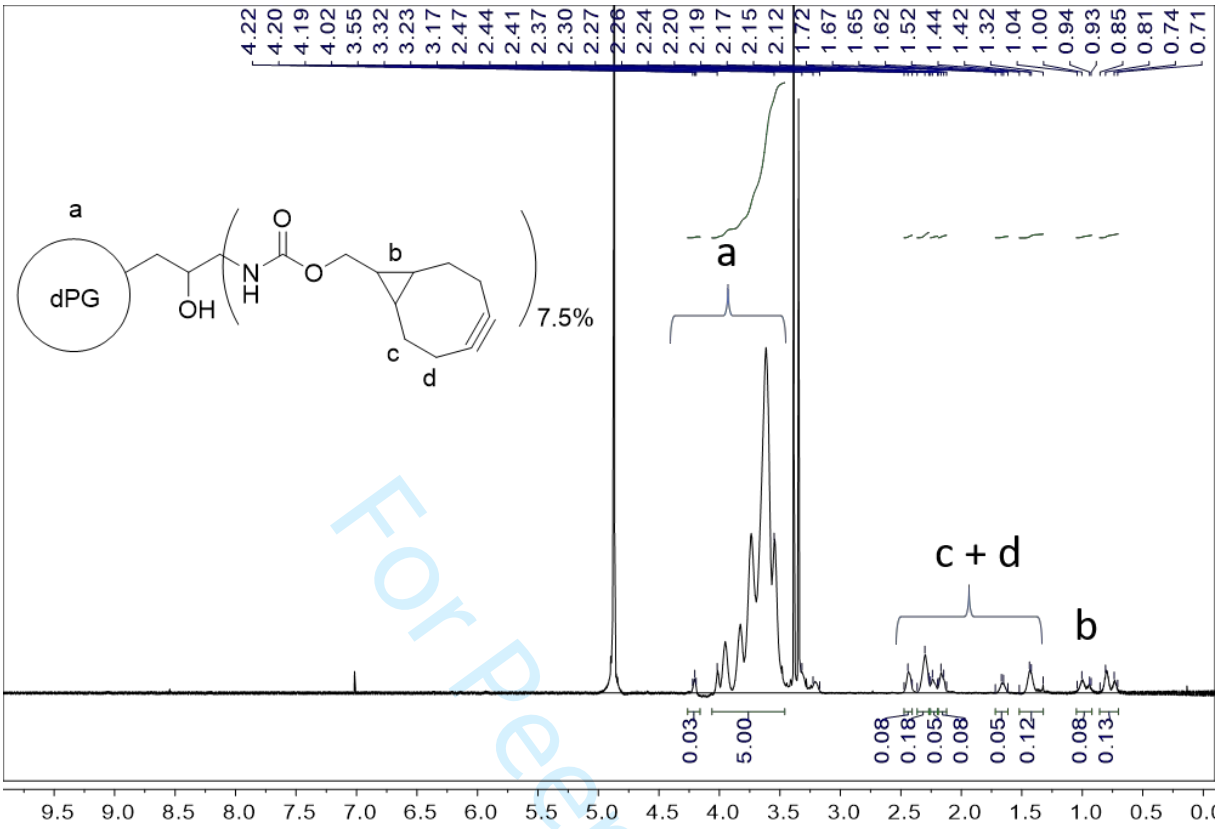

dPG-metTet (**MM3**) (^{1}H)

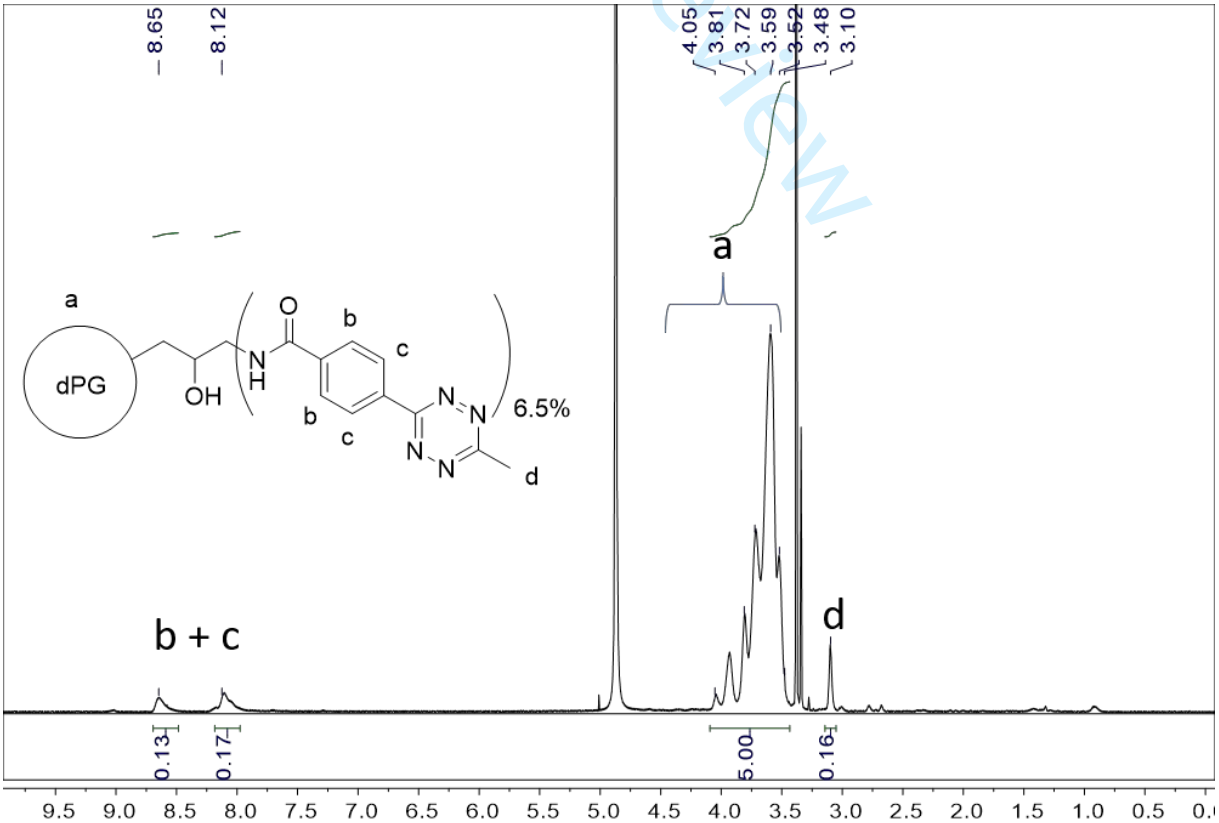

dPG-BA-N_3 (^{1}H)

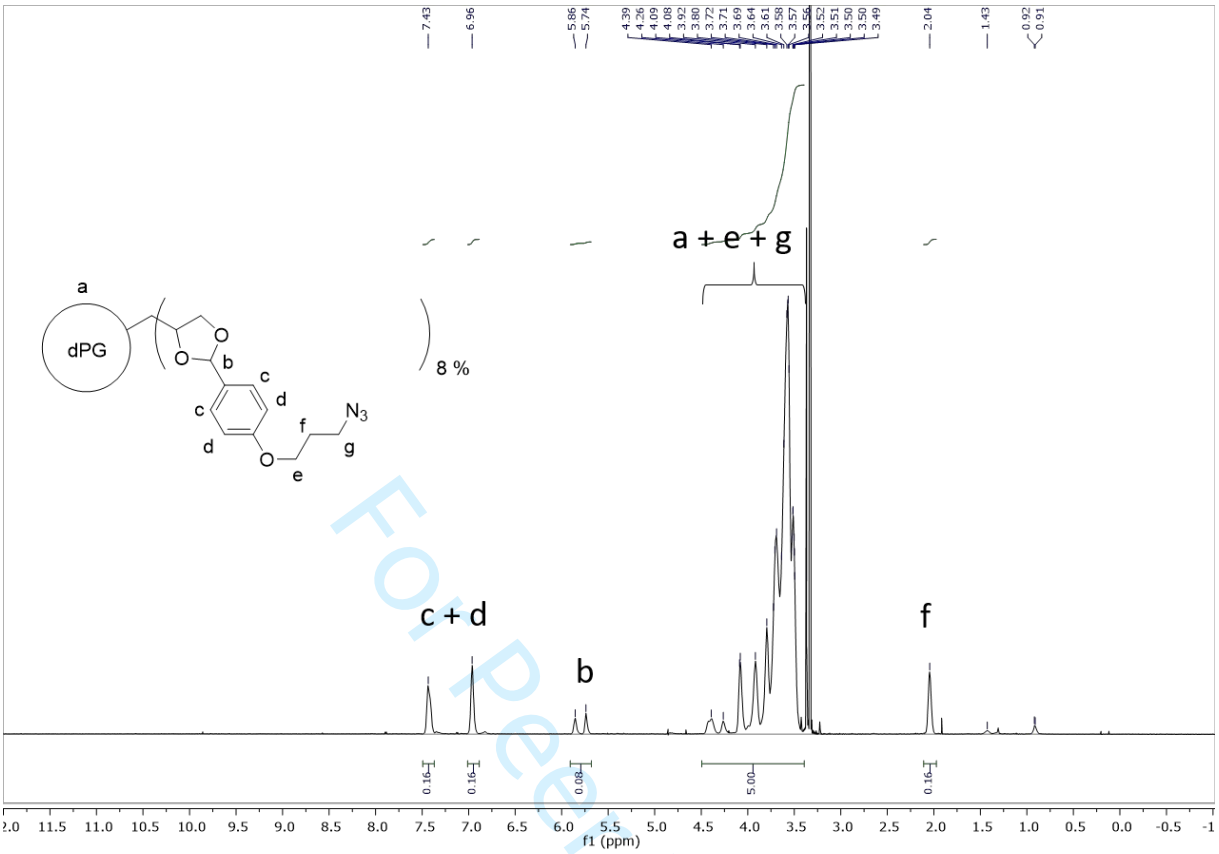

dPG-BA-NH_2 (^{1}H)

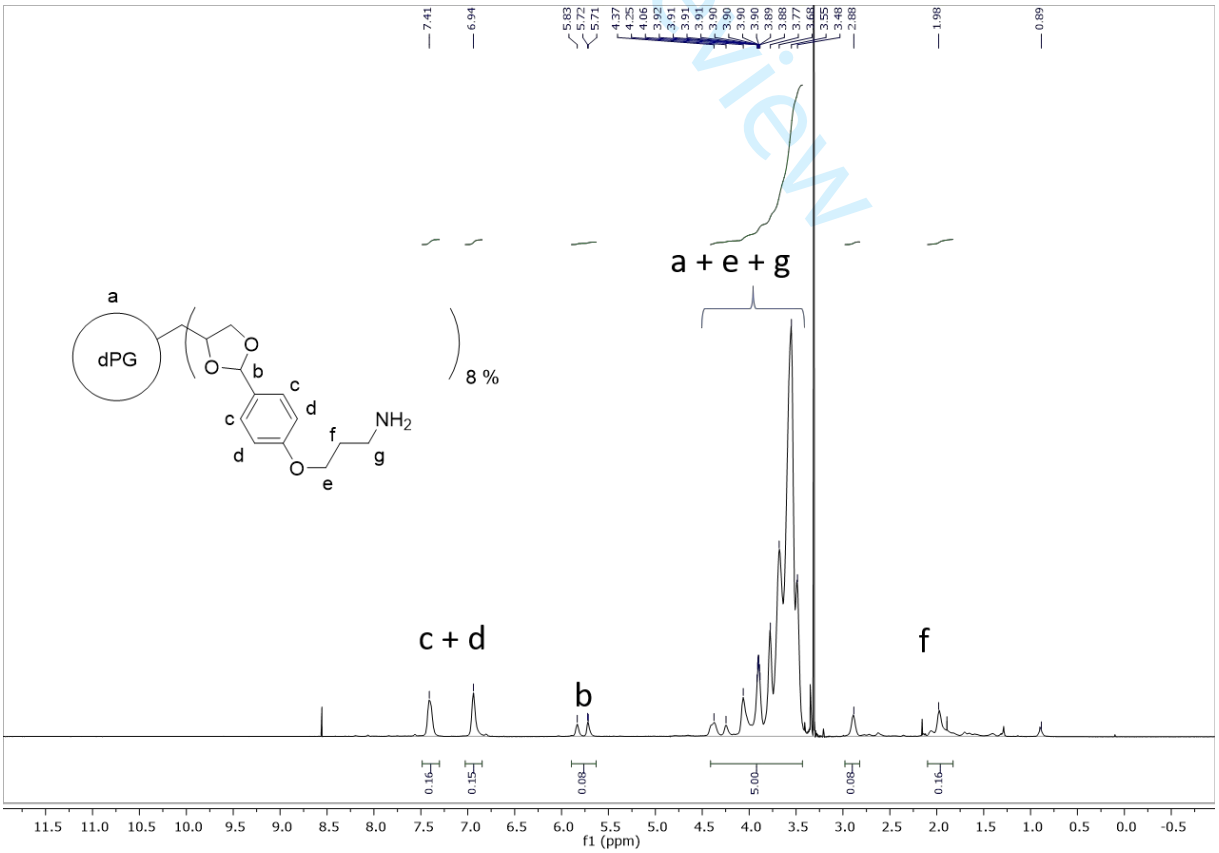

dPG-BA-norbonene (**MM4**) (^{1}H)

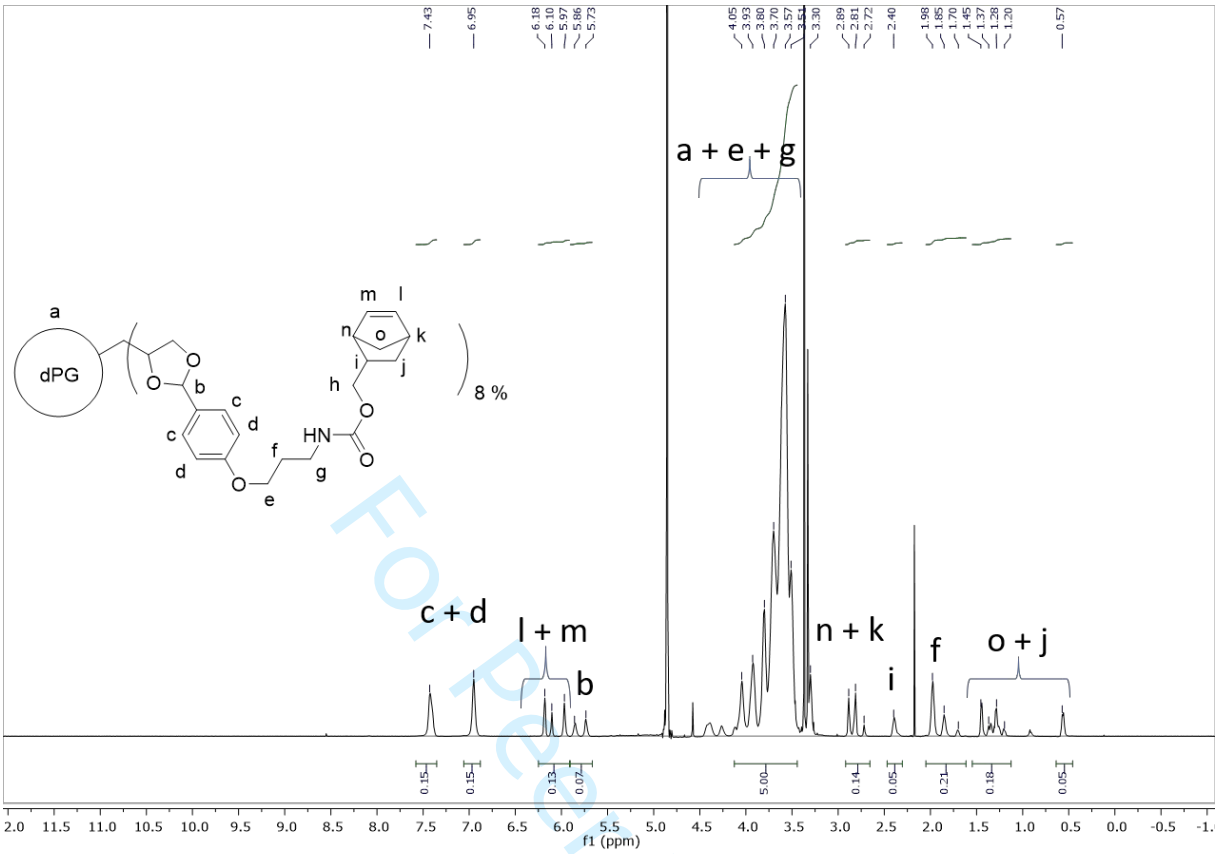

dPG-BA-norbonene (**MM4**) (^{13}C)

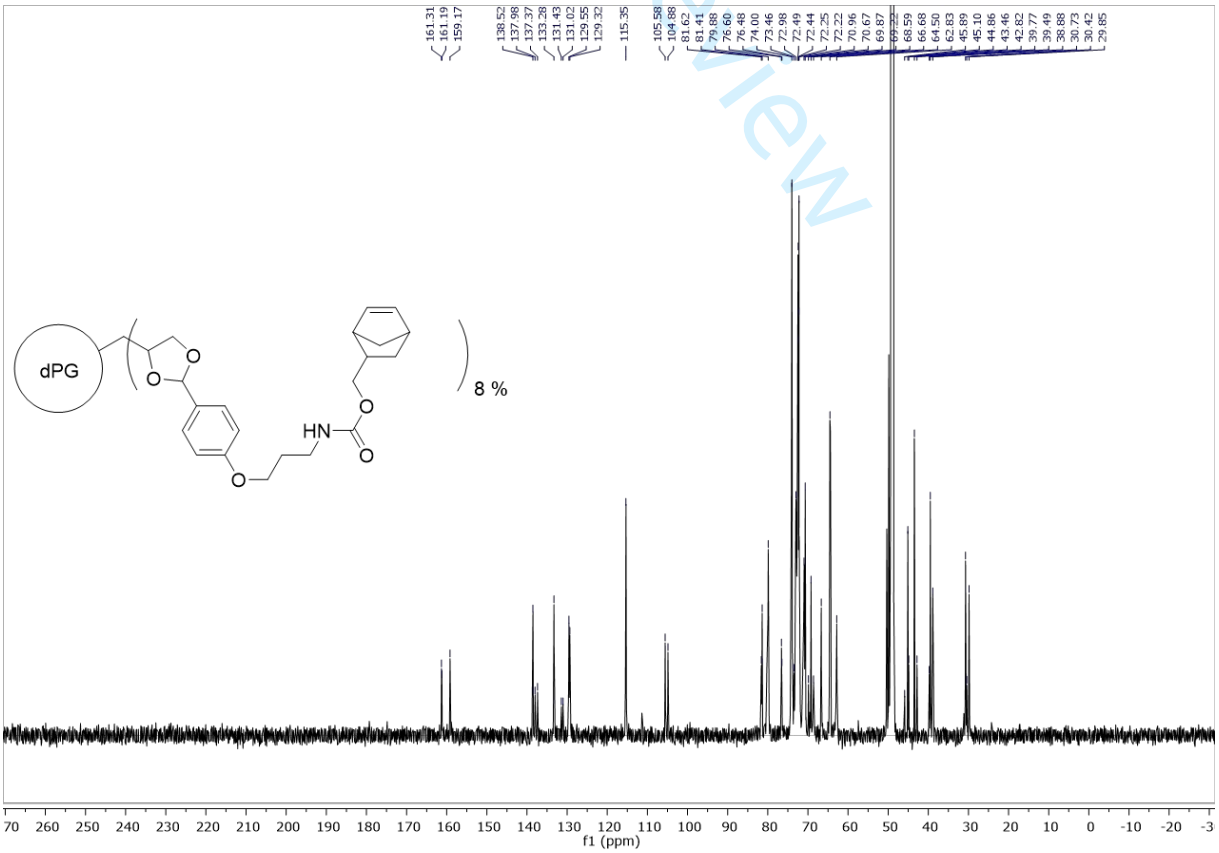

dPG-BA-BCN (**MM5**) (^{1}H)

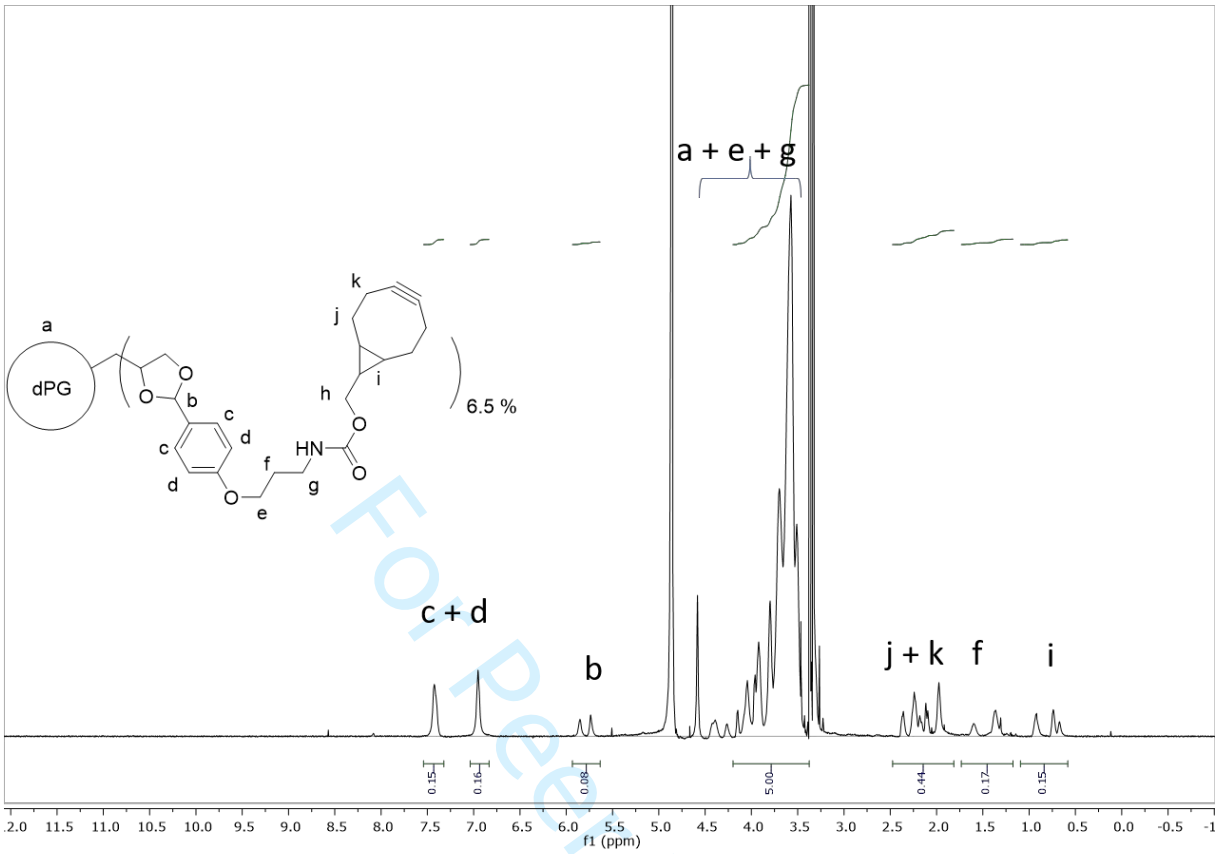

dPG-BA-BCN (**MM5**) (^{13}C)

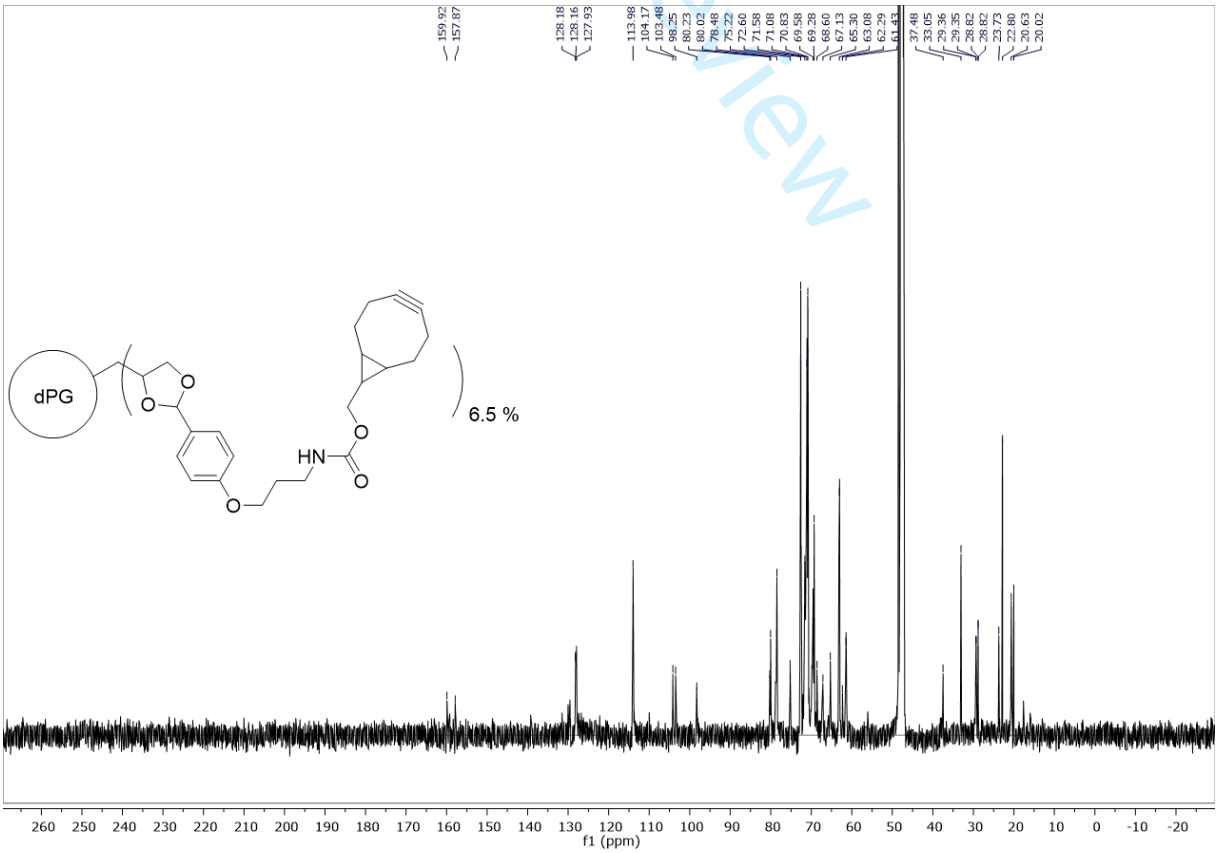

dPG-THP-azide (^{1}H)

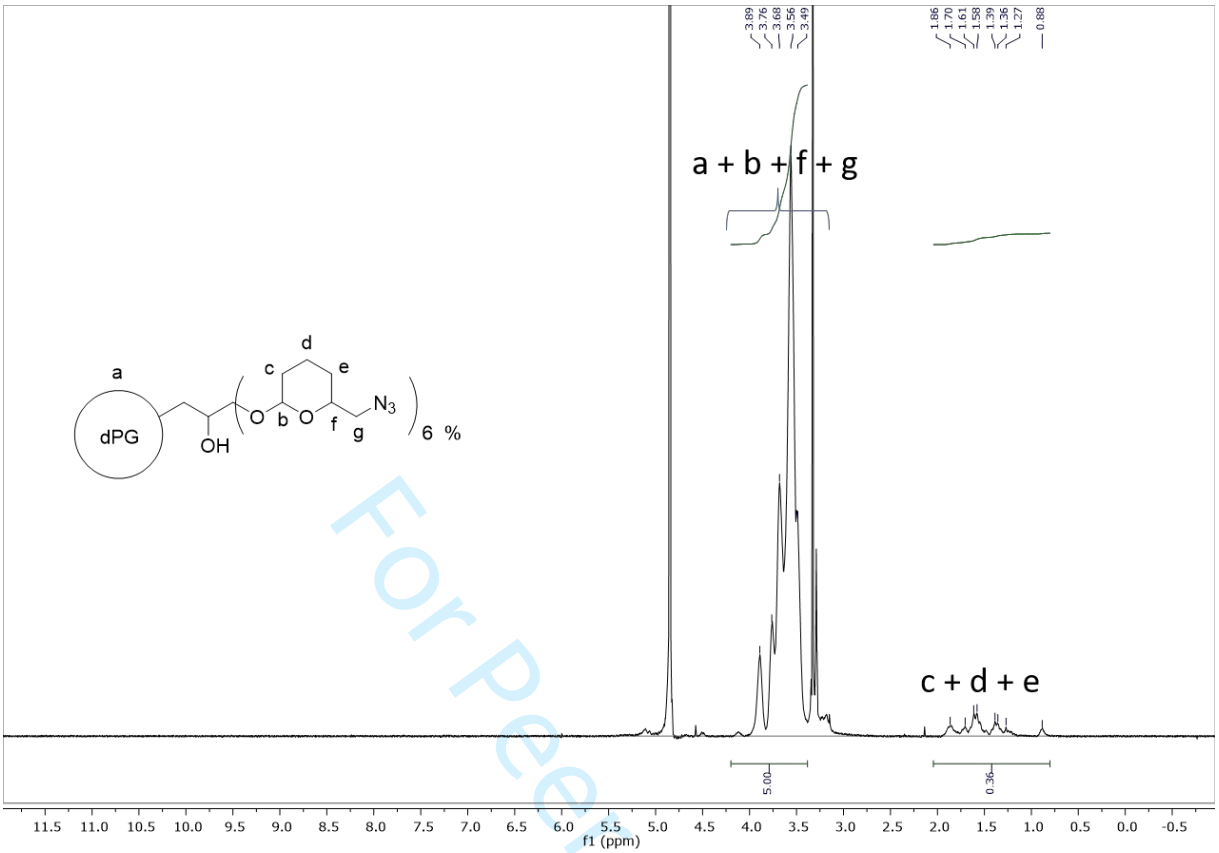

dPG-THP-amine (^{1}H)

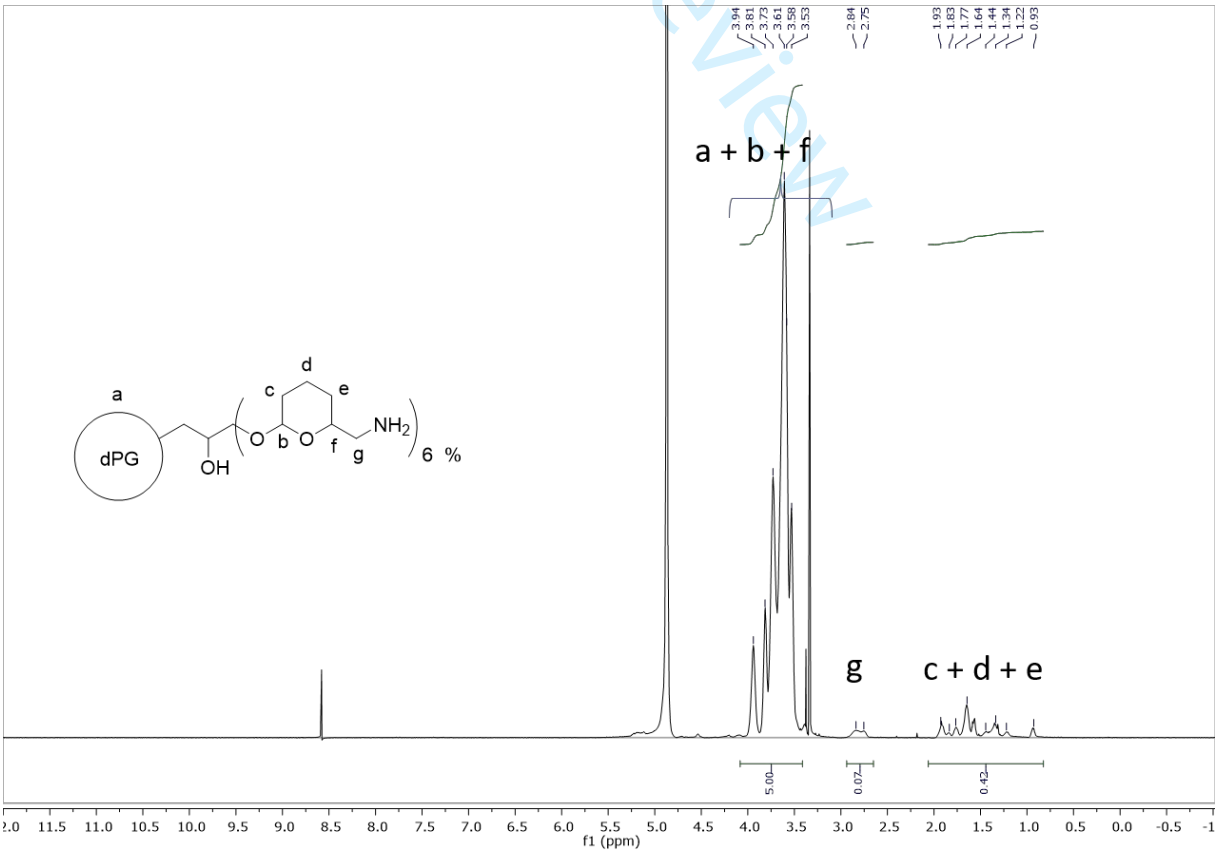

dPG-THP-norbonene (**MM6**) (^{1}H)

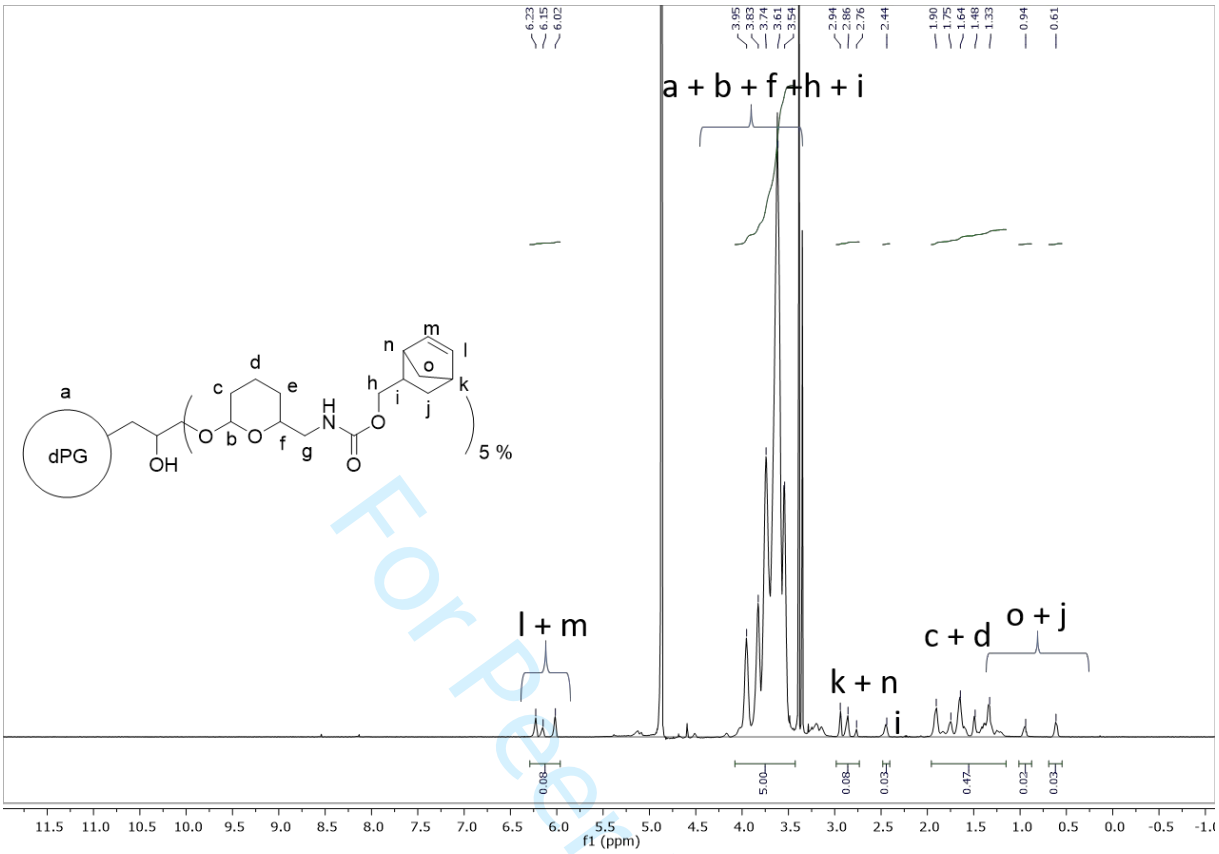

dPG-THP-norbonene (**MM6**) (^{13}C)

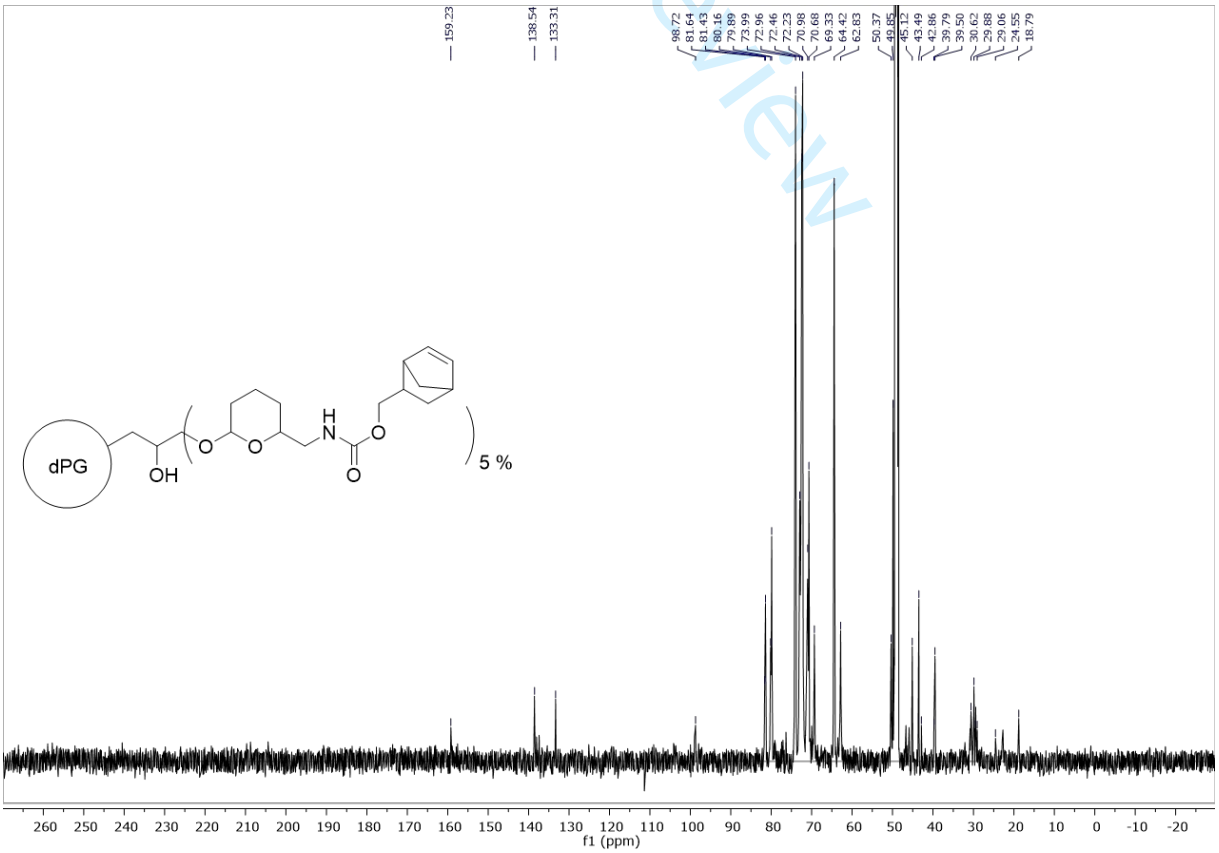

dPG-THP-BCN (**MM7**) (^{1}H)

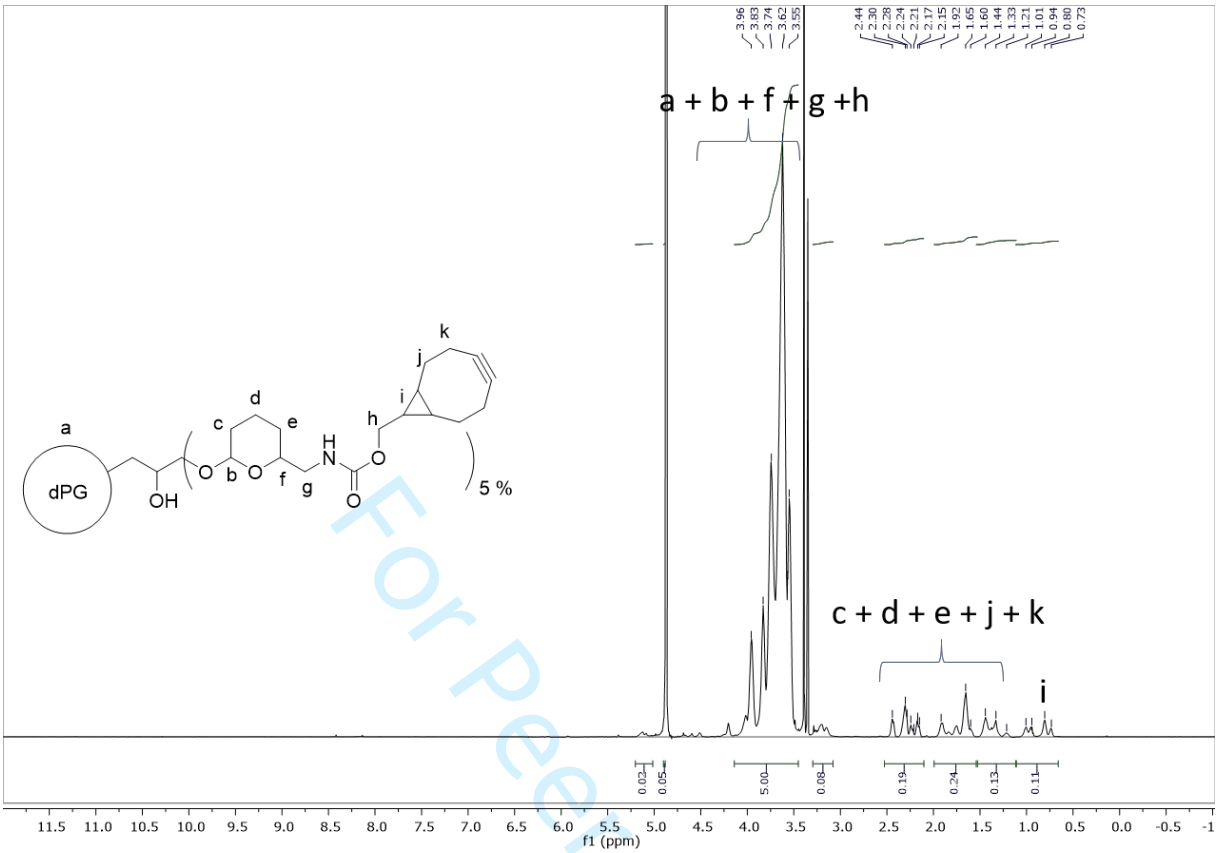

dPG-THP-BCN (**MM7**) (^{13}C)

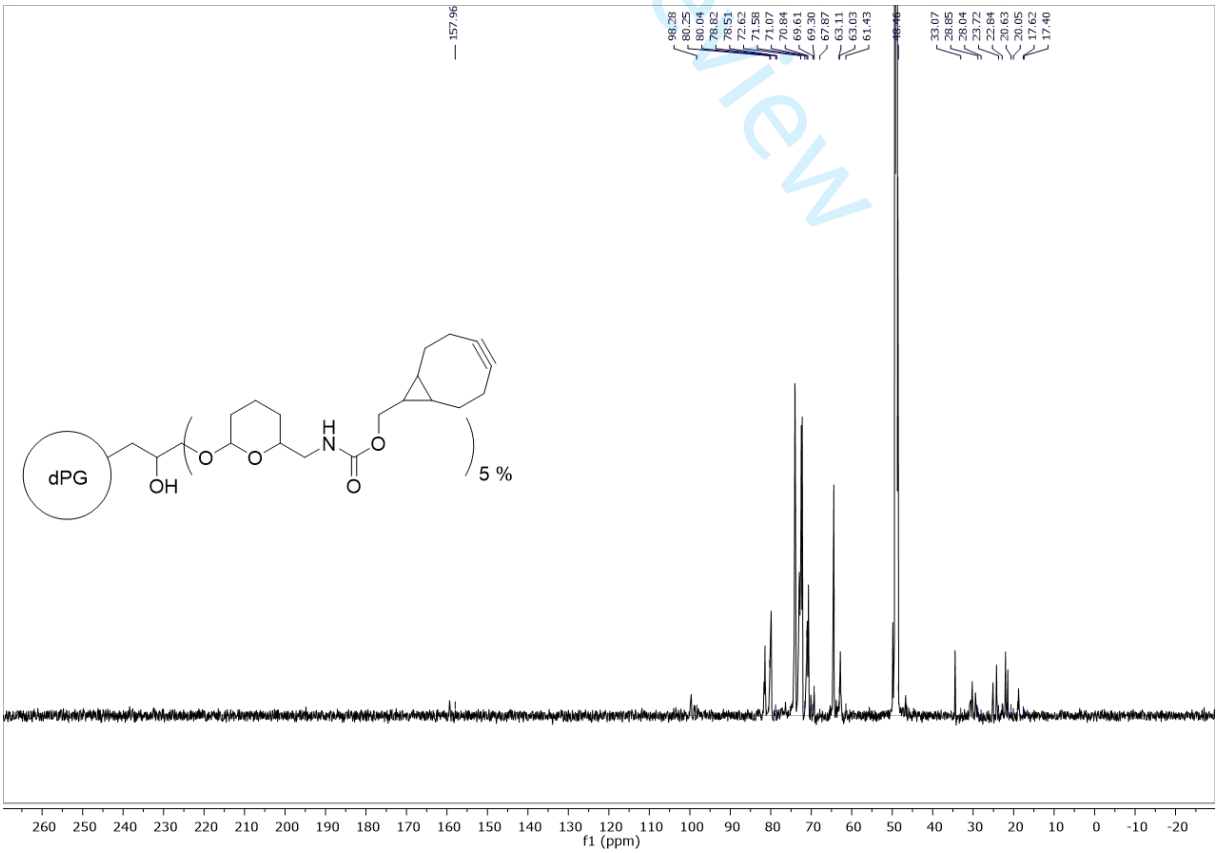

References

1. Dommerholt J, Schmidt S, Temming R, et al (2010) Readily Accessible Bicyclononynes for Bioorthogonal Labeling and Three-Dimensional Imaging of Living Cells. Angew Chem Int Ed 49:9422–9425. https://doi.org/10.1002/anie.201003761

2. Dey P, Bergmann T, Cuellar-Camacho JL, et al (2018) Multivalent Flexible Nanogels Exhibit Broad-Spectrum Antiviral Activity by Blocking Virus Entry. ACS Nano 12:6429–6442. https://doi.org/10.1021/acsnano.8b01616

3. Karver MR, Weissleder R, Hilderbrand SA (2011) Synthesis and evaluation of a series of 1,2,4,5-tetrazines for bioorthogonal conjugation. Bioconjug Chem 22:2263–2270. https://doi.org/10.1021/bc200295y

4. Sunder A, Hanselmann R, Frey H, Mülhaupt R (1999) Controlled synthesis of hyperbranched polyglycerols by ring-opening multibranching polymerization. Macromolecules 32:4240–4246. https://doi.org/10.1021/ma990090w

5. Roller S, Zhou H, Haag R (2005) High-loading polyglycerol supported reagents for Mitsunobu- and acylation-reactions and other useful polyglycerol derivatives. Mol Divers 9:305–316. https://doi.org/10.1007/s11030-005-8117-y

6. Steinhilber D, Rossow T, Wedepohl S, et al (2013) Ein Mikrogelbaukasten für die bioorthogonale Verkapselung und pH-gesteuerte Freisetzung von lebenden Zellen. Angew Chem 125:13780–13785. https://doi.org/10.1002/ange.201308005

4. Conclusion and Outlook

Smart and sensitive nanocarriers for the delivery of therapeutic proteins are needed as alternatives for covalent modification with the potentially immunogenic PEG. Nanogels as water swollen, highly hydrophilic polymer networks are promising candidates for protein delivery vehicles. However, scalable production, under sensitive and mild conditions, is still an active area of research. Inverse nanoprecipitation, as one of several production methods, offers the potential for the mild and non-destructive encapsulation of sensitive proteins. The gel networks are preferably formed by crosslinking of biocompatible, hydrophilic, and easily obtainable functionalized polymers. A variety of crosslinking chemistries, such as CuAAC, Thiol-Michael addition, and SPAAC have been studied for this purpose. Most of these chemistries, however, suffer from low biorthogonality, toxic catalysts, or the low synthetic accessibility of the precursors. IEDDA has emerged as an alternative for the other click chemistries, with fast reaction kinetics, high biorthogonality and easily accessible precursors.

The goal of this study was to design nanogels in a way that most of the mentioned criteria for a successful nanocarrier system are fulfilled. Nanogels, based on the biocompatible, scalable, hydrophilic and easily functionalizable dPG were presented in this work. Inverse nanoprecipitation was used as a mild gelation method, that lacks toxic surfactants or damaging ultrasound. The bioorthogonal and fast iEDDA click chemistry, based on tetrazines and dienophiles, was established for the first time in the use of nanogel production.

The first study focused on the search for suitable dienophiles for the iEDDA crosslinking chemistry. Reactivity and scalability were most important. This was achieved by screening of different iEDDA-reactive dienophile macromonomers. For this, the four different dienophile macromonomers dPG-norbonene, dPG-BCN, dPG-cyclopropene, and dPG-DHP were synthesized. As the tetrazine counterpart, the stable but still reactive dPG-metTet was obtained. The macromonomers were compared regarding their ability to form macro-and nanogels. Gelation times were determined and revealed that only dPG-norbonene and dPG-cyclopropene were able to form macrogels, while dPG-BCN showed incomplete, and dPG-DHP no gel formation at all. For nanogel formation, reaction parameters, such as rotation speed, macromonomer concentration, quenching times, and solvent to non-solvent ratios were screened. Solvent to non-solvent ratio and quenching time were the most influential parameters on nanogel size and polydispersity. The nanogels were obtained in the relevant size range of 40 to 200 nm and were stable for at least several months in aqueous solution.

Co-precipitation of the small model protein myoglobin was performed with the most promising macromonomer candidates dPG-norbonene and -cyclopropene. Encapsulation efficiencies of above 70% were achieved. Thus, it could be shown that a combination of dPG as the polymer scaffold, together with easily obtainable iEDDA reactive groups, such as norbonene and methyl tetrazine provide the toolbox for the design of a scalable and functional nanocarrier for proteins.

The second study aimed at transferring the gained knowledge on nanogel formation parameters, such as quenching time and solvent to non-solvent ratio on a smart, environmentally responsive version of the nanogel system. Environmentally responsiveness was achieved by the introduction of pH-cleavable acetal groups. One which is cleavable at pH values below 5 (benzacetal) and one which cleaves at values below 3 (THP). For this dPG was functionalized with the respective acetal linkers and then further functionalized with the dienophiles norbonene and BCN from the first study. Norbonene was the most promising candidate and BCN was used as a well-established comparison. The macromonomers showed no toxicity up to concentrations of 2.5 mg/mL in three different cell lines. Nanogels in the size range of 47-200 nm were obtained, which were stable in aqueous solution at pH 7.4 for several months, without decomposition or an increase of polydispersity. Upon exposure to acidic conditions, the benzacetal-based nanogels cleaved to small particles at pH 4.5 within 48 h, while the THP acetal-based nanogels cleaved only at pH 3 to small particles after 48 h. This proved the applicability of the nanogels for lysosomal cleavage and intracellular delivery for benzacetal gels and a potential delivery to the small intestine by the THP acetal functionalized gels. Co-precipitation of the therapeutic protein asparaginase led to encapsulation efficiencies of up to 93%. The degradability of the gels, the high encapsulation efficiencies, as well as the synthetic accessibility and biocompatibility of the macromonomer precursors, point out the potential of this nanocarrier platform for biomedical applications.

Based on the data that was obtained, the potential of the iEDDA based nanogels is evident. However, scalability must be improved at least for the nanogel production itself. Continuous flow methods, such as microfluidic based nanoprecipitation could potentially be used for the upscaling of the nanogels presented in this work. Furthermore, the addition of active targeting ligands to the nanogels or the macromonomers before inverse nanoprecipitation would even further increase the applicability of these nanogels for biomedical applications. One way of an easily obtainable active targeting moiety would be the sulfation of the dPG-macromonomers, which would introduce L-selectin binding affinity into the nanogels, thus targeting inflamed tissues.

5. Zusammenfassung

Intelligente und responsive Nanocarrier für die Verabreichung therapeutischer Proteine werden als Alternativen für die kovalente Modifikation mit dem potenziell immunogenen PEG benötigt. In diese Gruppe gehören Nanogele, die als geschwollene, wasserreiche, sehr hydrophile Polymernetzwerke vielversprechende Kandidaten für den Transport von therapeutischen Proteinen sind. Die skalierbare Produktion unter milden Bedingungen ist jedoch nach wie vor ein aktives Forschungsgebiet. Die umgekehrte Nanopräzipitation, als eines von mehreren Produktionsverfahren, bietet das Potenzial für die schonende und strukturerhaltende Verkapselung empfindlicher Proteine. Bei diesem Verfahren entstehen Gel-Netzwerke vorzugsweise durch die Vernetzung von biokompatiblen, hydrophilen und leicht herstellbaren funktionalisierten Polymeren. Eine Vielzahl von Klickreaktionen, wie CuAAC, Thiol-Michael-Addition und SPAAC, wurden für die Verwendung als Quervernetzungsreaktionen untersucht. Die meisten dieser Reaktionen haben jedoch verschiedene Nachteile, wie eine geringe Bioorthogonalität, die Verwendung toxischer Katalysatoren oder eine geringe synthetische Zugänglichkeit der Vorstufen. IEDDA hat sich hingegen als Alternative zu diesen Klickreaktionen herausgestellt, was an einer schnellen Reaktionskinetik, einer hohen Bioorthogonalität und leicht zugänglichen Vorstufen liegt.

Ziel dieser Arbeit war es, Nanogele so zu gestalten, dass die meisten der oben genannten Kriterien für ein erfolgreiches Nanocarrier-System erfüllt werden. Hierzu wurden Nanogele, die auf dem biokompatiblen, skalierbaren, hydrophilen und leicht funktionalisierbaren dPG basieren, in dieser Arbeit thematisiert. Die umgekehrte Nanopräzipitation wurde als milde Geliermethode eingesetzt, welche ohne toxische Tenside oder schädlichen Ultraschall auskommt. Diese wurde kombiniert mit der bioorthogonalen und schnellen iEDDA-Click-Chemie, wlche auf Tetrazin und Dienophilen basiert. Die Kombination dieser Methoden wurde hier zum ersten Mal für die Darstellung von Nanogelen etabliert und im Detail studiert.

Die erste Studie legte den Fokus auf die Suche nach geeigneten Dienophilen für die iEDDA-Vernetzungschemie, wobei Reaktivität und Skalierbarkeit im Vordergrund standen. Dies wurde durch das Screening verschiedener iEDDA-reaktiver Dienophil-funktionalisierter Makromonomere erreicht. Dazu wurden die vier verschiedenen Makromonomere dPG-Norbonen, dPG-BCN, dPG-Cyclopropen und dPG-DHP synthetisiert. Als Tetrazin-Gegenstück wurde das stabile, aber dennoch reaktive dPG-metTet erhalten. Die Makromonomere wurden hinsichtlich ihrer Fähigkeit, Makro- und Nanogele zu bilden,

verglichen. Die Gelierungszeiten wurden bestimmt und es zeigte sich, dass nur dPG-Norbonen und dPG-Cyclopropen Makrogele bilden konnten, während dPG-BCN eine unvollständige und dPG-DHP überhaupt keine Gelbildung zeigte. Für die Nanogelbildung wurden Reaktionsparameter wie Rotationsgeschwindigkeit, Makromonomerkonzentration, Quenchzeiten und das Verhältnis von Lösungsmittel zu Nicht-Lösungsmittel untersucht. Das Verhältnis von Lösungsmittel zu Nicht-Lösungsmittel und die Quenchzeit waren hierbei die wichtigsten Parameter zur Beeinflussung der Größe des Nanogels, sowie dessen Polydispersität. Die Nanogele wurden, im für biomedizinische Anwendungen relevanten, Größenbereich von 40 bis 200 nm hergestellt und waren in wässriger Lösung mindestens mehrere Monate lang stabil. Die Co-Präzipitation des kleinen Modellproteins Myoglobin wurde mit den vielversprechendsten Makromonomerkandidaten dPG-Norbonen und -Cyclopropen durchgeführt. Es wurden Verkapselungswirkungsgrade von über 70% erreicht. So konnte gezeigt werden, dass eine Kombination aus dPG als Polymergerüst, zusammen mit leicht erhältlichen iEDDA-reaktiven Gruppen wie Norbonen und Methyltetrazin, eine flexible Basis für skalierbare und funktionelle Nanotransporter für Proteine schafft.

Die zweite Studie zielte darauf ab, die gewonnenen Erkenntnisse über die Parameter der Nanogelbildung, wie z.B. die Quenchzeit und das Verhältnis von Lösungsmittel zu Nicht-Lösungsmittel auf eine bioabbaubare Version des Nanogelsystems zu übertragen. Die Abbaubarkeit wurde hierbei durch die Einführung von pH-spaltbaren Acetalgruppen erreicht. Es wurde ein Acetal verwendet, welches bei pH-Werten unter 5 (Benzacetal) spaltbar ist und eines, welches bei Werten unter 3 (THP) spaltet. Dazu wurde dPG mit den jeweiligen Acetal-Linkern funktionalisiert und dann mit den Dienophilen Norbonen und BCN aus der ersten Studie weiter funktionalisiert. Norbonen hatte sich bereits in der vorangegangenen Studie als der vielversprechendste Kandidat herausgestellt und wurde mit dem gut etablierten Reagenz BCN verglichen. Die Makromonomere zeigten bis zu einer Konzentration von 2,5 mg/ml in drei verschiedenen Zelllinien keine Toxizität. Mit den genannten Makromonomeren war es möglich Nanogele im Größenbereich von 47-200 nm zu synthetisieren, welche in wässriger Lösung bei pH 7,4, ohne Zersetzung oder Erhöhung der Polydispersität über mehrere Monate stabil waren. Unter sauren Bedingungen hingegen spalteten sich die Nanogele auf Benzacetalbasis innerhalb von 48 Stunden bei pH 4,5 in kleine Partikel, während die Nanogele auf THP-Acetalbasis erst nach 48 Stunden bei pH 3 in kleine Partikel zerfielen. Dies bewies die Anwendbarkeit von Benzacetal-Nanogelen für die lysosomale Spaltung und intrazelluläre Freisetzung von Proteinen, während THP-Acetal Nanogele für eine mögliche Freisetzung von Proteinen nach der Magenpassage im Dünndarm in Frage kommen. Die Co-

Präzipitation des therapeutischen Proteins Asparaginase zeigte eine Verkapselungseffizienz von bis zu 93%.
Die Abbaubarkeit der Gele, die hohen Verkapselungswirkungsgrade sowie die synthetische Zugänglichkeit und Biokompatibilität der Makromonomer-Vorstufen zeigen das Potenzial dieser Nanocarrier-Plattform für biomedizinische Anwendungen auf.

Basierend auf den gewonnenen Daten ist das Potenzial der iEDDA-basierten Nanogele offensichtlich. Die Skalierbarkeit muss jedoch zumindest für die Nanogel-Produktion selbst verbessert werden. Kontinuierliche Produktionsmethoden, wie die mikrofluidische Nanopräzipitation, könnten potenziell für das Upscaling der in dieser Arbeit vorgestellten Nanogele eingesetzt werden. Darüber hinaus würde die Funktionalisierung der Nanogele mit Liganden für das aktive Targeting den Nutzen dieser Nanogele für biomedizinische Anwendungen noch weiter erhöhen. Eine Möglichkeit einer leicht zugänglichen aktiven Targeting-Funktionalität wäre die Sulfatierung der dPG-Makromonomere, welche eine L-Selektin-Bindungsaffinität in die Nanogele einbringen würde. Damit könnte eine gezielte Bindung an Makrophagen in entzündetem Gewebe erreicht werden.

6. References

[1] C. M. Dawidczyk, C. Kim, J. H. Park, L. M. Russell, K. H. Lee, M. G. Pomper, P. C. Searson, *J. Control. Release* **2014**, *187*, 133–144.

[2] P. L. Turecek, M. J. Bossard, F. Schoetens, I. A. Ivens, *J. Pharm. Sci.* **2016**, *105*, 460–475.

[3] S. Mignani, S. El Kazzouli, M. Bousmina, J.-P. Majoral, *Adv. Drug Deliv. Rev.* **2013**, *65*, 1316–1330.

[4] M. B. Brown, G. P. Martin, S. A. Jones, F. K. Akomeah, *Drug Deliv.* **2006**, *13*, 175–187.

[5] M. M. Doherty, K. S. Pang, *Drug Chem. Toxicol.* **1997**, *20*, 329–344.

[6] J. Guo, I. Johansson, S. Mkrtchian, M. Ingelman-Sundberg, *Drug Metab. Rev.* **2016**, *48*, 369–378.

[7] P. D. Leeson, B. Springthorpe, *Nat. Rev. Drug Discov.* **2007**, *6*, 881–890.

[8] R. P. Heaney, *J. Nutr.* **2001**, *131*, 1344S-1348S.

[9] F. E. Stuurman, B. Nuijen, J. H. Beijnen, J. H. M. Schellens, *Clin. Pharmacokinet.* **2013**, *52*, 399–414.

[10] I. N. Kurniasih, J. Keilitz, R. Haag, *Chem. Soc. Rev.* **2015**, *44*, 4145–4164.

[11] M. E. Fox, F. C. Szoka, J. M. J. Fréchet, *Acc. Chem. Res.* **2009**, *42*, 1141–1151.

[12] R. Duncan, *Nat. Rev. Drug Discov.* **2003**, *2*, 347–360.

[13] A. Ruiz-Garcia, M. Bermejo, A. Moss, V. G. Casabo, *J. Pharm. Sci.* **2008**, *97*, 654–690.

[14] A. L. Sisson, I. Papp, K. Landfester, R. Haag, *Macromolecules* **2009**, *42*, 556–559.

[15] B. Chen, W. Dai, B. He, H. Zhang, X. Wang, Y. Wang, Q. Zhang, *Theranostics* **2017**, *7*, 538–558.

[16] B. D. Ulery, L. S. Nair, C. T. Laurencin, *J. Polym. Sci. Part B Polym. Phys.* **2011**, *49*, 832–864.

[17] K. Ulbrich, K. Holá, V. Šubr, A. Bakandritsos, J. Tuček, R. Zbořil, *Chem. Rev.* **2016**, *116*, 5338–5431.

[18] S. Bazban-Shotorbani, M. M. Hasani-Sadrabadi, A. Karkhaneh, V. Serpooshan, K. I. Jacob, A. Moshaverinia, M. Mahmoudi, *J. Control. Release* **2017**, *253*, 46–63.

[19] J. Suksiriworapong, V. Taresco, D. P. Ivanov, I. D. Styliari, K. Sakchaisri, V. B. Junyaprasert, M. C. Garnett, *Colloids Surfaces B Biointerfaces* **2018**, *167*, 115–125.

[20] X. Pang, Y. Jiang, Q. Xiao, A. W. Leung, H. Hua, C. Xu, *J. Control. Release* **2016**, *222*, 116–129.

[21] Y. Su, Y. Hu, Y. Du, X. Huang, J. He, J. You, H. Yuan, F. Hu, *Mol. Pharm.* **2015**, *12*, 1193–1202.

[22] F. Y. Qiu, M. Zhang, R. Ji, F. S. Du, Z. C. Li, *Macromol. Rapid Commun.* **2015**, *36*, 2012–2018.

[23] F. M. Veronese, G. Pasut, *Drug Discov. Today* **2005**, *10*, 1451–1458.

[24] A. Kakinoki, Y. Kaneo, Y. Ikeda, T. Tanaka, K. Fujita, *Biol. Pharm. Bull.* **2008**, *31*, 103–110.

[25] Y. Yu, J. Zou, L. Yu, W. Ji, Y. Li, W.-C. Law, C. Cheng, *Macromolecules* **2011**, *44*, 4793–4800.

[26] S. Dey, K. Sreenivasan, *Carbohydr. Polym.* **2014**, *99*, 499–507.

[27] Y. Wang, J. Zhou, L. Qiu, X. Wang, L. Chen, T. Liu, W. Di, *Biomaterials* **2014**, *35*, 4297–4309.

[28] W. She, N. Li, K. Luo, C. Guo, G. Wang, Y. Geng, Z. Gu, *Biomaterials* **2013**, *34*, 2252–2264.

[29] A. Wall, K. Nicholls, M. B. Caspersen, S. Skrivergaard, K. A. Howard, K. Karu, V. Chudasama, J. R. Baker, *Org. Biomol. Chem.* **2019**, *17*, 7870–7873.

[30] S. Lonial, M. Dimopoulos, A. Palumbo, D. White, S. Grosicki, I. Spicka, A. Walter-Croneck, P. Moreau, M.-V. Mateos, H. Magen, et al., *N. Engl. J. Med.* **2015**, *373*, 621–631.

[31] Q. J. Baca, B. Leader, D. E. Golan, *Protein Therapeutics*, Springer International Publishing, Cham, **2017**.

[32] D. Johnson, *Int. J. Mol. Sci.* **2018**, *19*, 3685.

[33] A. F. Hussain, H. R. Krüger, F. Kampmeier, T. Weissbach, K. Licha, F. Kratz, R. Haag, M. Calderón, S. Barth, *Biomacromolecules* **2013**, *14*, 2510–2520.

[34] M. L. Etheridge, S. A. Campbell, A. G. Erdman, C. L. Haynes, S. M. Wolf, J. McCullough, *Nanomedicine Nanotechnology, Biol. Med.* **2013**, *9*, 1–14.

[35] M. A. Dobrovolskaia, B. W. Neun, S. Man, X. Ye, M. Hansen, A. K. Patri, R. M. Crist, S. E. McNeil, *Nanomedicine Nanotechnology, Biol. Med.* **2014**, *10*, 1453–1463.

[36] E. Polo, M. Collado, B. Pelaz, P. Del Pino, *ACS Nano* **2017**, *11*, 2397–2402.

[37] R. Shrimanker, I. D. Pavord, **2017**, pp. 587–610.

[38] T. A. H. Järvinen, J. Rashid, T. Valmari, U. May, F. Ahsan, *ACS Biomater. Sci. Eng.* **2017**, *3*, 1273–1282.

[39] J. K. Dozier, M. D. Distefano, *Int. J. Mol. Sci.* **2015**, *16*, 25831–25864.

[40] Y. Wang, C. Wu, *Biomacromolecules* **2018**, *19*, 1804–1825.

[41] C. Ginn, H. Khalili, R. Lever, S. Brocchini, *Future Med. Chem.* **2014**, *6*, 1829–1846.

[42] F. Farjadian, A. Ghasemi, O. Gohari, A. Roointan, M. Karimi, M. R. Hamblin, *Nanomedicine* **2019**, *14*, 93–126.

[43] P. Zhang, F. Sun, S. Liu, S. Jiang, *J. Control. Release* **2016**, *244*, 184–193.

[44] M. Weinhart, I. Grunwald, M. Wyszogrodzka, L. Gaetjen, A. Hartwig, R. Haag, *Chem. - Asian J.* **2010**, *5*, 1992–2000.

[45] K. Knop, R. Hoogenboom, D. Fischer, U. S. Schubert, *Angew. Chem. - Int. Ed.* **2010**,

49, 6288–6308.

[46] D. F. Williams, *Biomaterials* **2008**, *29*, 2941–2953.

[47] T. Hayashi, *Prog. Polym. Sci.* **1994**, *19*, 663–702.

[48] J. Kopeček, *Biomaterials* **1984**, *5*, 19–25.

[49] R. B. Greenwald, Y. H. Choe, J. McGuire, C. D. Conover, *Adv. Drug Deliv. Rev.* **2003**, *55*, 217–250.

[50] C. L. Ferreira, C. A. Valente, M. L. Zanini, B. Sgarioni, P. H. Ferreira Tondo, P. C. Chagastelles, J. Braga, M. M. Campos, J. A. Malmonge, N. R. de Souza Basso, *Macromol. Symp.* **2019**, *383*, 1800028.

[51] I. Vroman, L. Tighzert, *Materials (Basel).* **2009**, *2*, 307–344.

[52] A. J. R. Lasprilla, G. A. R. Martinez, B. H. Lunelli, A. L. Jardini, R. M. Filho, *Biotechnol. Adv.* **2012**, *30*, 321–328.

[53] J. a. Czaplewska, T. C. Majdanski, M. J. Barthel, M. Gottschaldt, U. S. Schubert, *J. Polym. Sci. Part A Polym. Chem.* **2015**, *53*, 2163–2174.

[54] S. K. Shukla, A. K. Mishra, O. A. Arotiba, B. B. Mamba, *Int. J. Biol. Macromol.* **2013**, *59*, 46–58.

[55] G. D. Mogoşanu, A. M. Grumezescu, *Int. J. Pharm.* **2014**, *463*, 127–136.

[56] M. Hamidi, K. Rostamizadeh, M.-A. Shahbazi, in *Intell. Nanomater.*, John Wiley & Sons, Inc., Hoboken, NJ, USA, **2012**, pp. 583–624.

[57] K. Y. Lee, D. J. Mooney, *Prog. Polym. Sci.* **2012**, *37*, 106–126.

[58] A. Thomas, S. S. Müller, H. Frey, *Biomacromolecules* **2014**, *15*, 1935–1954.

[59] M. Weinhart, T. Becherer, N. Schnurbusch, K. Schwibbert, H. J. Kunte, R. Haag, *Adv. Eng. Mater.* **2011**, *13*, 501–510.

[60] D. Steinhilber, S. Seiffert, J. A. Heyman, F. Paulus, D. A. Weitz, R. Haag, *Biomaterials* **2011**, *32*, 1311–1316.

[61] S. Abbina, S. Vappala, P. Kumar, E. M. J. Siren, C. C. La, U. Abbasi, D. E. Brooks, J. N. Kizhakkedathu, *J. Mater. Chem. B* **2017**, 29.

[62] A. Sunder, R. Hanselmann, H. Frey, R. Mülhaupt, *Macromolecules* **1999**, *32*, 4240–4246.

[63] J. Khandare, A. Mohr, M. Calderón, P. Welker, K. Licha, R. Haag, *Biomaterials* **2010**, *31*, 4268–4277.

[64] C. Wu, C. Strehmel, K. Achazi, L. Chiappisi, J. Dernedde, M. C. Lensen, M. Gradzielski, M. B. Ansorge-Schumacher, R. Haag, *Biomacromolecules* **2014**, *15*, 3881–3890.

[65] R. Haag, J. F. Stumbé, A. Sunder, H. Frey, A. Hebel, *Macromolecules* **2000**, *33*, 8158–8166.

[66] X. Zhang, K. Achazi, D. Steinhilber, F. Kratz, J. Dernedde, R. Haag, *J. Control. Release* **2014**, *174*, 209–216.

[67] I. N. Kurniasih, H. Liang, V. D. Möschwitzer, M. a. Quadir, M. Radowski, J. P. Rabe, R. Haag, *New J. Chem.* **2012**, *36*, 371.

[68] M. Beigi, S. Roller, R. Haag, A. Liese, *European J. Org. Chem.* **2008**, *2008*, 2135–2141.

[69] D. Gröger, F. Paulus, K. Licha, P. Welker, M. Weinhart, C. Holzhausen, L. Mundhenk, A. D. Gruber, U. Abram, R. Haag, *Bioconjug. Chem.* **2013**, *24*, 1507–1514.

[70] S. Biffi, S. Dal Monego, C. Dullin, C. Garrovo, B. Bosnjak, K. Licha, P. Welker, M. M. Epstein, F. Alves, *PLoS One* **2013**, *8*, e57150.

[71] K. Oishi, Y. Hamaguchi, T. Matsushita, M. Hasegawa, N. Okiyama, J. Dernedde, M. Weinhart, R. Haag, T. F. Tedder, K. Takehara, et al., *Arthritis Rheumatol.* **2014**, *66*, 1864–1871.

[72] J. Dernedde, A. Rausch, M. Weinhart, S. Enders, R. Tauber, K. Licha, M. Schirner, U. Zugel, A. von Bonin, R. Haag, *Proc. Natl. Acad. Sci.* **2010**, *107*, 19679–19684.

[73] E. Mohammadifar, F. Zabihi, Z. Tu, S. Hedtrich, A. Nemati Kharat, M. Adeli, R. Haag,

Polym. Chem. **2017**, *8*, 7375–7383.

[74] V. P. Torchilin, *Adv. Drug Deliv. Rev.* **2006**, *58*, 1532–1555.

[75] Z. Gu, A. Biswas, M. Zhao, Y. Tang, *Chem. Soc. Rev.* **2011**, *40*, 3638–3655.

[76] D. D. Lasic, *Nature* **1996**, *380*, 561–562.

[77] P. S. Gill, J. Wernz, D. T. Scadden, P. Cohen, G. M. Mukwaya, J. H. von Roenn, M. Jacobs, S. Kempin, I. Silverberg, G. Gonzales, et al., *J. Clin. Oncol.* **1996**, *14*, 2353–2364.

[78] Y. H. Choi, H. K. Han, *J. Pharm. Investig.* **2018**, *48*, 43–60.

[79] K. Kataoka, A. Harada, Y. Nagasaki, *Adv. Drug Deliv. Rev.* **2001**, *47*, 113–131.

[80] Y. Li, T. Su, S. Li, Y. Lai, B. He, Z. Gu, *Biomater. Sci.* **2014**, *2*, 775–783.

[81] G. Seetharaman, A. R. Kallar, V. M. Vijayan, J. Muthu, S. Selvam, *J. Colloid Interface Sci.* **2017**, *492*, 61–72.

[82] T. Miller, S. Breyer, G. van Colen, W. Mier, U. Haberkorn, S. Geissler, S. Voss, M. Weigandt, A. Goepferich, *Int. J. Pharm.* **2013**, *445*, 117–124.

[83] S. Hönzke, C. Gerecke, A. Elpelt, N. Zhang, M. Unbehauen, V. Kral, E. Fleige, F. Paulus, R. Haag, M. Schäfer-Korting, et al., *J. Control. Release* **2016**, *242*, 50–63.

[84] J. Frombach, M. Unbehauen, I. N. Kurniasih, F. Schumacher, P. Volz, S. Hadam, F. Rancan, U. Blume-Peytavi, B. Kleuser, R. Haag, et al., *J. Control. Release* **2019**, *299*, 138–148.

[85] S. Liu, J. V. M. Weaver, Y. Tang, N. C. Billingham, S. P. Armes, K. Tribe, *Macromolecules* **2002**, *35*, 6121–6131.

[86] M. Karg, A. Pich, T. Hellweg, T. Hoare, L. A. Lyon, J. J. Crassous, D. Suzuki, R. A. Gumerov, S. Schneider, I. I. Potemkin, et al., *Langmuir* **2019**, *35*, 6231–6255.

[87] J. K. Oh, R. Drumright, D. J. Siegwart, K. Matyjaszewski, *Prog. Polym. Sci.* **2008**, *33*, 448–477.

[88] A. V. Kabanov, S. V. Vinogradov, *Angew. Chem. Int. Ed.* **2009**, *48*, 5418–5429.

[89] B. D. Chithrani, A. A. Ghazani, W. C. W. Chan, *Nano Lett.* **2006**, *6*, 662–668.

[90] M. Argenziano, C. Dianzani, B. Ferrara, S. Swaminathan, A. Manfredi, E. Ranucci, R. Cavalli, P. Ferruti, *Gels* **2017**, *3*, 22.

[91] Z. Shatsberg, X. Zhang, P. Ofek, S. Malhotra, A. Krivitsky, A. Scomparin, G. Tiram, R. Haag, R. Satchi-fainaro, *J. Control. Release* **2016**, *239*, 159–168.

[92] L. Nuhn, M. Hirsch, B. Krieg, K. Koynov, K. Fischer, M. Schmidt, M. Helm, R. Zentel, *ACS Nano* **2012**, *6*, 2198–2214.

[93] M. Dimde, F. Neumann, F. Reisbeck, S. Ehrmann, J. L. Cuellar-Camacho, D. Steinhilber, N. Ma, R. Haag, *Biomater. Sci.* **2017**, *5*, 2328–2336.

[94] J. K. Oh, R. Drumright, D. J. Siegwart, K. Matyjaszewski, *Prog. Polym. Sci.* **2008**, *33*, 448–477.

[95] S. J. Buwalda, T. Vermonden, W. E. Hennink, *Biomacromolecules* **2017**, *18*, 316–330.

[96] E. Fleige, M. A. Quadir, R. Haag, *Adv. Drug Deliv. Rev.* **2012**, *64*, 866–884.

[97] M. Giulbudagian, M. Asadian-Birjand, D. Steinhilber, K. Achazi, M. Molina, M. Calderón, *Polym. Chem.* **2014**, *5*, 6909–6913.

[98] M. Asadian-Birjand, J. Bergueiro, F. Rancan, J. C. Cuggino, R.-C. Mutihac, K. Achazi, J. Dernedde, U. Blume-Peytayi, A. Vogt, M. Calderon, *Polym. Chem.* **2015**, *6*, 5827–5831.

[99] M. Witting, M. Molina, K. Obst, R. Plank, K. M. Eckl, H. C. Hennies, M. Calderón, W. Frieß, S. Hedtrich, *Nanomedicine* **2015**, *11*, 1179–87.

[100] W. Chen, K. Achazi, B. Schade, R. Haag, *J. Control. Release* **2015**, *205*, 15–24.

[101] R. Kawasaki, Y. Sasaki, K. Katagiri, S. Mukai, S. Sawada, K. Akiyoshi, *Angew. Chem. Int. Ed.* **2016**, *55*, 11377–11381.

[102] S. Mura, J. Nicolas, P. Couvreur, *Nat. Mater.* **2013**, *12*, 991–1003.

[103] W. Chen, Y. Zou, Z. Zhong, R. Haag, *Small* **2017**, *13*, 1–9.

[104] S. Singh, F. Topuz, K. Hahn, K. Albrecht, J. Groll, *Angew. Chem. - Int. Ed.* **2013**, *52*, 3000–3003.

[105] D. Klinger, K. Landfester, *J. Polym. Sci. Part A Polym. Chem.* **2012**, *50*, 1062–1075.

[106] W. Chen, Y. Hou, Z. Tu, L. Gao, R. Haag, *J. Control. Release* **2017**, *259*, 160–167.

[107] D. Steinhilber, T. Rossow, S. Wedepohl, F. Paulus, S. Seiffert, R. Haag, *Angew. Chem. - Int. Ed.* **2013**, *52*, 13538–13543.

[108] K. Akiyoshi, S. Kobayashi, S. Shichibe, D. Mix, M. Baudys, S. Wan Kim, J. Sunamoto, *J. Control. Release* **1998**, *54*, 313–320.

[109] S. Daoud-Mahammed, P. Couvreur, R. Gref, *Int. J. Pharm.* **2007**, *332*, 185–191.

[110] H. Zhou, D. Steinhilber, H. Schlaad, A. L. Sisson, R. Haag, *React. Funct. Polym.* **2011**, *71*, 356–361.

[111] A. L. Sisson, D. Steinhilber, T. Rossow, P. Welker, K. Licha, R. Haag, *Angew. Chem. - Int. Ed.* **2009**, *48*, 7540–7545.

[112] M. Antonietti, *Angew. Chemie Int. Ed. English* **1988**, *27*, 1743–1747.

[113] J. Z. Du, T. M. Sun, W. J. Song, J. Wu, J. Wang, *Angew. Chem. - Int. Ed.* **2010**, *49*, 3621–3626.

[114] K. McAllister, P. Sazani, M. Adam, M. J. Cho, M. Rubinstein, R. J. Samulski, J. M. DeSimone, *J. Am. Chem. Soc.* **2002**, *124*, 15198–15207.

[115] R. Jenjob, T. Phakkeeree, F. Seidi, M. Theerasilp, D. Crespy, *Macromol. Biosci.* **2019**, *19*, 1–13.

[116] R. L. Grant, C. Yao, D. Gabaldon, D. Acosta, *Toxicology* **1992**, *76*, 153–176.

[117] Â. S. Inácio, K. A. Mesquita, M. Baptista, J. Ramalho-Santos, W. L. C. Vaz, O. V. Vieira, *PLoS One* **2011**, *6*, e19850.

[118] S. E. A. Gratton, P. D. Pohlhaus, J. Lee, J. Guo, M. J. Cho, J. M. DeSimone, *J.*

Control. Release **2007**, *121*, 10–18.

[119] S. Schubert, J. T. Delaney, U. S. Schubert, *Soft Matter* **2011**, *7*, 1581–1588.

[120] C. Zhang, V. J. Pansare, R. K. Prud'homme, R. D. Priestley, *Soft Matter* **2012**, *8*, 86–93.

[121] R. Tong, L. Yala, T. M. Fan, J. Cheng, *Biomaterials* **2010**, *31*, 3043–3053.

[122] D. Steinhilber, M. Witting, X. Zhang, M. Staegemann, F. Paulus, W. Friess, S. Küchler, R. Haag, *J. Control. Release* **2013**, *169*, 289–295.

[123] P. M. Valencia, P. A. Basto, L. Zhang, M. Rhee, R. Langer, O. C. Farokhzad, R. Karnik, *ACS Nano* **2010**, *4*, 1671–1679.

[124] E. M. Sletten, C. R. Bertozzi, *Acc. Chem. Res.* **2011**, *44*, 666–676.

[125] H. C. Kolb, M. G. Finn, K. B. Sharpless, *Angew. Chem. - Int. Ed.* **2001**, *40*, 2004–2021.

[126] B. L. Oliveira, Z. Guo, G. J. L. Bernardes, *Chem. Soc. Rev.* **2017**, *46*, 4895–4950.

[127] R. Huisgen, *Angew. Chemie* **1963**, *75*, 604–637.

[128] C. W. Tornøe, C. Christensen, M. Meldal, *J. Org. Chem.* **2002**, *67*, 3057–3064.

[129] V. V. Rostovtsev, L. G. Green, V. V. Fokin, K. B. Sharpless, *Angew. Chem. Int. Ed.* **2002**, *41*, 2596–2599.

[130] M. G. Finn, V. V. Fokin, *Chem. Soc. Rev.* **2010**, *39*, 1231.

[131] D. C. Kennedy, C. S. McKay, M. C. B. Legault, D. C. Danielson, J. A. Blake, A. F. Pegoraro, A. Stolow, Z. Mester, J. P. Pezacki, *J. Am. Chem. Soc.* **2011**, *133*, 17993–18001.

[132] J. Gierlich, G. A. Burley, P. M. E. Gramlich, D. M. Hammond, T. Carell, *Org. Lett.* **2006**, *8*, 3639–3642.

[133] E. Lallana, E. Fernandez-Megia, R. Riguera, *J. Am. Chem. Soc.* **2009**, *131*, 5748–5750.

[134] C. Barner-Kowollik, F. E. Du Prez, P. Espeel, C. J. Hawker, T. Junkers, H. Schlaad, W.

Van Camp, *Angew. Chem. Int. Ed.* **2011**, *50*, 60–62.

[135] V. Crescenzi, L. Cornelio, C. Di Meo, S. Nardecchia, R. Lamanna, *Biomacromolecules* **2007**, *8*, 1844–1850.

[136] G. Wittig, R. Pohlke, *Chem. Ber.* **1961**, *94*, 3276–3286.

[137] N. J. Agard, J. M. Baskin, J. A. Prescher, A. Lo, C. R. Bertozzi, *ACS Chem. Biol.* **2006**, *1*, 644–648.

[138] J. M. Baskin, J. A. Prescher, S. T. Laughlin, N. J. Agard, P. V. Chang, I. A. Miller, A. Lo, J. A. Codelli, C. R. Bertozzi, *Proc. Natl. Acad. Sci.* **2007**, *104*, 16793–16797.

[139] S. T. Laughlin, J. M. Baskin, S. L. Amacher, C. R. Bertozzi, *Science* **2008**, *320*, 664–667.

[140] J. Dommerholt, S. Schmidt, R. Temming, L. J. a Hendriks, F. P. J. T. Rutjes, J. C. M. van Hest, D. J. Lefeber, P. Friedl, F. L. van Delft, *Angew. Chem. Int. Ed.* **2010**, *49*, 9422–9425.

[141] M. F. Debets, S. S. Van Berkel, J. Dommerholt, A. J. Dirks, F. P. J. T. Rutjes, F. L. Van Delft, *Acc. Chem. Res.* **2011**, *44*, 805–815.

[142] S. Aubry, F. Burlina, E. Dupont, D. Delaroche, A. Joliot, S. Lavielle, G. Chassaing, S. Sagan, *FASEB J.* **2009**, *23*, 2956–2967.

[143] C. A. DeForest, K. S. Anseth, *Nat. Chem.* **2011**, *3*, 925–931.

[144] J. Xu, T. M. Filion, F. Prifti, J. Song, *Chem. - Asian J.* **2011**, *6*, 2730–2737.

[145] X.-M. Jiang, M. Fitzgerald, C. M. Grant, P. J. Hogg, *J. Biol. Chem.* **1999**, *274*, 2416–2423.

[146] R. A. Carboni, R. V. Lindsey, *J. Am. Chem. Soc.* **1959**, *81*, 4342–4346.

[147] G. Clavier, P. Audebert, *Chem. Rev.* **2010**, *110*, 3299–3314.

[148] J. Sauer, D. K. Heldmann, J. Hetzenegger, J. Krauthan, H. Sichert, J. Schuster, *European J. Org. Chem.* **1998**, 2885–2896.

[149] M. Wiessler, W. Waldeck, C. Kliem, R. Pipkorn, K. Braun, *Int. J. Med. Sci.* **2010**, *7*, 19–28.

[150] F. Thalhammer, U. Wallfahrer, J. Sauer, *Tetrahedron Lett.* **1990**, *31*, 6851–6854.

[151] A. Darko, S. Wallace, O. Dmitrenko, M. M. Machovina, R. A. Mehl, J. W. Chin, J. M. Fox, *Chem. Sci.* **2014**, *5*, 3770–3776.

[152] D. S. Liu, A. Tangpeerachaikul, R. Selvaraj, M. T. Taylor, J. M. Fox, A. Y. Ting, *J. Am. Chem. Soc.* **2012**, *134*, 792–795.

[153] J. Schoch, M. Staudt, A. Samanta, M. Wiessler, A. Jäschke, *Bioconjug. Chem.* **2012**, *23*, 1382–1386.

[154] J. Yang, J. Šečkute, C. M. Cole, N. K. Devaraj, *Angew. Chem. - Int. Ed.* **2012**, *51*, 7476–7479.

[155] M. R. Karver, R. Weissleder, S. A. Hilderbrand, *Bioconjug. Chem.* **2011**, *22*, 2263–2270.

7. Publications and Conference Contributions

1. **A. Oehrl**, S. Schötz, R. Haag, *Macromol. Rapid Commun*, accepted: DOI: 10.1002/marc.201900510
2. **A. Oehrl**, S. Schötz, R. Haag, *submitted*

Poster Presentation

A. Oehrl, R. Haag, Bioorthogonal preparation of dPG-based nanogels using iEDDA inverse nanoprecipitation, 255th ACS National Meeting & Exposition, New Orleans, LA, United States, March 18-22, 2018

8. Appendix

8.1 List of Abbreviations

API	Active Pharmaceutical Ingredient
BCA	Bicinchoninic Acid
BCN	bicyclo[6.1.0]non-4-yne
BSA	Bovine Serum Albumin
CMC	Critical Micelle Concentration
conc.	Concentrated
CuAAC	Cu Azide-Alkyne Cycloaddition
DCM	Dichloromethane
DHP	Dihydropyrane
DIPEA	*N*,*N*'-Diisopropylethylamine
DLS	Dynamic Light Scattering
DMF	*N*,*N*'-Dimethylformamide
DANN	Desoxyribonucleic Acid
dPG	Dendritic Polyglycerol
EPR	Enhanced Permeation and Retention Effect
eq.	Equivalents
ESI-MS	Electron Spray Ionization Mass Spectrometry
Et_2O	Diethylether
EtOAc	Ethyl Acetate
EtOH	Ethanol
FDA	Food and Drug Administration
GPC	Gel Permeation Chromatography
GSH	Gluthathion
H	Hour
HATU	Hexafluorophosphate Azabenzotriazole Tetramethyl Uronium
HOBt	1-hydroxybenzotriazol
HOMO	Highest Occupied Molecular Orbital
HPLC	High-Performance Liquid Chromatography
Hz	Hertz
iEDDA	Inverse Electron Demand Diels-Alder

J	Coupling Constant
LADMET	Liberation Administration Distribution Metabolism Excretion Toxicity
LCST	Lower Critical Solution Temperature
lPG	Linear Polyglycerol
LUMO	Lowest Unoccupied Molecular Orbital
MALDI-ToF	Matrix Assisted Laser Desorption Ionization Time-of-Flight
Me	Methyl
MeOH	Methanol
min(s)	Minute(s)
MPS	Mononuclear Phagocyte System
MWCO	Molecular Weight Cutoff
NG	Nanogel
NMR	Nuclear Magnetic Resonance
NTA	Nanoparticle Tracking Analysis
PCL	Polycaprolactone
PDI	Polydispersity Index
PEG	Polyethylene glycol
PLA	Polylactic Acid
PLGA	Polylactic-co-glycolic Acid
PPI	Polypropylene Imine
ppm	Parts Per Million
PRINT	Particle Replication In Non-wetting Templates
PS	Polystyrene
PVA	Polyvinyl Alcohol
quant.	Quantitative
r.t.	Room Temperature
RNA	Ribonucleic Acid
SPAAC	Strain-Promoted Azide Alkyne Cycloaddition
THP	Tetrahydropyran
TLC	Thin Layer Chromatography
UV	Ultraviolet

8.2 Curriculum Vitae

Der Lebenslauf ist in der Online-Version aus Gründen des Datenschutzes nicht enthalten.